

Photoactive antagonists for the GABA_A receptor

Rosemary Huckvale

In partial fulfilment of the requirements for the award of the degree of

DOCTOR OF PHILOSOPHY

at

UNIVERSITY COLLEGE LONDON

2016

Declaration

I, Rosemary Huckvale, confirm that the work presented in this thesis is my own. Where information has been derived from other sources, I confirm that this has been indicated in the thesis.

Abstract

GABA_A receptors are an integral part of regulating neuronal transmission. Through the action of their endogenous agonist, γ -aminobutyric acid, they control most neuronal signal inhibition. GABA_A receptors constantly move through the membrane, readily adapting to different stimuli, aided by transient interactions with scaffolding proteins. This thesis attempts to design and synthesise small, novel chemical tracking devices in order to gain insight into the driving forces of GABA_A receptor diffusion.

To this aim, photoaffinity labelled probe **1**, based on a GABA_A receptor antagonist gabazine, was synthesised. A benzophenone photoaffinity label was prepared, and installed onto a pyridazinyl-phenol core. A Sonogashira reaction, to install a carboxylic acid handle for the biotinylated linker, initially proved unsuccessful until the replacement of aryl bromide with an aryl iodide (Figure 1). Biotinylated probe **1** was associated with a quantum dot coated in streptavidin, and placed in live neurons. Real-time recording of the quantum dot trajectories show receptors moving in synaptic and extrasynaptic sites.

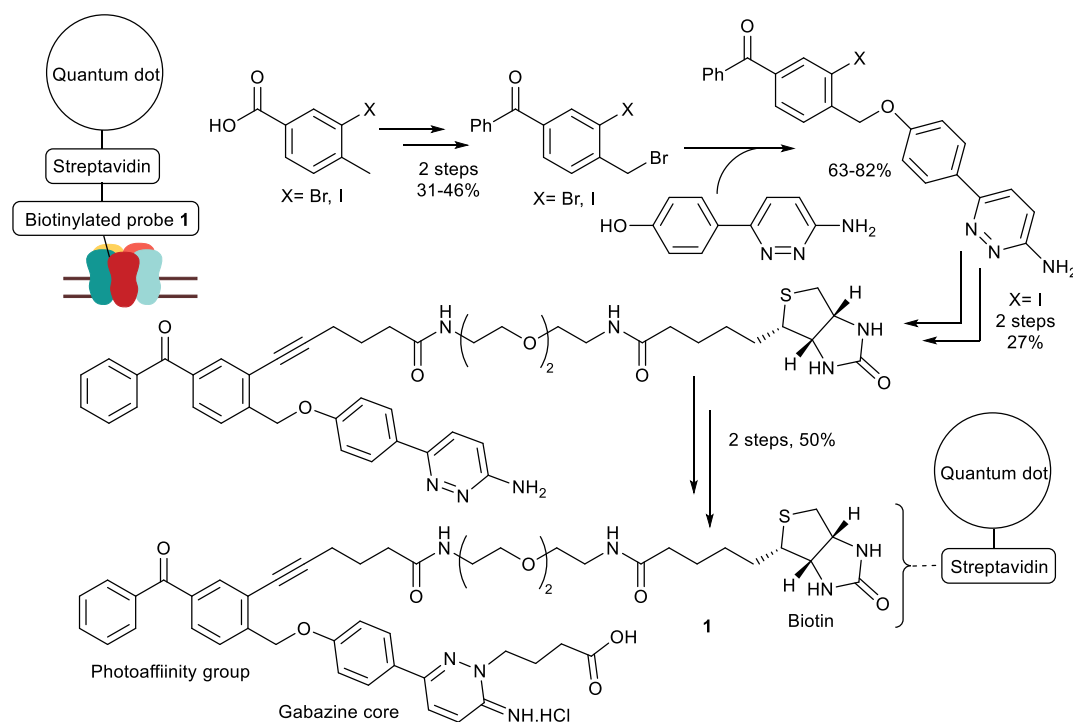


Figure 1: Photoaffinity probe **1** for tracking GABA_A receptors in cells.

This thesis also describes a modular synthetic strategy to build additional chemical tools. A “clickable” alkyne gabazine fragment **2** was synthesised and underwent copper catalysed alkyne-azide couplings to give probes **3** and **4**. These covalently bind to the receptor through an acrylamide electrophilic moiety, and cleavage of the directing gabazine fragment after UV light leaves a silently-tagged receptor. Further generations of these probes could be used to track unblocked, native receptors in order to compare the effects of antagonism on receptor movement (Figure 2).

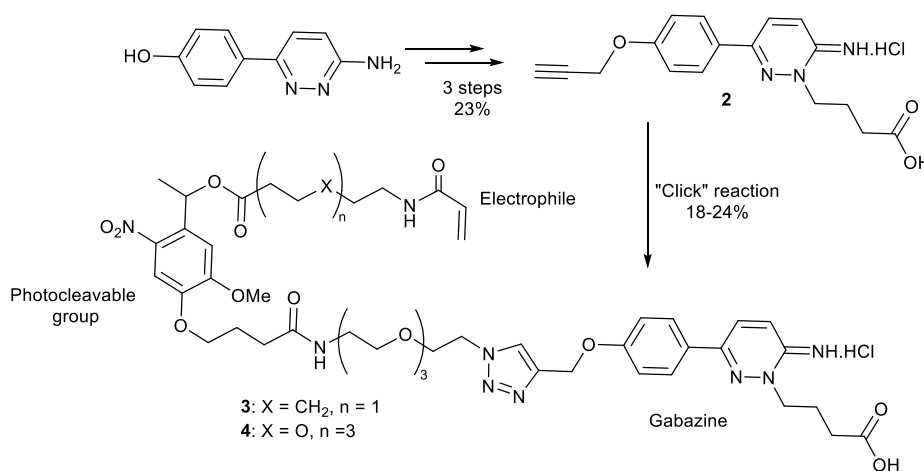


Figure 2: Photocleavable affinity antagonists **3** and **4**

In addition, this thesis discusses a novel photoswitchable antagonist, azo-gabazine **5**, which uses the *cis-trans* photoisomerisation of azobenzene to tune its potency under different wavelengths of light. It is synthesised and used to confer a photoswitching ability onto a native neuronal GABA_A receptors in a biological setting (Figure 3).

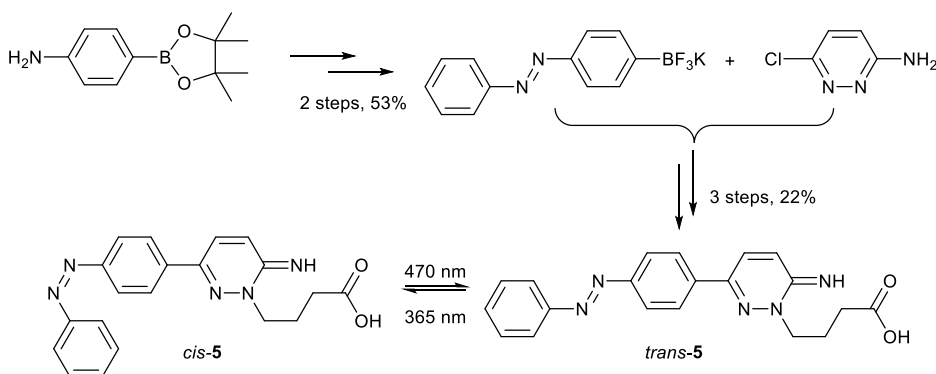


Figure 3: Development of a photoswitchable antagonist to the GABA_A receptor, azo-gabazine **5**.

Acknowledgements

Most of all I would like to thank Dr Jamie Baker for all his support and enthusiasm throughout this project. I would also like to thank our collaborators, Prof Trevor Smart and Dr Martin Mortensen, who carried out testing of our compounds and taught me a lot. Thanks go to Dr Favaad Iqbal, who laid the foundation for this work and was generous with time and help when I joined. Thank you also to my supervisor at Pfizer Neusentis, Dr David Pryde, for giving me support and guidance throughout this work.

Thank you to Dr Abil Aliev for the impeccable NMR service, and to Dr Kersti Karu, Dr Vincent Gray, Dr Eifion Robinson and Dr Lisa Haigh for mass spec.

Special thanks have also got to go to the people with whom it has been such a pleasure to work and get to know. To the members of the Baker group: Andrew, João and Cristina for always being around when I needed help; Dan, Liz, Sally and Nafsika for all the support and friendship.

I would also like to thank Rachel, Sam, Valerie and Sophie for being fabulous company, and allowing me to have the best of times. Thank you to Laure who always makes time for anyone with any question, profound or stupid. Thank you to Vincent and Matt for welcoming me into the lab, and making me laugh.

Whether it was up a hill, in a party cottage, in the pub or on the mezzanine – James, Emily, Antoine, Brian, Elena, Vijay, Marco and all other KLB adventurers, thank you for creating a remarkable and memorable space in which to work.

Grateful thanks also go my family for supporting and inspiring me. Finally, as we approach our ten year anniversary, I would like to thank David for his love and never-ending encouragement throughout these years.

Nothing can be more certain than this: we are *just beginning* to learn something of the wonders of the world on which we live and move and have our being.

WILLIAM RAMSAY, *Essays Biographical and Chemical*, **1908**

Still I had a lurking question. Would it not be better if one could really ‘see’ whether molecules as complicated as the sterols, or strychnine were just as experiment suggested?

DOROTHY HODGKIN, *Nobel Prize Lecture*, **1964**

Contents

Abbreviations	9
Chapter 1: Introduction	12
1.1 Introduction to GABA _A receptors	12
1.2 Introduction to photoaffinity labels	15
1.3 Photoaffinity labels for GABA receptors	17
1.4 Previous work on photoaffinity-labelled antagonists for the GABA _A receptor	19
1.5 Photoaffinity-fluorescent probes and GABA receptors.....	25
1.6 Introduction to quantum dot tracking of GABA receptors	26
1.7 Limitations of quantum dot tracking	31
1.8 Introduction to photocleavable probes for receptors.....	32
1.9 Introduction to photoswitching ligands	35
1.10 Introduction to photoswitchable ligands for receptors	37
1.11 Photoswitchable ligands and GABA _A Receptors	41
1.12 Thesis aims	45
Chapter 2: Photoaffinity antagonists for the GABA_A receptor	46
2.1 Synthesis of a photoaffinity labelled antagonist based on gabazine	46
2.2 Synthesis of a photoaffinity probe for quantum dot tracking of the GABA _A receptor	50
2.3 Quantum dot tracking of GABA _A receptors	62
2.4 Conclusions	69

Chapter 3: Testing alternative photoaffinity labels	71
3.1 UV spectra and photoaffinity labels.....	71
3.2 Testing potential photoaffinity labels	74
3.3 Conclusions	81
Chapter 4: Photocleavable antagonists for the GABA_A receptor	82
4.1 Photocleavable antagonists for the GABA _A receptor	82
4.2 A modular synthesis approach to a photocleavable antagonist for the GABA _A receptor	83
4.3 Development of a photocleavable antagonist for the GABA _A receptor	88
4.4 Conclusions	93
Chapter 5: Photoswitchable antagonists for the GABA_A receptor	94
5.1 Photoswitchable antagonists for the GABA _A receptor	94
5.2 Synthesis of azo-gabazine	95
5.3 Investigation of photoswitching ability by UV/Vis and NMR spectroscopy	100
5.4 Biological evaluation and azo-gabazine photoswitching in cells.....	104
5.5 Conclusions	108
Conclusions	109
Future work	111
General experimental	116
Experimental	118
References	180

Abbreviations

AChR	acetylcholine receptor
Aib	2-aminoisobutyric acid
AIBN	azobisisobutyronitrile
AMPA	α -amino-3-hydroxy-5-methyl-4-isoxazolepropionic acid
ANQX	6-azido-7-nitro-1,4-dihydroquinoxaline-2,3-dione
AP5	(2 <i>R</i>)-amino-5-phosphonovaleric acid
ATR	attenuated total reflection
au	arbitrary units
AziP <i>m</i>	<i>m</i> -Azipropofol
BIODIPY	dipyrrromethene boron difluoride
BisQ	(<i>E</i>)-1,1'-(diazene-1,2-diylbis(4,1-phenylene))bis(<i>N,N,N</i> -trimethylmethanaminium) bromide
Bpa	3-(4-benzoylphenyl)alanine
CI	chemical ionisation
CNB	α -carboxy-2-nitrobenzyl
CNQX	6-cyano-7-nitroquinoxaline-2,3-dione
18-crown-6	1,4,7,10,13,16-hexaoxacyclooctadecane
Cy3	cyanine 3 dye
dba	dibenzylideneacetone
DBCPP	5-[4-(3,3-dimethylbutoxycarbonyl)phenyl]-4-pentynoic acid
DCC	<i>N,N'</i> -dicyclohexylcarbodiimide
DCDHF	2-dicyanomethylene-3-cyano-2,5-dihydrofuran
DIPEA	diisopropylethylamine
DMAP	4-dimethylaminopyridine
DMBA	1,3-dimethylbarbituric acid
DMF	<i>N,N</i> -dimethylformamide
DMSO	dimethylsulfoxide
DPNI	4-[1,3-bis(dihydroxyphosphoryloxy)propan-2-yloxy]-7-nitroindoline
DTT	dithiothreitol
EDC	1-ethyl-3-(3-dimethylaminopropyl)carbodiimide
EI	electron ionisation
ES	electrospray

Fab	antigen binding fragment of an antibody
FT	Fourier transform
GABA	γ -aminobutyric acid
GFP	green fluorescent protein
HBTU	2-(1 <i>H</i> -benzotriazole-1-yl)-1,1,3,3-tetramethyluronium hexafluorophosphate
HEK293	human embryonic kidney 293 cells
HL-60	human promyelocytic leukemia cell
HOAt	1-hydroxy-7-azabenzotriazole
IC ₅₀	half maximal inhibitory concentration
iGluR	ionotropic glutamate receptor
IPSC	inhibitory post synaptic current
LC/MS/MS	liquid chromatography-tandem mass spectrometry
LED	light emitting diode
MAG	maleimide-azobenzene-glutamate
MES	2-(<i>N</i> -morpholino)ethanesulfonic acid
MscL	mechanosensitive channel of large conductance
MTSES	sodium 2-(sulfonatoethyl)methanethiosulfonate
nAChR	nicotinic acetylcholine receptors
NHS	<i>N</i> -hydroxysuccinimide
NBS	<i>N</i> -bromosuccinimide
nd	product not detected
NMDA	<i>N</i> -methyl-D-aspartate
NMP	<i>N</i> -methylpyrrolidinone
OEG	oligoethylene glycol
PEG	polyethylene glycol
petrol	petroleum ether
PTL	photoswitchable tethered ligand
QBr	(<i>E</i>)-1-(4-((4-(bromomethyl)phenyl)diazenyl)phenyl)- <i>N,N,N</i> - trimethylmethanaminium bromide
rt	room temperature (19-22 °C)
satd	saturated
SEP	superecliptic pHluorin fluorescent protein
sIPSC	spontaneous inhibitory post synaptic current

TBOB	2-nitro-4-[3-(trifluoromethyl)-3H-diazirin-3-yl]phenyl 4-(4-methoxycarbonyl-1-butynyl)benzoate
THPTA	<i>tris</i> (3-hydroxypropyltriazolylmethyl)amine
ToF	time of flight
TSPO	translocator protein
δ	chemical shift (ppm)
ν_{\max}	infra red absorption (cm^{-3})
μW	microwave

Chapter 1

Introduction

1.1 Introduction to GABA_A receptors

GABA_A receptors are ligand-gated chloride ion channels found mainly at postsynaptic membranes in the brain. Their principal agonist, the neurotransmitter γ -aminobutyric acid (GABA, **1**, Figure 1) mediates most neural synaptic and extrasynaptic inhibition.¹ This means that GABA receptors are responsible for preventing signals being transferred between neurons by preventing the postsynaptic membrane becoming depolarised and firing an action potential. As GABA binds to the receptor it induces a conformation change in the complex, making the membrane permeable to chloride ions. The resulting chloride ion influx hyperpolarises the membrane, reducing its excitability by sending the membrane potential further below the threshold required to fire an action potential.^{2,3}

In order to mediate this fast synaptic inhibition, the receptors need to accumulate in synapses opposite GABA-releasing neuron terminals. The concentration of GABA_A receptors in these synapses directly influences the strength of synaptic inhibition.¹ GABA_A receptors move into and out of the synapse, aided by complex interactions with scaffold proteins in the membrane. This localisation and dispersal is key for modulating neuronal transmission, as well as for enabling learning and memory (Figure 1 (ii)).⁴ The precise signals, timings and mechanisms by which GABA_A receptors are localised or dispersed from clusters remain unknown.⁵

Heterogeneity in receptor structure means there are variations in the transport and localisation of GABA_A receptors.⁶ GABA_A receptors have a pentameric structure, and are assembled from a wide range of subunits, of which 19 have been identified [α (1-

6), $\beta(1-3)$, $\gamma(1-3)$, δ , ϵ , θ , $\rho(1-3)$ and π] (Figure 1 (i)). Most GABA_A receptors expressed in the brain consist of two α subunits, two β subunits and one γ subunit. A binding site for GABA is formed at the interface of an α and β subunits. GABA receptors composed of different subunits accumulate at different regions of the synapse, have different membrane dynamics and different physiological and pharmacological properties.⁶

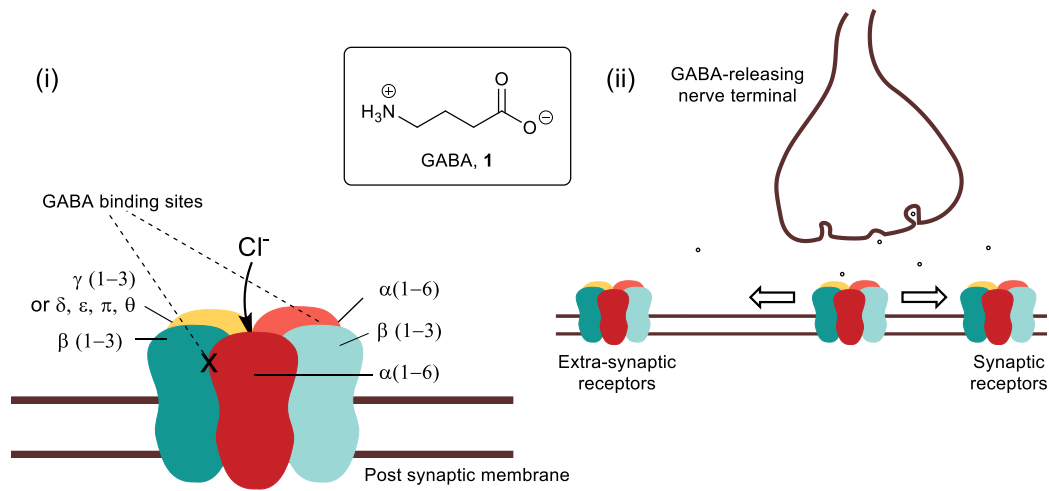


Figure 1: (i) Structure of a GABA_A receptor, showing subunit composition and location of the GABA binding sites between β and α subunits. (ii) Movement of GABA receptors between synaptic and extra-synaptic sites.

GABA_A receptors are assembled within the neuron and are then inserted into the plasma membrane at extrasynaptic sites, where they exhibit free Brownian diffusion. Once they diffuse into the synaptic cleft they are constrained by transient interactions with scaffolding molecules.⁷ There is continual exchange between diffuse receptor populations and clusters in synaptic and extrasynaptic sites (Figure 1 (ii)).³

There are several different classes of ligands for the GABA_A receptor, including agonists, antagonists and both positive and negative allosteric modulators. Agonists, such as muscimol **2** and isoguvacine **3** bind at the GABA binding site, along with competitive antagonists gabazine **4** and bicuculline **5** (Figure 2).

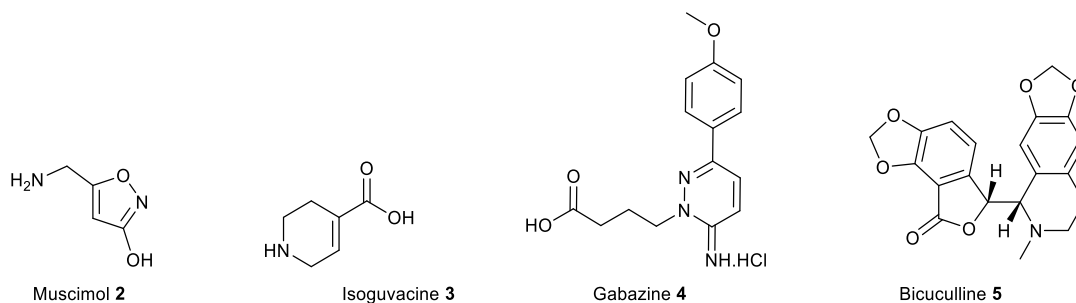


Figure 2: Ligands which bind at the α and β subunit interface on the GABA_A receptor.

A major class of drugs which bind to the GABA_A receptor at the interface of α and γ subunits are the benzodiazepines, of which there are currently fifty drugs on the market, including diazepam (Valium[®], 6) and chlordiazepoxide (Librium[®], 7, Figure 3).⁸ Through their positive allosteric modulation of GABA_A receptors they are used clinically to treat pain, anxiety, insomnia, epileptic seizures, alcohol-withdrawal and amnesia. GABA receptor ligands sometimes have varying affinities for particular receptor subtypes and this has an impact on their pharmacological properties, including unwanted side effects. Benzodiazepines which have additional selectivity for α_2 over α_1 subunit-containing receptors, for example, would be effective anti-anxiety drugs with low sedative effects. Zolpidem 8, in contrast, an allosteric modulator for GABA_A receptors, interacts preferentially with α_1 -containing receptors and is used as a sedative drug to treat insomnia (Figure 3). Agonists which act on α_3 subunit-containing receptors mediate pain relief, whilst there is investigation into α_5 -selective inverse agonists as learning and memory enhancers.⁹ GABA_A receptors containing α_4 or α_6 subunits, mainly found extrasynaptically, are insensitive to benzodiazepines.

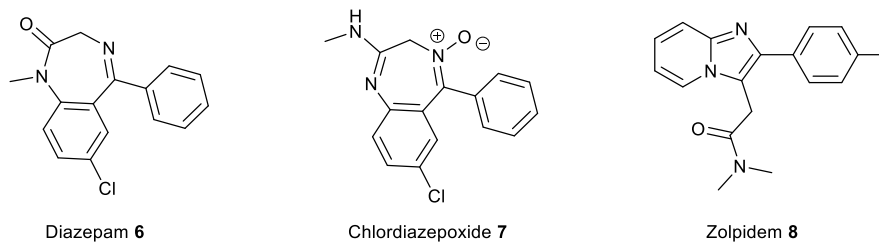


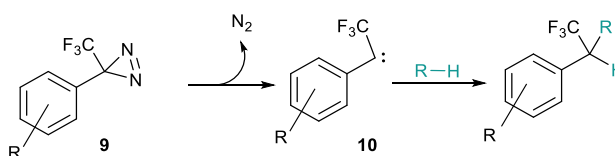
Figure 3: Ligands which bind at the α and γ subunit interface on the GABA_A receptor.

It has been shown that not only do GABA_A receptor ligands modulate the opening of the chloride ion channel, they have implications for the lateral diffusion of the receptors. The GABA_A agonist muscimol **2** has been shown to decrease the presence of GABA_A receptors at synapses, whilst the antagonist gabazine **4** increased this number.¹⁰ Benzodiazepines providing positive allosteric modulation, however, also increased the number of receptors at the synapse, and this gives rise to the hypothesis that the movement of the GABA_A receptor is dependent upon its conformation rather than just its occupancy.¹⁰

1.2 Introduction to photoaffinity labels

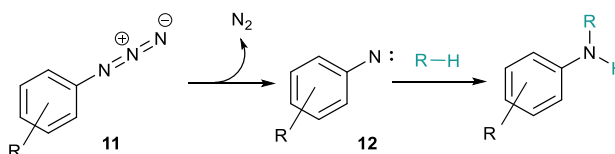
Photoaffinity labelling was pioneered in 1962¹¹ and is now a highly respected technique for studying the relationships between ligands and their target biomolecules *in vitro*. A ligand with high specificity to a receptor is modified to include a photoreactive group, which forms a highly reactive species upon UV/Vis irradiation at a requisite wavelength. This reactive species then generates a covalent bond between the probe and the receptor, irreversibly tagging it. In biological systems, it is important to be able to use irradiation of a wavelength higher than 350 nm, as this causes less protein degradation in the sample. The most popular photoaffinity labels include diazirines, aryl azides, and benzophenones.

Trifluoromethyldiazirine species **9**, which are the most stable of the commonly used diazirines, undergo photolysis very efficiently at 350-380 nm wavelength irradiation, losing nitrogen to form carbene **10** which reacts with nearby molecules (Scheme 1). Occasionally synthetically challenging, their preference for O-H bonds over C-H bonds means that their use is limited when there are water molecules in the binding pocket.¹²



Scheme 1: The photoreactivity of 3-phenyl-3-(trifluoromethyl)diazirines.

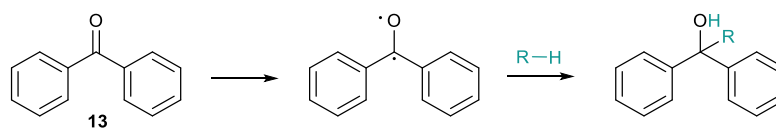
Aryl azides **11** are small and easily incorporated into ligand molecules with minimal structural disturbance. The loss of nitrogen upon excitation creates a highly reactive nitrene species **12** (Scheme 2).¹³ Their activation wavelength of 300 nm is more harmful to biological samples and they also have a tendency to form side products via rearrangement of the reactive nitrene species **12**.



Scheme 2: The photoreactivity of aryl azides.

Benzophenones **13** are chemically the most stable and they are inert to solvent effects, reacting with C-H bonds in preference to other bonds. Upon irradiation a benzophenone is excited via an n,π^* electron transition and reacts via H-abstraction and radical recombination (Scheme 3). The excitation occurs upon irradiation at 350-360 nm wavelengths, which is less damaging to cells. In addition the excited state relaxes back to the ground state if it does not react, which means repeated rounds of

excitation are possible. The disadvantages of using a benzophenone photoaffinity label in an aqueous biological system include its hydrophobicity and bulk.¹⁴



Scheme 3: The photoreactivity of benzophenones.

Photoaffinity labelling can be used to irreversibly block one specific protein component in a system, and it can also be used to establish the precise site of ligand-receptor binding. The receptor is tagged covalently and, after enzymatic or chemical degradation, a particular subunit or protein fragment can be identified by mass spectrometry, or an alternate spectroscopic technique, as the binding site. Photoaffinity labelling is particularly powerful when studying receptors which are embedded in membranes and otherwise difficult to visualise.¹⁵

1.3 Photoaffinity labels for GABA receptors

Photoaffinity labelling has been crucial to mapping the myriad binding sites of the GABA_A receptor. The progression of recombinant receptor technology over the last twenty years has allowed the expression of GABA_A receptors of known subunit composition in cells, and this has gradually diminished the idea of there being a handful of distinct binding sites on receptors.¹⁶ Instead, focus has shifted onto the actions of ligands towards receptors of different subunit composition. This strongly suggests that proposed sites on receptors overlap and interact, and are therefore difficult to quantify.¹⁶

Photoaffinity labelling studies have shown, however, likely positions for the binding of many classes of ligands on particular GABA_A receptors. General anaesthetic

(R)-etomidate (**R**)-**14** was the basis for the photoaffinity labelled analogue, (R)-azietomidate (**R**)-**15**, which helped construct a coherent and consistent model of general anaesthetic binding at the GABA site of the GABA_A receptor.^{17,18,19} The ‘convulsant’ binding site of GABA_A receptors, which interacts with the benzodiazepine site,²⁰ was first probed with the photoaffinity labelled agonist, the diazo derivative **16** of convulsant TBOB **17** (Figure 4).²¹

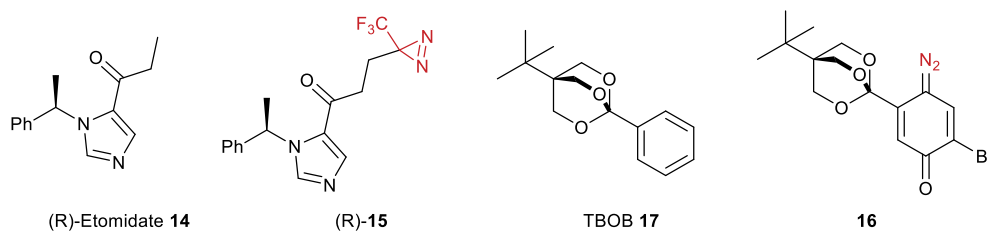


Figure 4: Photoaffinity analogues of GABA_A receptor ligands.

Photoaffinity labels based on non-competitive antagonists have also emerged, for example, NMB **18**,²² and diazirine fipronil **19** (which bind similarly to DBCPP **20** and fipronil **21** respectively) have both been used in binding site analysis (Figure 5).^{23,24}

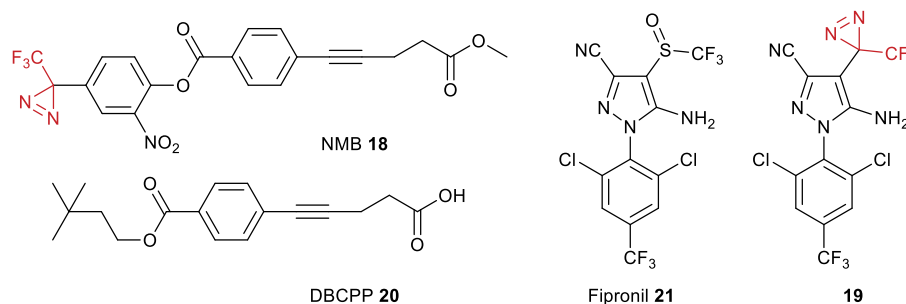


Figure 5: Photoaffinity analogues of non-competitive GABA_A receptor ligands.

Propofol **22**, an allosteric modulator of the GABA_A receptor and a commonly used sedative drug, has also been manipulated in order to ascertain where it binds on the receptor. A diazirine analogue of propofol (AziPm, **23**) was synthesised in 11 steps and 18% yield from Cumene **24** (Figure 6). It was irradiated in the presence of GABA_A receptors, which then underwent trypsin-mediated digestion. LC/MS/MS analysis of

the resulting peptides and residues highlighted the position at which AziPm **23** was covalently bound, and reinforced the location of the known propofol modulatory binding cavity, distinct from both the GABA and benzodiazepine binding sites.²⁵

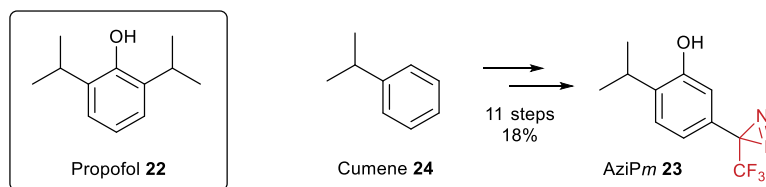
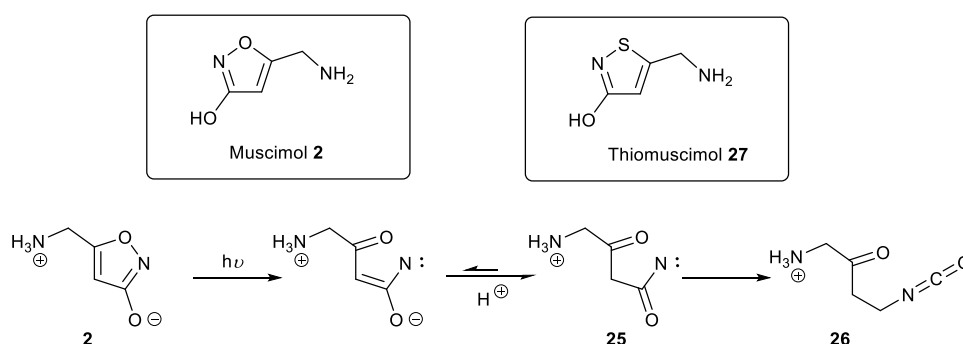


Figure 6: Propofol **22** and diazirine analogue AziPm, **23**.

Furthermore, muscimol **2** has been shown to act as both a competitive agonist and a photoaffinity label for the GABA_A receptor.²⁶ The reactive species **25** and **26** formed upon irradiation (Scheme 4) form covalent bonds with the binding site in the receptor. However, the requisite wavelength of below 210 nm would degrade the biological sample, so this technique could only be used for basic studies. Thiomuscimol **27** (with a UV maximum absorption peak slightly higher at 262 nm) has also been used as a photoaffinity label to the GABA_A receptor (Scheme 4).²⁷



Scheme 4: Photoreactivity of muscimol **2**. Thiomuscimol **27** has an analogous reactivity.

1.4 Previous work on photoaffinity-labelled antagonists for the GABA_A receptor

Previous work in the Baker and Smart groups has included the synthesis and evaluation of potent GABA_A receptor antagonists based on gabazine **4**.²⁸ Gabazine **4**, first synthesised in 1987,²⁹ is one of many synthetic antagonists which arose from the

knowledge that adding hydrophobic ring systems to a γ -aminobutyric acid core yields GABA_A receptor antagonists (Figure 7).²⁹ Gabazine **4** is also susceptible to certain modifications without loss of potency; indeed the replacement of the methoxy group with a benzoxy group leads to antagonist **28** which has an increased potency against GABA_A receptors, as do substituted benzoxy analogues in compounds **29** and **30** (Figure 7).³⁰

A useful measure of the effectiveness of antagonism of compounds is the half-maximal inhibitory concentration (IC₅₀), that is, the concentration of compound required to halve the maximum known response of the receptor. In the case of GABA_A receptors the response is quantified by the measurement of the current across the membrane of a cell. This is measured using whole-cell voltage-clamp electrophysiology where a glass electrode containing internal solution is sealed into the membrane of a cell expressing GABA_A receptors. An equal concentration of internal and external chloride ions and a negative holding potential ensure that observed changes in membrane potential arise from chloride ions driven through GABA_A receptors. This response is measured in the presence of varying concentrations of antagonist and a dose-response curve is plotted and interpreted to give the IC₅₀ value. The IC₅₀ values given in Figure 7 are derived from GABA-activated responses in HEK293 cells, which are human embryonic kidney cells which have been transfected to express GABA_A receptors with a particular subunit composition.

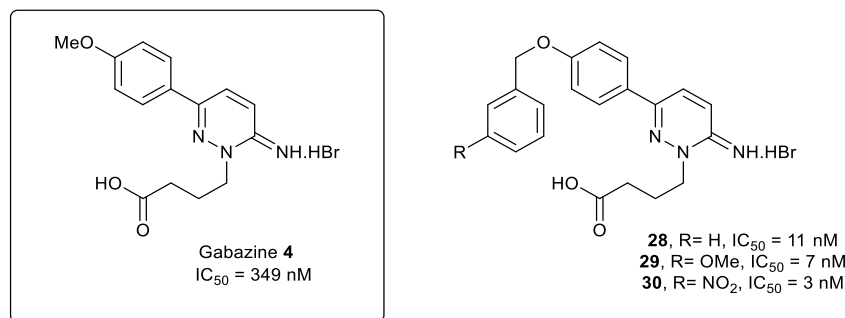
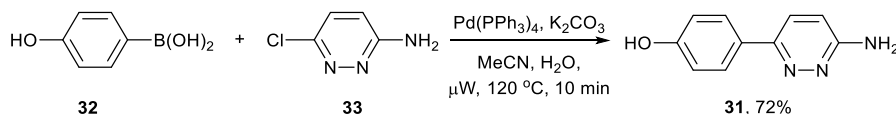


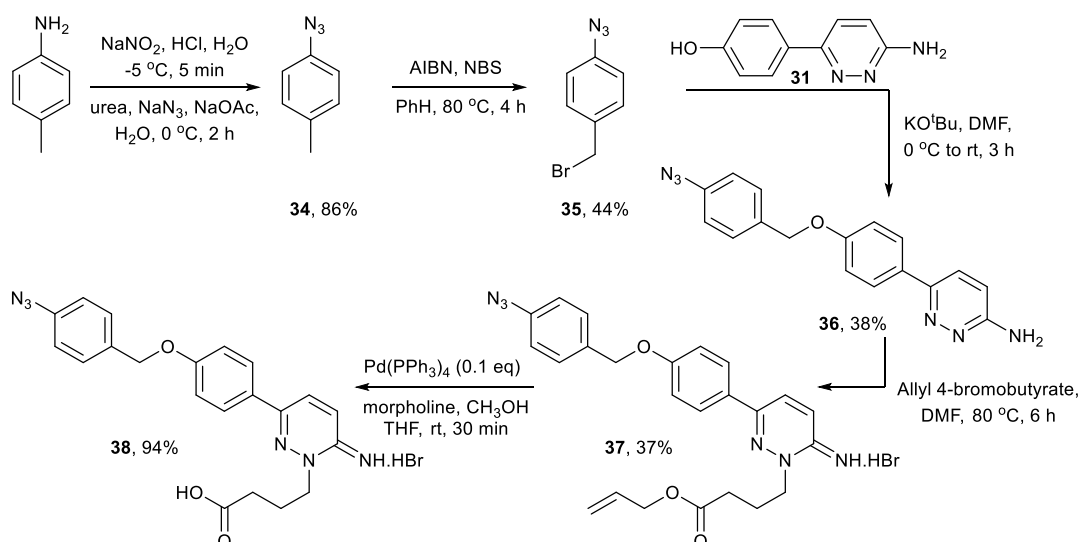
Figure 7: Gabazine **4**, antagonist to the GABA_A receptor, and analogues with increased potency in $\alpha 1\beta 2\gamma 2S$ GABA_A receptors transiently expressed in HEK293 cells.³⁰

The synthesis of three photoaffinity labelled antagonists based upon gabazine **4** has been reported, making use of diazirine, azide and benzophenone photoaffinity labels.³⁰ The pyridazine skeleton **31**, common to all syntheses was formed in a microwave-assisted Suzuki coupling reaction between commercially available starting materials 4-hydroxyphenylboronic acid **32** and 3-amino-6-chloropyridazine **33** in 72% yield (Scheme 5).

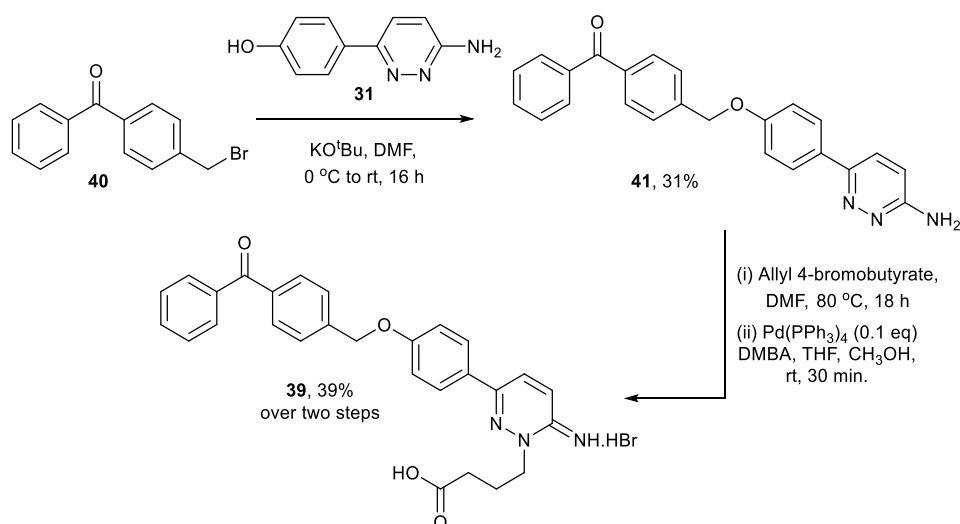


Scheme 5: Microwave-assisted Suzuki coupling reaction conditions.

In the synthesis of the azide analogue, 4-aminotoluene underwent oxidation to the diazonium salt, which then underwent displacement with sodium azide to give azide **34** in 86% yield (Scheme 6). Radical bromination with *N*-bromosuccinimide in the presence of AIBN led to formation of brominated azide **35** in 44% yield. A Williamson ether synthesis with potassium *tert* butoxide and pyridazine skeleton **31** furnished pyridazine **36** in 38% yield. *N*-Alkylation was achieved on heating with allyl 4-bromobutyrate in 37% yield, and subsequent deprotection of allyl ester **37** was achieved with tetrakis(triphenylphosphine)palladium and morpholine in 94% yield, giving azide analogue **38** in a total of 5 steps and 5% overall yield (Scheme 6).

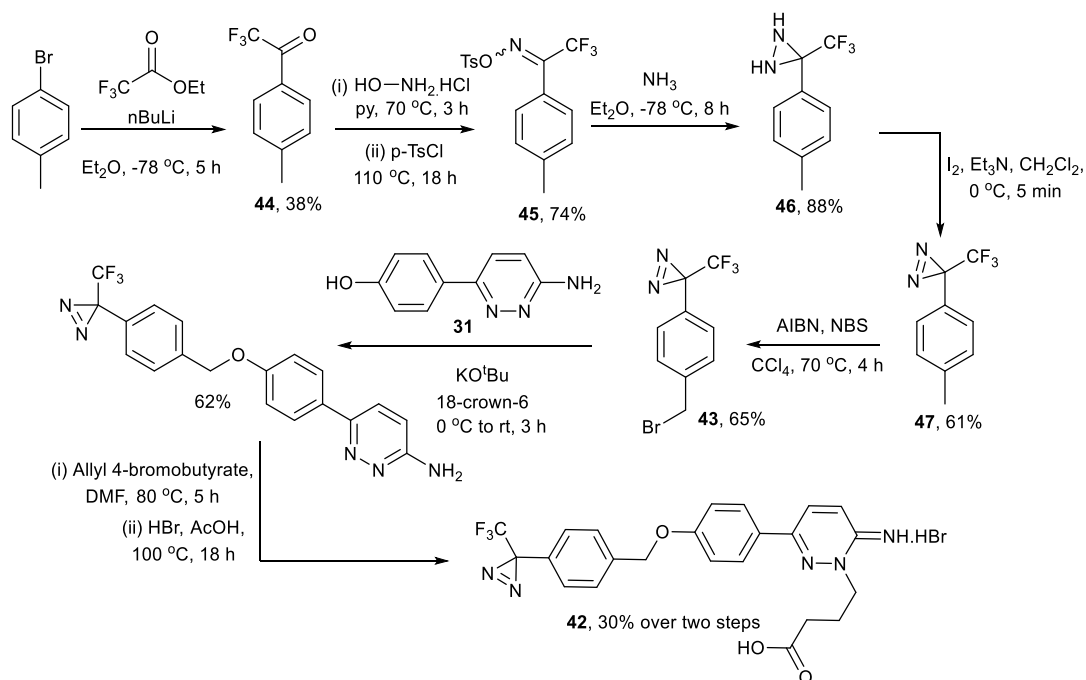
Scheme 6: Synthesis of azide photoaffinity label based upon gabazine **4**.

The benzophenone analogue **39** was synthesised relatively easily in three steps in 12% overall yield. The requisite benzophenone bromide **40** is commercially available, and the ether synthesis was achieved with potassium *tert* butoxide and **31** in 31% yield. The *N*-alkylation of pyridazine **41** and subsequent ester deprotection were accomplished in 60 and 65% yield respectively to give benzophenone **39** (Scheme 7).

Scheme 7: Synthesis of benzophenone photoaffinity label based upon gabazine **4**.

The trifluorodiazirine analogue **42** was synthetically more challenging; the brominated species **43** itself requiring a six step synthesis. 4-Bromotoluene was reacted with *n*-

butyllithium and quenched with ethyl trifluoroacetate to give ketone **44** in 38% yield. Oxime **45** was synthesised in 99% yield as a mixture of isomers upon reaction of ketone **44** with hydroxylamine hydrochloride. Tosylation of the oxime was accomplished in 75% yield upon reaction with *p*-toluenesulfonyl chloride giving tosyl oxime **45**, which was when reacted with ammonia condensed in a sealed vessel at -78 °C to give diaziridine **46** in 88% yield. The subsequent oxidation to diazirine **47** was achieved upon reaction with iodine and triethylamine in dichloromethane in 61% yield. Diazirine **47** then underwent radical bromination with *N*-bromosuccinimide and AIBN to furnish bromide **43** in 65% yield. A Williamson ether synthesis was achieved in 62% yield, and the *N*-alkylation and ester deprotection in 41 and 59% respectively, which afforded diazirine analogue **42** in nine steps and 2% overall yield (Scheme 8).



Scheme 8: Synthesis of diazirine photoaffinity label based upon gabazine **4**.

The potency and photoactivity of these compounds was measured by calculation of the IC_{50} value, and measurement of the photolytic block. Whole-cell patch clamp electrophysiology was used to record the membrane current from multiple ion

channels on a cell. GABA was applied and the postsynaptic membrane current was measured. The photoactive antagonist was then applied and exposed to UV radiation in brief ten second flashes. The cells were washed to remove any non-covalently bound antagonist, then GABA was reapplied and the membrane current recorded again. The difference in the transmembrane current before and after the UV irradiation is called the photolytic block, and denotes the percentage of GABA receptors which have been inactivated.

The IC_{50} value of gabazine **4** in recombinant $\alpha 1\beta 2\gamma 2S$ receptors in HEK293 cells was 349 nM. Photoaffinity compounds **38**, **39** and **42** all had lower IC_{50} values than gabazine **4**, denoting that they were all more potent antagonists. In addition, the benzophenone analogue **39** gave a 49% photolytic block in these recombinant $\alpha 1\beta 2\gamma 2S$ receptors. Azide **38** and diazirine **42** gave 29 and 21% photolytic block respectively (Figure 8).

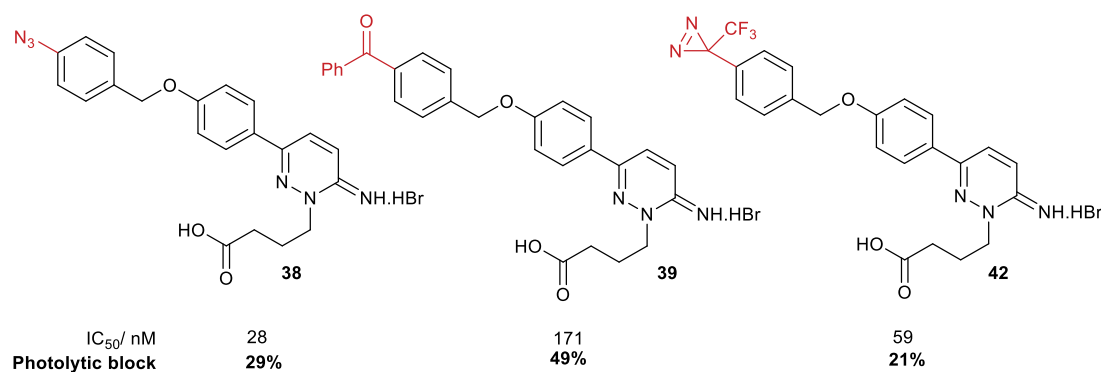


Figure 8: Photoaffinity labelled antagonists for the $GABA_A$ receptor.

Once the receptor is blocked irreversibly in a recombinant cell system, there is no effective mechanism by which receptors could be replaced. In a primary culture of hippocampal neurons however, the biological structure is in place for the receptors to be replenished. The timescale and mechanisms of this receptor trafficking are an ongoing and important area of research, and further experiments using benzophenone

39 on a primary culture would be highly beneficial. Chapter 2 of this thesis describes new routes in a scale-up synthesis of this photoaffinity labelled antagonist **38** in order for additional biological experiments in primary neuronal cultures to be carried out.

1.5 Photoaffinity-fluorescent probes and GABA receptors

The strength of inhibitory synaptic transmission is dependent upon the local concentration of GABA receptors on the postsynaptic membrane. It is known that GABA_A receptors are mobile on the membrane, and that this mobility occurs not just when they are being inserted into the membrane after synthesis.³¹ To study this, photoaffinity labels have been tagged with fluorescent probes to visualise the movement of a labelled protein (Figure 9). The ligand would bind to the receptor, and irradiation of the photoaffinity label will tag the receptor covalently, whilst the fluorescent reporter can be tracked under a microscope.

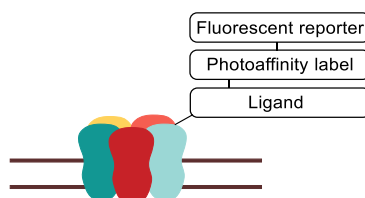


Figure 9: Photoaffinity-fluorescent probe for a membrane bound receptor.

Li *et al.* successfully synthesised a fluorescent probe **48** for photoaffinity labelling GABA_B receptors in living cells (Figure 10). Based on a high-affinity, GABA_B-specific antagonist **49**, probe **48** incorporates a photolabile diazirine group, as well as a fluorescent tag derived from BODIPY. Following irradiation, probe **48** was successful in significantly preventing GABA_B receptors (transfected into HEK293 cells) being activated by GABA, which shows that it is a potential technique for providing, via fluorescence imaging, important information about the localisation of GABA_B receptors expressed in live cells.

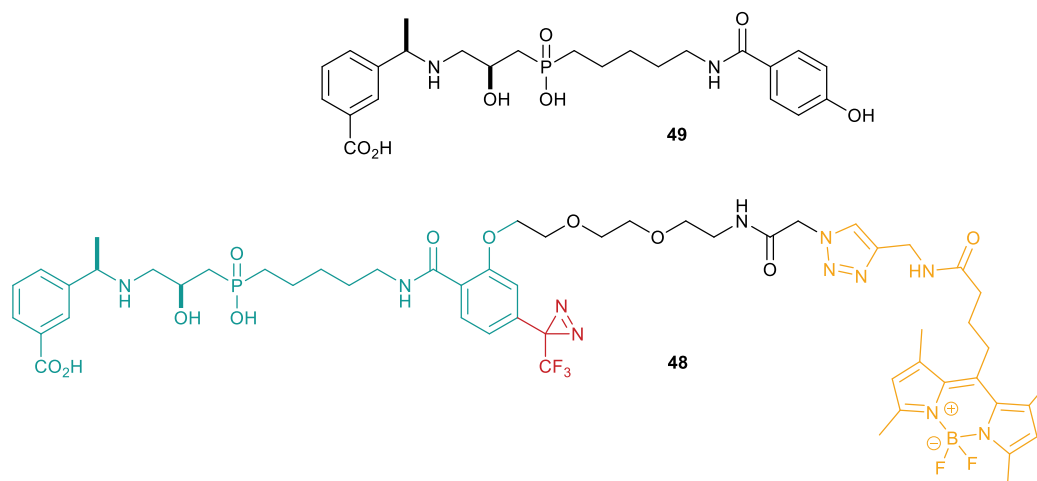


Figure 10: Antagonist to the GABA_B receptor **49** and the photoaffinity probe for the GABA_B receptor **48**, showing the receptor ligand group (blue), the photoaffinity label (red) and the BODIPY-derived fluorophore tag (gold).³²

1.6 Introduction to quantum dot tracking of GABA receptors

In many cases, this tracking of receptors in membranes is carried out using quantum dots, which are particularly well suited for visualising and tracking molecular processes in cells by standard fluorescence microscopy.³³ Quantum dots are nanometre-sized fluorescent probes, generally composed of a heavy metal core (for example CdSe) responsible for the fluorescence; a non-emissive stabilising shell (for example ZnS); and a coating which provides binding sites for organic molecules. They surpass other organic fluorophores and fluorescent protein tags as they are stable to photobleaching, and, as they are highly tuneable in terms of colour, different quantum dots can be used to study more different proteins in the same experiment.³⁴

There are various ways to incorporate a quantum dot onto a molecule. The quantum dot can be coated in a polyacrylamide, and covalently bound via linkers to the ligands. Quantum dots can also be coated in proteins such as streptavidin, meaning they can be strongly but non-covalently bound to nearly any compound containing a biotin **50** moiety (Figure 11).³⁵ In addition there are quantum dots which have a surface coating

with reactive chemical functional groups, including primary amines, thiols, maleimides and carboxylic acids. These provide a variety of conjugation strategies to ensure selective binding of the quantum dot in a biological system. There are relatively few reported uses of small molecule-quantum dot conjugates, despite their ready synthesis and their potential to target proteins which do not have target-specific antibodies or peptides available.³⁶

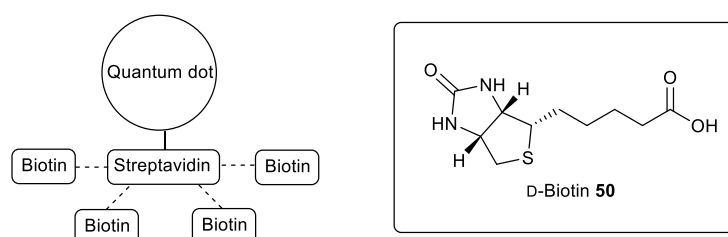
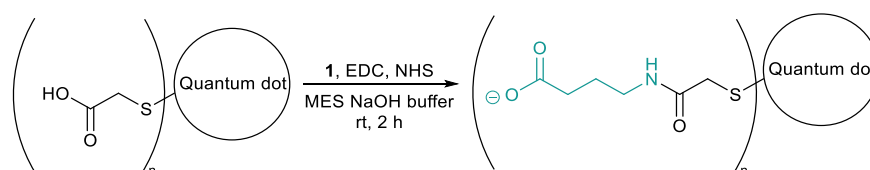


Figure 11: D-Biotin **50** is used to recognise a streptavidin-coated quantum dot.

Quantum dots have opened new perspectives for the study of GABA receptor trafficking, as they enable measurements at a single molecule level and can give information about the organisation and mobility of receptors in the membrane.³⁴ For example, the presence of GABA receptors in tobacco plants was reportedly first detected by the use of GABA directly linked via an amide bond to a quantum dot coated in mercaptoacetic acid (Scheme 9).³⁷



Scheme 9: GABA-quantum dot conjugate

Gussin *et al.* have achieved the conjugation of a quantum dot to GABA_C receptors using the specificity of the agonist, muscimol **2**.³⁶ GABA_C receptors have pentameric structures and are assembled from ρ 1-3 subunits. Here, GABA_C receptors were expressed in a model cell system as homopentamers of ρ 1 subunits. GABA receptor

agonist muscimol **2** was bound to a quantum dot which was coated in polyacrylamide via a polyethylene glycol (PEG) linker chain, in a test to study the biological activity of such a compound (Figure 12). The long PEG linker of 3400 units was used to achieve sufficient distance between the quantum dot and the GABA_C – muscimol binding site, and enabled several (150-200) muscimol ligands to be joined to one quantum dot. The positive and specific biological activity of this conjugate **51** is encouraging for future investigations into neurotransmitter membrane receptors.

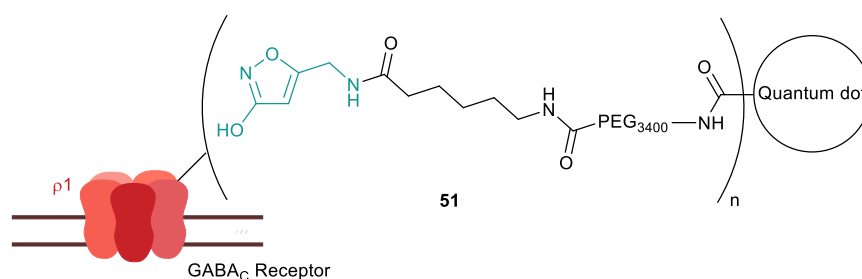


Figure 12: Muscimol – quantum dot conjugate **51**, where $n = 150-200$.

Another approach, using antibodies and protein recognition to tag the target protein or biomolecule, has been used successfully to show how the distribution of GABA_A receptors on the postsynaptic membrane changes upon application of a GABA gradient.³⁸ Bouzigues *et al.* saw asymmetric redistribution of GABA_A receptors when they followed single receptors with quantum dots. The $\gamma 2$ subunits of GABA_A receptors on the membrane of rat spinal neurons were labelled with a $\gamma 2$ -specific antibody. This antibody was then labelled with a secondary, biotinylated antibody, which was associated with a streptavidin-coated quantum dot (Figure 13 (i)). It was found that on membranes with no GABA, the average position of the 10-30 tagged receptors had a statistically random motion. In a uniform GABA concentration, the receptors still maintained a statistically random motion (Figure 13 (ii), grey), but on the application of a GABA gradient, the GABA_A receptors had a directed motion towards the higher GABA concentration (Figure 13 (ii), black). Upon removal of the

GABA concentration gradient, the spread of GABA receptors returned to a symmetric distribution. This is important in showing how GABA_A receptors adapt to stimuli and influence the propagation of synaptic inhibition.³⁸

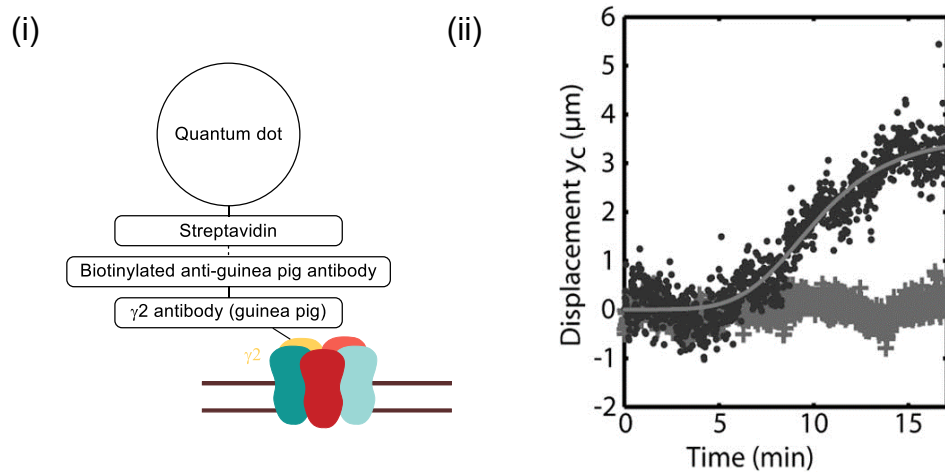


Figure 13: (i) schematic of quantum dot tagged GABA_A Receptors; (ii) Displacement of the centre of mass of receptors in the presence of no GABA gradient (grey) and GABA gradient (black).³⁸

Muir *et al.* used quantum dots bound to single, non-native receptors to investigate the effect that the activation of glutamate receptors in excitatory synapses have on the lateral mobility of GABA_A receptors in inhibitory synapses. The pH-sensitive superecliptic pHluorin (SEP) fluorescent protein was used to visualise only receptors at the *surface* of cells (the pH inside the cell is unfavourable to SEP fluorescence). $\alpha 2^{\text{SEP}}$ -GABA_A receptors (assembled from SEP-tagged $\alpha 2$ subunits alongside endogenous GABA_A receptor subunits) could be seen on the cell surface in live hippocampal neurons. Imaging revealed the initial intensities and location of $\alpha 2^{\text{SEP}}$ -GABA_A receptor clusters (groups of 20-30 receptors). It was shown that glutamate receptor activation led to a decrease in the fluorescence at these clusters, but no decrease in the overall fluorescence. This suggested that there must be a redistribution, rather than removal, of GABA_A receptors. This technique could not, however, resolve the behaviour of a single GABA_A receptor. In order to do this, a quantum dot (anti-

mouse) antibody conjugate was attached to a receptor via an antibody that recognised the SEP tag (Figure 14 (i)). The trajectory of a single quantum dot- $\alpha 2^{\text{SEP}}$ -GABA_A receptor into and out of a cluster was then tracked under a microscope, and its diffusion rate increased on glutamate receptor activation (Figure 14 (iii)). It was concluded that glutamate receptor activation led to the dispersal of GABA_A receptor clusters by increasing GABA_A receptor mobility.³⁹

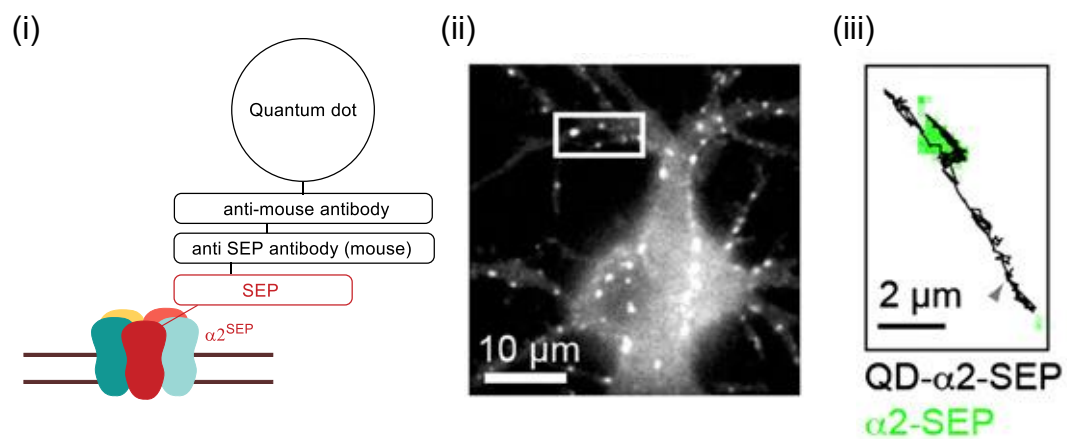


Figure 14: (i) Schematic of a quantum dot-tagged $\alpha 2^{\text{SEP}}$ GABA_A receptor; (ii) $\alpha 2^{\text{SEP}}$ GABA_A receptors expressed in a hippocampal neuron;³⁹ (iii) trajectory of a quantum dot-tagged $\alpha 2^{\text{SEP}}$ GABA_A receptor shown (black) into and out of a GABA_A receptor cluster (green).³⁹

One of the advantages of this research is that it enabled the simultaneous visualisation of single GABA_A receptors movement alongside the real location of receptor clusters (Figure 14, (ii)). One disadvantage is the size and bulk of the SEP-tagged receptors, which could be showing a different dynamic behaviour than unmodified GABA_A receptors in the brain. A second limitation is the fact that the receptors here are not native, and this may also affect the way they diffuse through the membrane. The combination of a photoaffinity labelled antagonist and a fluorescent probe could be very powerful in investigating the movement of native receptors in the plasma membrane.

1.7 Limitations of quantum dot tracking

There are many questions to be considered about the efficacy of using quantum dots to study membrane receptor diffusion.⁴⁰ It is important, firstly, to consider whether the presence of a quantum dot influences the surface diffusion. It is generally thought that the diffusion of the receptor is not hindered by the presence of a quantum dot, instead the rate limiting factor is the viscosity of the membrane itself, reported to be 100-1000 times more viscous than the extracellular medium.⁴¹ A comparison between the diffusion rates of AMPA receptors tagged with a variety of sized quantum dot conjugates were deemed to not be significantly different.⁴¹ [AMPA receptors are ligand-gated cation channels, activated by glutamate, and are excitatory synaptic receptors].⁴¹ However, when discussing receptors inside the synaptic cleft, there seems to be more doubt on the issue. Dahan *et al.* tracked synaptic glycine receptors, and showed that the quantum dots were small enough to penetrate into the synaptic cleft.⁴² On the other hand, the diffusion rates of a quantum dot coated in a large protein were different to that of a quantum dot coated in a relatively small Fab fragment, which supports the rationale that the smaller the probe the more accurate the tracking of synaptic receptors.⁴¹

A second point to consider is whether an endogenous receptor and mutated recombinant receptors have the same surface diffusion. This is a limitation in many of the methods outlined above, and it is not possible to form pertinent controls for many of these experiments.

The ideal tool for studying lateral mobility of GABA_A receptors would be one which could track individual native receptors. This could be mediated by a small GABA_A-specific ligand covalently bound to the receptor. This covalent bond could come from

an electrophilic moiety in the molecule, or from the excitation of a photoaffinity label, the latter also allowing additional spatial control (Figure 15).

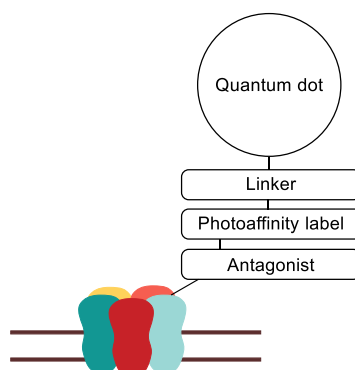


Figure 15: A photoaffinity labelled fluorescent probe to track the lateral mobility of GABA_A receptors.

A better picture would be gained if the modification of the GABA_A receptors remained as small as possible. The fluorescent probe should be small enough to fit inside the synaptic cleft, as well as being far enough away from the receptor-ligand binding site to not cause steric interference. A quantum dot has many advantages over fluorescent proteins and organic fluorophores. Furthermore, in general it is more effective to measure the effect of an antagonist as opposed to an agonist, as the block of ion current over the membrane is easier to quantify than an incremental increase, which is highly dependent on agonist concentration. The development of a chemical tool upon this basis, such as that shown in Figure 15, is attempted in Chapter 2 of this thesis.

1.8 Introduction to photocleavable probes for receptors

The movement of receptors in the membrane has been shown to be highly dependent upon the conformation of the receptor.^{43,4} It has already been mentioned that in the presence of a GABA gradient, the GABA_A receptors move non-randomly. In addition, recent work has highlighted that GABA_A receptors disperse in the presence of agonists, but in the presence of antagonists they remain more stationary in the synapse.

This is due to changes in the interaction of GABA_A with large proteins on the cytoskeleton. More widely, neuronal activity modifies the diffusion properties of GABA_A receptors. Most tracking methods described above reveal the location and movement of their targets, but seldom reveal information about the activation state of the channel.⁴⁴ A probe based upon a photoaffinity labelled antagonist will necessarily only give information about the movement of a blocked receptor. A receptor with a free binding site may well move differently, and in probes which rely upon ligand specificity to direct fluorescent attachment, this calls for a photocaging strategy, whereby the ligand is cleaved once the fluorescent probe is installed.

An example of this technique is the nanoprobe **52**, which was designed as a ligand-targeted and photocleavable probe for delivering a fluorophore to native AMPA receptors in order to carry out studies on receptor trafficking. Nanoprobe **52** is comprised of a polyamine receptor-specific ligand [gold] attached, via a nitroindoline photocage [red], to an acrylamide electrophile [black] and a Cy3 fluorescent dye [blue] (Figure 16). The electrophilic acrylamide would form a covalent bond with a residue near the binding site in the ion channel, and photolysis of the photocage would cause ligand release, leaving a covalently tagged receptor in a non-antagonised state.^{44,45}

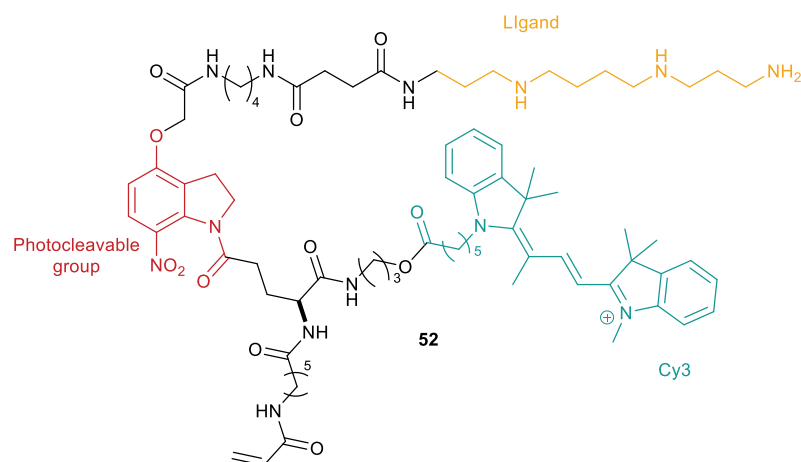


Figure 16: Nanoprobe **52** for 'silent' fluorescent labelling of neuronal receptors, showing the ligand group (gold), the photocleavable group (red) and the Cy3 fluorophore tag (blue).

There are many different electrophilic moieties which have been used to facilitate protein-ligand covalent attachment, including epoxides, aryl halides, haloacetamides, maleimides and carbonates.⁴⁶ The benzodiazepine ligand Ro15-4513 **53**, as well as diazepam **6**, were modified to include an electrophilic isothiocyanate group, giving **54** and **55** respectively (Figure 17). These compounds were incubated with GABA_A receptors of different subunit compositions, which had been mutated to include cysteine residues at various points in the benzodiazepine binding site. The cases in which irreversible binding was observed were used to generate an experimental picture of how each ligand sits in the binding pocket.^{47,48}

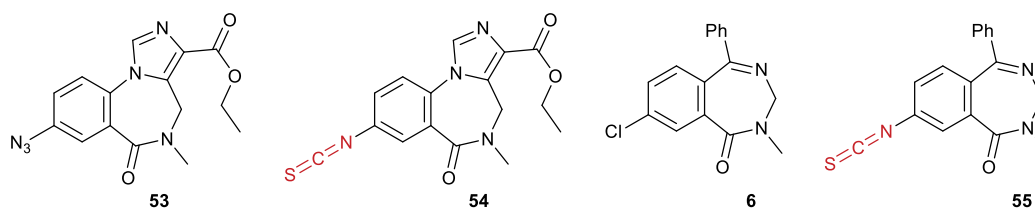


Figure 17: Isothiocyanate electrophilic analogues **54** and **55**, of allosteric modulators **53** and **6** to probe the benzodiazepine binding site.

The photorelease of a compound can be facilitated by many different photocleavable groups, allowing the compound to leave as a variety of molecular functionalities

including phosphates, carboxylates, phenols, thiols, amines and amides.⁴⁹ Several of these photocaged ligands, which are inactive until uncaged, have been used effectively in neuronal cultures, in the form of photocaged neurotransmitters.⁵⁰ Of these, various nitroindoliny- and nitrobenzyl-based photocages, for example DPNI-GABA **56** and CNB-L-glutamate **57**, are commercially available and widely used (Figure 18).

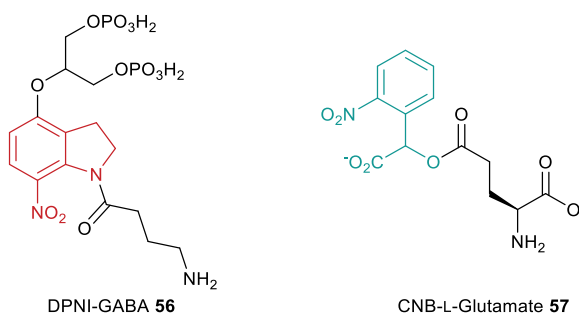


Figure 18: Commercially available photocaged neurotransmitters.

A nanoprobe with the functionality described above and based on gabazine, could release its ligand from the GABA binding site of a GABA_A receptor upon irradiation, leaving a fluorescent probe covalently tethered. With further development and optimisation, it could track unblocked GABA_A receptors in a live neuronal system. Research into a system such as this is described in Chapter 3 of this thesis.

1.9 Introduction to photoswitching ligands

Photoaffinity labelling, and the above photocleavable ligands are irreversible optopharmacological tools.⁵¹ Chemical photoswitches, in contrast, are bistable photochromic compounds which can be activated and deactivated in cycles. These could be used to reversibly control the function of a biological system, using a mode of reactivity which is orthogonal to most cellular processes, light. Synthetic bistable molecules include azobenzenes **58**, stilbenes **59**, and hemithioindigos **60**, which form

photostationary states consisting of different ratios of *cis* and *trans* photoisomers under different wavelengths of light or thermal conditions (Figure 19).

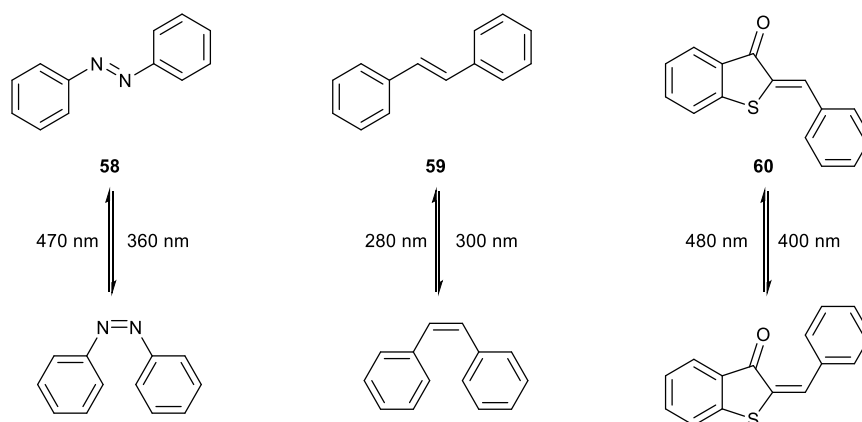


Figure 19: Compounds which undergo *cis-trans* photoisomerisation.

In addition, spiropyrans **61**, diarylethenes **62** and thiophenefulgides **63**, are synthetic photoswitches which reversibly switch between open and closed forms (Figure 20).

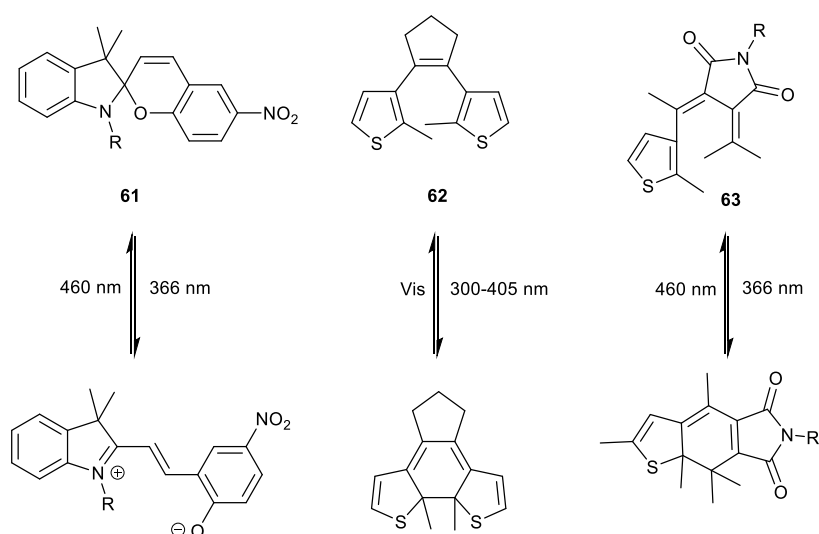


Figure 20: Ring opening and closing photochromic compounds.

By far the most well-known and well-used photoswitch is azobenzene **58**, first reported in 1937,⁵² which upon irradiation with UV light forms a *cis*-enriched photostationary state. This can be relaxed to a majority *trans* equilibrium thermally or upon visible light irradiation.⁵³ In order to be of use in a biological system, a synthetic

photoswitch would need to undergo rapid switching, and have a high extinction coefficient with a high quantum yield at wavelengths that are not harmful to living cells.⁵⁴

Substituents on the phenyl rings greatly affect the photoisomerism of the azobenzene, including the wavelength at which isomerisation is optimised. The use of UV irradiation in a working biological system has the great disadvantage of causing cell damage, and for this reason substituted azobenzenes with red-shifted absorbance have been synthesised.⁵⁵ Many of these either have *ortho*- or *para*-amino-, *para*-amido-groups, or invoke a push-pull electron effect by having acceptor and donor groups in opposing *para*- positions.⁵⁶

1.10 Introduction to photoswitchable ligands for receptors

In biological systems, photochromic ligands to a protein can provide precise spatial and temporal control of function. Photodynamic properties can be conferred onto a receptor via an untethered ligand with active and inactive photoswitchable states.⁵⁷ Another method would be a tethering approach, through which a photoswitch is bound via a covalent bond between a genetically introduced nucleophilic residue and a complementary electrophilic moiety on the ligand. Once bound, application of the light stimulus will cause the photoswitchable tethered ligand (PTL) to change conformation and retract its binding motif from the binding pocket (Figure 21). This is then reversed upon application of a light stimulus of a different wavelength. In this way the receptor is reversibly activated/deactivated upon UV exposure.

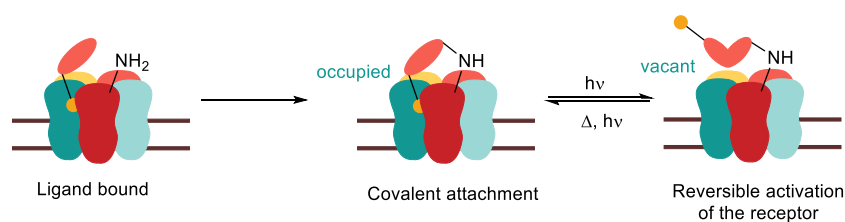
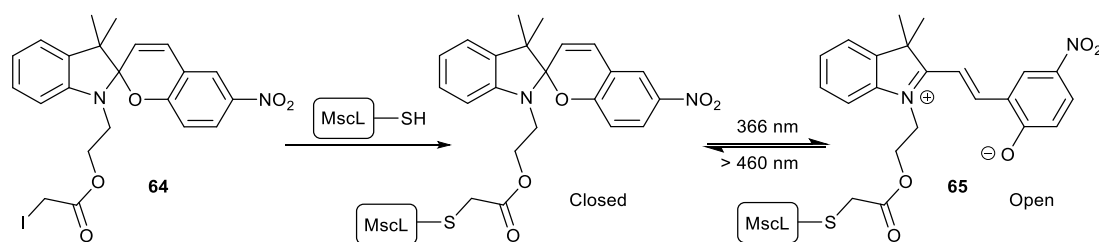


Figure 21: General mechanism of use for a tethered photoswitchable ligand.

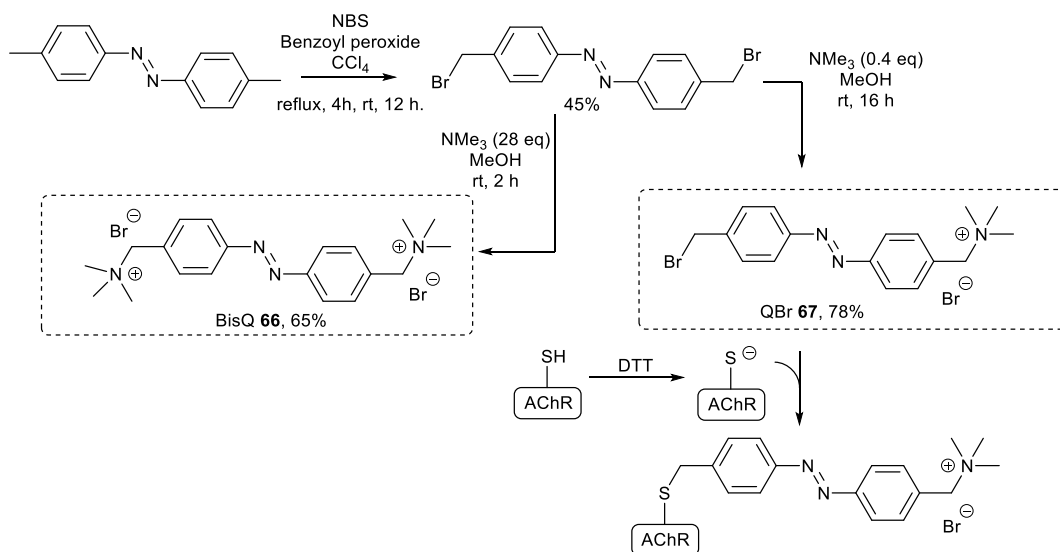
Photoswitchable ligands and PTLs in the literature mostly contain azobenzenes, although some others have been used. For example, the spiropyran iodoacetate **64** has been successfully used to regulate the opening and closing of a mechanosensitive channel of large conductance (MscL). Cysteine residues, genetically introduced in the channel pore, covalently bind to **64**, and irradiation of the system causes ring-opening formation of the dipolar merocyanine structural isomer **65**, the dipolar nature of which forces the channel open. This releases liposomal material which can be quantified using fluorescence readings (Scheme 10).⁵⁸ In fact, spiropyrans can undergo structural isomerisation under a number of different stimuli including light, temperature, redox potentials, presence of metal ions and mechanical stress, and the vastly different polarity of the two isomers can be used to refine solvation and chelation properties.⁵⁹



Scheme 10: Light induced photoisomerisation of a spiropyran derivative.

In 1971 Erlanger *et al.* synthesised two photoswitchable activators of acetylcholine receptors (AChRs), having previously demonstrated the use of azobenzenes in regulating the activities of chymotrypsin and acetylcholinesterase enzymes. BisQ **66**, synthesised in two steps from 1,2-di-*p*-tolylidiazene (Scheme 11), has two quaternary

methyl ammonium salts, which block the receptor's binding site. It was found that a *trans*-BisQ is over 500-fold more potent than BisQ in a majority *cis*- photostationary state. In addition, following reduction with dithiothreitol (DTT), the receptor binds covalently to the second antagonist, QBr **67**, and to some extent still confers photoswitchable activity to the receptor (Scheme 11).⁶⁰



Scheme 11: Synthesis and of non-tethered BisQ **66** and tethered QBr **67** photoswitchable ligands to the acetylcholine receptor.

The photo control of ion channels in particular was substantially extended by Trauner and colleagues during the 2000s.⁵⁶ They developed maleimide-azobenzene-glutamate (MAG) compounds, for example **68**, which were able to demonstrate receptor conjugation and light activation of an ionotropic glutamate receptor (iGluR6), itself mutated to include a strategically placed single cysteine residue (Figure 22).

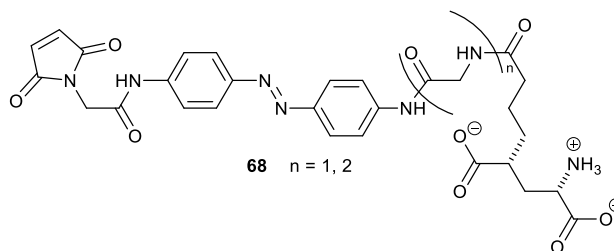


Figure 22: Example of MAG photoswitch **68** for an AChR.

Furthermore, Trauner *et al.* built a range of photoswitchable tethered ligands, which used the affinity and selectivity of the ligand to accelerate covalent attachment, this time onto native nucleophilic residues near the binding site. A variety of electrophilic moieties were used in the investigation of wild-type Shaker channels expressed in HEK293 cells.⁶¹ Of these, acrylamide **69**, chloroacetamide **70** and epoxide **71** imparted photosensitivity to the endogenous channels. In cultured hippocampal neurons, acrylamide **69** and chloroacetamide **70** were again successful, essentially yielding a photoswitchable ion channel (Figure 23).

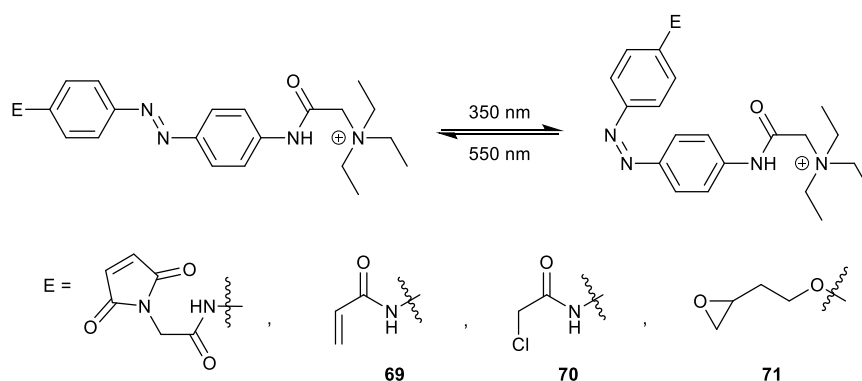
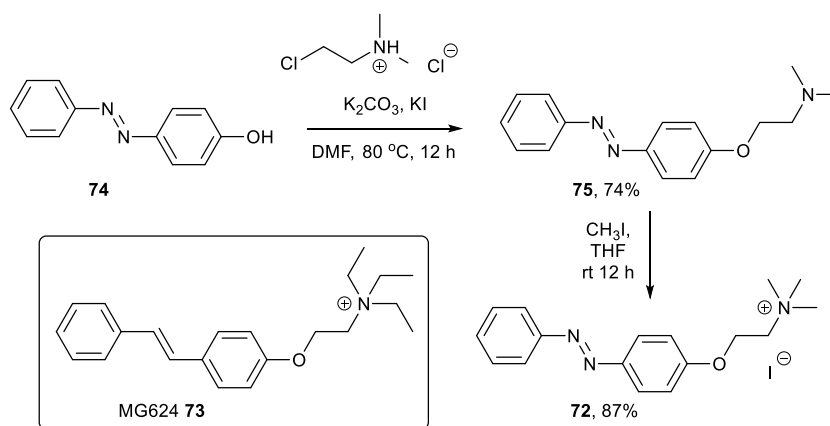


Figure 23: Photosensitive affinity ligands for endogenous K⁺ ion channels.

More recently, the same group have enabled optical control of $\alpha 7$ nicotinic acetylcholine receptors (nAChRs) with a freely diffusible ligand. AzoCholine **72** was similar to BisQ **66** and resembles $\alpha 7$ nAChR antagonist MG624 **73**.⁶² 2-Chloro-*N,N*-dimethylethylamine hydrochloride underwent nucleophilic substitution with 4-hydroxyazobenzene **74** to form 4-(dimethylaminoethyl)oxyazobenzene **75**, which then underwent quaternisation with iodomethane to give AzoCholine **72** in two steps and 64% overall yield (Scheme 12).

Scheme 12: Synthesis of AzoCholine **72**.

Upon the comparison of AzoCholine **72** with BisQ **66**, it was found that, whilst AzoCholine **72** was a potent agonist in its *trans* state and could be used as a photoswitchable ligand on a chimeric model of neuronal $\alpha 7$ nAChRs in HEK293T cells, BisQ **66** showed no activation. However, when subunits for muscle nAChRs were expressed in these cells, BisQ **66** proved to be a photoswitchable agonist where AzoCholine **72** did not. Upon application of AzoCholine **72**, extracellular electrophysiology of mouse hippocampal slices showed that activity of the receptors could be modulated by alternating between 360 and 460 nm wavelengths of light.

1.11 Photoswitchable ligands and GABA_A Receptors

Alongside success with neuronal voltage-gated potassium ion channels and nicotinic acetylcholine receptors, Trauner *et al.* also worked on developing photoswitchable ligands for GABA_A receptors. Propofol **22**, an allosteric modulator to the GABA receptor, is known to tolerate modification at the *para*- position of the phenol, and sixteen azo-propofols were designed and synthesised. The most promising of these, the *para*-amino compound **74**, was found to have the most favourable characteristics for a photochromic potentiator of GABA_A receptors (Figure 24).⁶³ It has a red-shifted absorption spectrum, with a majority *cis* photostationary state under 404 nm light. This

compound also quickly reverts thermally to the *trans* isomer once the light is switched off. Application of azo-propofol **74** alongside GABA to *Xenopus* oocytes resulted in an increased GABA response through positive allosteric modulation. Irradiation using 390-450 nm light during this time prevented this potentiation, which then returned when the light was turned off. This photoswitching ability was also shown in $\alpha 1\beta 2\gamma 2$ GABA_A receptors expressed in HEK cells. The use of this compound as a light-dependent anaesthetic was then investigated by looking at righting reflexes in tadpoles, which was significantly potentiated in the presence of photoswitchable azo-propofol **74**.

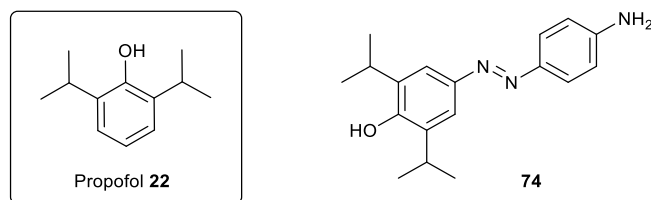


Figure 24: Photoswitchable analogue of allosteric modulator for GABA_A receptors.

In the same year Pepperberg *et al.* made a propofol analogue **75** for photoregulation of GABA_A receptors (Figure 25).⁶⁴ The *trans* isomer of this compound potentiates the GABA response and, at high concentrations, directly activates the receptor. The *cis* isomer produces little receptor potentiation both in $\alpha 1\beta 2\gamma 2$ GABA_A receptors expressed in *Xenopus laevis* oocytes and in native GABA_A receptors in retinal ganglion cells.

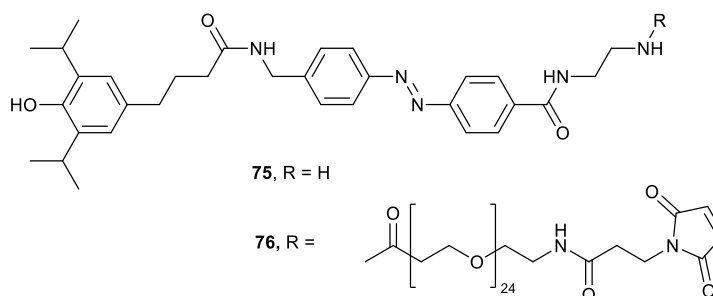
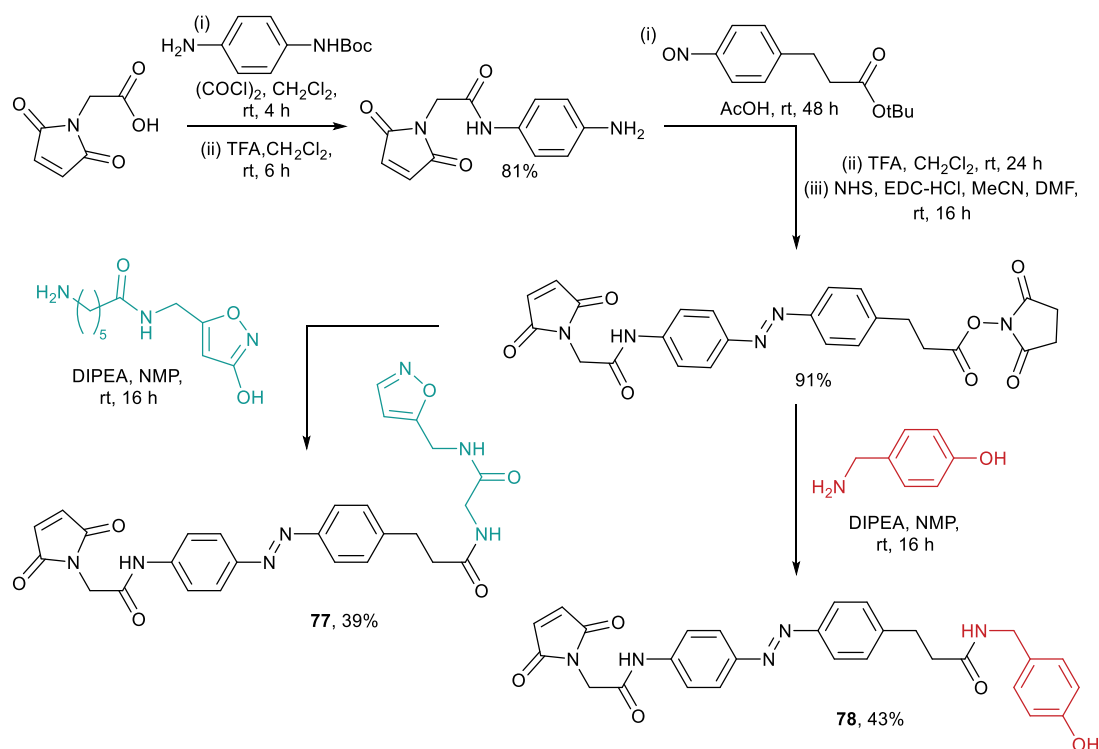


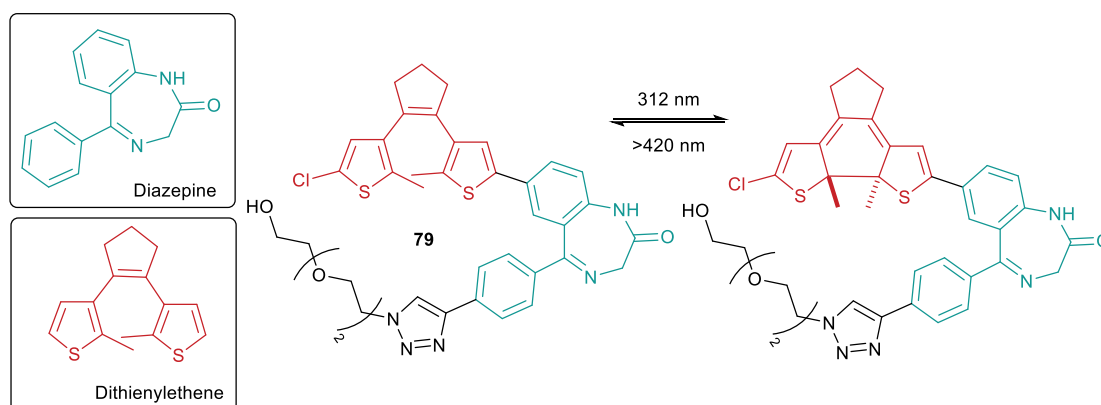
Figure 25: Tethered **75** and non-tethered photoswitchable ligand **76** for GABA_A receptors.

Further to this, a tethered analogue **76** was synthesised, which incorporated a maleimide-terminated PEG linker, and was tested on oocytes expressing $\alpha 1\beta 2\gamma 2$ GABA_A receptors which had a cysteine substituted into the 79-position of the γ subunit. This cysteine covalently anchored the ligand to the receptor. In the presence of GABA, and with picrotoxin, the tethered ligand also showed analogous potentiation and depotentiation of the receptors controlled by UV and visible light irradiation.

Another optogenetic strategy towards engineering a light-regulated GABA_A receptor was recently developed by Lin *et al.*, and involved the synthesis initially of a photoswitchable tethered ligand **77**, comprising a maleimide, azobenzene and muscimol moiety and synthesised in three steps from maleimidoacetic acid in 29% yield (Scheme 13).⁶⁵ Despite muscimol **2** being an agonist for the GABA_A receptor, compound **77** acted as a photoswitchable antagonist, and replacement of the muscimol moiety with a hydroxybenzylamine group **78** in fact increased the distinction between the *cis* and *trans* isomers in terms of inhibition. This inhibition was measured in $\alpha 1^{T125C}\beta 2\gamma 2S$ receptors in HEK293T cells, as well as in cultured hippocampal neurons, showing direct photocontrol and the formation of light regulated GABA_A receptors.

Scheme 13: Synthesis of tethered photoswitchable ligands for the GABA_A receptor.

A recent dissertation from the Krönig group describes the synthesis of a water soluble photoswitchable benzodiazepine derivative **79**, which utilises the photoisomerisation of dithienylethenes. Dithienylethene **79**, despite its limited use as a photoswitchable allosteric modulator for GABA_A receptors in cells, is a further sign that optical control of receptors continues to interest and excite the scientific community.⁶⁶

Figure 26: Water soluble photoswitchable benzodiazepine ligands for the GABA_A receptor.

It was hypothesised that a non-tethered photoswitchable antagonist for the GABA_A receptor could be designed and, through a short burst of UV or visible light, produce reversible antagonism of the receptors on cells. A compound of this type could give spatial and temporal control of receptors, giving valuable information on the effect of antagonism in different areas of a neuron.

1.12 Thesis aims

Light is an important tool when it comes to orthogonal control of biological systems. On systems which are not inherently light sensitive, this requires the use of light-activatable compounds. This thesis describes the organic synthesis of different light-activatable antagonists for the GABA_A receptor. These include a photoaffinity probe, which would direct the attachment of a tracking device, in this case a quantum dot, to the receptors in order to help understand their movement at different locations on the neuronal membrane. The synthesis of a second photoactivatable antagonist, was designed so that once covalently bound to the receptor, UV light would release the binding moiety, leaving a silently-tagged receptor. The tracking of this would provide a comparison between the movement of a blocked and un-blocked receptor. A third antagonist, which could change its potency towards the receptor upon application of different wavelengths of light, would also be synthesised and shown to be a powerful tool in locating GABA_A receptors as well as in spatial and temporal control of neuronal inhibition.

Chapter 2

Photoaffinity antagonists for the GABA_A receptor

2.1 Synthesis of a photoaffinity labelled antagonist based on gabazine

A photoaffinity labelled antagonist has two main components: a binding moiety and a photoactive group. Previous work in the Baker and Smart groups has shown highly promising biological activity of photoaffinity labelled antagonist **39**, based on gabazine **4**. To further explore the biological applications of this analogue, and to carry out biological testing on GABA_A receptors in a primary neuronal culture, the first goal of this project was to scale up the synthesis of **39** to obtain sufficient material (Figure 27).

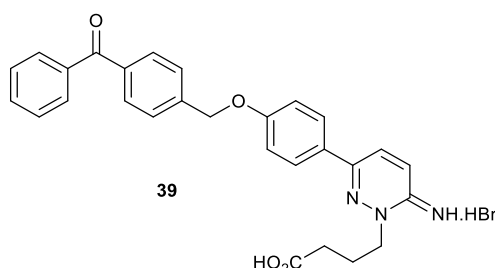
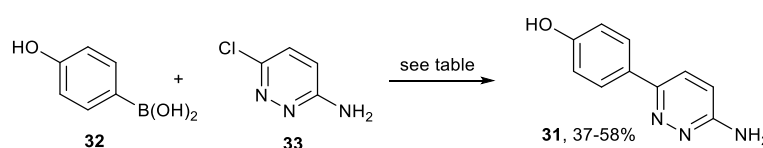


Figure 27: Photoaffinity labelled antagonist for the GABA_A receptor **39**.

Firstly, 3-arylpyridazine **31** was synthesised via a Suzuki-type palladium coupling reaction between 4-hydroxyphenylboronic acid **32** and 3-amino-6-chloropyridazine **33**. After initial reactions using the previously reported microwave irradiation³⁰ gave the product **31** in 58% yield, it became apparent that it would be useful if larger scale reactions were not hindered by the small scale limit of the microwave. Various reaction conditions were then attempted.^{67,68,69} Attempts to increase the product formation by using a more reactive palladium (0) species, Pd(PPh₃)₄, were unsuccessful, with no product being detected by TLC, potentially due to rapid

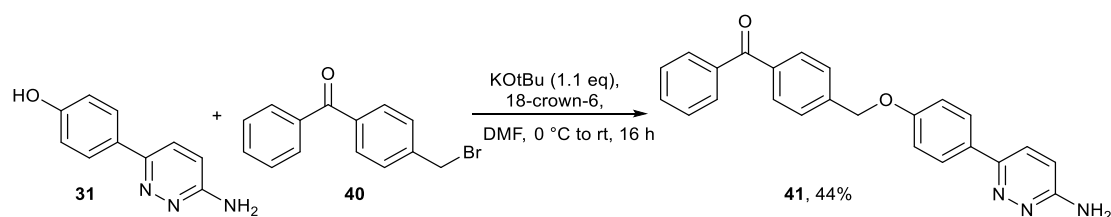
oxidation of the catalyst before the reaction. Another palladium (0) catalyst, Pd₂(dba)₃ along with tributylphosphine ligand, gave only slightly more success, with the low yield of 37% partially ascribed to degradation the oxygen-sensitive phosphine ligand. It was found that the optimal conditions involved the use of Pd(PPh₃)₂Cl₂ catalyst, with aqueous Na₂CO₃ in 1,4-dioxane. Though none of the yields were excellent, they enabled reaction to be performed on a gram scale in 56% yield and on a ten gram scale in 47% yield.



Palladium source	Reaction conditions	Yield
Pd(PPh ₃) ₂ Cl ₂ (5 mol%)	K ₂ CO ₃ , MeCN:H ₂ O (1:1), μW 120 °C, 10 min	58%
Pd(PPh ₃) ₄ (5 mol%)	2M aq Na ₂ CO ₃ (2.2 eq), PhMe: EtOH (10:1), 82 °C, 42 h	nd
Pd ₂ (dba) ₃ (2 mol%), tBu ₃ P (4 mol%)	K ₂ CO ₃ (2.0 eq), 1,4-dioxane, 101 °C, 24 h	37%
Pd(PPh ₃) ₂ Cl ₂ (5 mol%)	1M aq Na ₂ CO ₃ (3.0 eq), 1,4-dioxane, 101 °C, 16 h	56%
Pd(PPh ₃) ₂ Cl ₂ (5 mol%)	1M aq K ₂ CO ₃ (3.0 eq), 1,4-dioxane, 101 °C, 16 h	53%

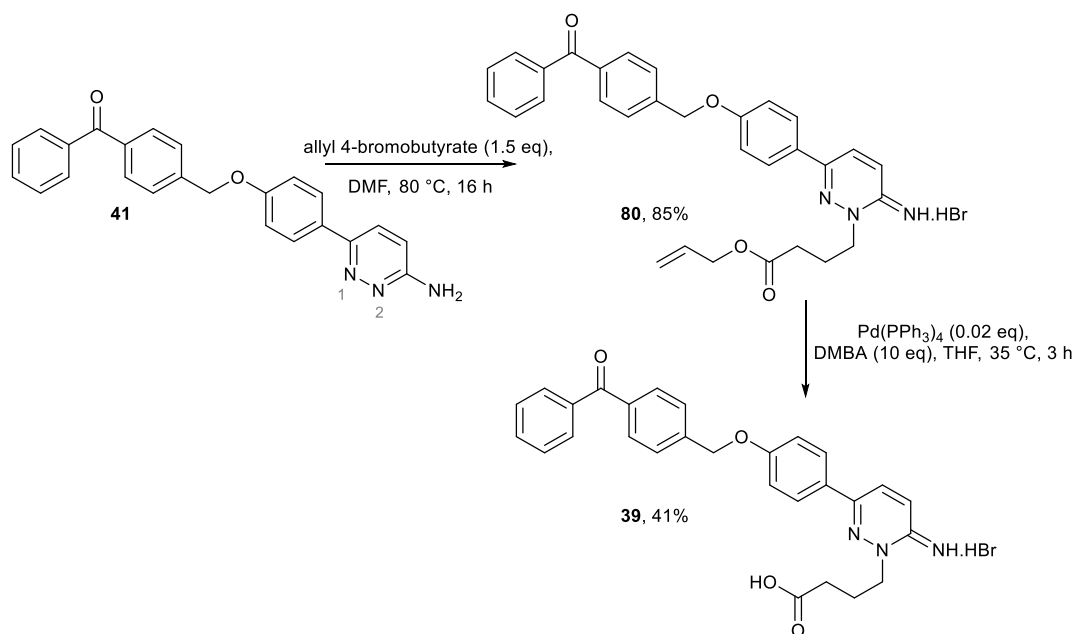
Table 1: Optimisation of reaction conditions in the formation of **31**. nd: not detected.

Benzophenone derivative **41** was then synthesised in a 44% yield via deprotonation of alcohol **31** at 0 °C with KO^tBu, followed by addition of commercially available bromomethyl benzophenone **40** (Scheme 14). The reaction was carried out in DMF, as the starting materials are relatively insoluble in other solvents.



Scheme 14: Ether synthesis reaction conditions.

The pyridazine nitrogen then underwent *N*-alkylation in the presence of allyl 4-bromobutyrate in DMF at 80 °C giving pyridazinyl ester **80** in 85% yield (Scheme 15). *N*-Alkylation occurs at the *N*(2) nitrogen when there is an aromatic group in the 6-position of the pyridazine skeleton, thought to be due to deactivation of the *N*(1) position, alongside steric factors.²⁹ Hydrolysis of allyl ester **80** was achieved upon reaction with Pd(PPh₃)₄ in the presence of the allyl group scavenger DMBA, yielding photoaffinity-labelled antagonist **39**, in an overall 9% yield over four steps (Scheme 15).

Scheme 15: *N*-Alkylation and subsequent allyl-ester hydrolysis reaction conditions.

This material **39** was then used by Dr Martin Mortensen in the Smart group, for further biological testing including its application onto live cerebellar granule cells. In a live

system it is possible for inhibitory signals to be regained after a time, as new, unblocked endogenous receptors are inserted into the membrane by the cell, or as unblocked receptors make their way through the membrane to the blocked site. However, by measuring the response of neuron, via whole-cell patch clamping, to 1 mM of applied GABA at different times after 20 s irradiation at 365 nm, it was shown that even after forty minutes, the time course of the experiment, GABA signals remained suppressed (Figure 28, (i)). In addition, recording spontaneous inhibitory post synaptic currents (sIPSCs) from a single cell, [spikes in current due to endogenous release of GABA from neighbouring pre-synaptic terminals] thirty minutes after irradiation in the presence of **39**, showed no discernible recovery of inhibitory signals, suggesting that the arrival of new receptors via membrane insertion must be a slow process. (Figure 28, (ii)).

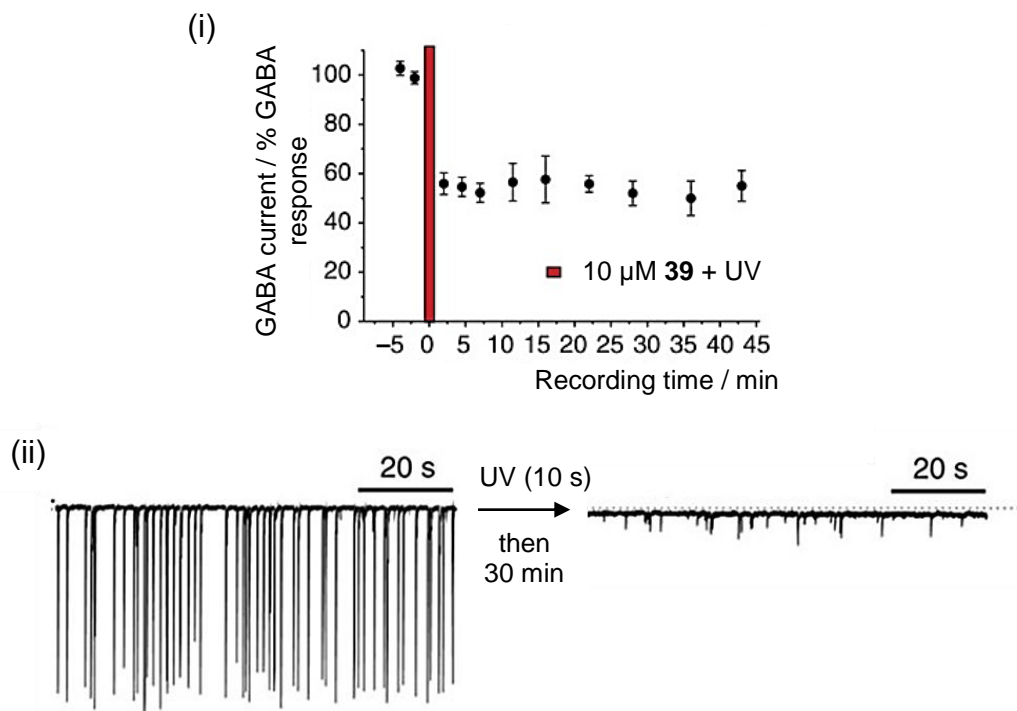


Figure 28: (i) Time profile for 1 mM GABA-activated currents before and after treatment with 10 μ M **39** and 20 s UV; (ii) sIPSCs from a single cerebellar granule cell 3 minutes before, and 29 minutes after treatment with **39** and UV.

2.2 Synthesis of a photoaffinity probe for quantum dot tracking of the GABA_A receptor

This section concerns the design and synthesis of a chemical tool which can photocrosslink to the receptor and is also able to relay information about the lateral movement of GABA_A receptors. The photocrosslinking, as before, would be directed by the binding of a gabazine core and facilitated by a benzophenone photoaffinity label. The incorporation of a biotin via a solubilising ethylene glycol linker would enable connection to a streptavidin-coated quantum dot (Figure 29). Once irreversibly bound to receptors on cells, the quantum dot movement can be recorded, showing the precise routes of these receptor-quantum dot constructs over time. The site of attachment for the linker on benzophenone was devised from computational docking studies, which suggested that, once in the binding site, there would be space in the 3-position for a straight linker segment.⁷⁰

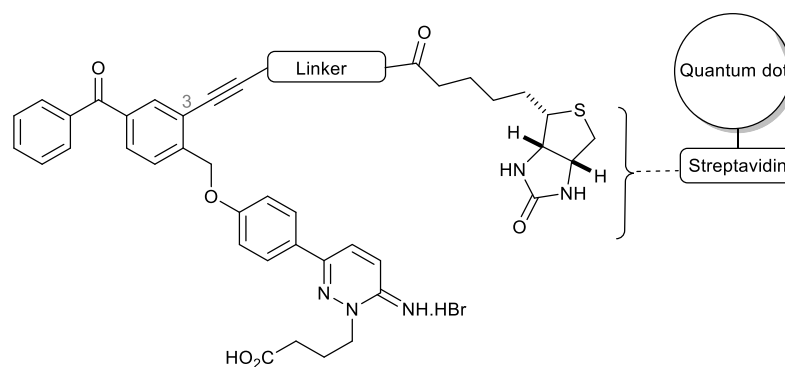
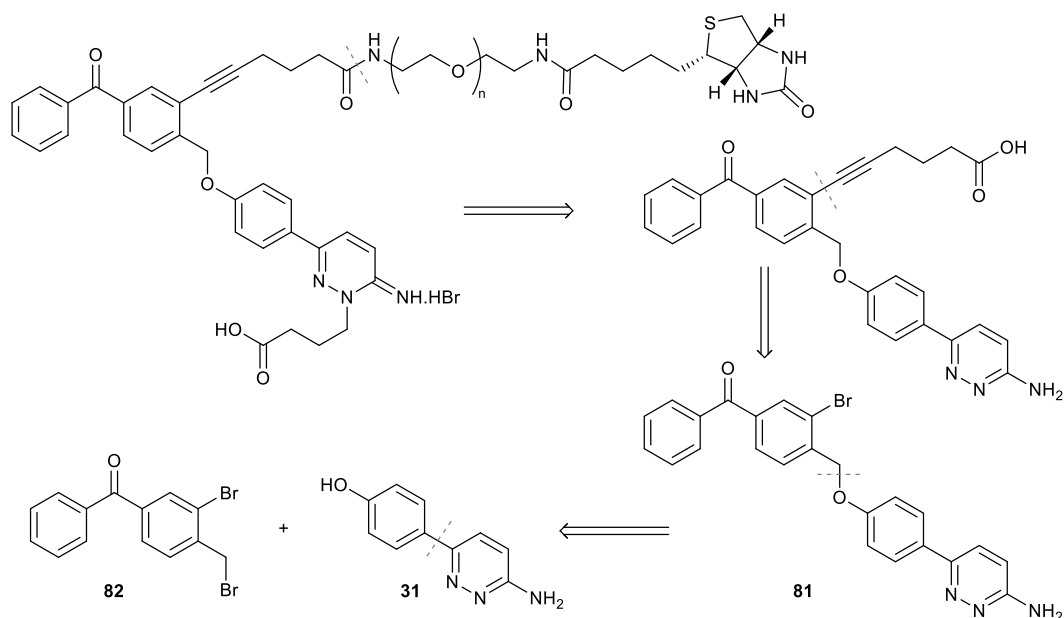


Figure 29: Photoaffinity labelled probe for the GABA_A Receptor.

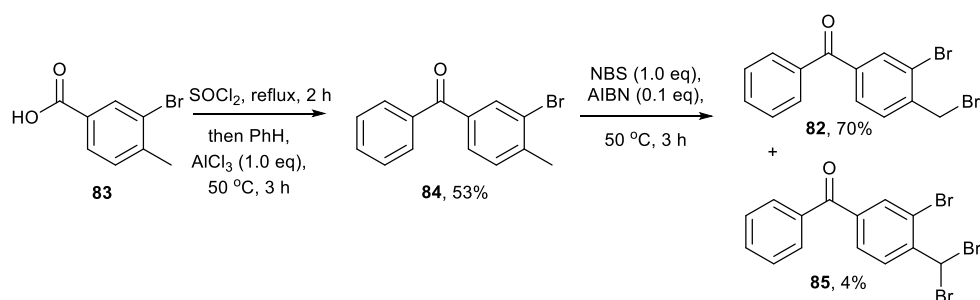
In a retrosynthetic analysis, the biotin and linker fragments were installed via amide bond couplings, and a Sonogashira-type reaction installed a linear alkyne section in the most tolerated position (Scheme 16). The intermediate **81** was synthesised by the strategy similar to one described in Schemes 5 and 6, starting with 4-(6-aminopyridazin-3-yl)phenol **31** (Scheme 16). A previous, unoptimised attempt at this

route yielded insufficient material,²⁸ and in order to generate biological data and quantum dot tracking of receptors, an optimised route and scale up production of the probe was required.



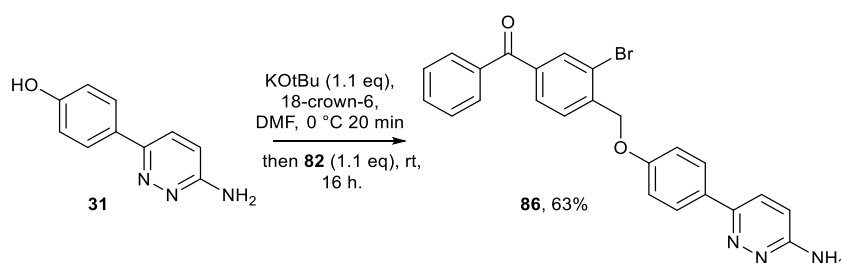
Scheme 16: Retrosynthetic analysis of photoaffinity labelled probe for the GABA_A receptor.

Benzylic bromide **82** was synthesised in two steps from 3-bromo-4-methylbenzoic acid **83**. Acid **83** was refluxed in thionyl chloride to give the acid chloride intermediate, and then heated in benzene with AlCl₃ to yield (3-bromo-4-methylphenyl)(phenyl)methanone **84** in 53% yield. Upon treatment with *N*-bromosuccinimide in the presence of AIBN, mono bromination at the benzylic position to give **82** was accomplished in 70% yield. In this reaction the doubly brominated species **85** was also isolated in 4% yield, whilst 16% of starting material **84** was returned (Scheme 17).



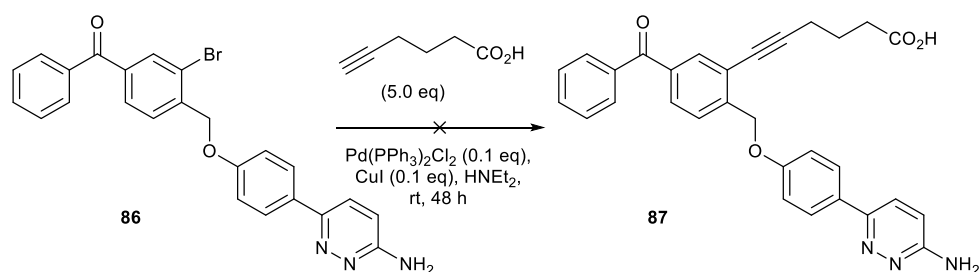
Scheme 17: Construction of benzophenone fragment.

The displacement reaction was then accomplished upon treatment of arylpyridazine **31** with KO^tBu and 18-crown-6, followed by addition of bromomethylbenzophenone **82**. This gave benzophenone derivative **86** in 63% yield (Scheme 18).



Scheme 18: Introduction of pyridazine core.

The next step in the synthesis was the Sonogashira-type coupling⁷¹ between arylbromide **86** and 5-hexynoic acid to give acid **87**. The Songogashira conditions shown in Scheme 19 had previously been applied in the group, but only with limited success.²⁸ Application of these conditions to bromide **86** proved unsuccessful so further optimisation was undertaken.

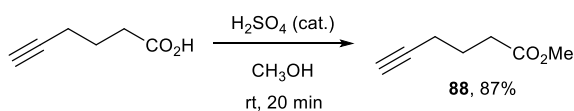


Scheme 19: Unsuccessful Sonogashira reaction conditions.

It was thought that a copper catalysed alkyne-alkyne homocoupling could be competing in this reaction, as the carboxylic acid could not be recovered. Accordingly all solvent was degassed with argon and the hexynoic acid was added to the reaction mixture slowly.⁷² However, no desired product, nor homocoupled product were detected.

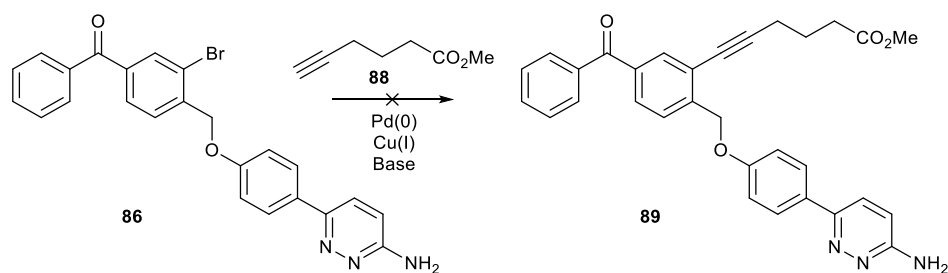
Sonogashira reaction conditions in the literature are quite varied, and the reaction is very substrate dependant. The main components include a palladium (0) source, which is either added to the reaction or formed *in situ*. A copper source and a base are required to activate the alkyne to undergo carbometallation onto the palladium. Varying sources of palladium, including Pd(PPh₃)₂Cl₂ and Pd(PhCN)₂Cl₂, were used alongside amine bases, for example diethylamine and DIPEA, and CuI, at room temperature, according to literature conditions but with no success.^{73,74} An attempt using Pd/C and CuI with Cs₂CO₃ at 80 °C was also unsuccessful.

One problem with the reaction could be the presence of the carboxylate anion formed by salt formation of 5-hexynoic acid and the base, as there are few reported cases of Sonogashira reactions involving a carboxylic acid.⁷⁵ Accordingly 5-hexynoic acid methyl ester **88** was synthesised from 5-hexynoic acid in 87% yield (Scheme 20).



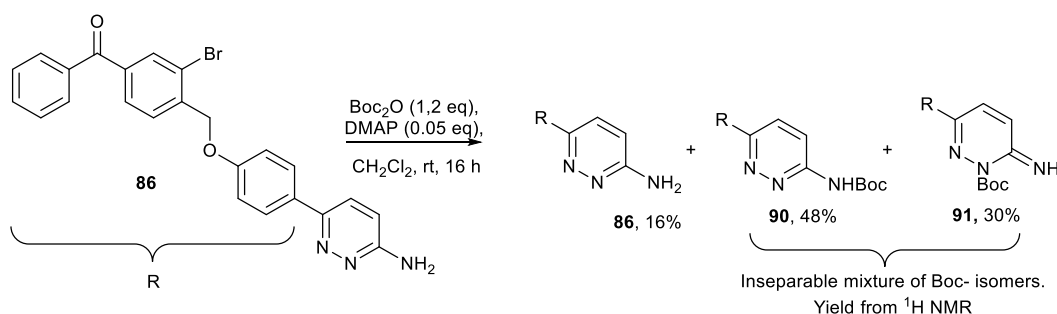
Scheme 20: Hexynoic acid methyl ester formation.

However, after subsequent application of 5-hexynoic acid methyl ester **88** to various reaction conditions, including with Pd(PPh₃)₂Cl₂ and Pd(PhCN)₂Cl₂ catalyst at room temperature with CuI and a requisite base, no desired product **89** was detected (Scheme 21).



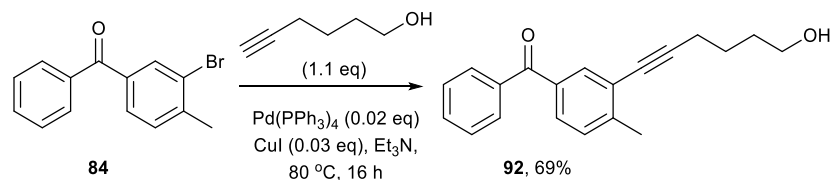
Scheme 21: Unsuccessful Sonogashira reaction conditions.

A second reason for the failure of the required Sonogashira reaction could have been the co-ordination of the amine group in **86** to the palladium catalyst. To avoid this, the synthesis of a Boc-protected analogue of **86** was attempted (Scheme 22). However, unreacted starting material was isolated in 16% yield along with an inseparable 1.6:1 mixture of Boc-isomers, which was not taken on to the Sonogashira reaction. These Boc-isomers were tentatively assigned via ¹H NMR spectroscopy and known regioisomer chemical shifts to be **90** and **91**, in 48 and 30% yields respectively.



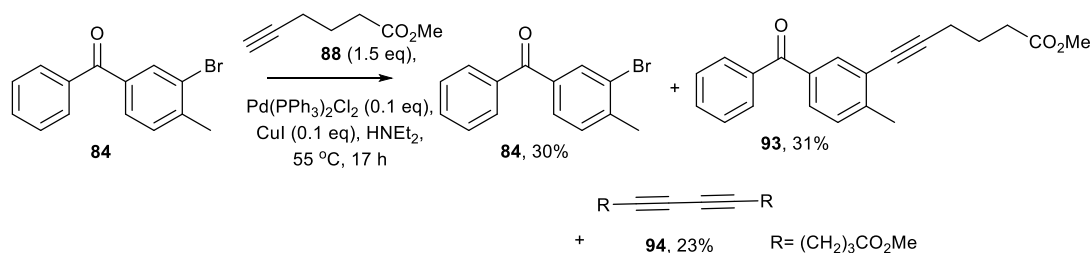
Scheme 22: Attempted Boc-protection of pyridazine.

As a model system, 5-hexyn-1-ol was reacted with benzophenone derivative **84** under literature conditions in order to pinpoint the reactivity problem.⁷⁶ The reagents were treated with Pd(PPh₃)₄ and CuI at a lower catalyst loading in triethylamine, but at a higher temperature of 80 °C for 16 h. Encouragingly the desired product **92** in this reaction was isolated in 69% yield (Scheme 23).



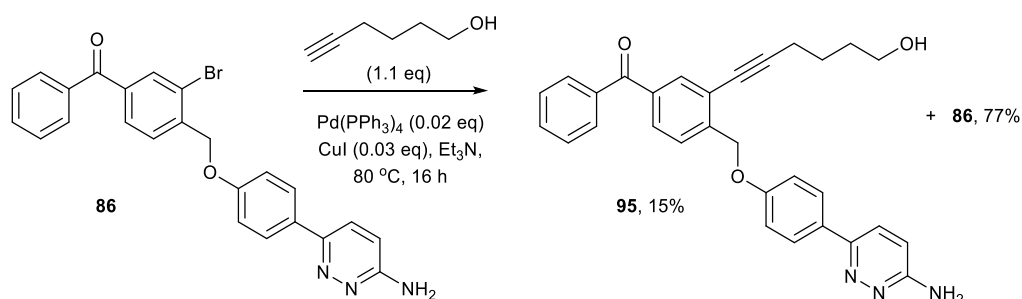
Scheme 23: Sonogashira reaction conditions - increased temperature.

Concurrently, a reaction between model benzophenone **84** with 5-hexynoic acid methyl ester **88** with $\text{Pd}(\text{PPh}_3)_2\text{Cl}_2$, CuI and diethylamine at 55°C yielded the product **93** in 31% isolated yield (Scheme 24). In this case returned starting material **84** was isolated in 30% yield, whilst the homocoupled product **94** was isolated in 23% yield with respect to the ester starting material, despite best-effort inert conditions.



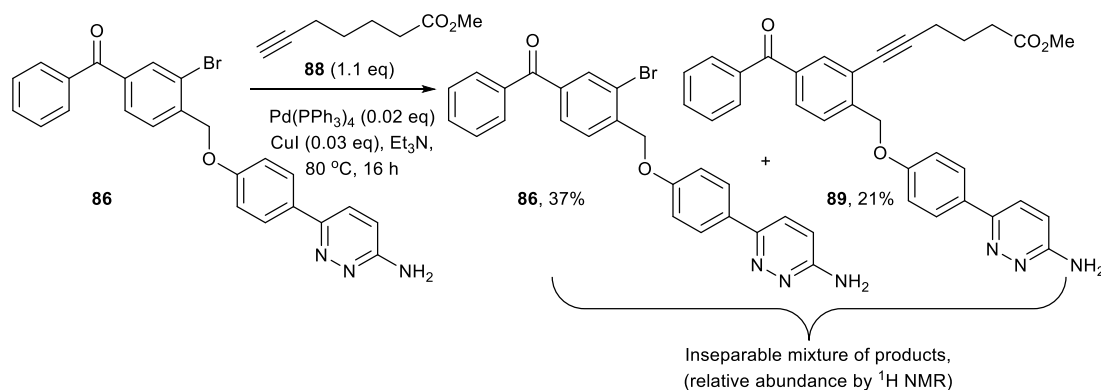
Scheme 24: Sonogashira reaction conditions - increased temperature.

Application of 5-hexyn-1-ol reactants to the desired pyridazine arylbromide substrate **86** yielded the desired alcohol product **95** in 15% yield, whilst 77% of the starting material **86** was returned (Scheme 25). It was noted that alcohol **95** could still be useful in the synthetic pathway as it could form the amide linker after oxidation.



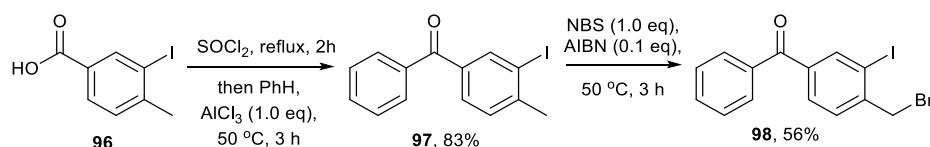
Scheme 25: Sonogashira reaction conditions.

Unfortunately, in the reaction between **86** and 5-hexynoic methyl ester **88**, the product was detected by ¹H NMR spectroscopy along with starting material **86** but the product was not isolable (Scheme 26).



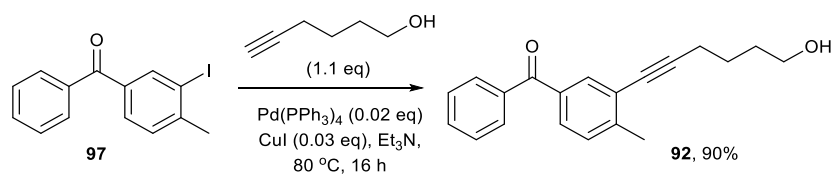
Scheme 26: Sonogashira reaction conditions.

It was thought that the failure of this reaction was due mainly to slow conversion and the competing homocoupling reaction. As such it was envisaged that replacement of the bromide with an iodide would aid the reaction. It is well reported that the rate-limiting step of a Sonogashira reaction is the oxidative addition of palladium into the carbon–halogen bond.⁷⁷ This goes some way to explain the reactivity of the *sp*² species towards the Sonogashira reaction as the relative reactivities are as follows: aryl iodide > aryl triflate ≥ aryl bromide >> aryl chloride, i.e. inversely to the strength of the carbon–halogen bond.⁷⁷ With this in mind, an iodo analogue of **84** was synthesised in two steps in 46% overall yield following previous reaction conditions (Scheme 25). 3-Iodo-4-methylbenzoic acid **96** was reacted with thionyl chloride and the resulting acid chloride was heated in benzene in the presence of AlCl₃ to give analogue **97**, which was brominated to give **98** in 46% overall yield (Scheme 27). A small percentage of de-iodination (3%) was detected when the reagent was heated in the presence of AlCl₃, which is in accordance with literature precedent.⁷⁸



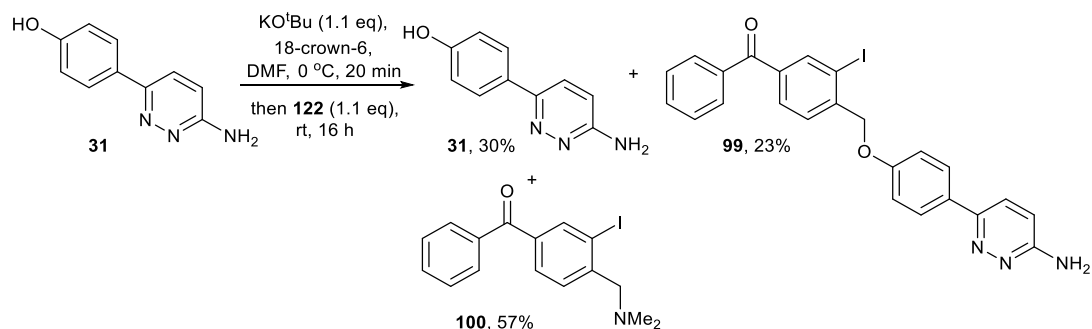
Scheme 27: Iodine analogue of benzophenone fragment.

For a direct comparison between the reactivity of aryl-iodide **97** and aryl-bromide **84**, iodide **97** was reacted with 5-hexyn-1-ol in the presence of Pd(PPh₃)₄, CuI and triethylamine to give alcohol **95** in 90% yield, encouragingly higher in yield than the bromo analogue {69%} (Scheme 28).



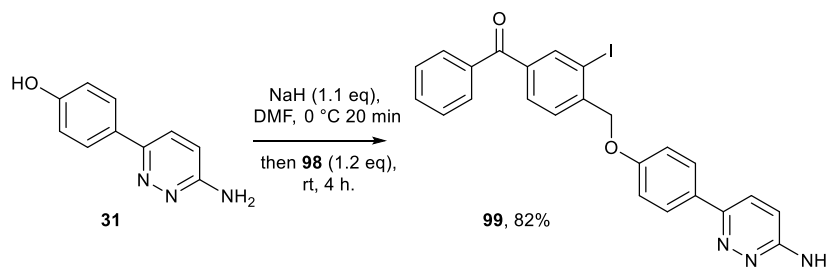
Scheme 28: Sonogashira reaction conditions.

The next step in the synthesis of the iodo analogue, the ether synthesis, was attempted between 6-arylpyridazine **31** and benzophenone derivative **98** using the previously reported reaction conditions {KO^tBu, 18-crown-6 and DMF}. This led to the synthesis of the required product **99** in 23% yield, but also to the formation of an amino-dimethyl derivative **100** in 57% yield, alongside 30% returned starting material **31** (Scheme 29). The side product **100** is formed through nucleophilic substitution by dimethylamine, a degradation product of DMF. In this case, however, freshly distilled DMF did not eliminate the formation of dimethylamino derivative **100**, which suggests that the presence of dimethylamine arises from interactions between KO^tBu and DMF.⁷⁹



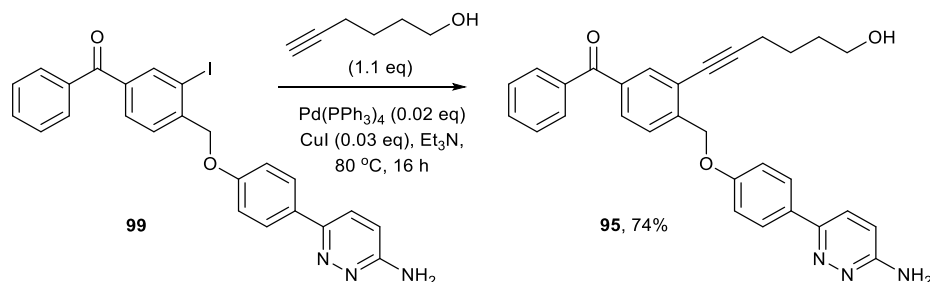
Scheme 29: Product distribution in the ether synthesis of iodo analogue.

The formation of this side product was eliminated with the use of NaH as the base, and **99** was formed in 82% yield (Scheme 30).



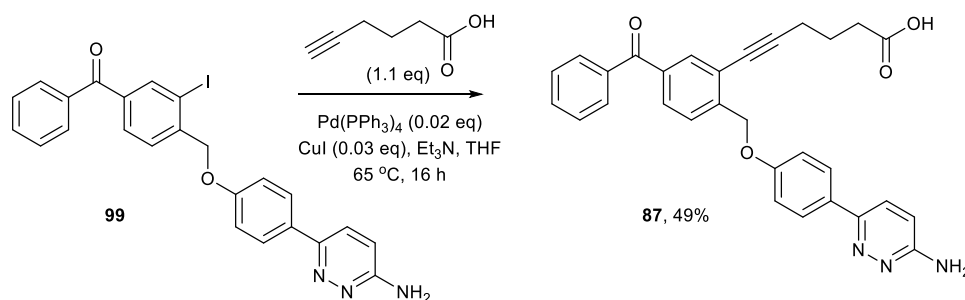
Scheme 30: Optimised ether synthesis reaction conditions.

With this in hand, a Sonogashira reaction was undertaken, following previous reaction conditions, between iodo analogue **99** and 5-hexyn-1-ol, yielding alcohol **95** in 74% yield (Scheme 31).



Scheme 31: Sonogashira reaction conditions.

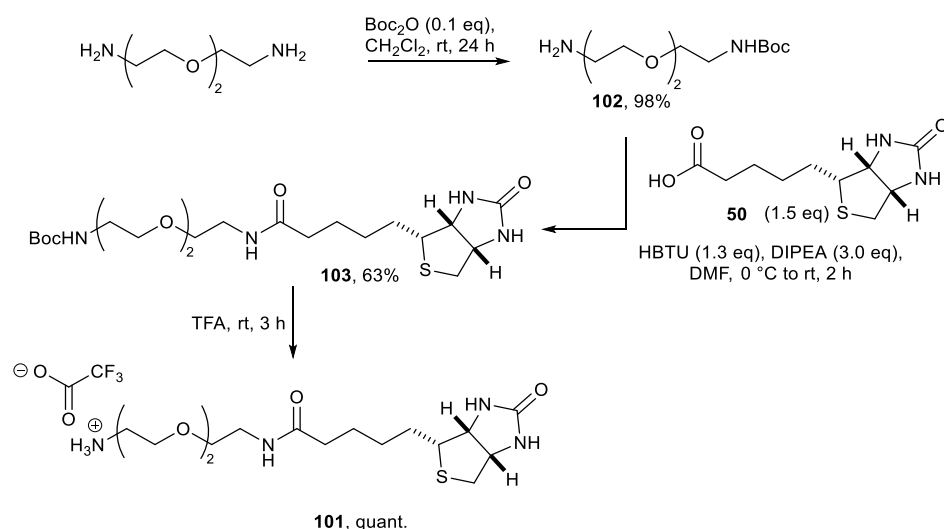
Given the great improvement in yield between the iodo analogue **99** and bromo analogue **86** {74% compared to 15%}, the Sonogashira reaction with 5-hexynoic acid was undertaken and yielded **87** in 49% yield as an insoluble white solid (Scheme 32).



Scheme 32: Successful Sonogashira reaction conditions.

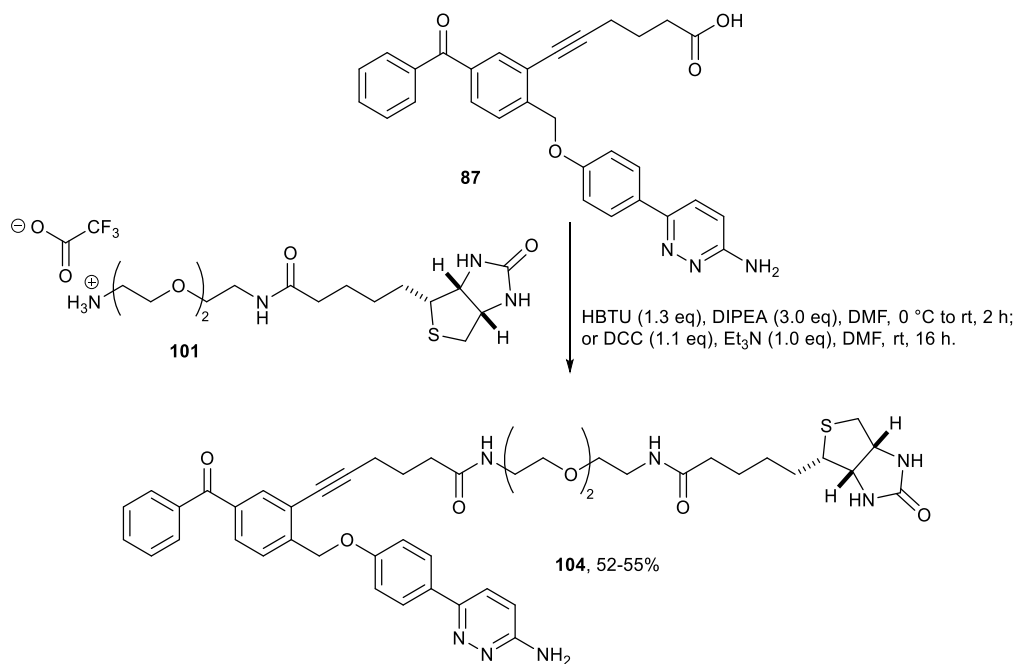
Acid **87** was insoluble in a wide range of organic solvents, including THF and DMSO, and as such, only a broad ¹H NMR spectrum was obtained. A tentative assignment was made, and after the compound's derivatisation in the next step of the synthesis, alongside mass spectrometry results, this assignment was confirmed. Its insolubility could be due to the crystallisation into a zwitterion after column chromatography.

Attention was then turned to the synthesis of the ethylene glycol tether **101**, initially of three units length, which would be connected to the photoaffinity labelled pyridazine **87**. The tether was synthesised in 3 steps in 62% overall yield following literature conditions.^{80,81} Commercially available 2,2'-(ethane-1,2-diylbis(oxy)) diethanamine was mono-Boc protected with 0.1 equivalent of Boc-anhydride to give **102** in 98% yield with respect to Boc-anhydride. Amine **102** was then reacted with D-biotin **50** in the presence of HBTU and DIPEA to give **103** in 63% yield. Boc-deprotection was accomplished upon addition of TFA, to give biotinyl-PEG amine **101** in quantitative yield (Scheme 33).



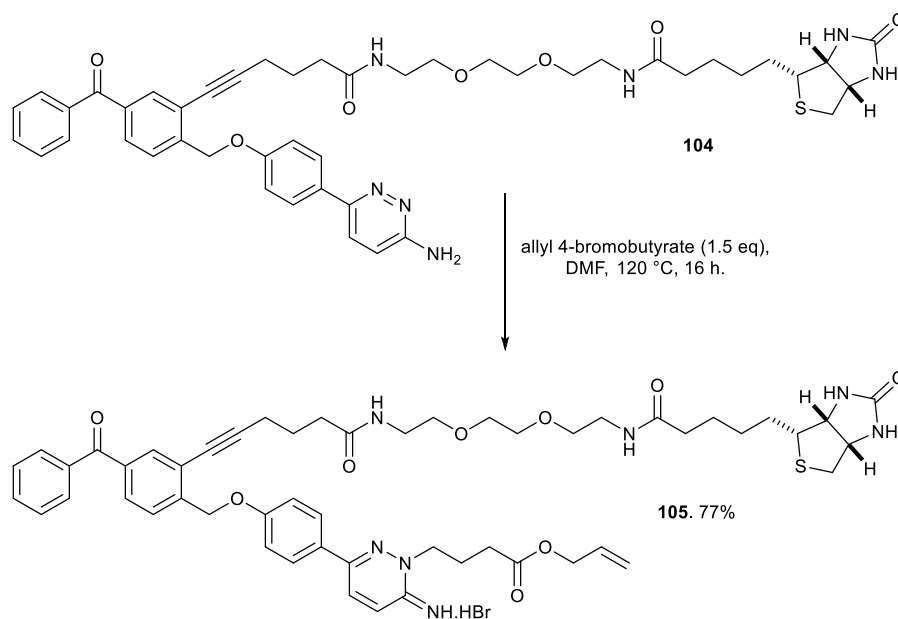
Scheme 33: Preparation of the biotin linker for incorporation into the probe structure.

The coupling between biotinylated amine **101** and Sonogashira product **87** was achieved using HBTU and DIPEA, and yielded **104** in 55% yield. Isolation of the pure product proved lengthy due to HBTU contamination, so the reaction was attempted with DCC and triethylamine which yielded **104** in a comparable 52% yield, but with a more straightforward purification (Scheme 34).



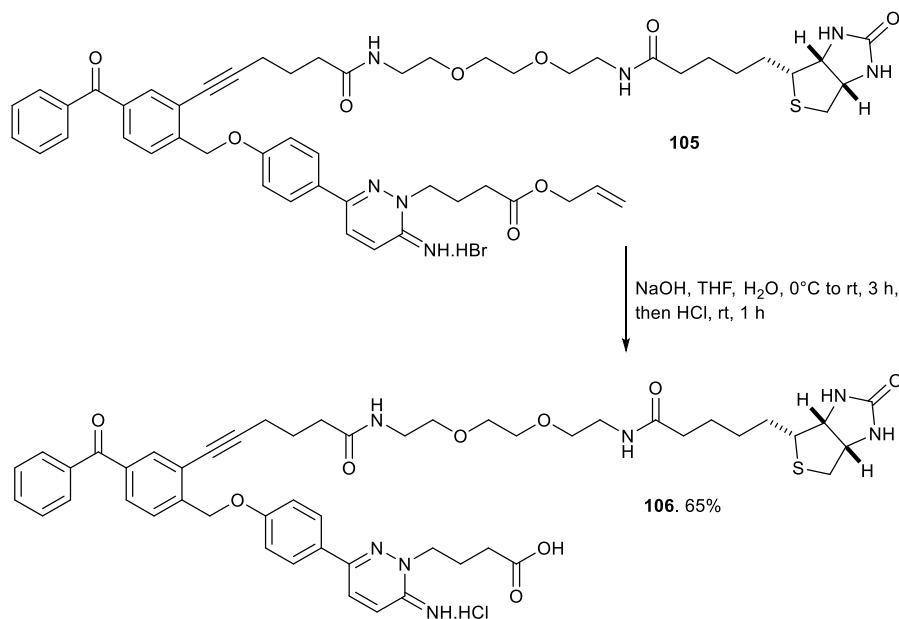
Scheme 34: Incorporation of the linker and biotin functionality.

The next stage in the synthesis was the alkylation of the pyridazine *N*(2) nitrogen with allyl 4-bromobutyrate, initially reacted in DMF at 50 °C for 5 h according to the previously reported protocol,³⁰ but this led only to a return of starting material. The reaction conditions were altered to 120 °C for 16 h, which yielded the *N*-alkylated product **105** in 77% yield (Scheme 35).



Scheme 35: *N*-Alkylation reaction conditions.

The final deprotection step was achieved via base-catalysed hydrolysis of the allyl ester group with sodium hydroxide, and yielded the target molecule **106** in 65% yield (Scheme 36).



Scheme 36: Allyl ester hydrolysis as the final step in the synthesis of photoaffinity labelled probe **109**.

This then completed the targeted synthesis of the photoaffinity labelled probe for the GABA_A receptor **106** from commercially available 4-hydroxyphenylboronic acid **32** and 3-amino-6-chloropyridazine **33** in an overall yield of 7%.

2.3 Quantum dot tracking of GABA_A receptors

The biological evaluation of gabazine probe **106** was then conducted by Dr Martin Mortensen in the Smart group. Firstly an IC₅₀ value was obtained from inhibition experiments in recombinant $\alpha 1\beta 2\gamma 2S$ GABA_A receptors expressed in HEK293 cells, which was measured as 1.49 μ M (Figure 30). Whilst this is less potent than previous, smaller analogues it still gave an acceptable activity for further experiments.

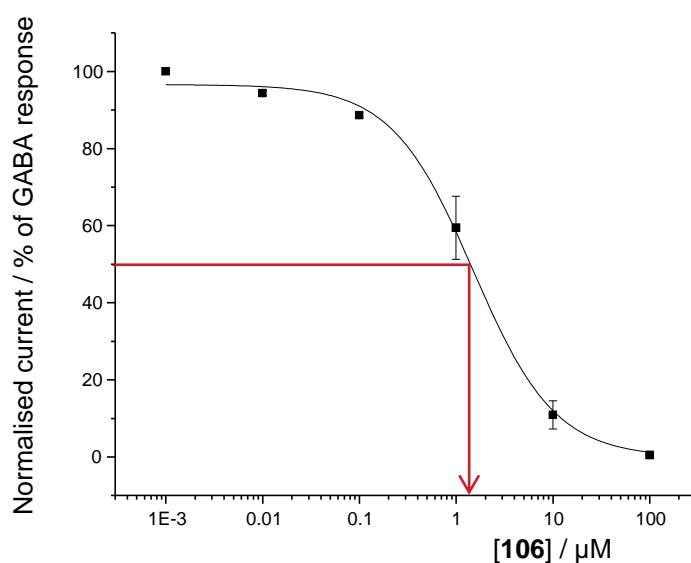


Figure 30: Dose response curve, showing the response of different concentrations of **106** relative to maximal GABA response, giving an IC₅₀ of 1.49 μM.

Secondly, the photolytic block of the probe was measured to assess the efficacy of the benzophenone photoaffinity label. Encouragingly a photolytic block of ~30% was seen as probe **106** underwent the irradiation protocol reported *vide supra* (Figure 31).

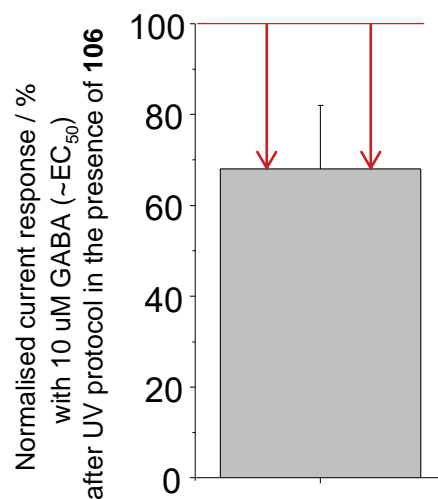


Figure 31: Photolytic block of biotinylated probe **106**.

With the knowledge that probe **106** was successfully antagonising GABA_A receptors, and that it was forming a covalent attachment with the receptor upon irradiation with UV light, experiments to track native GABA_A receptors in live neurons were then undertaken.

The quantum dot-streptavidin nanocrystals used in these experiments were purchased from Invitrogen Molecular Probes[®], which have a narrow maximum in their emission spectrum at 655 nm, independent of excitation wavelength. They are comprised of CdSe core which is coated in an additional semiconductor shell made from ZnS. This core-shell material is further coated with a polymer shell, which is covalently coupled to 5-10 streptavidin molecules per quantum dot (Figure 32).⁸²

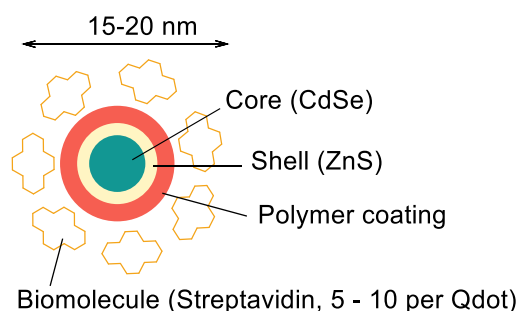


Figure 32: Schematic of a quantum dot-streptavidin conjugate used in these experiments.

The hippocampal cells used for these imaging experiments were prepared as a primary culture from rats. Live hippocampal cells, isolated via enzyme dissociation and trituration, were placed on a cover slip and grown in a monolayer containing astroglial cells, which provide support for the hippocampal cell development. Over ten days, dendrites grew out from the soma of the cells to make a synaptically connected network, similar to neuronal tissue.⁸³ For localisation purposes, some cells were transfected with green fluorescent protein (GFP) to visualise the network of dendrites belonging to any one of the transfected cells and allow identification after the cover slip was removed for washes and returned.

The cover slips containing the cells were loaded into a microscope sample holder to be imaged. The microscope set-up allowed the cells to be viewed through several light filters, allowing the transmission of defined wavelengths of light. These filters were used to visualise GFP at 488 nm, quantum dots at 655 nm, and the whole cells with white light (Figure 39). The set-up also contained a UV irradiation source, which could be directed onto regions of the cover slip.

After the cells were treated with the quantum dot-**106** conjugates and a section was irradiated, the whole cover slip was removed from the microscope and washed with Krebs's solution⁸⁴ to remove any non-covalently bound quantum dot-**106** constructs. The dish was then replaced on the microscope stage, and the region previously UV exposed was located using the particular shape of the GFP transfected neurons at 488 nm. Viewing this area through a 655 nm light filter showed the quantum dots which were still bound to the cells (Figure 33). The movement of these quantum dots was recorded for several seconds.

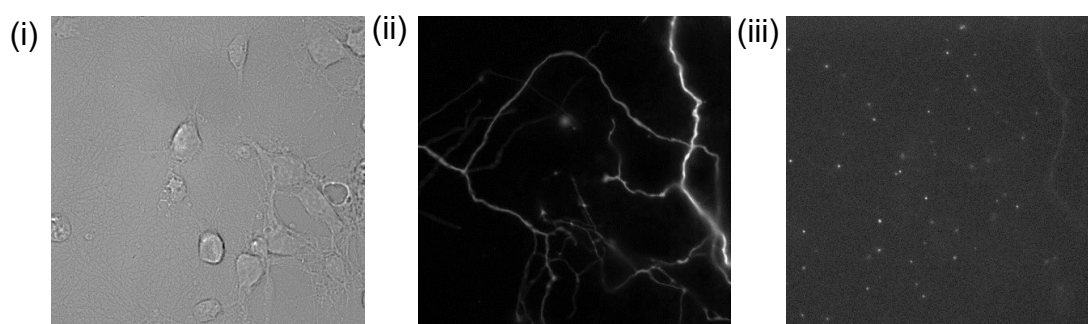


Figure 33: (i) Hippocampal cells seen under visible light; (ii) Cells seen with 488 nm light, highlighting the GFP used for recognition of particular cells on the slide; (iii) Cells seen with 655 nm light, showing the presence of quantum dots on GABA receptors at synapses. Each quantum dot could be filmed and followed.

Control experiments were conducted to ascertain the specificity of the quantum dot-**106** construct to GABA_A receptors, and the efficacy of the photoaffinity label in the presence of the quantum dot. In these experiments, it was shown that quantum dots

alone were washed away easily during our procedure. However, it was also discovered that quantum dot-106 constructs, despite not being irradiated, persisted even after washes, and this accounted for on average eight quantum dots per cell area (Figure 40).

Further experiments also showed no significant difference in the numbers of quantum dots bound to the cells, after washing, in the area of the cells directly under the beam of UV light, and those in surrounding areas, not directly exposed. This could potentially be due to the scattering of UV light over the entire dish (Figure 34).

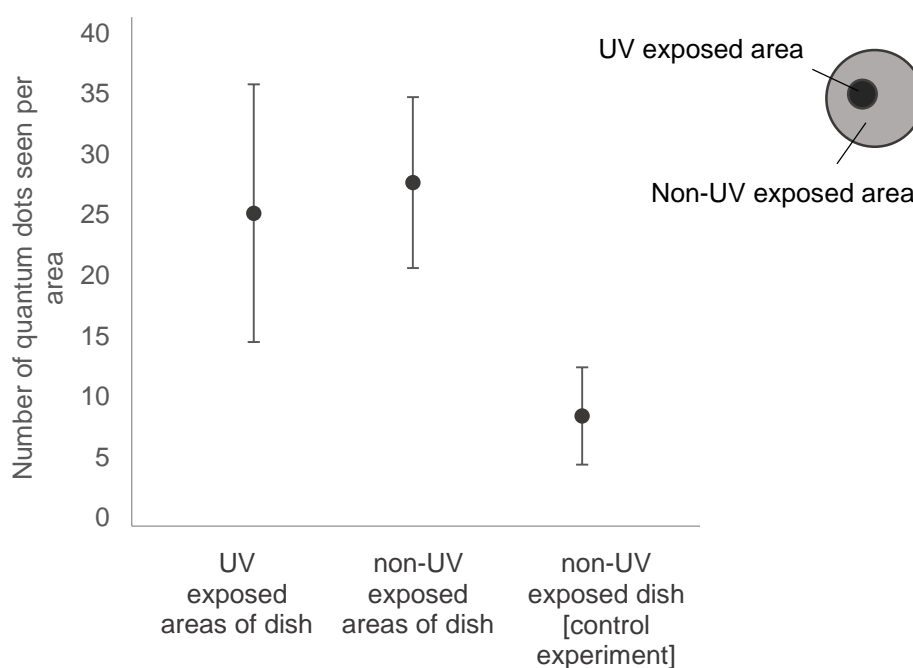


Figure 34: Numbers of quantum dots seen in control experiments; some quantum dots appeared strongly bound despite not being irradiated in the control experiment.

With confidence that a significant number of the quantum dots seen through the 655 nm filter were indeed covalently bound to GABA_A receptors, the recordings of quantum dot movement were analysed and their individual trajectories were plotted (Figure 35). These show a mixture of mobile and confined quantum dots, indicating whether the receptor is freely diffusing along the membrane, or whether it is confined by a synapse.

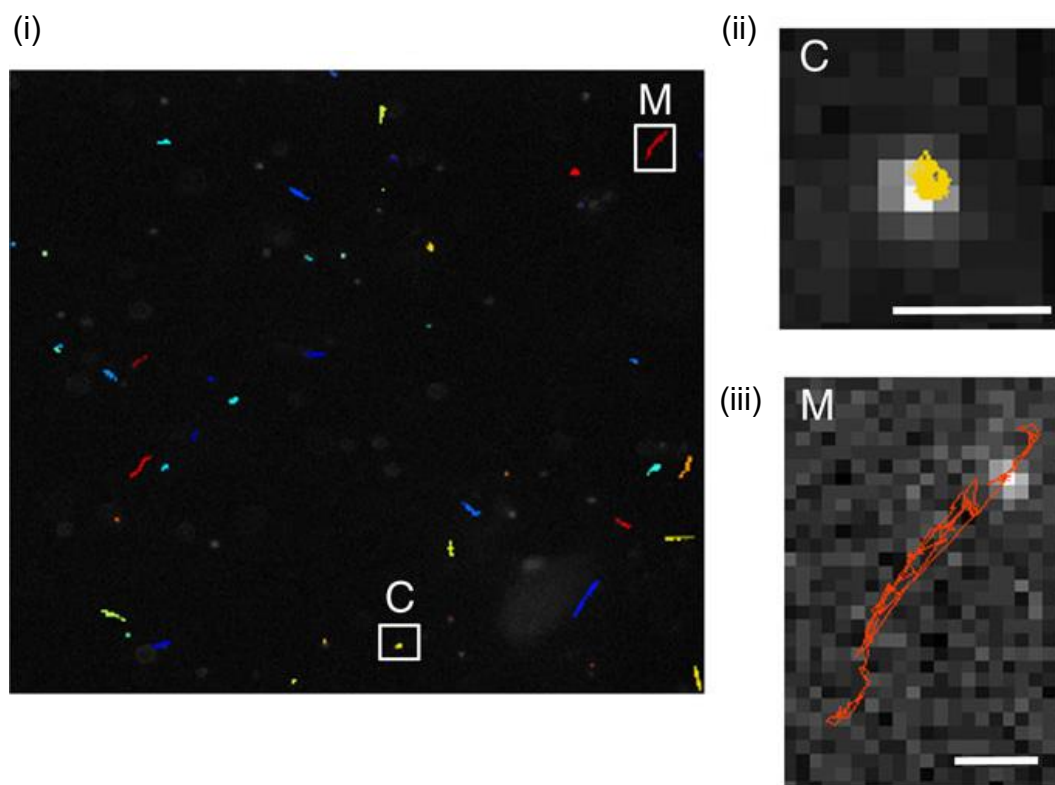
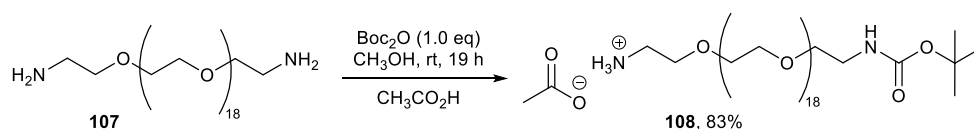


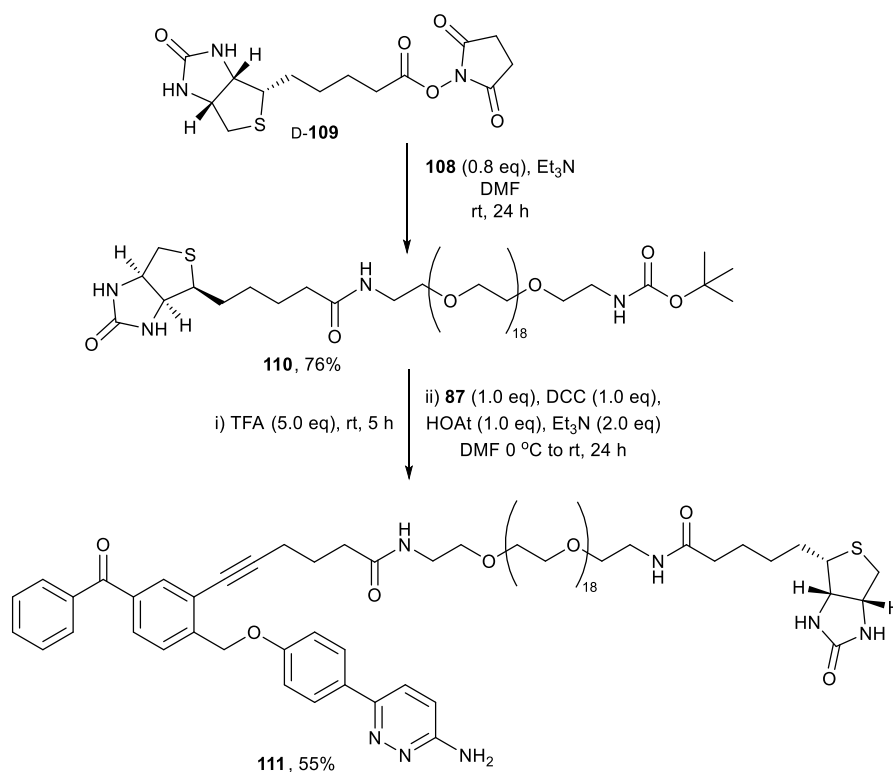
Figure 35: (i) Trajectories (coloured lines) of quantum dots photolinked to GABA_A receptors via probe **106**; Highlighted are trajectories of (ii) a mobile extrasynaptic receptor (M), and; (iii) a constrained synaptic receptor (C).

This work has shown the use of a photoaffinity labelled probe, conjugated with a quantum dot, to investigate the movement of native GABA_A receptors in a live system. They provided an excellent opportunity to study single native GABA_A receptors, although having some bound quantum dot-**106** conjugates present in the control experiment was not optimal. A second biotinylated compound with a longer ethylene glycol linker was designed to increase the distance between the quantum dot and the binding site. It was thought that this would allow the gabazine binding motif to be more flexible and bind more strongly to the receptor. If this occurred, the background presence of non-specific membrane-binding quantum dots would have less significance. The longer, 19 unit, oligo ethylene glycol (OEG) linker was prepared by mono-Boc protection of the commercially available diamine OEG **107** and stored as an acetic acid salt **108** (Scheme 37).



Scheme 37: Preparation of the longer PEG linker section.

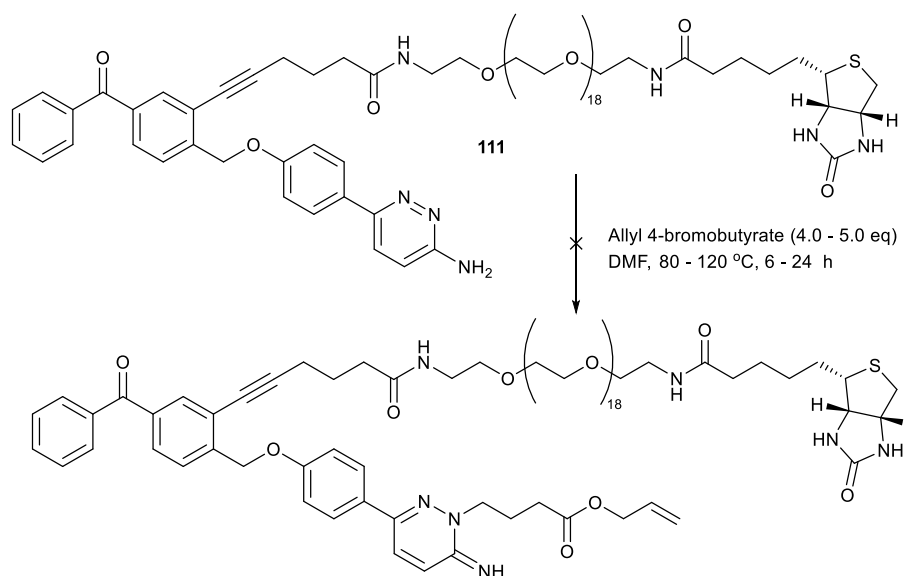
This acetic acid salt **108** was reacted with D-biotin *N*-hydroxysuccinimide ester **D-109**, in the presence of triethylamine to give fragment **110** in 76% yield. Then a DCC-mediated amide bond formation gave biotinylated pyridazine skeleton **111** in 55% yield (Scheme 38).



Scheme 38: Construction of longer PEG linker chemical probe.

Unfortunately the next step, the *N*-alkylation of the pyridazine core proved unsuccessful, despite numerous applied reaction conditions (Scheme 39). The oligomeric ethylene glycol chain may have prevented the precipitation of the product, although subsequent column chromatography yielded returned starting material only. It was hypothesised that the hydrophilic nature of the long chain enfolded the

pyridazine nitrogen, making it less accessible for nucleophilic attack. Further reaction conditions were tried with up to five equivalents of allyl 4-bromobutyrate and with heating up to 120 °C in DMF. However, no product was observed in any case, and the starting pyridazine was always returned. This led to attention being turned away from the synthesis of this chemical probe.



Scheme 39: Unsuccessful *N*-alkylation reaction conditions.

2.4 Conclusions

This chapter describes the successful use of a benzophenone photoaffinity antagonist for GABA_A receptors, and then goes on to describe the synthesis of a novel photo-activatable probe for the GABA_A receptor. This probe formed an adduct with a streptavidin-coated quantum dot, and was incubated with neurons. UV irradiation created a covalent link between neuronal receptors and the probe, irreversibly blocking and tagging it. Microscopy then followed the movement of quantum dots, as they tracked the movement of GABA receptors in synaptic and extra-synaptic sites.

Membrane dynamics of GABA_A receptors are incredibly varied, and are reliant on numerous factors, including the presence of ligands. This means that there is a

remaining need for another type of chemical tool, one which could track unblocked GABA_A receptors in the membrane. A synthesis of a photocleavable probe, with this aim, is described in Chapter 4.

Chapter 3 describes a short investigation into alternative benzophenone analogues, and the development of an assay to discover a way to quantify H-abstraction ability.

Chapter 3

Testing alternative photoaffinity labels

3.1 UV spectra and photoaffinity labels

Alongside this work on functionalised chemical probes to track the GABA_A receptor, a study was initiated to explore alternative benzophenone analogues that could be used in photoaffinity labelling. The reactivity of benzophenone **13** is derived from excitation with a requisite wavelength, usually around 350 nm, of light to form a n,π^* electronic state, which readily undergoes *H*-abstraction followed by intermolecular radical recombination to form a photoadduct.⁸⁵ The UV spectra of benzophenone comprises of an absorbance at 250 nm, which is ascribed to a π,π^* electronic transition, and a weaker absorbance corresponding to the n,π^* transition at 345 nm (Figure 36). The UV spectra taken of benzophenone **13** was considerably altered upon the introduction of electron donating or withdrawing substituents onto the phenyl rings, as shown with the *p*-methoxy and *p*-nitro analogues **112** and **113** respectively.

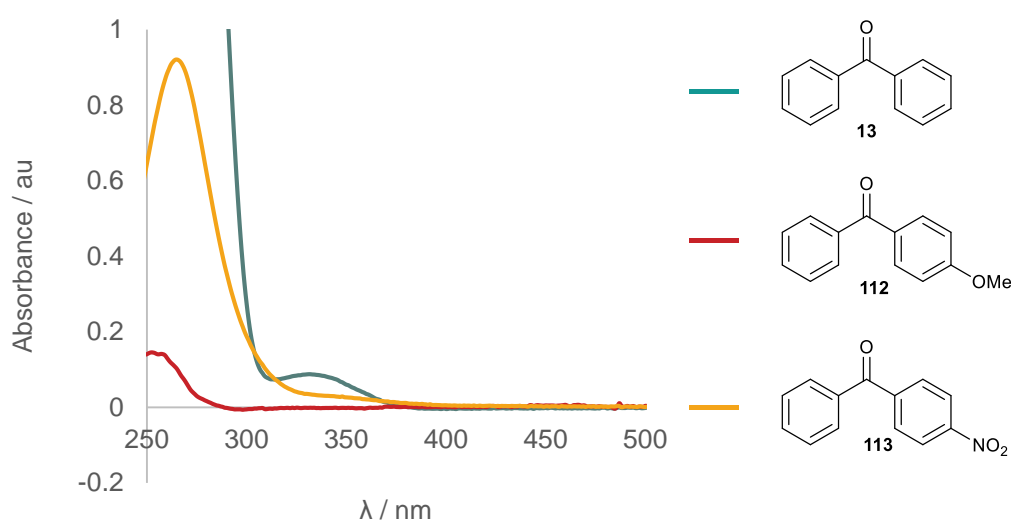


Figure 36: UV spectra of substituted benzophenones, with particular look at transition at 350 nm.
C = 5×10^{-4} M.

In the first instance, it was a dramatic increase in n,π^* absorbance at a wavelength greater than 350 nm which was desired, as this wavelength is less harmful to biological samples. At this point the search was broadened to include, amongst others, naphthalene analogue **114** (Figure 37).

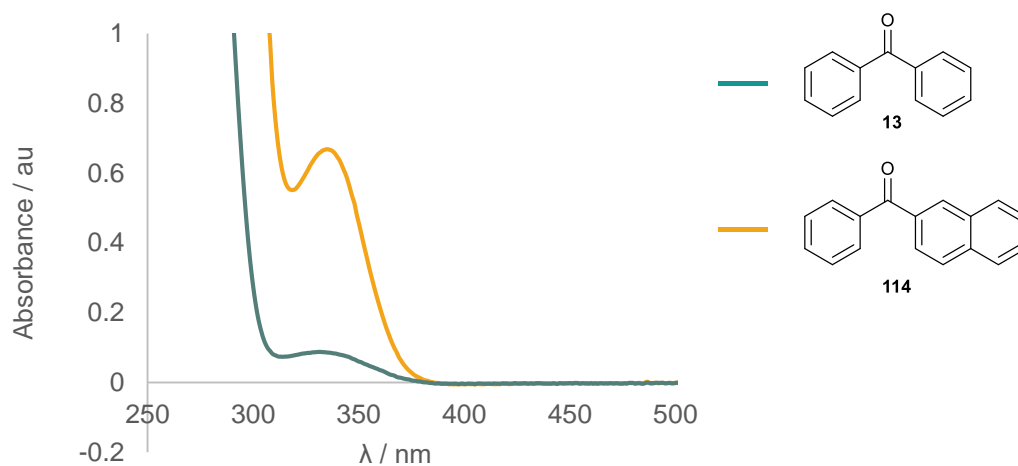
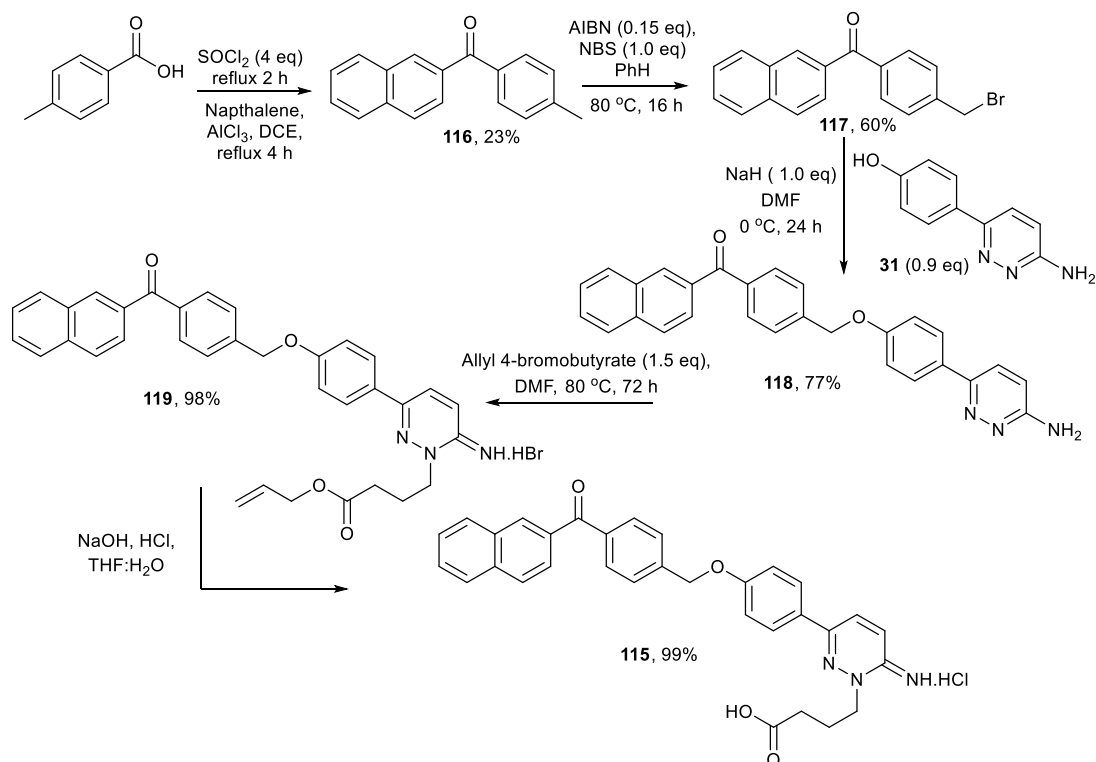


Figure 37: UV spectra of benzophenone **13** and naphthalen-2-yl(phenyl)methanone **114**, highlighting absorbance at $\lambda = 340 - 360$ nm. $c = 5 \times 10^{-4}$ M.

This naphthalenylphenylmethanone **114** had a very much increased intensity of absorbance at 355 nm. With this in mind, the six step synthesis of a naphthalenyl gabazine analogue **115** was undertaken. An electrophilic aromatic addition of naphthalene to 4-methylbenzoic acid gave ketone **116** in 23% yield. This was then brominated to give **117** and underwent an ether synthesis with phenol **31** to give pyridazine **118**. This was then subjected to *N*-alkylation, giving allyl ester **119** and the resulting ester was hydrolysed to give naphthalene analogue **115** in an overall, unoptimised yield of 10% over five steps (Scheme 40).



Scheme 40: Synthesis of naphthalenyl photoaffinity label **115** for the GABA_A receptor.

However, once made, the UV spectra of the naphthalene analogue **115** and benzophenone photoaffinity label **30** turned out to be similar, with absorbance at 350 nm being slightly stronger for the original benzophenone analogue **39** (Figure 38).

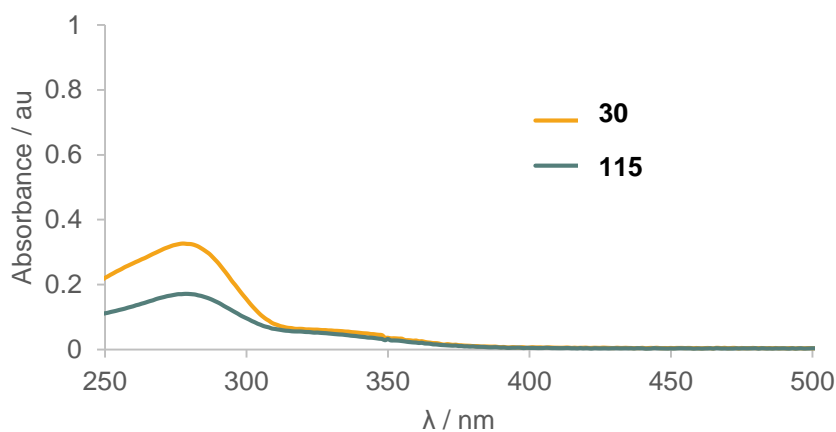


Figure 38: UV absorbance spectra of gabazine based antagonists, **39** and **115**; $c = 2.0 \times 10^{-4}$ M.

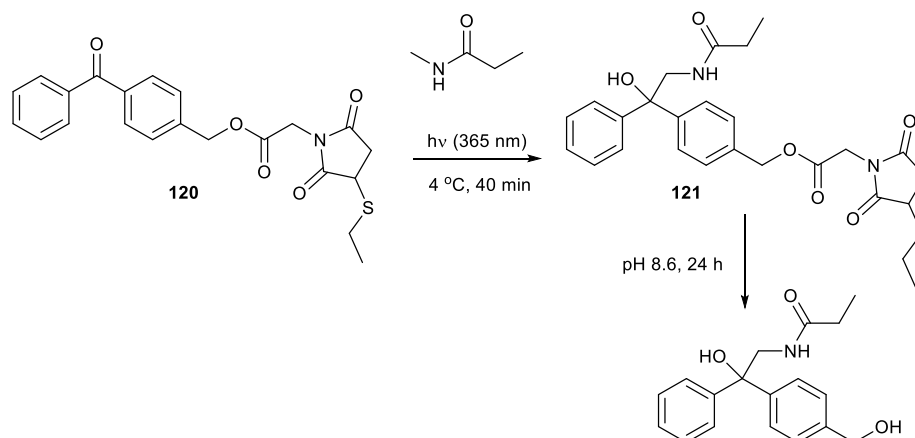
This result, along with the increased hydrophobicity of analogue **115**, leading to its insolubility in polar solvents, meant that it became a non-viable alternative to benzophenone gabazine analogue **39**.

3.2 Testing potential photoaffinity labels

The completion of an analogue synthesis was the impetus for the development of an assay to test the H-abstraction ability of other potential photoaffinity labels. The H-abstraction reaction by benzophenone is widely known, and could be used as a standard to compare the potential of other photoaffinity labels. There is evidence that an excited benzophenone in a protein environment would preferentially react with a methionine residue, even when other abstractable hydrogens are closer,⁸⁶ and this, alongside other literature results, directed our research.

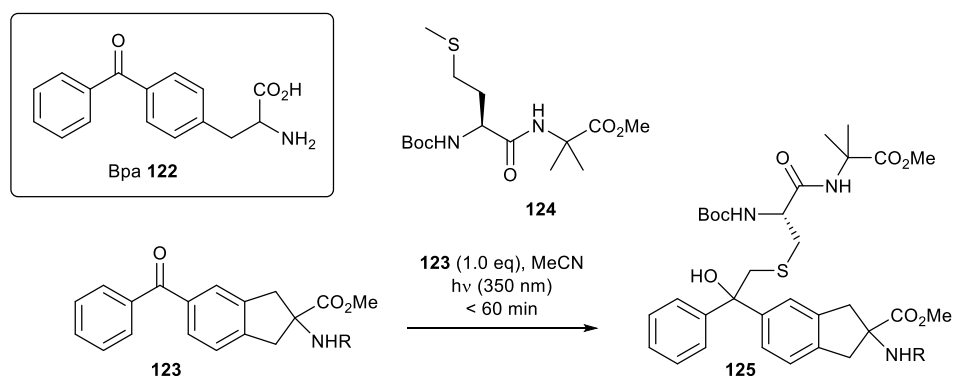
There are few reports describing testing of new photoaffinity labels, although many groups report irradiation in the presence of a hydrogen source. A brief description of some known literature techniques are given here to contextualise the direction of our efforts. Firstly, the irradiation of benzophenone in the presence of 2-propanol is well documented, and indeed is a popular undergraduate practical experiment.⁸⁷

Secondly, in order to test the reactivity of heterobifunctional benzophenone **120**, it was irradiated in the presence of a ‘protein mimicking’ solvent, namely *N*-methylpropionamide, to arrive at pH-dependent cleavable protein crosslinker **121** (Scheme 41).⁸⁸



Scheme 41: Testing photoaffinity label in 'protein mimicking' solvent, N-methylpropanamide.

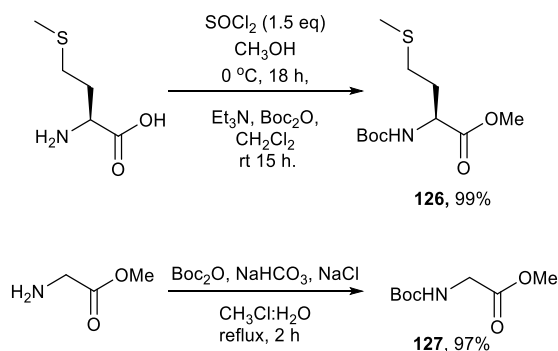
Another way to mimic protein conditions to test for H-abstraction ability is to irradiate in the presence of a small peptide as shown for the case of 3-(4-benzoylphenyl)alanine (Bpa **122**), a popular probe for photoaffinity labelling. Good results were obtained when Bpa **122** was irradiated in the presence of a hexapeptide, which showed that excited benzophenone reacted preferentially with Gly α -, Met γ - and Met ϵ -hydrogens.⁸⁹ The photoreactivity of a partially constrained analogue of Bpa, **123**, was probed using dipeptide Boc-Met-Aib-OMe **124**, a reaction which yielded photoadduct **125**, as seen by ¹H NMR spectroscopy and ESI-ToF mass spectrometry (Scheme 42).⁹⁰



Scheme 42: Testing photoaffinity label **123** with methionine-containing dipeptide **124**.

From this short literature review, it was envisaged that an assay could be developed in which potential photoaffinity labels could be irradiated in the presence of a protected

methionine or glycine amino acid. The syntheses of these protected amino acids **126** and **127** were then undertaken following well known protocols in excellent yields (Scheme 43).



Scheme 43: Synthesis of protected methionine and glycine.

An irradiation procedure was devised in which the potential photoaffinity label was mixed with the amino acids in degassed acetonitrile in a photoreactor immersion well. Irradiation of benzophenone with a 125 W medium power mercury lamp as a control led to the formation of benzopinacol **128** and benzopinacolone **129** homoaddition and rearrangement products in good yield (Figure 39).

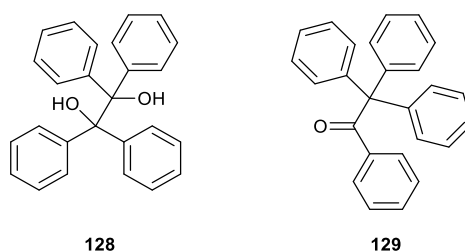
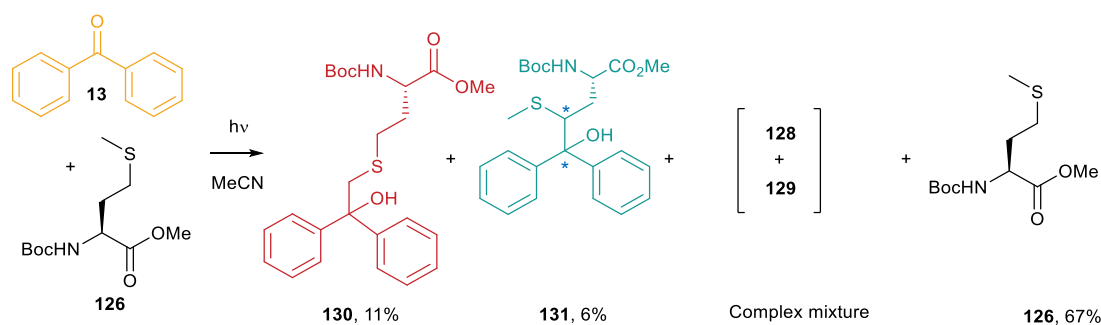
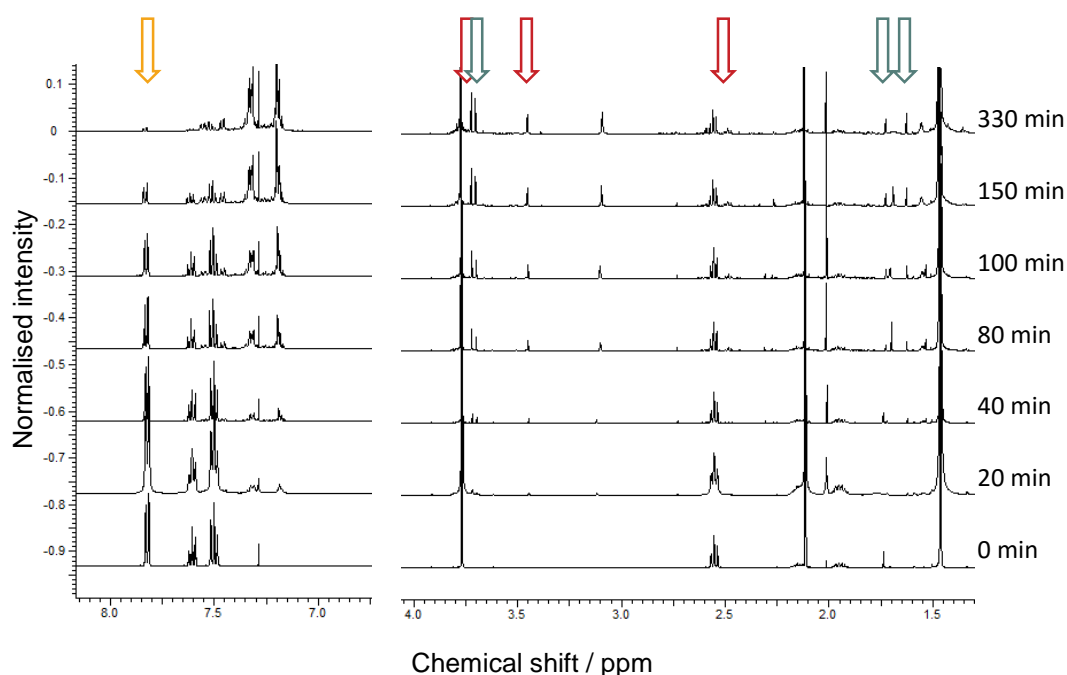


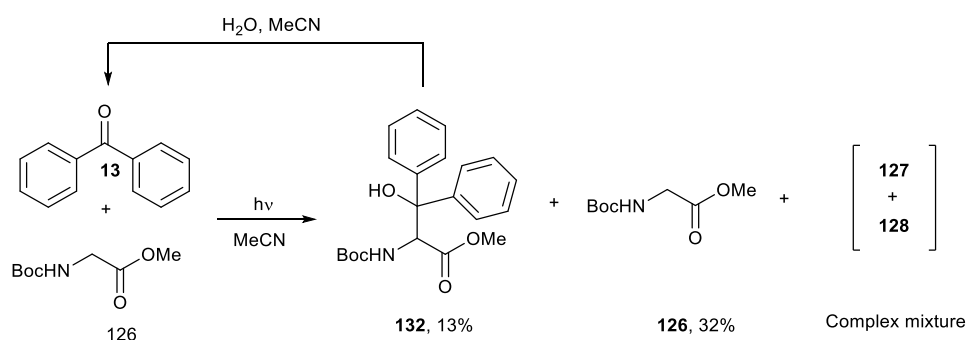
Figure 39: Benzopinacol **128** and benzopinacolone **129**.

In addition, irradiation of benzophenone in the presence of Boc-Met-OMe **126** produced a mixture of products, the formation of which were traced by ¹H NMR spectroscopy (Figure 40). Typical isolated yields for this reaction after 100 min irradiation are shown in Scheme 44.

Scheme 44: Product distribution from irradiation of benzophenone **13** with methionine **125**.Figure 40: ^1H NMR spectroscopic analysis of benzophenone **13** irradiation with methionine **125**.

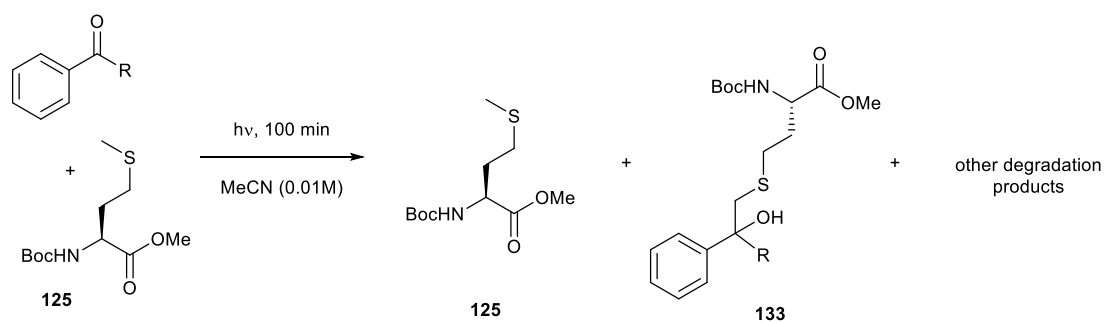
The formation of photoadducts **130** and **131** seemed to require at least 20 minutes of irradiation, and disappearance of all benzophenone starting material takes at least 5.5 hours (330 minutes). Although this is not the time scale upon which cross-linking in cells seems to occur,^{46,28} this assay still shows which photoadducts are likely formed upon irradiation. In this case it is the diastereomeric γ -adduct **131**, alongside the ϵ -adduct **130** and a complex mixture containing benzopinacol **128** and benzopinacolone **129**.

Irradiation of benzophenone in the presence of Boc-Gly-OMe **127** forms an α -glycine adduct **132**, isolated in 13% yield after a 100 minute irradiation. Again, the majority of the material was isolated as a mixture of aromatic byproducts (Scheme 45). Photoadduct **132**, was thought to be unstable, undergoing a retro-aldol reaction under the reaction conditions, and indeed upon stirring **132** in water and acetonitrile, benzophenone was recovered after extraction in organic solvent.



Scheme 45: Irradiation of benzophenone **13** in the presence of glycine **126**.

An irradiation time of 100 minutes in degassed acetonitrile was chosen as an assay to test the efficacy of a photoaffinity label to abstract a hydrogen from a methionine residue. The results are given as a ratio between remaining amino acid **125** and requisite major photoadduct **133**, which should give an indication of H-abstraction ability by 1H NMR analysis (Scheme 46). Other aromatic degradation pathways proved difficult to quantify. The potential photoactive groups, alongside UV spectra highlighting a relevant λ_{max} and molar extinction co-efficient (ϵ), are reported in Table 2 alongside their assay results.



Scheme 46: General assay for determining H-abstraction ability.

Photoactive group (R)	UV spectra	Assay result 126 : 133
<p>13</p>	<p>$c = 5 \times 10^{-4} \text{ M}$ $\epsilon_{(333 \text{ nm})} = 170 \text{ M}^{-1}\text{cm}^{-1}$</p>	1 : 0.4
<p>112</p>	<p>$c = 5 \times 10^{-4} \text{ M}$ $\epsilon_{(254 \text{ nm})} = 290 \text{ M}^{-1}\text{cm}^{-1}$</p>	1 : 0.2
<p>134</p>	<p>$c = 5 \times 10^{-4} \text{ M}$ $\epsilon_{(273 \text{ nm})} = 9360 \text{ M}^{-1}\text{cm}^{-1}$</p>	1 : 0

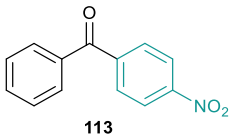
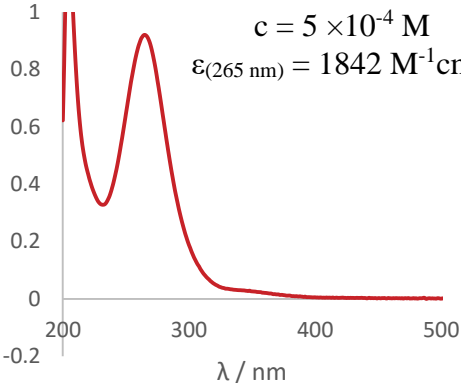
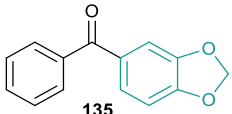
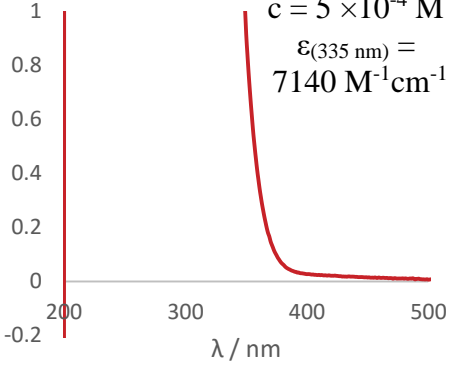
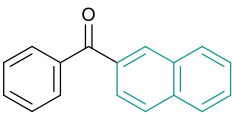
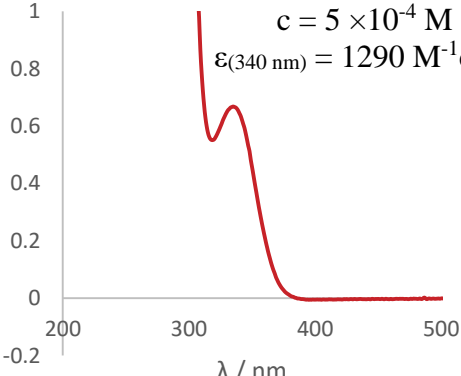
 <p>113</p>	 <p>$c = 5 \times 10^{-4} \text{ M}$ $\epsilon_{(265 \text{ nm})} = 1842 \text{ M}^{-1}\text{cm}^{-1}$</p>	1 : 0
 <p>135</p>	 <p>$c = 5 \times 10^{-4} \text{ M}$ $\epsilon_{(335 \text{ nm})} = 7140 \text{ M}^{-1}\text{cm}^{-1}$</p>	1 : 0.3
 <p>114</p>	 <p>$c = 5 \times 10^{-4} \text{ M}$ $\epsilon_{(340 \text{ nm})} = 1290 \text{ M}^{-1}\text{cm}^{-1}$</p>	1 : 0

Table 2: UV spectra and [unreacted methionine **91**: requisite photoadduct **96**] ratio after 100 min irradiation; R group shown in blue.

The assay also gave negative results for acetophenone **136**, succinimide **137**, phthalimide **138**, benzil **139** and benzophenone imine **140**: no photoadducts were observed (Figure 41).

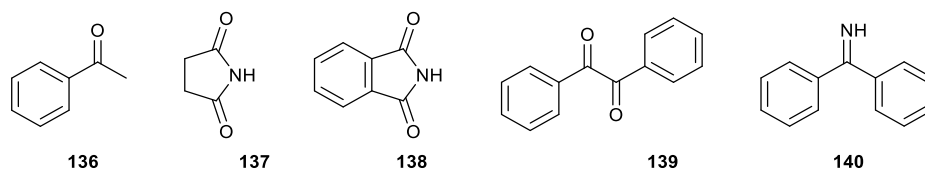


Figure 41: Other potential photoaffinity labels which showed no H-abstraction under irradiation conditions.

This led to the result that only benzophenone **13**, methoxy- and dioxole- substituted benzophenones **112** and **134** were able to undergo *H*-abstraction from methionine **91**. Of these, the benzophenone **13** remained the most successful, with an unreacted methionine **125** : photoadduct **132** ratio of 1.0 : 0.4.

3.3 Conclusions

This chapter describes a method to compare potential photoaffinity labels, by irradiating them in an assay containing a methionine or glycine amino acid. The products of this irradiation were analysed by ^1H NMR spectroscopy, in an attempt to quantify the ability of a compound to undergo H-abstraction reactions to estimate its potential as a photoaffinity label in a protein binding site.

Despite this largely negative result for H-abstraction in this chapter, the list of potential photoaffinity labels tested was by no means exhaustive, and a method to experimentally test the ability of a chromophore to undergo photochemical reactions remains an interesting and understudied area of research.

Chapter 4

Photocleavable antagonists for the GABA_A receptor

4.1 Photocleavable antagonists for the GABA_A receptor

It is known that the conformation of the receptor affects how it interacts with scaffolding proteins, and how it moves in the membrane.¹⁰ The differences in lateral dynamics between blocked and unblocked receptors is an understudied area, and the photoaffinity probe described in Chapter 2 will necessarily only give information about blocked receptors. It became apparent that an imaging tool for unblocked receptors, conducted with our useful gabazine analogue, would have to include a method to cleave off the gabazine fragment, leaving the binding site unblocked, but the fluorescent probe still attached. The dynamics of these unblocked receptors could be compared to those which were followed whilst blocked, for example with previous probe **106** {Scheme 36, Chapter 2}. A gabazine moiety will bring the compound into the binding site, and the covalent attachment onto the acrylamide would be accelerated by the proximity of a nucleophilic residue. Irradiation of the receptor-probe construct would release the gabazine moiety, which would diffuse out of the binding site, leaving a tagged receptor with an open GABA binding site (Figure 42).

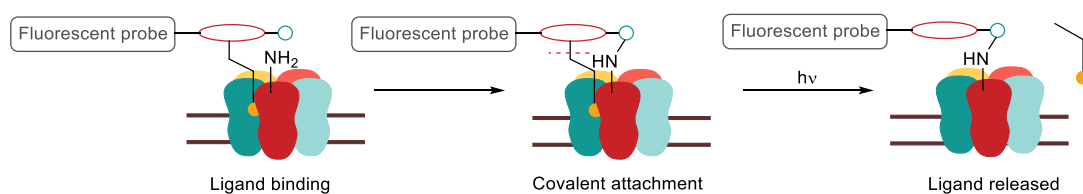


Figure 42: General mechanism of action for a photocleavable-affinity ligand.

4.2 A modular synthesis approach to a photocleavable antagonist for the GABA_A receptor

In this task, the development of a different, modular approach to the synthesis was deemed beneficial. This ‘building blocks’ method would include the addition of a complete gabazine fragment directly onto the rest of the structure in the last stages, allowing for a faster turnover in a screen of linker length and photocaging moiety. It would remove the need for allyl ester hydrolysis in the presence of the photolabile ester, and, furthermore, a modular approach would allow the capricious *N*-alkylation reaction to be undertaken earlier in the synthesis on simpler, reliable substrates.

There were many different alternatives for the precise structure of this complete gabazine fragment. Alkyne derivative **141**, which had previously been synthesised in the group and shown to have an IC₅₀ value on HEK293 GABA_A receptors of 40 nM, alongside azide analogue **38**, also previously synthesised as a photoaffinity label with an IC₅₀ of 28 nM,³⁰ were chosen (Figure 43). These both could conceivably be joined to the rest of the molecule at a late stage in the synthesis via a copper catalysed alkyne-azide click reaction.⁹¹

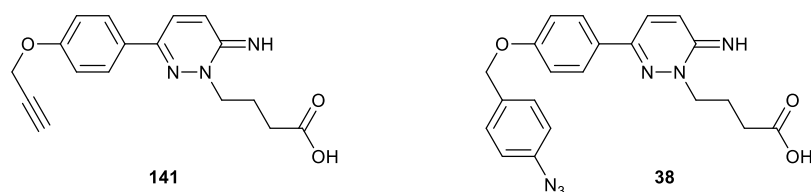
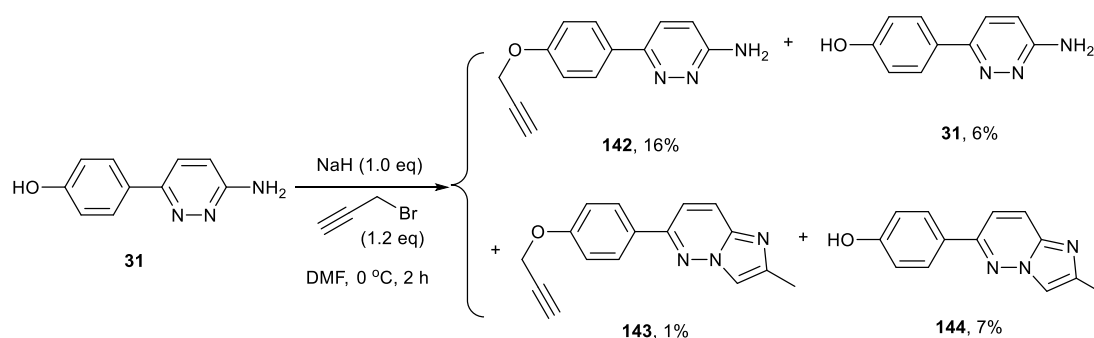


Figure 43: “Clickable” gabazine fragments.

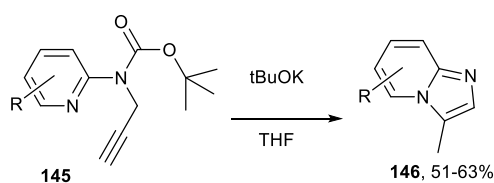
The first step of the synthesis of alkyne **141**, the Williamson ether synthesis between pyridazinyl phenol **31** and propargyl bromide, was attempted. This initially yielded the desired product **142** in 16% yield, with a further 6% starting material isolated. Also isolated from this reaction were imidazo[1,2-*b*]pyridazine compounds **143** and **144** as

byproducts (Scheme 47). This is an interesting and novel mode of reactivity, and was subject to a slight further investigation.



Scheme 47: Product distribution in ether synthesis.

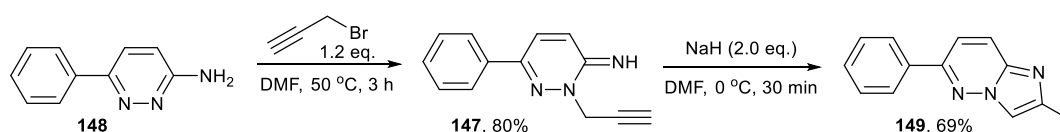
It was hypothesised that in the absence of a fully deprotonated alkoxide anion, the pyridazine *N*(2) reacted with propargyl bromide and the resulting compound forms an imidazo[1,2-*b*]pyridazine compound in the presence of sodium hydride. This is similar to the reported reactivity of *N*(2)-propargyl pyridin-2-amines, such as **145**, which are known to cyclise upon treatment with base, forming imidazopyridine 3-isomer **146** (Scheme 48). Reported ¹H NMR reaction studies on this reaction suggested the intermediate formation of an allene promoted by the potassium tert butoxide as the first mechanistic step.⁹²



Scheme 48: Formation of imidazo[1,2]pyridines.⁹²

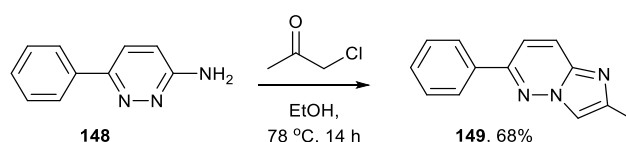
In order to establish the likely regioselectivity of our byproducts and investigate this novel mode of reaction further, *N*(2)-alkylated pyridazine **147** was synthesised in 80% yield upon reaction of propargyl bromide on 6-phenylpyridazin-3-amine **148** (Scheme 49). Treatment of the *N*(2)-alkylated product **148** with sodium hydride lead to

complete conversion to imidazopyridazine **149** via TLC, with product isolation in 69% yield (Scheme 49).



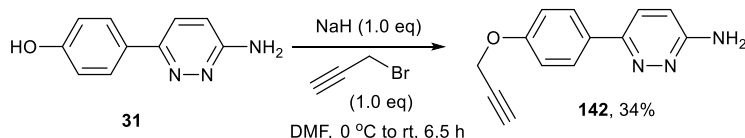
Scheme 49: Investigating a novel reaction to form methyl imidazo[1,2-b]pyridazine **149**.

The regiochemistry of this compound **149** was assigned through ¹H and ¹³C NMR spectroscopic comparison with the product of a condensation of 6-phenylpyridazin-3-amines with chloroacetone, which is known to give the 2-isomer according to literature precedent (Scheme 50).⁹³



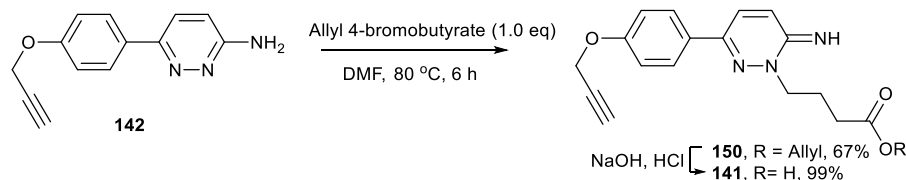
Scheme 50: Chloroacetone condensation reaction conditions.

In order to suppress the formation of these imidazo[1,2-b]pyridazine byproducts in our synthesis, phenol **31** was treated with sodium hydride to form the alkoxide ion for an additional hour, and the equivalents of propargyl bromide were lowered from 1.2 equivalents to 1.0. This slightly optimised procedure yielded desired product **142** in 34% yield (Scheme 51).

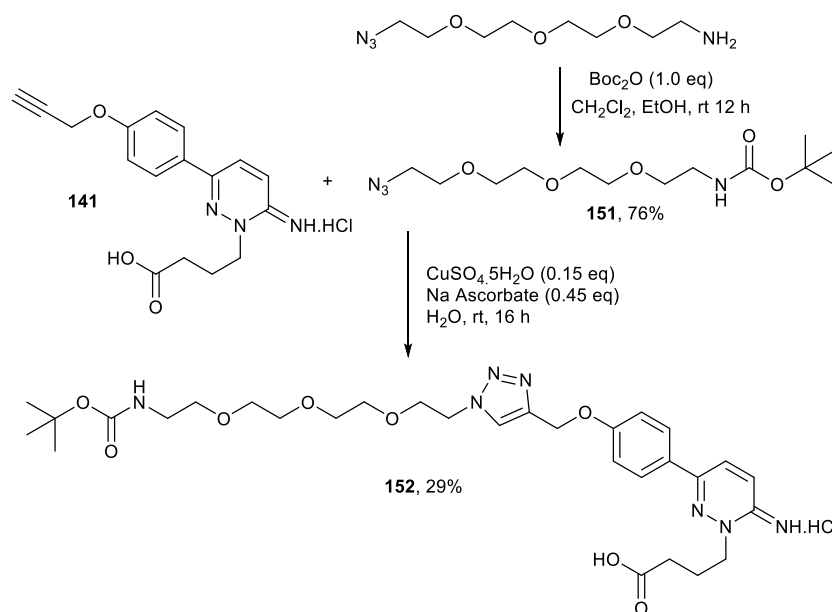


Scheme 51: Ether synthesis reaction conditions.

N-Alkylation of alkyne **142** proceeded in 67% yield, and subsequent deprotection of the allyl ester **150** was achieved quantitatively (Scheme 52).

Scheme 52: *N*-Alkylation and ester deprotection reaction conditions.

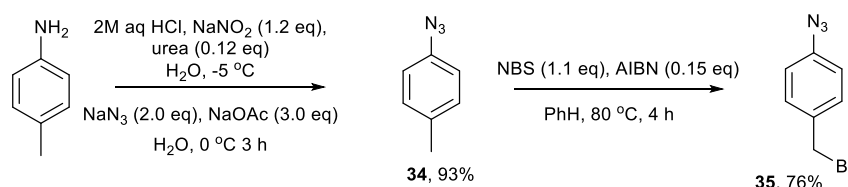
An alkyne-azide click reaction was performed between alkyne-gabazine fragment **141** and Boc-protected amine azide PEG unit **151**, in a model system, and triazole **152** was generated in 29% yield (Scheme 53).



Scheme 53: Model click reaction conditions.

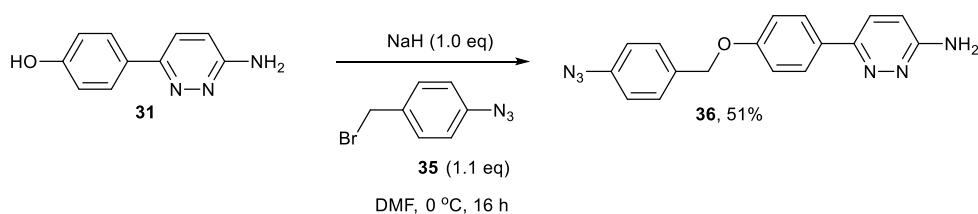
This triazole **152** was tested for potency as an antagonist for GABA_A receptors transiently expressed in HEK293 cells, by Dr Martin Mortensen in the Smart group. It has an IC₅₀ value of 435 nM, which is comparable to the value for gabazine **4** itself. Moreover, triazole **152** does not exhibit any non-competitive antagonism, which had been shown with other triazoles in the literature.⁹⁴ This was an encouraging result in the search for a versatile gabazine ‘block’ from which to develop highly functionalised molecules.

Meanwhile, the synthesis of the azide analogue **38** was attempted, with less success. Benzylbromide **35** was synthesised in two steps from *p*-toluidine in 76% overall yield (Scheme 54).



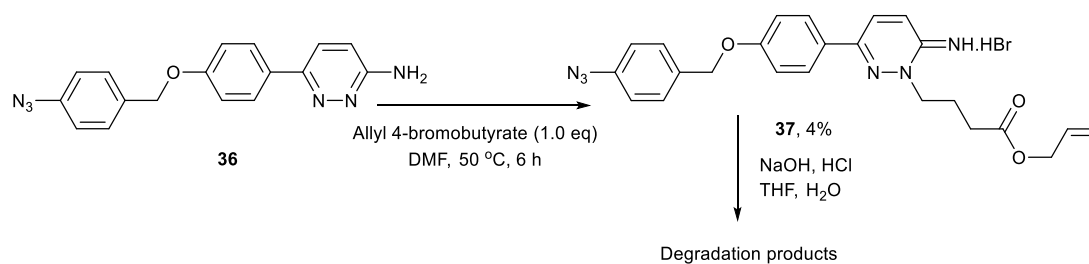
Scheme 54: Construction of azide fragment.

This benzyl bromide **35** was then introduced onto the pyridazine skeleton in a Williamson ether synthesis to form compound **36** in a 51% yield (Scheme 55).



Scheme 55: Ether synthesis reaction conditions.

Application of previously used *N*-alkylation conditions, yielded **37**, which was isolated upon recrystallisation from a mixture of starting material and product, in a disappointing 4% yield (Scheme 56). The returned starting material was reapplied to the reaction conditions, at an elevated temperature of 80 °C, but this led to the degradation of the compound. In addition the attempted ester deprotection of the *N*-alkylated species **37** led to a complex mixture of degradation products, potentially via reactions involving the azide, or cleavage of the benzyl ether previously seen in the group.^{28,95}

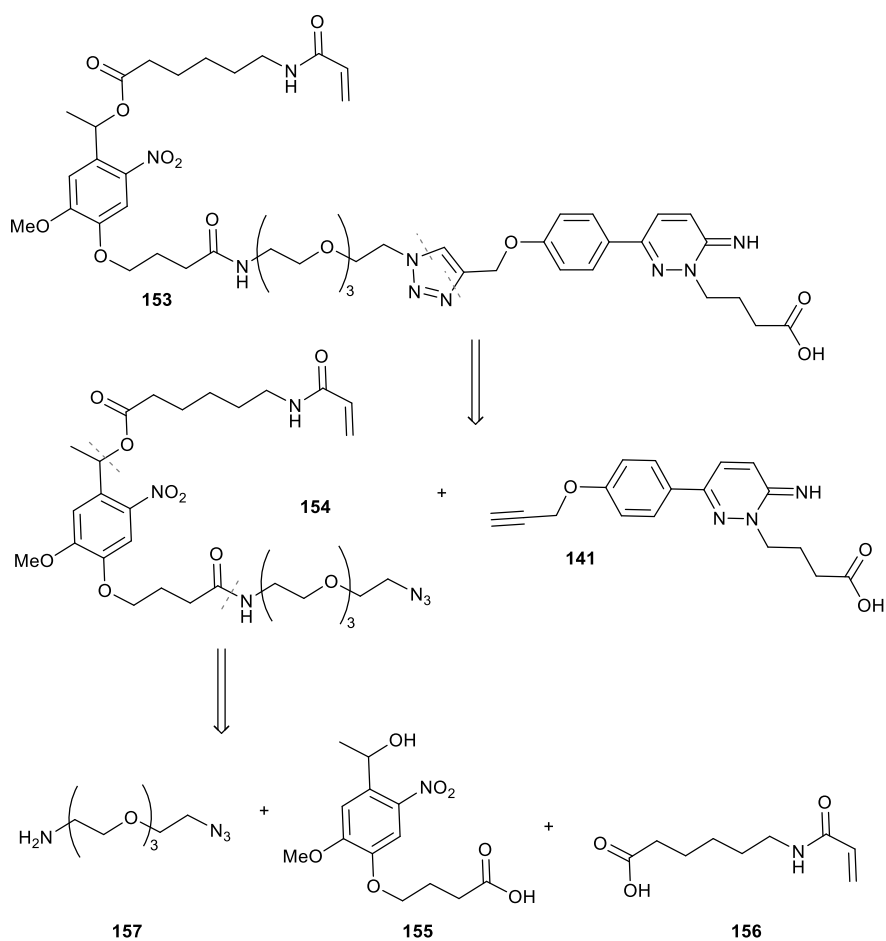


Scheme 56: *N*-alkylation and ester deprotection reaction conditions.

This result led to the progression of the alkyne gabazine fragment **141**, over the azide variant **39**, in the development of a modular, adaptable synthesis for further tools to study the GABA_A receptor.

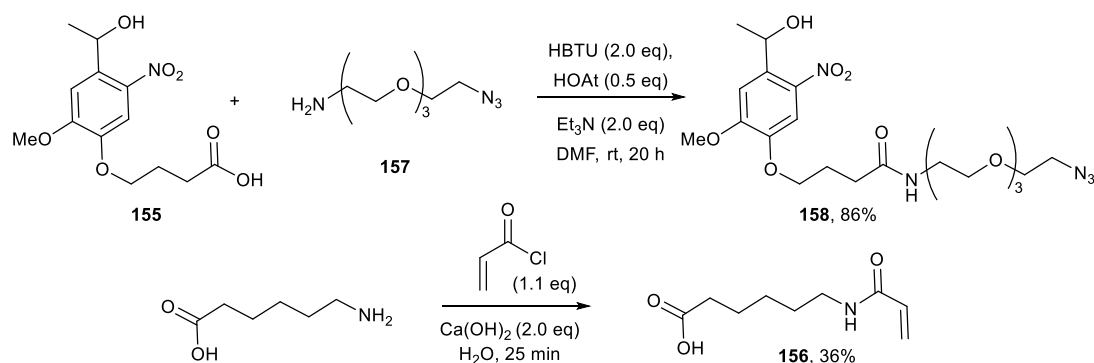
4.3 Development of a photocleavable antagonist for the GABA_A receptor

A modular, retrosynthetic pathway to the first tethered photocleavable affinity probe for the GABA_A receptor was devised. A probe, such as that described in Figure 42, has a vast array of functionality. In order to test for retained potency of the analogue, to discover the efficacy of photouncaging, as well as to test a new modular synthetic ethos, a simpler structure **153** was designed and synthesised. In this structure the attachment of the fluorescent probe was left out. The synthesis of this simpler model system involved a photocaging fragment **154** (synthesised from commercially available hydroxyethylphotolinker **155**), an acrylamide with a carboxylic acid moiety **156**, and installation of an azide via an azide – amine OEG chain **157** (Scheme 57).

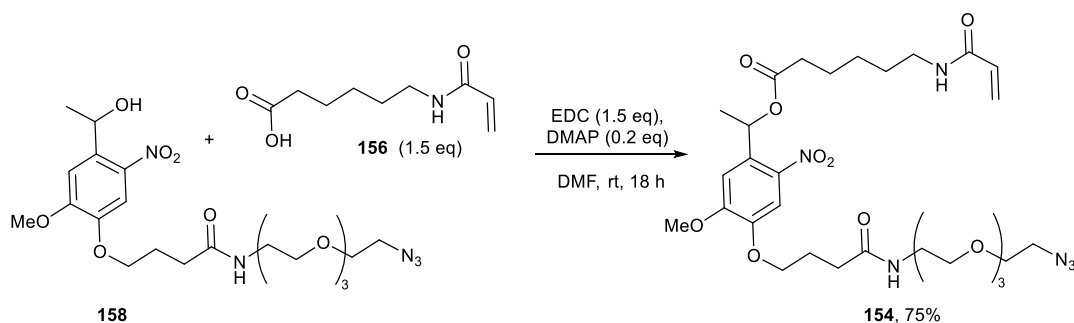


Scheme 57: Retrosynthetic analysis of photocleavable affinity ligand **153**, initially without a fluorescent probe attachment.

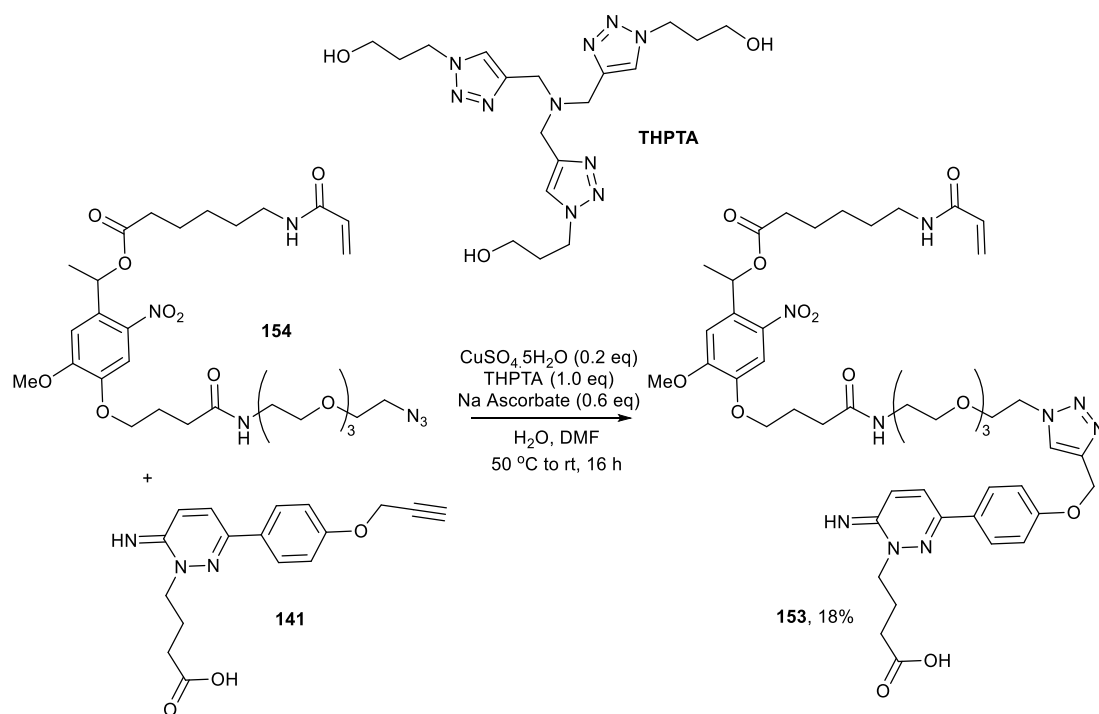
Firstly the amine OEG chain **157** underwent HBTU amide bond formation on the acid functionality of the hydroxyethyl photolinker **155** to give fragment **158** in 86% yield, and the acrylamide acid fragment **156** was synthesised from 6-aminohexanoic acid and acryloyl chloride in 36% yield (Scheme 58).

Scheme 58: Synthesis of photocaging fragment **158** and electrophile fragment **156**.

The installation of the photolabile ester was facilitated by an EDC coupling between hydroxyethylphotolinker fragment **158** and carboxylic acid **156**, which proceeded in 75% yield (Scheme 59).

Scheme 59: Completion of the photocleavable affinity fragment **154**.

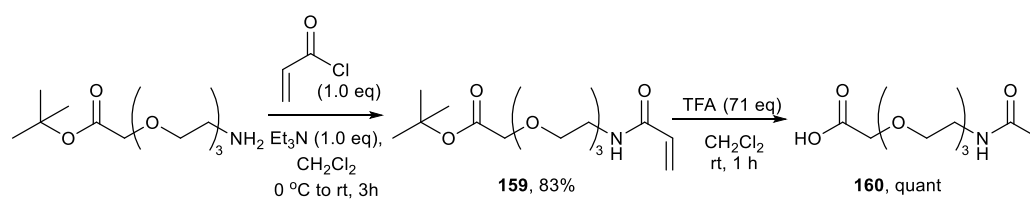
Initial attempts at the alkyne-azide click reaction following the previous protocol (Scheme 50) were unsuccessful. However, a low but sufficient yield of 18% desired product **153** was achieved through optimising the procedure, which involved a higher catalyst loading, a higher temperature of 50 °C and the addition of THPTA⁹⁶ as a ligand to stabilise the copper (I) species formed *in situ* (Scheme 60).



Scheme 60: Copper catalysed azide-alkyne click reaction to form photocleavable affinity probe **153**.

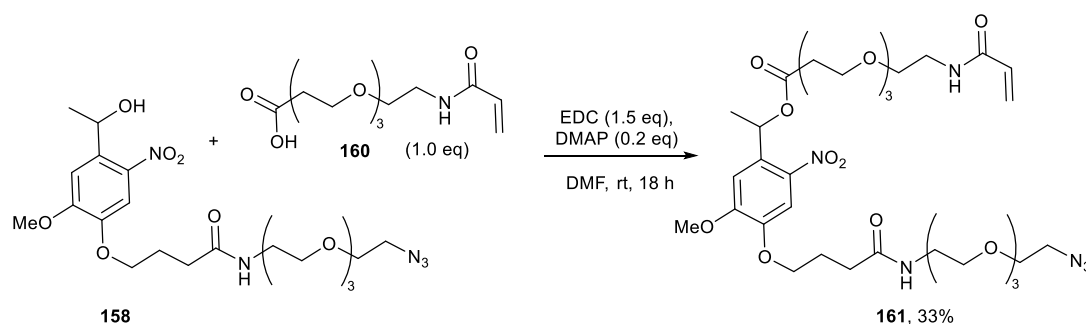
In proximity-accelerated electrophilic attachment, a covalent bond is formed between the ligand and the receptor via a nucleophilic residue from, in this case, an unknown location near the binding site. With the exact location unknown, it seemed prudent to vary the length of linker between the photocaging group and the acrylamide in a second compound. This was achieved with the substitution of the hexanoic acid linker, which provided a ten atom bridge between the photolabile carbonyl carbon and the electrophilic terminal carbon, with a longer ethylene glycol chain, providing a bridge of sixteen atoms.

The ethylene glycol linker for this second variant was synthesised from commercially available *tert* butyl-12-amino-4,7,10-trioxadodecanoate, which underwent addition to acryloyl chloride yielding **159** followed by *tert*-butyl ester hydrolysis to give **160** in 83% overall yield (Scheme 61).



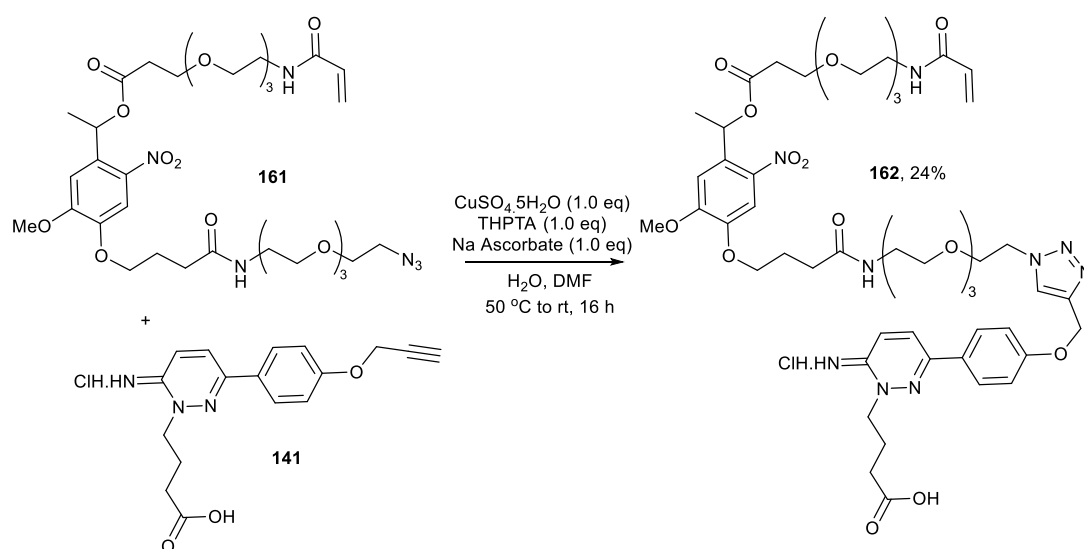
Scheme 61: Preparation of longer linker fragment.

Acrylamide **160** was then reacted in an EDC coupling reaction with azide **158** to give **161** in 33% yield (Scheme 62).



Scheme 62: Completion of a photocleavable affinity ligand with a longer linker.

This was then reacted in a copper catalysed alkyne-azide click reaction with alkyne-gabazine, to form the second variant **162** in 24% yield, to be used alongside the initial variant **153** in electrophilic tagging of the GABA_A receptors (Scheme 63).



Scheme 63: Copper catalysed azide-alkyne click reaction conditions.

4.4 Conclusions

These chemical tools **153** and **162** are currently undergoing biological testing by Dr Martin Mortensen in the Smart group, and will firstly be analysed in the dark for potency against recombinant GABA_A receptors. Any covalent attachment will be apparent as antagonism which persists even after flushing of the cells with buffer solution. UV irradiation and further washing will be able to demonstrate the release of gabazine from the binding site as a drop in receptor inhibition i.e. reappearance of a GABA response (Figure 44).

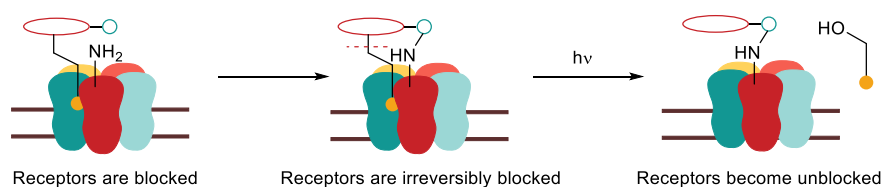


Figure 44: General mechanism for the action of affinity antagonists **153** and **162**.

Once GABA_A receptor specificity and covalent attachment is proven, and the efficacy of the photocaging motif is established, the next stage would be the tracking of receptors. This would require an additional functionality – a fluorescent probe, incorporated near the electrophile. Potentially this could be a streptavidin coated quantum dot (associated, as in the previous chapter, via a biotin moiety). This future construct would be able to track these unblocked receptors in a vital comparison of conformation-dependent receptor dynamics.

Chapter 5

Photoswitchable antagonists for the GABA_A receptor

5.1 Photoswitchable antagonists for the GABA_A receptor

The small molecular probes reported in Chapters 2 and 4 provide unique functionality to track GABA_A receptors as they move in the membrane, adapting to chemical and electrical signals. All previous constructs rely on a light-induced irreversible change. This next chapter describes the design and synthesis of a photoswitchable antagonist, one which continues to change shape in alternating wavelengths of light. By being able to turn functionality of the receptors on and off reversibly, additional information will be afforded about how the conformation of the receptor affects its movement. In another application it also allows the activation of receptors under a defined spot of UV irradiation, compared to previous photoaffinity labels deactivating the receptors. This activation can be quantified and so can help build a picture of which areas on the cell contain the most GABA_A receptors (Figure 45).

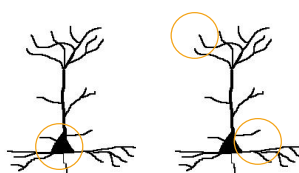


Figure 45: Use of photoswitching ligand and UV spot light to block and then unblock receptors at different points on the neurons.

The process for designing both tethered and non-tethered photoswitching compounds for GABA_A receptors has been described and encouraged in the literature.⁹⁷ The development of such compounds is often reported as beginning with an evaluation of ligands for their potential to include a photoswitching group. It is necessary that this group does not alter the specificity of a ligand for the target, and instead confers a

‘switch’ at a position likely to modulate binding efficacy. A rational introduction of an azobenzene photoswitch would be, for example, in place of a similarly-shaped moiety already present in the ligand. Such “azosters” could include stilbenes, 1,2-diphenyl ethanes, 1,2-diphenyl hydrazines, *N*-benzyl anilines, benzyl-phenyl ethers, benzyl-phenyl thioethers, diaryl esters and diaryl amides.⁹⁸

Following this rationale, “azologization” of one antagonist to the GABA_A receptor, the benzyl analogue of gabazine **26**, previously made in the group and shown to have a greatly increased potency to gabazine itself,³⁰ could result in an azogabazine synthetic target **156**, whereby an azobenzene moiety replaces a benzyl-phenyl ether in a position where receptor-ligand interactions are important for potency (Figure 46).

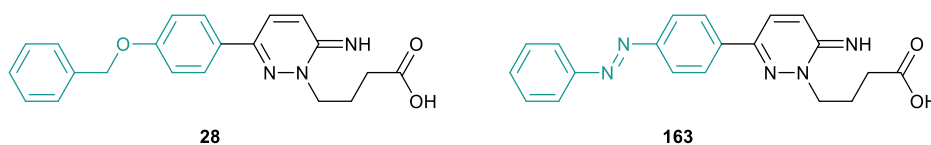
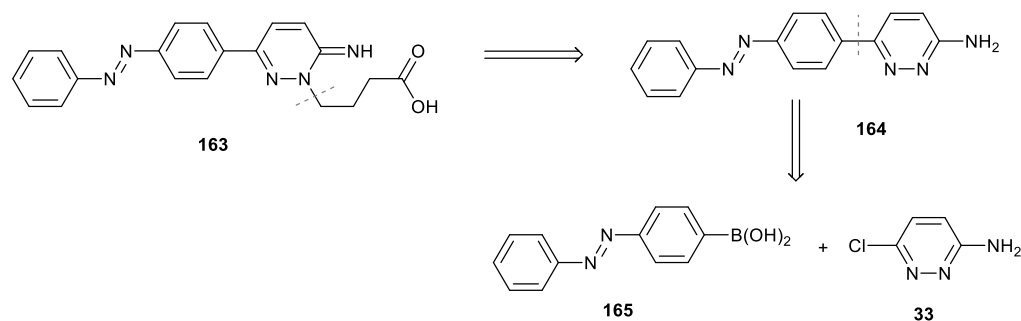


Figure 46: “Azologization” of benzyl gabazine analogue **28**.

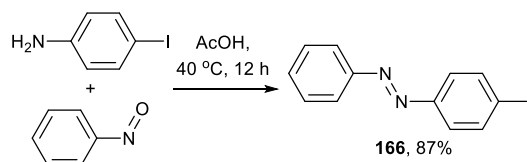
This azo-gabazine could allow for the photomodulation of GABA_A receptors, which would mean that a short burst of UV or indeed visible light could produce reversible antagonism of the receptors in recombinant cells or in a primary culture. This would lead to spatial and temporal control of receptors, giving valuable information on the effect of antagonism in different areas of a neuron.

5.2 Synthesis of azo-gabazine

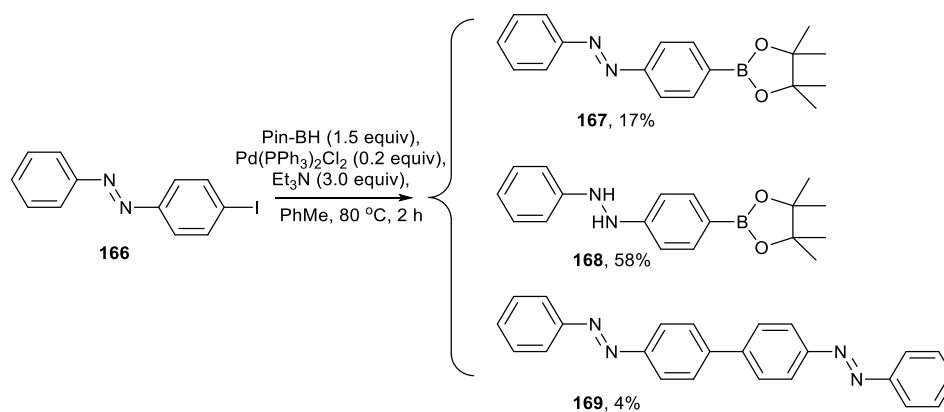
A retrosynthetic analysis of azo-gabazine **163** leads, via our previous *N*-alkylation strategy to Suzuki coupling product **164**, potentially formed from commercially available 3-chloro-2-aminopyridazine **33**, and azobenzene boronic acid **165** (Scheme 64).

Scheme 64: Retrosynthetic analysis of azogabazine derivative **163**.

Firstly, the synthesis of azobenzene fragment **165** was attempted, for which 4-iodoaniline was refluxed with nitrosobenzene in glacial acetic acid for 24 h to yield 4-iodo-azobenzene **166** in an excellent yield (Scheme 65).

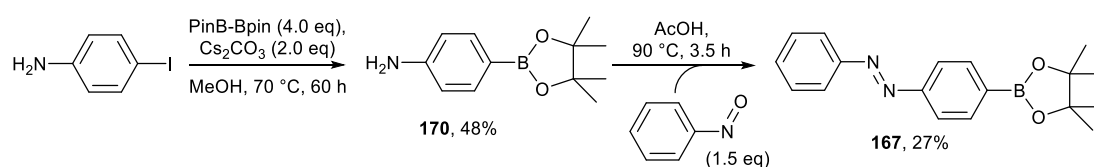
Scheme 65: Condensation reaction conditions to form azobenzene **166**.

A boronylation reaction was then attempted, firstly by heating **166** with pinacolborane and Pd₂(PPh₃)₂Cl₂ in triethylamine and toluene for 2 h. However, this only resulted in a 17% yield of azobenzene pinacol borane **167**, with the hydrazine **168** and homodimer **162** side products formed in 58 and 4% yield respectively (Scheme 66). Further attempts using bis(pinacolato)diboron were also low yielding.



Scheme 66: Product distribution of pinacolboronate installation reaction conditions.

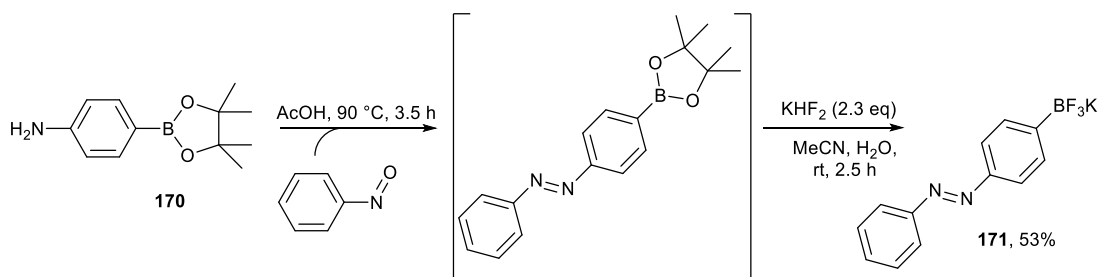
A synthetic route which involved the pre-installation of the pinacolborane was then undertaken, with more success. 4-Iodoaniline was heated to 90 °C in the presence of caesium carbonate and bis-(pinacolato)diboron, and yielded 4-aminophenylboronic acid pinacol ester **170** in 48% yield. This product then underwent condensation with nitrosobenzene to yield the desired azobenzene-boronic acid pinacol ester **167** in 27% yield (Scheme 67). The low yield of the latter reaction was attributed to difficulty in purification using column chromatography; the collection of the clean material was prohibitively slow.



Scheme 67: Formation of pinacol boronate azobenzene **167**.

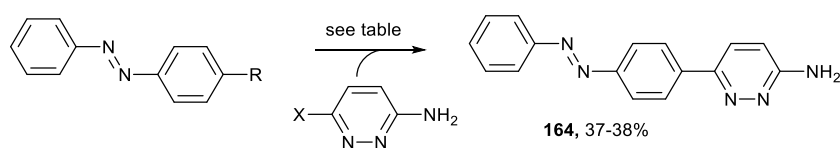
A trifluoroborate salt of this azobenzene had been reported to undergo Suzuki couplings directly on a variety of substrates with [bis(diphenylphosphino)ferrocene]-palladium dichloride catalyst.⁹⁹ The conversion of pinacolborane **167** to the corresponding trifluoroborate salt **171** was facilitated with potassium hydrogen fluoride in good yield. The synthesis of this complete azobenzene fragment **171** was further optimised by omitting the purification of azobenzene-boronic acid pinacol ester **167**, and taking forward the crude mixture to form the trifluoroborate salt in 53% overall yield from 4-aminophenylboronic acid pinacol ester **170** (Figure 68). The procedure was developed as follows: petroleum ether was added to the crude product of the condensation reaction, and the suspension was filtered. The filtrate was then concentrated *in vacuo*, redissolved in acetonitrile and water (10:1 ratio), and three equivalents of potassium hydrogen fluoride were added. The reaction mixture was stirred at room temperature for 2.5 h, before being quenched with saturated sodium

hydrogen carbonate solution. The solvent was removed *in vacuo* and triturated with petroleum ether and the product purified by recrystallisation from acetone.



Scheme 68: Optimised reaction conditions for the formation of trifluoroborate salt **171**.

The use of **171** in the subsequent Suzuki coupling under literature conditions unfortunately gave a poor result; the pyridazine product was produced in a low 38% yield (Scheme 69).



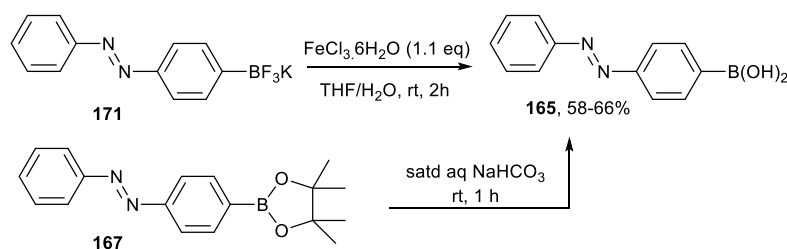
Scheme 69: Suzuki reaction conditions.

R	X	Conditions	Yield of 164
BF ₃ K	Cl	PdCl ₂ (dppf) K ₂ CO ₃ , MeOH, 70 °C, 2 h.	38%
B(OH) ₂	Cl	PdCl ₂ (dppf) K ₂ CO ₃ , MeOH, 70 °C, >16 h.	0%
BF ₃ K	I	PdCl ₂ (dppf) K ₂ CO ₃ , MeOH, 70 °C, >16 h.	0%
BF ₃ K	Cl	Pd(PPh ₃) ₂ Cl ₂ , MeCN, H ₂ O, μW 120 °C, 10 min.	37%

Table 3: Azobenzene Suzuki reaction conditions.

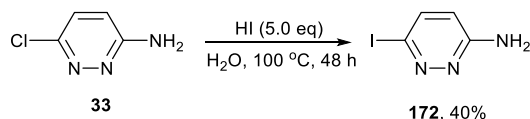
In order to optimise this Suzuki reaction, the boronic acid **165** was formed from the trifluoroborate salt **171** upon reaction with iron trichloride in 66% yield (Scheme 70).

The boronic acid was also formed in 58% yield upon reaction of pinacolborane **167** with saturated aqueous ammonium chloride (Scheme 66).



Scheme 70: Hydrolysis of trifluoroborate salt **171** and boron pinacol ester **167** yield boronic acid **165**.

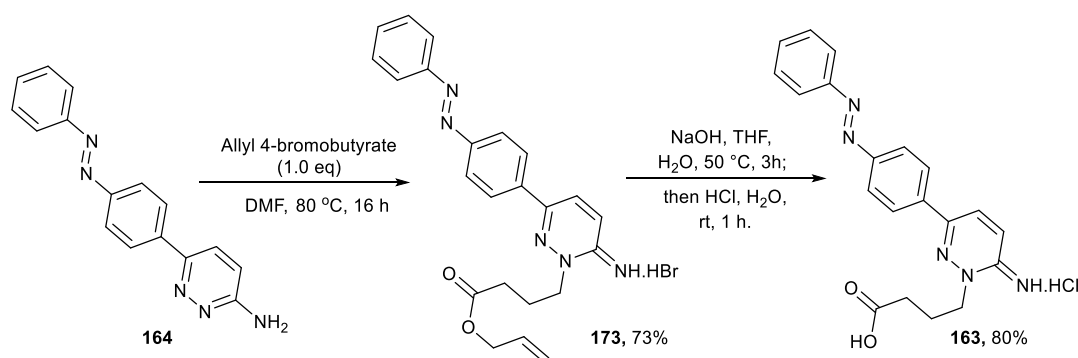
However, when reacted under the stated Suzuki conditions, no product formation was detected. In a second strategy, iodo-pyridazine **172** was synthesised from the reaction of 3-amino-6-chloropyridazine **33** with hydrogen iodide in reasonable yield (Scheme 71); however this also proved unsuccessful at forming the desired product under various Suzuki reaction conditions (Scheme 69).



Scheme 71: Halogen exchange reaction of pyridazine fragment.

Finally it was a return to our previous Suzuki conditions involving microwave irradiation in the presence of $\text{Pd}(\text{PPh}_3)_2\text{Cl}_2$, which allowed us to improve on the reaction time for this reaction, if not the product yield (Table 3).

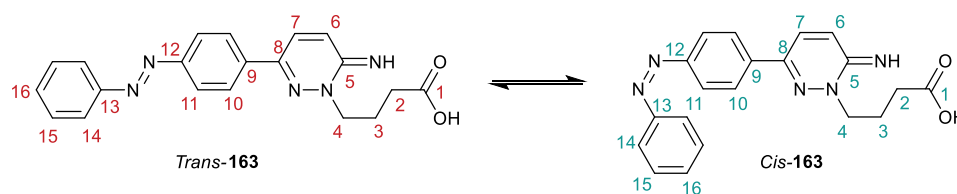
The Suzuki product **164** was then *N*-alkylated under conditions reported *vide supra*, to yield **173** in 73% yield, which was subsequently deprotected to give acid **163** in 80% yield (Scheme 72).

Scheme 72: Endgame in the synthesis of azo-gabazine **156**.

This gives the azo-gabazine **163** compound in four steps and 12% overall yield from aminophenylboronic pinacol ester **170**.

5.3 Investigation of photoswitching ability by UV/Vis and NMR spectroscopy

In order to characterise the photoisomerisation of azobenzene **163** (Figure 47), firstly UV/Vis and ¹H NMR spectroscopic analysis was carried out.

Figure 47: Photoisomerisation of azo-gabazine **163**.

A UV spectrum of the thermodynamic mixture was taken, which showed characteristic peaks for a *trans* azobenzene-containing compound (Figure 48).¹⁰⁰ These include a large absorbance with λ_{max} of 342 nm describing a π, π^* transition. After 30 seconds of irradiation from a hand-held torch containing LEDs of 365 nm wavelength placed on top of the cuvette, a further UV spectrum was taken immediately. This was now characteristic of a *cis* azobenzene-containing compound, with an increase in absorbance at 435 nm, describing an n, π^* transition (Figure 48). The cuvette was left in the dark for a further twelve minutes, with UV spectra taken every four minutes.

The UV spectra of these were identical to the spectrum acquired immediately after irradiation.

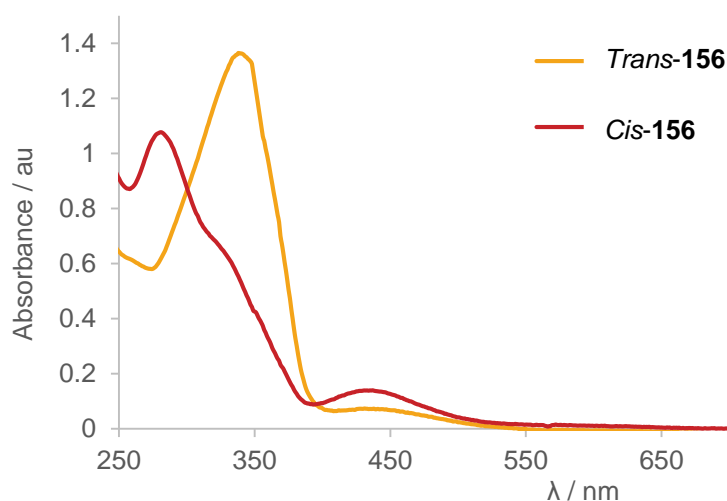


Figure 48: UV/Vis spectrum of azo-gabazine **163** pre- and post- irradiation; $c = 5.5 \times 10^{-5} \text{ mol dm}^{-3}$.

Secondly, for ^1H NMR analysis, a solution of **163** (10 mM in DMSO- d_6) was diluted ten-fold with deuterium oxide, to give a clear yellow 1 mM solution, which was ascertained to be the minimum concentration necessary to allow for defined 600 MHz ^1H NMR signals for the minor isomer. In order to crudely replicate the set-up of electrophysiology experiments and to achieve effective sample irradiation, an LED was clamped just above a 0.7 mL droplet of the 1 mM solution as it rested on a square of laboratory film. After irradiation the sample was transferred via syringe to an NMR tube, which was then placed onto the carousel and loaded into the NMR machine by the automaton. In general the NMR tube was in ambient light for around 20 seconds before reaching the darkness inside the instrument, and a complete spectrum was obtained in around 4 minutes.

By comparing integration for non-overlapping ^1H NMR signals for each isomer a *trans* : *cis* ratio was calculated. It became clear that the *trans* : *cis* resting point in ambient light was solvent dependent, and that it could take up to 1 h for this ratio to

equilibrate. The isolated material, previously concentrated *in vacuo* from methanol, formed a 92:8 ratio initially in DMSO-*d*₆, but this relaxed to 75:25 under ambient light in less than an hour. Addition of sodium chloride to the sample did not change the *trans* : *cis* ratio.

Five different LEDs were used, with wavelengths of 365, 405, 470, 530 and 565 nm and the percentage of *cis* isomer was ascertained after 2, 10, 60 and 300 seconds of irradiation (Figure 49).

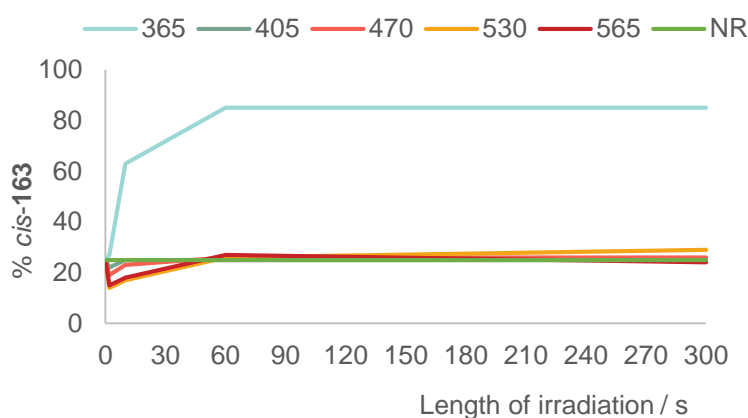


Figure 49: Graph showing percentage *cis* isomer after *t* seconds of irradiation with LEDs with different wavelengths. NR: non radiated sample.

Pleasingly after just two seconds of irradiation with the 365 nm LED, a large percentage of *cis* isomer was obtained, and an 80% *cis* enriched photostationary point was reached in under 60 seconds. This was illustrated clearly in the ¹H NMR analysis of the aromatic region of the spectra (Figure 50).

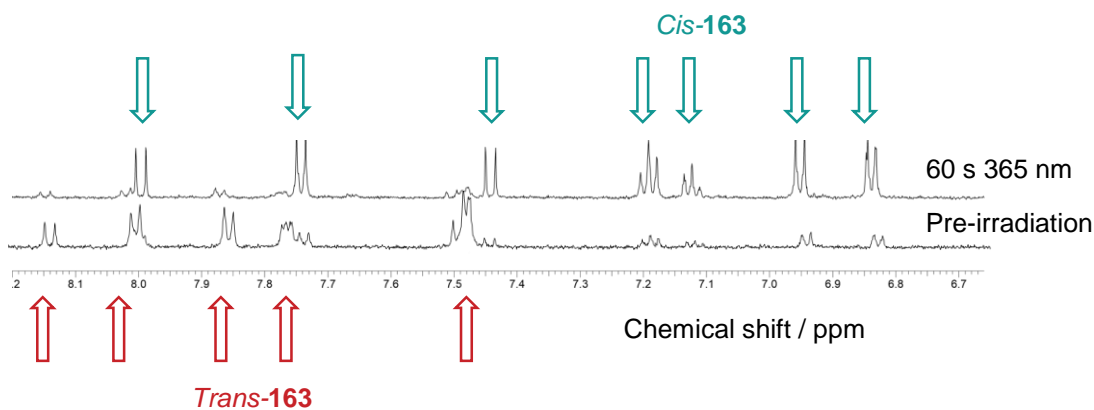


Figure 50: ¹H NMR spectroscopic analysis of aromatic region of **163** spectrum showing signals arising from formation of majority *cis*-**163** photostationary state from a *trans*-rich mixture, upon irradiation with 365 nm light for 60 s.

Disconcertingly at first, none of the other LEDs appeared to change the ratio at all, and indeed it appeared that two seconds of irradiation decreased the percentage of *cis* isomer more than a longer irradiation time for 470, 530 and 565 nm LEDs (Figure 47). This was due to the fact that the time spent in ambient light, though only seconds, was deemed enough to convert the mixture to its ambient *cis* : *trans* resting ratio of around 25:75 in DMSO:H₂O. Greater conversion to *trans* isomer (99%) was seen when additional steps were taken to ensure that the sample was in ambient light for less than two seconds, with the removal of a shield for the NMR tube removed moments before it was entered into the NMR machine. This was also true when applied after UV light irradiation, with the *cis* isomer reaching 91% after 60 s of illumination. This is in line with current literature protocols, which suggests constant illumination during spectrum acquisition.¹⁰¹ Unfortunately, equipment limitations meant this was unfeasible for us at this time.

In order to observe thermal relaxation from *cis*-**163** to *trans*-**163**, a UV irradiated and a sample that had equilibrated at an 80:20 ratio in ambient light were placed in darkness, with a ¹H NMR taken after 0.5, 1.5, 6 and 24 hours (Figure 51). The thermal relaxation for both was observable, but slow. In contrast, relaxation of a UV irradiated

sample to the ambient photostationary state, if left in ambient light, took only six hours.

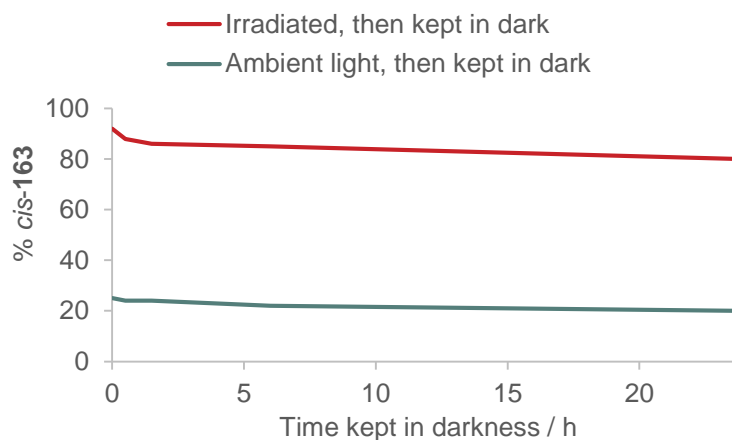


Figure 51: Relaxation of *cis* isomer to *trans* isomer in dark conditions over time after 60 s 365 nm irradiation.

A ¹H NMR spectrum of both samples after ten days in the dark showed a decrease in *cis* isomer from 95 to 46% in the irradiated sample, and from 25 to 0% *cis* in the non-irradiated sample. After fourteen days kept in the dark, the irradiated sample had also converted to 99% the thermodynamic *trans* isomer.

These UV/Vis and ¹H NMR spectroscopy results combine to show that azo-gabazine **163** does undergo robust photoswitching with these LEDs, and provides a foundation for biological testing experiments.

5.4 Biological evaluation and azo-gabazine photoswitching in cells

With the knowledge that *cis* and *trans* isomerisation could be efficiently induced with our LEDs, the compound was taken onto a biological system, and tested for potency on $\alpha 1\beta 2\gamma 2$ GABA_A receptors expressed in HEK293 cells (Figure 52). Work by Dr Martin Mortensen in the Smart group showed azo-gabazine **163** to be a very potent antagonist for the receptor, with an IC₅₀ of 12.2 nM at ambient light; similar to the

benzoxy gabazine analogue **28** (IC₅₀ = 11 nM), and also over ten times more potent than gabazine **4**.

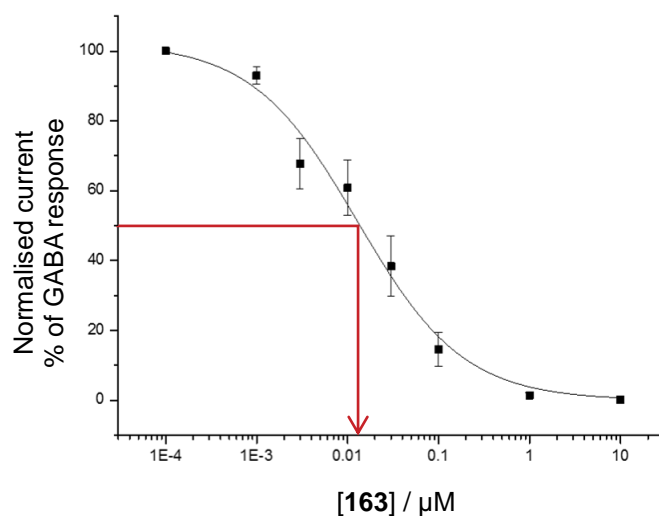


Figure 52: Dose response curve for azo-gabazine **163**, giving an IC₅₀ of 12.2 nM.

Experiments to investigate the antagonist properties of azo-gabazine **163** under different wavelengths of light were carried out by Dr Martin Mortensen, firstly in synaptic GABA_A receptors comprised of $\alpha 1\beta 2\gamma 2\text{S}$ subunits expressed in HEK293 cells. Azo-gabazine was applied to the cell along with GABA, and the current across the membrane was measured by whole cell patch clamping. Application of 365 nm light elicits a large GABA response suggesting the *cis* isomer is a less potent antagonist, and azo-gabazine in this conformation allows more GABA into the binding site to activate the receptor. However, it also appears in the first instance that irradiation with 470 nm light elicits a lesser response, but in the same direction. This could suggest that the act of switching *cis* to *trans* also frees the binding site momentarily to allow an influx of GABA and consequently hyperpolarises the membrane (Figure 53).

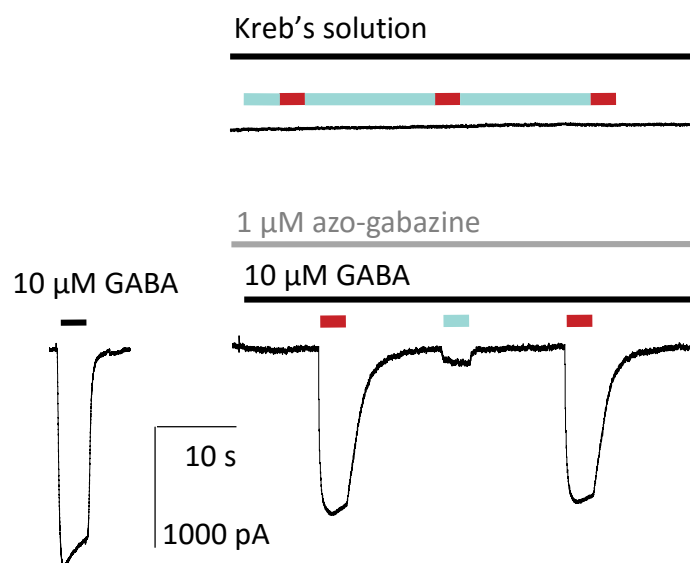


Figure 53 Whole cell patch clamp recordings of GABA_A receptors expressed in HEK293 cells and tested with *cis*- and *trans*-**163**.¹⁰²

It was shown that azo-gabazine **163** could indeed be used as a photoswitch, to activate these expressed GABA_A receptors in cycles when alternately irradiated with 470nm light and 365 nm light, shown as blue and purple bars respectively in Figure 54.

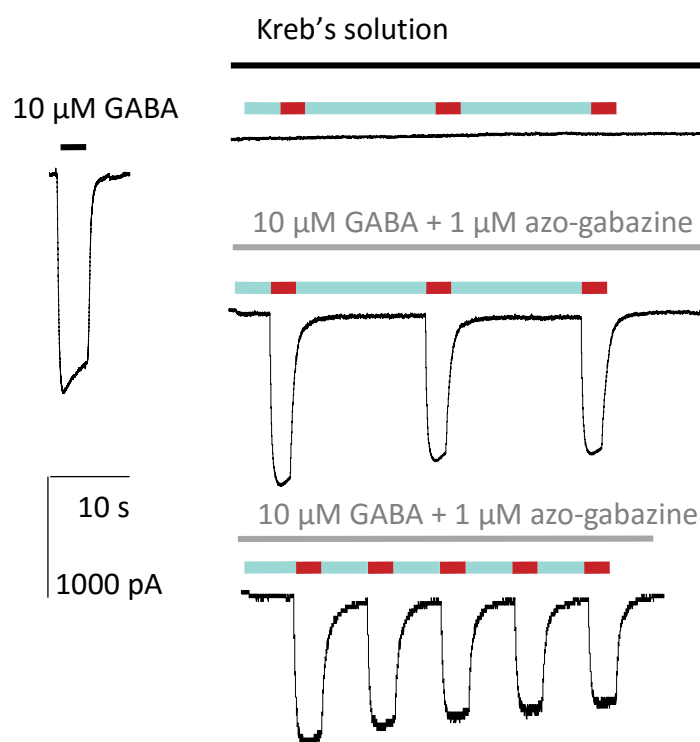


Figure 54: Photoswitching in three different GABA_A receptors expressed in HEK293 cells.¹⁰²

With these experiments demonstrating that alternating between 470 nm and 365 nm light produces cycles of GABA receptor activation, azo-gabazine was taken onto cerebellar granule cells. These were treated with CNQX and AP5 to block excitatory post synaptic currents, and underwent whole cell patch clamp recording. Spontaneous inhibitory post synaptic currents (sIPSCs) were apparent, arising from the action of endogenous GABA on the receptors, but these were inhibited upon perfusion with the azo-gabazine antagonist **163**, including in the presence of 470 nm light – as expected. Irradiation with 365 nm light restored the sIPSCs. Once the perfusion was stopped, sIPSCs were reinstated (Figure 55).

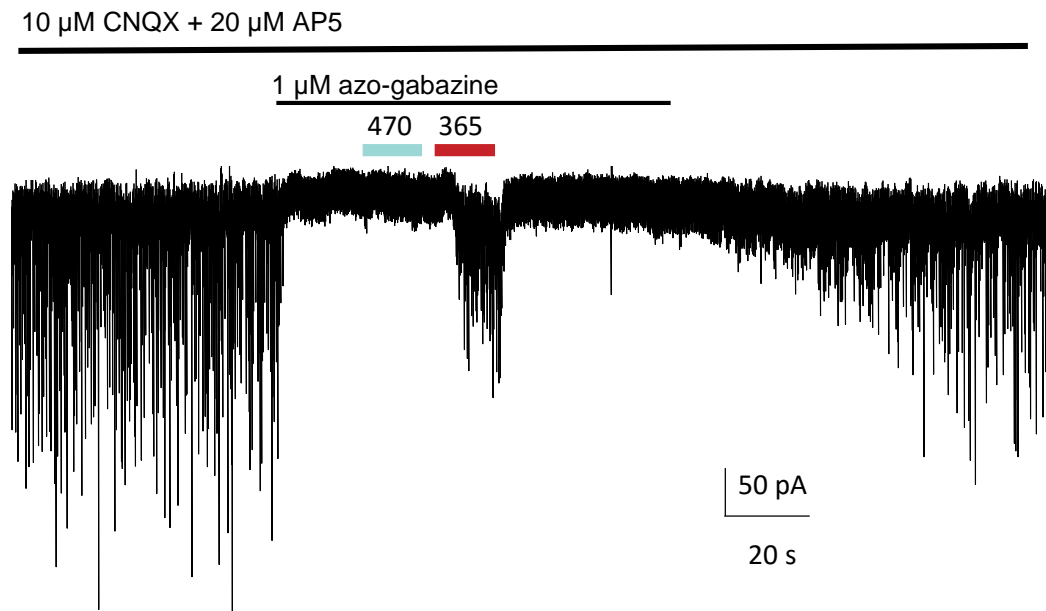


Figure 55: Photoswitchable GABA_A receptors in cerebellar granule cells.

Currently further work in the Smart group is ongoing to include spatial control of photoswitching, by irradiating a neuron at different points, for example on the soma or along the dendrites. Any differences in intensity of the sIPSCs during UV irradiation between the two areas could give valuable information about the distribution of GABA_A receptors, and how each area recovers from receptor blockage.

5.5 Conclusions

This chapter describes how the replacement of a benzylphenyl ether with an azobenzene moiety in a potent GABA_A receptor antagonist created a photoswitchable ligand for the GABA_A receptor. This promising ligand was used to reversibly unblock GABA_A receptors in recombinant cells as well as live neurons. Azo-gabazine **163** is currently undergoing further experiments in cells, which will demonstrate the power of being able to switch on neuronal inhibition with spatial and temporal control.

Conclusions

This thesis has shown the development of a range of small molecule chemical probes to elucidate the mechanisms of GABA_A receptor movement. Quantum dots were photocrosslinked to GABA_A receptors, via a highly functionalised small molecule. These constructs were followed as they moved in the membrane of live neuronal cells (Figure 56). This revealed free diffusion of GABA_A receptors in extrasynaptic sites, and more constrained movement of GABA_A receptors in the synaptic cleft.

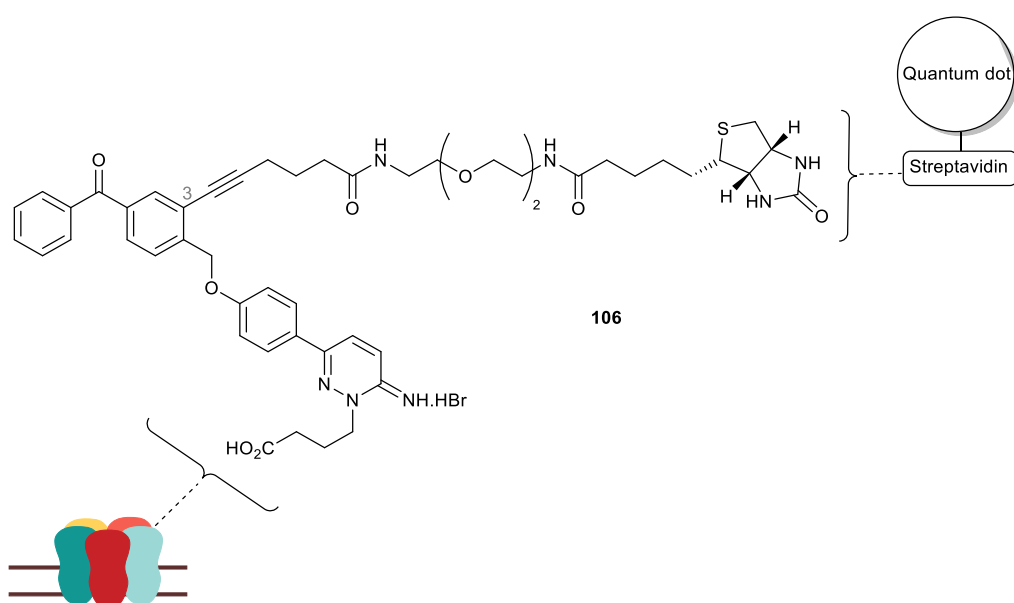


Figure 56: A photoaffinity labelled probe for the GABA_A receptor

An assay was developed and tested for a small number of potential aryl ketone photoaffinity labels. The products of an irradiation of benzophenone in the presence of amino acids were isolated and analysed. An unreliable link between UV spectrum absorbance and H-abstraction ability was highlighted, as even after the assay, benzophenone remained the front runner in ability to form photoadducts.

A photocleavable chemical probe was also designed, in order to track unblocked GABA_A receptors in live cells. To this end a modular synthetic ethos was developed,

providing methodology for the rapid turnover of various characteristics required in the search for an optimised chemical probe (Figure 57).

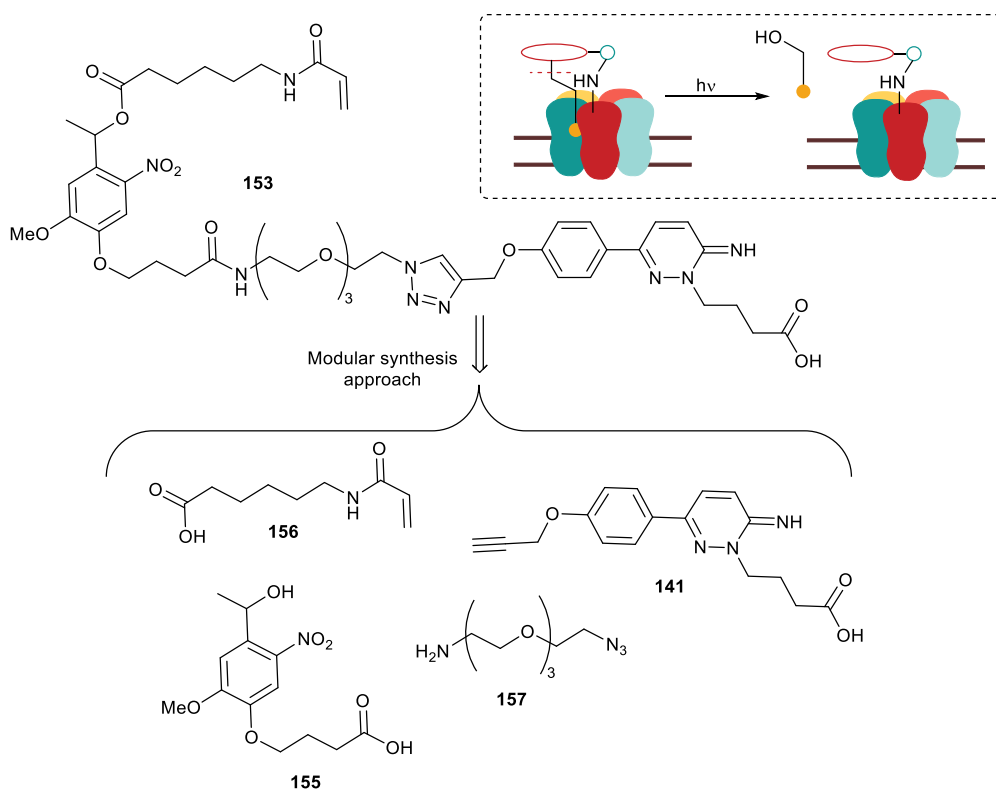


Figure 57: Photocleavable antagonist for the GABA_A receptor

This thesis also describes the synthesis of photoswitchable GABA_A receptors, through the development of an azobenzene molecule with high affinity for the receptor. This photoswitching has been shown both in recombinant cells as well as in live neuronal cultures (Figure 58).

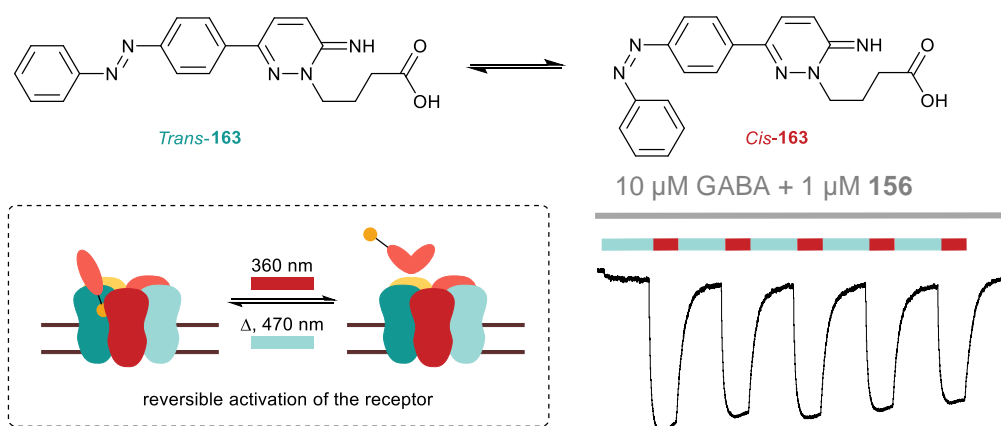


Figure 58: Photoswitchable antagonist **163** for the GABA_A receptor.

Future work

Photocleavable fluorescent probes for tracking the GABA_A receptor

A further iteration on the design for a photocleavable antagonist (Chapter 4) could be the addition, not only a fluorescent probe to track the receptors, but one which would be photoactivatable. Upon irradiation with low intensity 407 nm light, azido-2-dicyanomethylene-3-cyano-2,5-dihydrofuran (Azido-DCDHF, **174**) converts to the fluorescent **175** (Figure 59).^{103,104} This would allow the single-molecule tracking of bound, unblocked receptors. Spot photolysis at particular points on the membrane would release ligands just from this area, and trigger a fluorescent response just from specific populations of GABA_A receptors. From this the number of GABA_A receptors at certain points could be quantified, and the dispersal of the fluorescence would give information about how the receptors move.

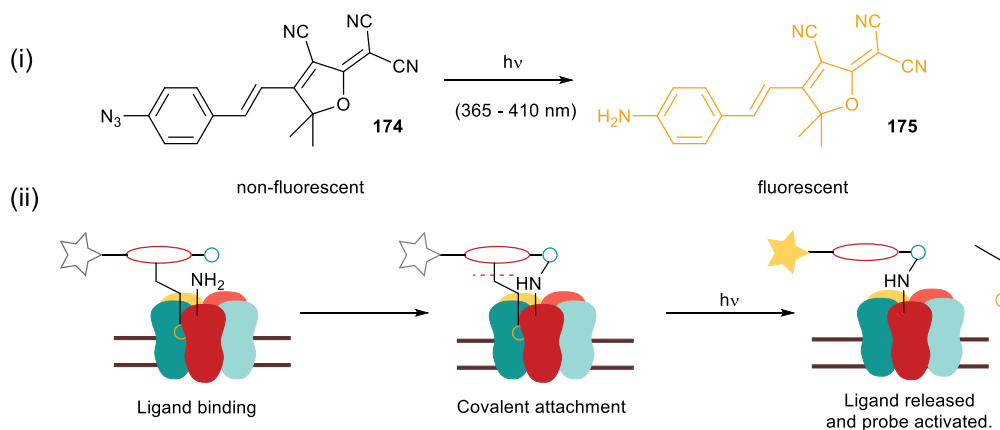


Figure 59: (i) Azido-DCDHF **174** photoconverts to the fluorescent DCDHF **175**; (ii) General mechanism showing spatial control of fluorescence in cells.

“Turn on” fluorescent affinity labels for the GABA_A receptor

Another method to label and track receptors, could be to use the affinity properties of the ligand itself to ‘turn on’ fluorescence. Yamaguchi *et al.* describe the synthesis of an small bifunctional chemical probe, bearing a ligand bound to a non-fluorescent O-

nitrobenzoxadiazole unit **176**. Upon ligand-target interaction, a nearby lysine residue irreversibly binds, forming a fluorescent monoalkylamino-nitrobenzoxadiazole species **177** and releasing the ligand from the binding site (Figure 60).

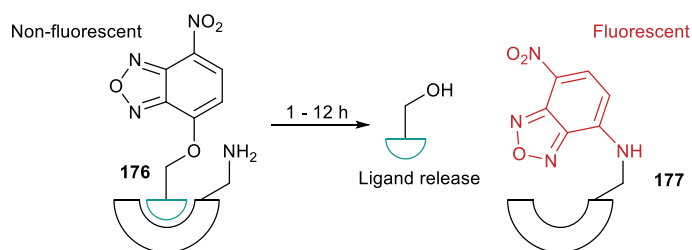


Figure 60: General mechanism for “turn-on” fluorescent affinity labelling.

It was shown that that, with a biotin ligand and linker lengths of over 11.9 Å, their O-nitrobenzoxadiazole probe was very selective for the lysine residue, K-111, on avidin, even in the presence of lysine-rich bovine serum albumin and a whole cell lysate, HL-60, which contains many non-target proteins. The group also synthesised an O-nitrobenzoxadiazole derivative **178** of *N,N*-dialkyl-2-phenylindol-3-ylglyoxylamide **179**, which is a recently developed ligand for the translocator protein and peripheral-type benzodiazepine receptor, TSPO, found in the outer mitochondrial membrane (Figure 61). Interestingly here, it was the partner protein of TSPO, a voltage dependent anion channel which was labelled, reflecting its relative abundance of available lysine residues, and giving the location of the binding site as where these two proteins meet.¹⁰⁵

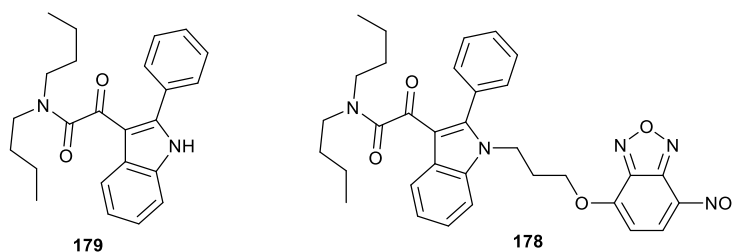


Figure 61: Bifunctional probes for turn-on fluorescent labelling.

With its focus on generating small, highly functionalised chemical probes to follow receptors, an approach such as above has many merits. Any fluorescence of monoalkylamino-compounds originates from tagged proteins, from which the ligand is displaced. Although this strategy relies somewhat on available lysine residues, a correct linker length between ligand and probe can make a compound, such as **180**, specific to certain GABA_A receptors, and even to certain α and β subunits (Figure 62).

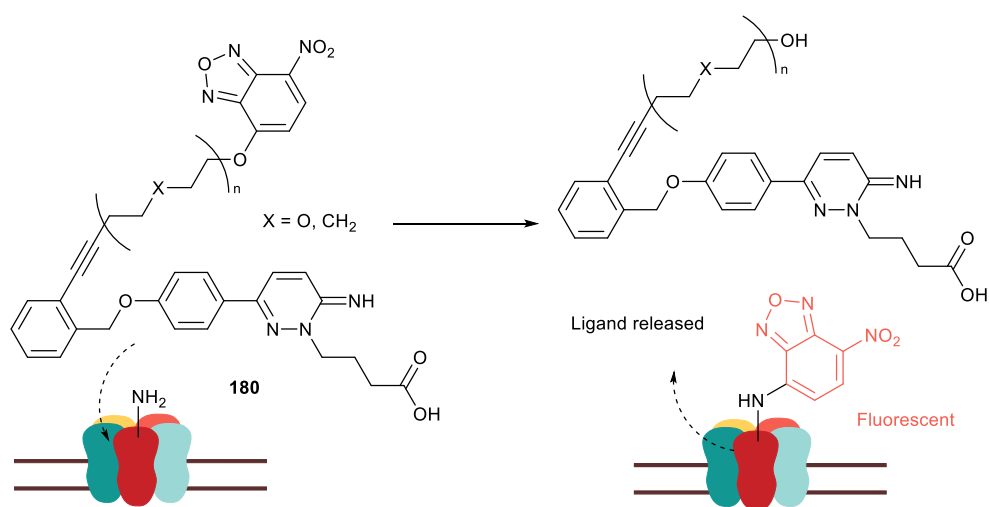


Figure 62: Potential affinity probe for the GABA_A receptor.

Future perspectives for tracking the GABA_A receptor

There are many small molecular probes for the GABA_A receptor which could be envisaged. These, for example, could include chemical probes which themselves change as a bound GABA_A receptor experiences different stimuli. It could be a probe targeting GABA_A receptors alongside a complementary probe targeting a different protein and could potentially show interactions between the receptor and the membrane.

Photoswitchable ligands show the use of molecular mechanics in controlling receptors, and inspiration for future molecular machines could come from the

mechanical proteins which exist in the biological GABA_A receptor trafficking system: transporters, filaments, scaffolding proteins and even organelles.

Work to discover more about how receptors and membrane proteins work together to respond and adapt to chemical and electrical stimuli is still only just beginning. Just last year, the first crystal structure of a GABA_A receptor was published.¹⁰⁶ This, alongside existing homology modelling, can now be used in the design of chemical probes, particularly helpful for those which rely upon particular residues for affinity labelling. Elucidation of working biological systems is also advancing due to progresses being made in imaging, in particular two-photon excitation microscopy. The dysfunction of GABA-mediated inhibition is implicated in many diseases, and progression in medicinal chemistry will continue to accelerate as GABA_A receptor trafficking is further understood, and perhaps new proteins are highlighted as drug targets.

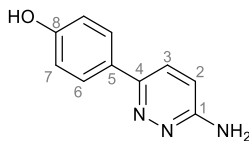
General experimental

All reactions were carried out at atmospheric pressure with stirring unless otherwise stated. All reagents and solvents were purchased from suppliers and used without further purification unless otherwise stated. *N*-Bromosuccinimide was recrystallised from water prior to use. Photoreactions were carried out in pyrex immersion well (Photochemical Reactors Ltd), which was cooled via running water, and irradiated with a 125 W, medium pressure mercury lamp (Photochemical Reactors Ltd). All reactions were monitored by TLC or ^1H NMR as stated. TLC plates pre-coated with silica gel 60 F254 on aluminium (Merck KGaA) were used, being visualized by UV (254 or 365 nm) or chemical stain (KMnO_4 , I_2 , ninhydrin). Normal phase silica gel (BDH) was used for flash chromatography and the eluting solvent or solvent gradient given. ^1H NMR and were recorded at 500 or 600 MHz and ^{13}C NMR spectra were recorded at 125 or 150 MHz on a Bruker AMX500 or AMX600-cryoprobe respectively, at ambient temperature, unless otherwise stated; all chemical shifts are measure in ppm and referenced to the residual proton impurity of the deuterated solvent. The multiplicity of the signal is indicated as s (singlet), d (doublet), t (triplet), dd (doublet of doublets), dt (doublet of triplets), quint (quintet) or a m (multiplet) which is defined as all signals where overlap or complex coupling makes definitive descriptions of peaks difficult. All peaks should be taken as sharp unless otherwise described. Coupling constants are defined as J given in Hz. For NMR experiments, CDCl_3 denotes deuterated (d_3) chloroform, DMSO denotes deuterated (d_6) dimethylsulfoxide, and CD_3OD denotes deuterated (d_4) methanol. Deuterated solvents were chosen according to the position of solvent peak in spectra and solubility of substrate. High and low resolution mass spectrometry was performed using a VG70 SE operating in modes CI, EI, ES and FAB. Infrared spectra were obtained on a Perkin

Elmer Spectrum 100 ATR FTIR Spectrometer or a Bruker Alpha Platinum ATR FT-IR spectrometer. Melting points were measured with a Gallenkamp apparatus and given with recrystallisation solvent where appropriate. Room temperature (rt) is defined as between 19-22 °C. *In vacuo* is used to describe solvent removal by rotary evaporation between 20 °C and 60 °C, at approximately 10 mmHg unless otherwise stated. The term “dried” refers to the process of adding then filtering away solid magnesium sulfate or sodium sulfate from an organic solvent to remove trace amounts of water. The term ‘degassed’ refers to the process of removing oxygen from a solution by bubbling argon through the solution prior to use. Microwave irradiation was carried out in a CEM 150W microwave reactor.

Experimental

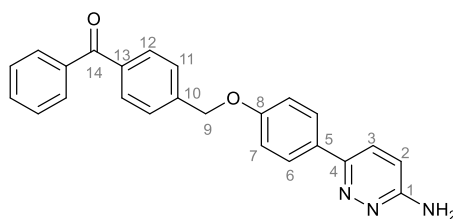
5-(1-Amino-pyridazin-4-yl)-phenol, **31**.³⁰



Method A: A microwave vial containing 4-hydroxyphenylboronic acid **32** (163 mg, 1.26 mmol), 3-amino-6-chloropyridazine **33** (102 mg, 0.74 mmol), Pd(PPh₃)₂Cl₂ (27 mg, 0.04 mmol) and K₂CO₃ (202 mg, 1.46 mmol) in MeCN (2.0 mL) and H₂O (1.3 mL) was degassed for 5 min, then irradiated for 10 min at 120 °C. The reaction mixture was diluted with H₂O (50 mL), then extracted with EtOAc (3×100 mL). The combined organic layers were washed with brine (100 mL), dried and concentrated *in vacuo*. Purification via flash column chromatography (EtOAc) gave **31** (81 mg, 58%) as a white solid.

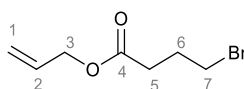
Method B: 4-Hydroxyphenylboronic acid **32** (1.00 g, 7.25 mmol), 3-amino-6-chloropyridazine **33** (817 mg, 6.30 mmol) and Pd(PPh₃)₂Cl₂ (221 mg, 0.32 mmol) were added sequentially to degassed 1,4-dioxane (50 mL) and stirred at rt for 10 min. Degassed 1 M aqueous Na₂CO₃ (18.9 mL) was added and the reaction mixture was heated rapidly to reflux for 16 h. The resulting mixture was then concentrated *in vacuo*. Purification via flash column chromatography (EtOAc : CH₃OH, 50:1) gave **31** (659 mg, 56%) as a white solid.

δ_{H} (500 MHz, CD₃OD) 6.87 (2H, d, *J* 8.8, 2×C(7)H), 6.97 (1H, d, *J* 9.5, C(2)H), 7.70 (1H, d, *J* 9.5, C(3)H), 7.71 (2H, d, *J* 8.8, 2×C(6)H), δ_{C} (125 MHz, CD₃OD); 116.6 (C(7)H), 117.6 (C(2)H), 128.0 (C(3)H), 128.6 (C(6)H), 129.3 (C(5)), 153.1 (C(4)), 159.7 (C), 160.6 (C); ν_{max} (ATR) 3463, 3326, 3200, 1628, 1605, 1458; mp (PhMe) 262-263 °C {lit:³⁰ 250-252 °C}; *m/z* (EI⁺) 187 (100%, [M]⁺); HRMS (EI) C₁₀H₈N₃O⁺ ([M-H]⁺) requires 186.06619, measured 186.06679.

(4-((4-(6-aminopyridazin-3-yl)phenoxy)methyl)phenyl)(phenyl)methanone, 41.⁷⁰

To a solution of KO^tBu (197 mg, 1.76 mmol) and 18-crown-6 (10 mg, 0.04 mmol) in DMF (15 mL) was added a solution of alcohol **31** (300 mg, 1.60 mmol) in DMF (15 mL) at 0 °C and the reaction mixture was stirred at 0 °C for 20 min. (4-Bromomethylphenyl)(phenyl)methanone **40** (485 mg, 1.76 mmol) was added in one portion and the reaction was allowed to warm to rt and stirred for 16 h. The reaction mixture was partitioned between saturated aqueous LiCl (50 mL) and EtOAc (200 mL). The aqueous layer was extracted with EtOAc (3×100 mL) and the combined organic layers were dried and concentrated *in vacuo*. Purification via flash column chromatography (EtOAc) gave **41** (266 mg, 44%) as a white solid.

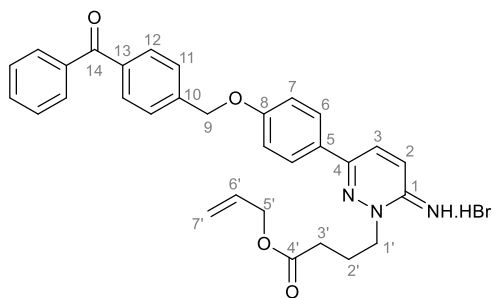
δ_{H} (500 MHz, DMSO-*d*₆) 5.29 (2H, s, C(9)H₂), 6.36 (2H, s, NH₂), 6.82 (1H, d, *J* 9.1, C(2)H), 7.12 (2H, d, *J* 9.1, 2×C(7)H), 7.56 (2H, t, *J* 7.7, 2×*o*-PhH), 7.63-7.70 (3H, m, C(3)H, 2×C(11)H), 7.72-7.79 (5H, m, C(2)H, 2×*m*-PhH, 2×C(12)H), 7.91 (2H, d, *J* 9.1, C(6)H); δ_{C} (125 MHz, DMSO-*d*₆) 68.6 (C(9)H₂), 114.3 (C(2)H), 115.0 (C(7)H), 124.9 (CH), 126.7 (CH), 127.4 (C(3)H), 128.6 (C(11)), 129.6 (CH), 129.9 (CH), 130.1 (C), 132.7 (C), 136.4 (C), 137.0 (C), 142.0 (C), 149.6 (C), 158.4 (C), 159.5 (C), 195.5 (C(1)); ν_{max} (solid) 3307, 3053, 2917, 2873, 2849, 1645; mp (PhMe) 200-203 °C ; *m/z* (ES⁺) 382 (100%, [M+H]⁺), HRMS (ES⁺) C₂₄H₂₀N₃O₂⁺ ([M+H]⁺) requires 382.1556, measured 382.1551.

Allyl 4-bromobutyrate.¹⁰⁷

4-Bromobutyryl chloride (2.00 mL, 17.3 mmol) was added dropwise to allyl alcohol (6.00 mL, 138 mmol) at 0 °C over 2 h and the resulting mixture stirred at rt for a further 4 h. Excess allyl alcohol was removed *in vacuo* and the residue was redissolved in CH₂Cl₂ (50 mL), washed with saturated aqueous NaHCO₃ (50 mL) and brine (50 mL), dried and concentrated *in vacuo* to give allyl 4-bromobutyrate (3.17 g, 89%) as a colourless oil.

δ_{H} (600 MHz, CDCl₃) 2.18 (2H, quin, J 7.2, C(6)H₂), 2.53 (2H, t, J 8.0, C(5)H₂), 3.46 (2H, t, J 7.5, C(7)H₂), 4.59 (2H, dd, J 6.0, 1.1, C(3)H₂), 5.24 (1H, d, J 10.5, C(1)H_A), 5.32 (1H, d, J 17.3, C(1)H_B), 5.87-5.95 (1H, m, C(2)H); δ_{C} (150 MHz, CDCl₃) 27.8 (C(6)H₂), 32.5 (CH₂), 32.8 (CH₂), 65.4 (C(3)H₂), 118.5 (C(1)H₂), 132.1 (C(2)H), 172.3 (C(4)); m/z (CI⁺) 209 (90%, [⁸¹M+H]⁺), 207 (100%, [⁷⁹M+H]⁺).

Allyl 4-(3-(4-((4-benzoylbenzyl)oxy)phenyl)-6-iminopyridazin-1(6H)-yl)butanoate hydrobromide, **80.**⁷⁰

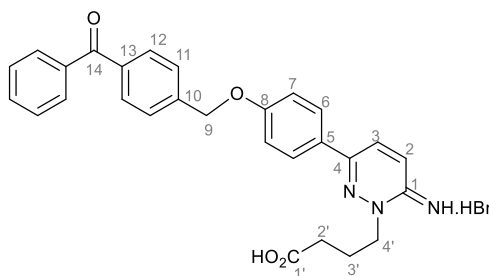


A reaction mixture of allyl 4-bromobutyrate (97 mg, 0.47 mmol) and pyridazine **41** (120 mg, 0.31 mmol) in DMF (0.4 mL) was heated to 80 °C for 16 h. The product precipitated upon addition of cold EtOAc (3 mL) and filtered to give **80** (135 mg, 85%) as a grey solid.

δ_{H} (500 MHz, CD₃OD:CDCl₃, 1:1) 2.25 (2H, quint. J 6.9, C(2')H₂), 2.59 (2H, t, J 6.8, C(3')H₂), 4.42, (2H, t, J 7.1, C(1')H₂), 4.50 (2H, d, J 5.7, C(5')H₂), 5.16 (1H, dd, J 10.6, 1.1, C(7')H_A), 5.24 (1H, dd, J 17.0, 1.4, C(7')H_B), 5.26 (2H, s, C(9)H₂), 5.81 (1H,

ddt, J 17.0, 10.6, 5.7, C(6' H), 7.12 (2H, d, J 8.8, 2×C(7) H), 7.48 (2H, t, J 7.3 2× o -Ph H), 7.56-7.63 (3H, m, p -Ph H , 2×C(11) H), 7.66 (1H, d, J 9.8 C(3) H), 7.75 (2H, d, J 7.3, 2× m -Ph H), 7.80 (2H, d, J 8.2, 2×C(12) H), 7.88 (2H, d, J 9.1, 2×C(6) H), 8.19 (1H, d, J 9.8 C(2) H); δ_C (125 MHz, CD₃OD:CDCl₃, 1:1) 22.8 (C(2')H₂), 31.5 (C(3')H₂), 57.0 (C(1')H₂), 67.0 (C(5')H₂), 70.7 (C(9)H₂), 117.0 (C(7)H), 119.7 (C(7')H₂), 126.6 (C), 127.0 (C(3)H), 128.4 (C(11)H), 129.6 (CH), 129.7 (CH), 131.1 (CH), 131.7 (CH), 132.8 (CH), 133.0 (CH), 134.1 (p -PhH), 138.4 (C), 138.7 (C), 142.9 (C), 152.1 (C), 162.5 (C), 174.1 (C(14)), 198.6 (C(1)); ν_{\max} (solid) 3218, 3019, 1735, 1651, 1607, 1581, 1536, 1510; mp 210-214 °C; m/z (ES⁺) 508 (90%, [M+H]⁺), 351 (100%, [M-C₆H₈O₂]⁺); HRMS C₃₁H₃₀N₃O₄⁺ ([M+H]⁺) requires 508.2236, measured 508.2236.

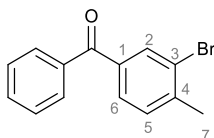
4-(3-(4-((4-benzoylbenzyl)oxy)phenyl)-6-iminopyridazin-1(6H)-yl)butanoic acid hydrobromide, 39.



To a mixture of **80** (121 mg, 0.238 mmol) and DMBA (376 mg, 2.38 mmol) in degassed CH₂Cl₂ (2.5 mL) was added Pd(PPh₃)₄ (23 mg, 0.02 mmol). The reaction mixture was stirred at 35 °C for 3 h in the dark. The resulting mixture was partitioned between CH₂Cl₂ (10 mL) and saturated aqueous NaHCO₃ (10 mL). The aqueous layer was extracted with CH₂Cl₂ (2×30 mL), and the combined organic layers were washed with brine (30 mL) then dried and concentrated *in vacuo*. Purification via flash column chromatography (CHCl₃: CH₃OH, 10:1) gave **39** (53 mg, 41%) as a white solid.

δ_{H} (500 MHz, CDCl_3 : CD_3OD , 1:1) 2.04-2.12 (2H, m, $\text{C}(3')\text{H}_2$), 2.32-2.36 (2H, m, $\text{C}(2')\text{H}_2$), 3.28-3.31 (2H, m, $\text{C}(4')\text{H}_2$), 5.25 (2H, s, $\text{C}(9)\text{H}_2$), 7.11 (2H, d, J 8.8, $2\times\text{C}(7)\text{H}$), 7.48 (2H, d, J 7.8, $2\times m\text{-PhH}$), 7.56-7.62 (4H, m, $\text{C}(3)\text{H}$, $2\times\text{C}(11)\text{H}$, $p\text{-PhH}$), 7.73-7.77 (2H, m, $2\times o\text{-PhH}$), 7.78-7.81 (2H, m, $2\times\text{C}(12)\text{H}$), 7.86 (2H, d, J 8.8, $2\times\text{C}(6)\text{H}$), 8.09 (1H, d, J 9.8, $\text{C}(2)\text{H}$); δ_{C} (125 MHz, CDCl_3 : CD_3OD , 1:1) 23.8 ($\text{C}(3')$), 32.8 ($\text{C}(2')$), 57.9 ($\text{C}(4')$), 69.1 ($\text{C}(9)\text{H}_2$), 116.9 (CH), 126.7 (CH) 126.8 (C), 128.4 (CH), 129.5 (CH), 129.7 (CH), 131.3 (CH), 131.7 (CH), 132.5 (CH), 134.2 (CH), 138.4 (C), 138.6 (C), 143.0 (C), 151.7 (C), 153.6 (C), 162.3 (C), 179.5 ($\text{C}(14)$), 198.6 ($\text{C}(1)$); ν_{max} (solid) 3340 (O-H), 2935, 1738, 1650 (C=O), 1609, 1567, 1535, 1510; mp 234 °C; m/z (ES^+) 468 (100%, $[\text{M}+\text{H}]^+$); HRMS (ES^+) $\text{C}_{28}\text{H}_{26}\text{N}_3\text{O}_4^+$ ($[\text{M}+\text{H}]^+$) requires 468.1923, measured 468.1945.

(3-Bromo-4-methylphenyl)(phenyl)methanone, **84.**¹⁰⁸

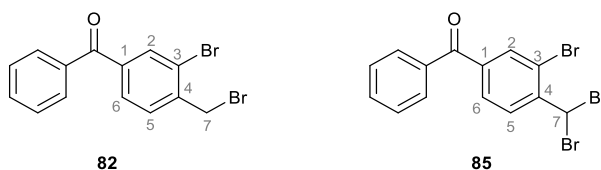


Thionyl chloride (5 mL) was added dropwise to 3-bromo-4-methylbenzoic acid **83** (1.00 g, 4.65 mmol) and stirred at rt for 2 min. The reaction mixture was then heated to reflux and stirred for 2 h. The reaction mixture was cooled to rt, concentrated *in vacuo*, and the residue was redissolved in benzene (5 mL). A solution of AlCl_3 (0.7 g) in benzene (5 mL) was then added dropwise and the reaction mixture was heated to 50 °C for 3 h. The resulting mixture was washed with 3 M aqueous HCl (25 mL) and brine (25 mL), dried and concentrated *in vacuo*. Purification via flash column chromatography (40-60 °C petrol: Et_2O , 10:1) gave **84** (676 mg, 53%) as a white crystalline solid.

δ_{H} (500 MHz, CDCl_3) 2.49 (3H, s, C(7) H_3), 7.35 (1H, d, J 7.6, C(5) H), 7.49 (2H, ddt, J 7.9, 7.6, 1.6, 2 \times *m*-Ph H), 7.60 (1H, ddt, J 7.9, 7.6, 1.6, *p*-Ph H), 7.65 (1H, dd, J 7.6, 1.6, C(6) H), 7.78 (2H, ddt, J 7.9, 1.4, 1.4, 2 \times *o*-Ph H), 7.98 (1H, d, J 1.6, C(2) H); δ_{C} (125 MHz, CDCl_3) 23.3 (C(7) H_3), 125.0 (C(3)), 128.5 (*m*-Ph H), 129.1 (C(6) H), 130.0 (*o*-Ph H), 130.7 (C(5) H), 132.7 (*p*-Ph H), 134.0 (C(2) H), 137.0 (C), 137.4 (C), 140.0 (C(4)), 195.1 (C); ν_{max} (solid) 3056, 2567, 1734, 1651, 1593, 1579, 1549; mp 76-77 °C; m/z (EI $^+$) 276 (50%, [^{81}M] $^+$), 274 (51%, [^{79}M] $^+$), 199 (48%, [$^{81}\text{M-C}_6\text{H}_5$] $^+$), 197 (50%, [$^{79}\text{M-C}_6\text{H}_5$] $^+$), 105 (100%, [$\text{M-C}_7\text{H}_6\text{Br}$] $^+$); HRMS (EI) $\text{C}_{14}\text{H}_{11}\text{O}^{79}\text{Br}$ (M^+) requires 273.9988, measured 273.9991.

[(3-Bromo-4-bromomethyl)phenyl](phenyl)methanone 82,^{108,109}

[3-Bromo-4-(di-bromomethyl)phenyl](phenyl)methanone 85.



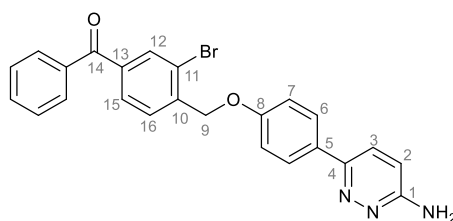
N-Bromosuccinimide (398 mg, 2.23 mmol) and AIBN (48 mg, 0.29 mmol) were added sequentially to benzophenone **84** (614 mg, 2.23 mmol) in benzene (12 mL). The mixture was heated to 80 °C for 16 h, before the reaction solvent was removed *in vacuo*. Purification via flash column chromatography (40-60 °C petrol : Et_2O , 50:1) gave **85** (40 mg, 4%), starting material **84** (101 mg, 16%) followed by **82** (555 mg, 70%).

Data for 85: δ_{H} (500 MHz, CDCl_3) 7.10 (1H, s, C(7) H), 7.51 (2H, t, J 7.6, 2 \times *m*-Ph H), 7.63 (1H, t, J 7.6, *p*-Ph H), 7.78-7.82 (3H, m, C(5) H , 2 \times *o*-Ph H), 7.93 (1H, d, J 1.6, C(2) H), 8.13 (1H, d, J 8.2, C(6) H); δ_{C} (125 MHz, CDCl_3) 38.8 (C(7) H), 119.8 (C), 128.1 (*m*-Ph H), 129.1 (C(5) H), 130.1 (*o*-Ph H), 131.1 (C(6) H), 133.2 (*p*-Ph H), 133.9 (C(2) H), 136.6 (C), 134.0 (C), 143.9 (C), 194.1 (C); ν_{max} 3073, 1735, 1650 (C=O),

1592, 1578, 1551; mp 68-69 °C; m/z (EI⁺) 436 (28%, [^{79,81,81}M]⁺), 432 (86%, [^{79,79,81}M]⁺), 430 (29%, [^{79,79,79}M]⁺), 106 (100%, [M-C₇H₄Br₃]⁺); HRMS (EI) C₁₄H₉OBr₃⁺ (^{79,79,79}M⁺) requires 429.81980, measured 429.81912.

Data for 82: δ_H (500 MHz, CDCl₃) 4.64 (2H, s, C(7)H₂), 7.50 (2H, t, J 7.6, 2 \times *m*-PhH), 7.57 (1H, d, J 7.9, C(5)H), 7.62 (1H, t, J 7.6, *p*-PhH), 7.71 (1H, d, J 7.6, C(6)H), 7.77 (2H, d, J 7.6, 2 \times *o*-PhH), 8.01 (1H, s, C(2)H); δ_C (125 MHz, CDCl₃) 32.4 (CH₂), 124.5 (C(3)), 128.6 (*m*-PhH), 129.4 (C(6)H), 130.1 (*o*-PhH), 131.1 (C(5)H), 133.0 (*p*-PhH), 134.7 (C(2H)), 136.8 (C), 139.2 (C), 141.2 (C(4)), 194.5 (C); ν_{max} (solid) 3057, 1651, 1595, 1579, 1555, 1480; mp 59-60 °C {lit¹⁰⁹ 68-69 °C}; m/z (EI⁺) 356 (6%, [^{81,81}M]⁺), 354 (13%, [^{79,81}M]⁺), 352 (6%, [^{79,79}M]⁺), 276 (37%), 275 (100%), 274 (38%), 273 (97%), 199 (24%, [⁸¹M-C₆H₅Br]⁺), 197 [⁷⁹M-C₆H₅Br]⁺, 105 (50%, [M-C₇H₅Br₂]⁺); HRMS (EI) C₁₄H₁₀OBr₂ (^{79,79}M⁺) requires 351.90929, measured 351.908979.

(4-((4-(6-aminopyridazin-3-yl)phenoxy)methyl)-3-bromophenyl)(phenyl)methanone, 86.

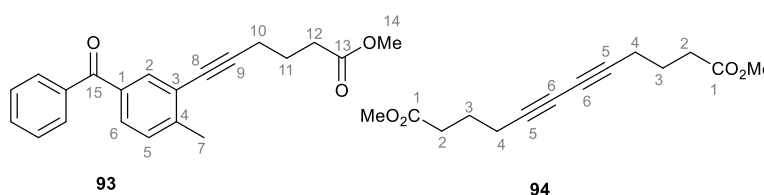


A solution of arylpyridazine **31** (240 mg, 1.28 mmol) in DMF (15 mL) was added to a solution of KO^tBu (172 mg, 1.54 mmol) and 18-crown-6 in DMF (7 mL) at 0 °C and the reaction mixture was stirred at 0 °C for 20 min. Benzophenone **82** (500 mg, 1.41 mmol) was added in one portion and the reaction was allowed to warm to rt over 16 h. The reaction mixture was partitioned between saturated aqueous LiCl (50 mL) and EtOAc (200 mL). The aqueous layer was extracted with EtOAc (3 \times 100 mL) and the combined organic layers were dried and concentrated *in vacuo*. Purification via flash

column chromatography (40-60 °C petrol : Et₂O, 50:1) gave **86** (375 mg, 63%) as a white solid.

δ_{H} (500 MHz, CDCl₃:CD₃OD, 1:1) 5.26 (2H, s, C(9)H₂), 6.96 (1H, d, *J* 9.1, C(2)H), 7.09 (2H, d, *J* 9.0, 2×C(7)H), 7.51 (2H, t, *J* 7.7, 2×*o*-PhH), 7.63 (1H, t, *J* 6.9, *p*-PhH), 7.66 (1H, d, *J* 9.1, C(3)H), 7.71-7.77 (4H, m, 2×*m*-PhH, C(15)H, C(16)H), 7.81 (2H, d, *J* 9.0, 2×C(6)H), 8.00 (1H, d, *J* 1.6, C(12)H); δ_{C} (125 MHz, CDCl₃:CD₃OD, 1:1) 70.5 (C(9)H₂), 115.5 (C(7)H), 116.6 (C(2)H), 122.4 (C), 127.1 (CH), 127.9 (CH), 128.8 (CH), 128.8 (CH), 129.5 (CH), 130.3 (CH), 130.4 (C), 130.5 (C), 133.4 (CH), 134.2 (CH), 137.1 (C), 138.7 (C), 141.2 (C), 159.3 (C), 161.0 (C), 194.4 (C); ν_{max} (ATR) 3200, 3057, 2929, 1657, 1608, 1460; mp 170-172 °C; *m/z* (EI⁺) 461 (49%, [⁸¹M]⁺), 459 (48%, [⁷⁹M]⁺), 275 (35%, [⁸¹M-C₁₀H₈N₃O]⁺), 273 (35%, [⁷⁹M-C₁₀H₈N₃O]⁺), 186 (100%, [M-C₁₃H₁₀BrO]⁺); HRMS (EI) C₂₄H₁₈O₂N₃Br⁺ (⁷⁹M⁺) requires 459.05769, measured 459.05709.

[3-(6'-Methyl hex-5'-ynoate)-4-methylphenyl](phenyl)methanone, 93, and Dimethyl dodeca-5,7-diynedioate, 94.¹¹⁰



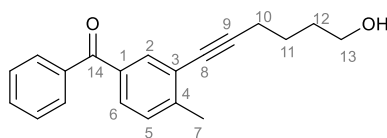
Degassed diethylamine (5 mL) was added to a mixture of **84** (75.0 mg, 0.273 mmol), Pd(PPh₃)₂Cl₂ (18.0 mg, 0.027 mmol) and CuI (5.1 mg, 0.027 mmol). 5-Hexynoic acid methyl ester **50** (51.7 mg, 0.410 mmol) was then added dropwise and the reaction mixture was stirred at 55 °C for 16 h. The reaction solvent was removed *in vacuo* and purification via flash column chromatography (40-60 °C petrol : EtOAc, 50:1) firstly

gave **93** (24 mg, 31%) as a colourless oil, and with further elution gave **94** (12 mg, 23%) as a colourless oil.

Data for 93: δ_{H} (500 MHz, CDCl_3) 1.94 (2H, quint, J 7.2, C(11) H_2), 2.49 (3H, s, C(9) H_3), 2.52 (4H, app q, J 7.2, C(10) H_2 , C(12) H_2), 3.68 (3H, s, C(14) H_3), 7.29 (1H, d, J 8.2, C(5) H), 7.48 (2H, t, J 7.6, 2 \times *m*-Ph H), 7.58 (1H, t, J 7.6, *p*-Ph H), 7.63 (1H, dd, J 7.9, 1.9, C(6) H), 7.75-7.78 (2H, m, 2 \times *o*-Ph H), 7.79 (1H, d, J , 1.6, C(2) H); δ_{C} (125 MHz, CDCl_3) 19.1 (C(12) H_2), 21.1 (C(9) H_3), 24.0 (C(11)), 33.0 (C(10)), 51.7 (C(14) H_3), 79.5 (C(8)), 94.0 (C(9)), 123.9 (C(3)), 128.4 (*m*-Ph), 129.3, 129.5 (C(5) H , C(6) H), 130.0 (*o*-Ph H), 132.4 (*p*-Ph H), 133.7 (C(2) H), 135.2 (C), 137.7 (C), 145.0 (C(4)), 173.6 (C(13)), 196.0 (C(15)); ν_{max} (oil) 3444, 2952, 1736; m/z (EI $^+$) 320 (16%, [M] $^+$), 207 (100%, [M-C $_7$ H $_9$ O $_2$] $^+$), 105 (33%, [M-C $_{14}$ H $_{15}$ O $_2$] $^+$); HRMS (EI) C $_{21}$ H $_{20}$ O $_3$ $^+$ (M $^+$) requires 320.14070, measured 320.14064.

Data for 94: δ_{H} (500 MHz, CDCl_3) 1.84 (4H, quint. J 7.1, 2 \times C(3) H_2), 2.33 (4H, t, J 7.1, 2 \times C(2) H_2), 2.44 (4H, t, J 7.1, 2 \times C(4) H_2), 3.67 (6H, s, 2 \times CH $_3$); δ_{C} (125 MHz CDCl_3) 18.7 (C(4) H_2), 23.5 (C(3) H_2), 32.7 (C(2) H_2), 51.7 (CH $_3$), 66.1 (C(6)), 76.5 (C(5)), 173.5 (C(1)); ν_{max} 3444, 2952, 1736; m/z (EI $^+$) 250 (13%, [M] $^+$), 219 (54%, [M-C $_2$ H $_6$] $^+$), 177 (58%, [M-C $_3$ H $_5$ O $_2$] $^+$), 117 (100%, [M-C $_5$ H $_8$ O $_4$] $^+$); HRMS (EI) C $_{14}$ H $_{18}$ O $_4$ $^+$ (M $^+$) requires 250.11996, measured 250.12030.

[3-(6'-Hydroxyhex-1'-yn-1'-yl)phenyl](phenyl)methanone, **92**.



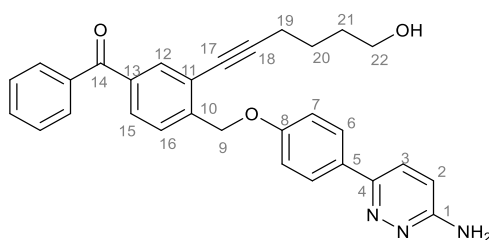
Method A: A solution of aryl bromide **84** (50.0 mg, 0.182 mmol), in degassed Et $_3$ N (2 mL) was treated with 5-hexyn-1-ol (22.0 μ L, 0.200 mmol), Pd(PPh $_3$) $_4$ (4.2 mg, 0.004 mmol) and CuI (1.0 mg, 0.005 mmol) and the reaction mixture was stirred in the dark

at 80 °C for 16 h. The solvent was concentrated *in vacuo* and the resulting residue was treated with saturated aqueous NH₄Cl (5 mL), extracted with Et₂O (3×10 mL) and the combined organic layers were dried and concentrated *in vacuo*. Purification via flash column chromatography (40-60 °C petrol : Et₂O, 1:1) gave **92** (37 mg, 69%) as a yellow oil.

Method B: A solution of aryl iodide **61** (37.0 mg, 0.115 mmol), in degassed Et₃N (2 mL) was treated with 5-hexyn-1-ol (13.9 μL, 0.126 mmol), Pd(PPh₃)₄ (2.7 mg, 0.002 mmol) and CuI (0.7 mg, 0.004 mmol) and the reaction mixture was stirred in the dark at 80 °C for 16 h. The solvent was concentrated *in vacuo* and the resulting residue was treated with saturated aqueous NH₄Cl (5 mL), extracted with Et₂O (3×10 mL) and the combined organic layers were dried and concentrated *in vacuo*. Purification via flash column chromatography (40-60 °C petrol: Et₂O, 1:1) gave **92** (30.2 mg, 90%) as a yellow oil.

δ_{H} (500 MHz, CDCl₃) 1.67-1.79 (4H, m, C(11)H₂, C(12)H₂), 2.49 (3H, s, C(7)H₃), 2.49 (2H, overlapping t, *J* 6.9, C(10)H₂), 3.70 (2H, t, *J* 6.2, C(13)H₂), 7.29 (1H, d, *J* 7.9, C(5)H), 7.47 (2H, t, *J* 7.6, 2×*m*-PhH), 7.58 (1H, t, *J* 7.6, *p*-PhH), 7.62 (1H, dd, *J* 7.9, 1.9, C(6)H), 7.75-7.80 (3H, m, C(2)H, 2×*o*-PhH); δ_{C} (125 MHz, CDCl₃) 19.5 (C(10)H₂), 21.1 (C(7)H₃), 25.1 (C(11)H₂), 32.0 (C(12)H₂), 62.5 (C(13)H₂), 79.0 (C), 95.1 (C), 124.1 (C), 128.4 (CH), 129.2 (C(6)H), 129.6 (C(5)H), 130.0 (CH), 132.4 (*p*-PhH), 133.7 (C(2)H), 135.2 (C), 137.7 (C), 145.0 (C), 196.1 (C(14)); ν_{max} (oil) 3388, 3060, 2930, 2227, 1654, 1597, 1578; *m/z* (EI⁺) 292 (51%, [M]⁺), 105 (100%, [M-C₁₃H₁₅O]⁺); HRMS (EI) C₂₀H₂₀O₂⁺ (M⁺) requires 292.14578, measured 292.14633.

(4-((4-(6-Aminopyridazin-3-yl)phenoxy)methyl)-3-(6-hydroxyhex-1-yn-1-yl)phenyl)(phenyl)methanone, 95.



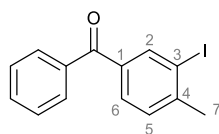
Method A: A solution of **86** (31.9 mg, 0.068 mmol), in degassed Et₃N (1 mL) was treated with 5-hexyn-1-ol (8.2 μL, 0.075 mmol), Pd(PPh₃)₄ (1.6 mg, 0.001 mmol) and CuI (0.4 mg, 0.002 mmol) and the reaction mixture was stirred at 80 °C in the dark for 16 h. The solvent was concentrated *in vacuo* and the resulting residue was treated with saturated aqueous NH₄Cl (5 mL) and extracted with Et₂O (3×10 mL). The combined organic layers were dried and concentrated *in vacuo*. Purification via flash column chromatography (EtOAc: CDCl₃, 100:1) gave starting material **86** (24.1 mg, 77%) as a yellow solid. Further elution gave **95** (4.5 mg, 15%) as a yellow solid.

Method B: A solution of **99** (15.4 mg, 0.030 mmol), in degassed Et₃N (1 mL) under Ar was treated with 5-hexyn-1-ol (3.7 μL, 0.033 mmol), Pd(PPh₃)₄ (0.7 mg, 0.001 mmol) and CuI (0.2 mg, 0.001 mmol) and the reaction mixture was stirred at 80 °C in the dark for 16 h. The solvent was concentrated *in vacuo* and the resulting residue was treated with saturated aqueous NH₄Cl (5 mL) and extracted with Et₂O (3×10 mL). The combined organic layers were dried and concentrated *in vacuo*. Purification via flash column chromatography (EtOAc: CDCl₃, 100:5) gave **95** (10.6 mg, 74%) as a yellow solid.

δ_H (500 MHz, CDCl₃:CD₃OD 1:1) 1.60-1.70 (4H, m, C(20)H₂, C(21)H₂), 2.46 (2H, t, *J* 6.6, C(19)H₂), 3.55 (2H, t, *J* 6.1, C(22)H₂), 5.31 (2H, s, C(9)H₂), 6.93 (1H, br d, *J* 8.7, C(2)H), 7.07 (2H, d, *J* 8.7, 2×C(7)H), 7.48 (2H, t, *J* 7.9, 2×*m*-PhH), 7.57-7.64 (3H, m, *p*-PhH, C(16)H, C(15)H), 7.69 (1H, dd, *J* 8.0, 1.7, C(3)H), 7.75 (2H, dd, *J*

8.5, 1.3, 2×*o*-PhH), 7.78 (2H, d, *J* 8.9, 2×C(6)H), 7.81 (1H, d, *J* 1.7, C(12)H); δ_C (125 MHz, CDCl₃:CD₃OD, 1:1) 20.7 (C(19)H₂), 26.3 (C(20)H₂), 33.0 (C(21)H₂), 62.8 (C(22)H₂), 69.4 (C(9)H₂), 78.9 (C), 98.5 (C), 115.3 (C), 116.5 (C(7)H), 118.0 (C(2)H), 124.0 (C), 124.0 (C) 128.4, 128.4 (C(16)H, C(15)H), 129.0 (C(6)H), 129.8 (*m*-PhH), 130.7 (C(3)H), 130.9 (C), 131.4 (*o*-PhH), 134.3 (*p*-PhH), 135.0 (C(12)H), 144.2 (C), 159.2 (C), 160.0 (C), 160.8 (C), 160.8 (C), 198.0 (C(14)); ν_{\max} (solid) 3316, 3193, 2931, 2861; mp (CH₃OH) 82-84 °C; *m/z* (EI⁺) 477 (6%, [M]⁺), 207 (26%, [M-C₁₆H₁₅N₃O₂]⁺), 84 (100%, [M-C₂₅H₁₈N₃O₃]⁺); HRMS (EI) C₃₀H₂₇N₃O₃⁺ (M⁺) requires 477.20469; measured 477.20513.

(3-Iodo-4-methylphenyl)(phenyl)methanone, 97.

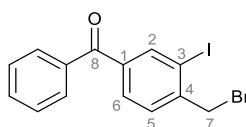


Thionyl chloride (7.00 mL, 96.5 mmol) was added dropwise to 2-iodo-4-methylbenzoic acid **96** (5.00 g, 19.1 mmol) and the reaction mixture was heated to reflux for 2 h. The reaction mixture was allowed to cool and then was concentrated *in vacuo*. The residue was redissolved in benzene (20 mL) and AlCl₃ (2.80g, 21.0 mmol) was added. The mixture was then heated to 50°C for 3 h. After having cooled, the reaction mixture was partitioned between 3 M aqueous HCl (20 mL) and EtOAc (20 mL). The aqueous layer was extracted with EtOAc (3×20 mL), and the combined organic layers were washed with brine (50 mL), dried and concentrated *in vacuo*. Purification via flash column chromatography (40-60 °C petrol:Et₂O, 9:1) gave **97** (5.09 g, 83%) as a white solid.

δ_H (500 MHz, CDCl₃) 2.52 (3H, s, C(7)H₃), 7.34 (1H, d, *J* 7.9, C(5)H), 7.49 (2H, dd, *J* 7.9, 7.6, 2×*m*-PhH), 7.60 (1H, tt, *J* 7.3, 1.3, *p*-PhH), 7.68 (1H, dd, *J* 7.9, 1.7, C(6)H), 7.76-7.79 (2H, m, 2×*o*-PhH), 8.25 (1H, d, *J* 1.6, C(2)H); δ_C (125 MHz, CDCl₃) 28.5

(C(7)H₃), 100.8 (C), 128.5 (*m*-PhH), 129.5 (C(5)), 130.0 (C(6)), 130.0 (*o*-PhH), 132.7 (*p*-PhH), 136.9 (C), 137.3 (C), 140.5 (C(2)), 146.4 (C), 194.9 (C=O); ν_{\max} (solid) 3050, 1722, 1652, 1595, 1587, 1577, 1544; mp 78-79 °C; m/z (EI⁺) 322 (100%, M⁺), 245 (62%, [M-C₆H₅]⁺), 105 (51%, [M-C₇H₆I]⁺); HRMS (EI) C₁₄H₁₁OI⁺ (M⁺) requires 321.98491, measured 321.98516.

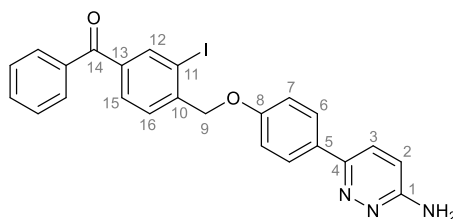
(4-(Bromomethyl)-3-iodophenyl)(phenyl)methanone, 98.



NBS (527 mg, 2.96 mmol) and AIBN (63 mg, 0.39 mmol) were added sequentially to **97** (955 mg, 2.96 mmol) in benzene (20 mL). The mixture was then heated to 80 °C for 16 h then the reaction solvent was removed *in vacuo*. Purification via flash column chromatography (40-60 °C petrol: Et₂O, 100:1) gave starting material **97** (372 mg, 39%) and further elution gave **98** (666 mg, 56%) as a yellow solid.

δ_{H} (500 MHz, CDCl₃) 4.63 (2H, s, C(7)H₂), 7.50 (2H, t, J 7.6, 2×*m*-PhH), 7.57 (1H, d, J 7.9, C(5)H), 7.62 (1H, tt, J 7.6, 1.9, *p*-PhH), 7.74 (1H, dd, J 7.9, 1.9, C(6)H), 7.79 (2H, dt, J 7.6, 1.9, 2×*o*-PhH), 8.27 (1H, d, J 1.9, C(2)H); δ_{C} (125 MHz, CDCl₃) 37.8 (C(7)H₂), 99.7 (C(3)), 128.6 (*m*-PhH), 130.1 (*o*-PhH), 130.2 (CH), 130.4 (CH), 133.1 (*p*-PhH), 136.8 (C), 140.0 (C), 141.3 (C(2)H), 144.3 (C(4)), 194.4 (C(8)); ν_{\max} (solid) 3030, 2927, 1734, 1649, 1594, 1562, 1550, 1510; mp (Et₂O) 54-56 °C; m/z (EI⁺) 402 (16%, [⁸¹M]⁺), 400 (16%, [⁷⁹M]⁺), 321 (100%, [M-Br]⁺); HRMS (EI) C₁₄H₁₀BrIO⁺ (⁷⁹M⁺) requires 399.89542, measured 399.89584.

**(4-((4-(6-Aminopyridazin-3-yl)phenoxy)methyl)-3-iodophenyl)
(phenyl)methanone, 95.**



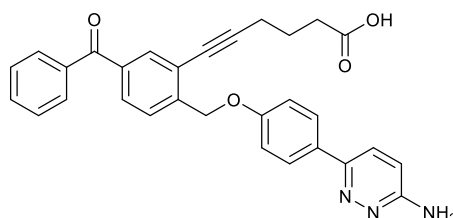
Method A: To a solution of KO^tBu (322 mg, 2.89 mmol) in DMF (5 mL) was added a solution of **31** (448 mg, 2.39 mmol) in DMF (15 mL) at 0 °C and the reaction mixture was stirred at 0 °C for 20 min. Benzylbromide **98** (1.06 g, 2.63 mmol) was added in one portion and the reaction was allowed to warm to rt over 16 h. The reaction mixture was concentrated *in vacuo*, and the residue was partitioned between saturated aqueous LiCl (100 mL) and EtOAc (200 mL). The aqueous layer was extracted with EtOAc (3×300 mL) and the combined organic layers were dried and concentrated *in vacuo*. Purification via flash column chromatography (EtOAc) **100** (358 mg, 57%). Further elution gave **99** (278 mg, 23%) as a white solid. Further elution gave starting material **31** (70 mg, 30%).

Method B: To a solution of NaH (131 mg, 3.56 mmol) in DMF (5 mL) at 0 °C was added **31** (606 mg, 3.24 mmol) in one portion. The resulting solution was stirred at 0 °C for 20 min, before a solution of **98** (1.56 g, 3.88 mmol) in DMF (5 mL) was added via cannula. The reaction mixture was stirred at rt for 4 h, quenched with H₂O (2 mL), and concentrated *in vacuo*. Purification via flash column chromatography (EtOAc) gave **95** (1.25 g, 82%) as a white solid.

δ_{H} (600 MHz, CDCl₃) 4.82 (2H, br s, NH₂), 5.16 (2H, s, C(9)H₂), 6.84 (1H, d, *J* 8.9, C(2)H), 7.09 (2H, d, *J* 8.9, 2×C(7)H), 7.50 (2H, t, *J* 7.7, 2×*o*-PhH), 7.59-7.63 (2H, m, C(3)H, C(15)H), 7.65 (1H, d, *J* 8.0, *p*-PhH), 7.77-7.81 (3H, m, 2×*m*-PhH, C(16)H), 7.94 (2H, d, *J* 8.9, 2×C(6)H), 8.31 (1H, d, *J* 1.5, C(12)H); δ_{C} (150 MHz, CDCl₃) 73.8

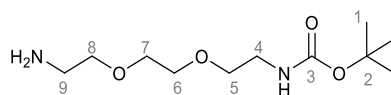
(C(9)H₂), 96.4 (C(11)), 115.1 (C(2)H), 115.3 (2×C(7)H), 125.9 (C(15)H), 127.7 (*p*-PhH), 128.0 (C(6)H), 128.6 (*o*-PhH), 130.1 (C(16)H), 130.2 (*m*-PhH), 130.3 (C), 133.0 (C(3)H), 137.0 (C), 138.6 (C), 140.5 (C(12)H), 143.4 (C), 153.3 (C), 158.1 (C), 159.0 (C), 194.9 (C(14)); ν_{\max} (solid) 3420, 3312, 3168, 2928, 2349, 1653; mp (CH₃OH) 90-91 °C; m/z (EI⁺) 507 (100%, [M]⁺); HRMS (EI) C₂₄H₁₈IN₂O₂⁺ (M⁺) requires 507.04382, measured 507.04450.

6-(2-((4-(6-Aminopyridazin-3-yl)phenoxy)methyl)-5-benzoylphenyl)hex-5-ynoic acid, **87.**



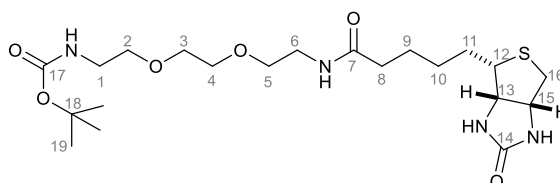
A solution of **99** (160 mg, 0.32 mmol) in degassed Et₃N (5 mL) and THF (5 mL), was treated sequentially with 5-hexynoic acid (38 μ L, 0.35 mmol), Pd(PPh₃)₃ (7.3 mg, 0.006 mmol) and CuI (1.8 mg, 0.010 mmol), and the reaction was heated to 65 °C for 16 h in the dark. The crude product was redissolved in CH₃OH (20 mL) and the reaction mixture was concentrated *in vacuo*. Purification via flash column chromatography (CHCl₃: CH₃OH, 10:1) gave **87** (76.6 mg, 49%) as an insoluble white solid.

¹H and ¹³C NMR data was unavailable for this compound due to its high insolubility in deuterated solvents (yes, including DMSO-d₆); ν_{\max} (solid) 3521, 2917, 2235, 1689; mp 239-240 °C; m/z (ES⁺) 492 (100%, [M+H]⁺); HRMS (ES⁺) C₃₀H₂₆N₃O⁺ ([M+H]⁺) requires 492.1923, measured 492.1901.

***tert* Butyl *N*-{2-[2'-(2''-aminoethoxy)ethoxy]ethyl}carbamate, **102**.¹¹¹**

A solution of Boc₂O (1.18 g, 5.40 mmol) in CH₂Cl₂ (20 mL) was added dropwise to a solution of 2-[2-(2-aminoethoxy)ethoxy]ethanamine (8.00 g, 54.0 mmol) in CH₂Cl₂ (20 mL) at 0 °C, and the reaction mixture left to stir at rt for 16 h before being concentrated *in vacuo*. The resulting residue was redissolved in CH₂Cl₂ (40 mL) and washed with H₂O (40 mL). The aqueous layer was extracted with CH₂Cl₂ (2×40 mL) and the combined organic layers were dried and concentrated *in vacuo* to give **102** (1.38 g, 99%) as a colourless oil.

δ_{H} (500 MHz, CDCl₃) 1.43 (9H, s, 3×C(1)H₃), 1.87 (2H, br s, NH₂), 2.89 (2H, t, *J* 5.2, C(9)H₂), 3.32 (2H, q, *J* 5.2, C(4)H₂), 3.51-3.56 (4H, m, C(5)H₂, C(8)H₂), 3.61 (4H, s, C(6)H₂, C(7)H₂), 5.16 (1H, br s, NH); δ_{C} (125 MHz, CDCl₃) 28.5 (3×C(1)H₃), 40.4 (C(4)H₂), 41.4 (C(9)H₂), 70.2 (CH₂), 70.2 (CH₂), 70.3 (CH₂), 72.6 (C(8)H₂), 79.2 (C(2)), 156.1 (C(3)); ν_{max} (oil) 3366, 2973, 2927, 2865, 1703; *m/z* (CI⁺) 249 (20%, [M]⁺), 193 (100%, [M-C(CH₃)₃]⁺), 149 (79%, [M-CO₂C(CH₃)₃]⁺), 57 (81%, [C(CH₃)₃]⁺); HRMS (CI⁺) C₁₁H₂₄N₂O₄⁺ (M⁺) requires 249.18088, measured 249.17974.

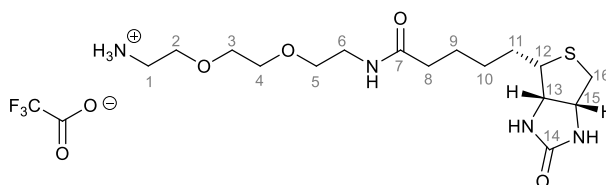
***N*-(2-(2'-(2''-(*N*-Boc-amino)ethoxy)ethoxy)ethyl)biotinylamine, **103**.¹¹²**

A solution of D-biotin (221 mg, 0.91 mmol), HBTU (298 mg, 0.79 mmol) and DIPEA (310 μ L, 1.81 mmol) in DMF (3 mL) was stirred for 20 mins at rt before being added

via cannula to a solution of **65** (150 mg, 0.60 mmol) in DMF (5 mL). The reaction mixture was stirred for 2 h before the solvent was removed *in vacuo*. Purification via flash column chromatography (CH₂Cl₂ : CH₃OH, 20:1) gave **103** (183 mg, 63%) as a colourless oil.

δ_{H} (600 MHz, CD₃OD); 1.42-1.48 (11H, m, 3×C(19)H₃, C(11)H_A, C(10)H_A), 1.56-1.77 (4H, m, C(9)H₂, C(11)H_B, C(10)H_B), 2.22 (2H, t, *J* 7.2, C(8)H₂), 2.71 (1H, d, *J* 12.7, C(16)H_A), 2.93 (1H, dd, 12.7, 4.8, C(16)H_B), 3.19-3.24 (3H, m, C(12)H, C(1)H₂), 3.37 (2H, t, *J* 5.5, C(6)H₂), 3.52 (2H, t, *J* 5.7, C(2)H₂), 3.55 (2H, t, *J* 5.5, C(5)H₂), 3.61 (4H, app s, C(3)H₂, C(4)H₂), 4.31 (1H, dd, *J* 7.8, 4.8, C(13)H), 4.50 (1H, dd, *J* 7.8, 4.3, C(15)H); δ_{C} (125 MHz, CD₃OD) 26.9 (C(9)H₂), 28.9 (C(19)H₃), 29.5 (C(11)H₂), 29.8 (C(10)H₂), 36.7 (C(8)H₂), 40.3 (C(6)H₂), 41.1 (C(16)H₂), 41.2 (C(1)H₂), 57.0 (C(12)H), 61.6 (C(15)H), 63.4 (C(13)H), 70.6 (CH₂), 71.1 (CH₂), 71.2 (CH₂), 71.3 (CH₂), 80.1 (C(18)), 158.4 (C(17)), 166.1 (C(14)), 176.2 (C(7)); ν_{max} (oil) 3292, 2930, 2867, 1693; *m/z* (FTMS) 497 (37%, [M+Na]⁺), 375 (100%, [M-C₅H₁₄O₂]⁺); HRMS (FTMS) C₂₁H₃₈O₆N₄NaS⁺ ([M+Na]⁺) requires 497.2404, measured 497.2394.

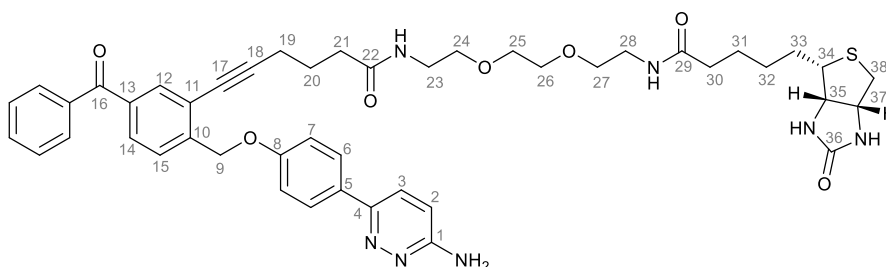
***N*-(2-(2'-(2''-Aminoethoxy)ethoxy)ethyl)biotinylamine TFA salt, 101.**



TFA (4 mL, 52.2 mmol) was added to a solution of **103** (700 mg, 1.48 mmol) in CH₂Cl₂ (4 mL) and stirred at rt for 3 h. The reaction mixture was then concentrated *in vacuo* to give **101** (725 mg, quant) as a yellow oil.

δ_{H} (600 MHz, CD_3OD) 1.41-1.48 (2H, m, $2\times\text{C}(10)\text{H}$), 1.55-1.77 (4H, m, $\text{C}(9)\text{H}_2$, $2\times\text{C}(11)\text{H}$), 2.23 (2H, t, J 7.3, $\text{C}(8)\text{H}_2$), 2.71 (1H, d, J 12.8, $\text{C}(16)\text{H}_{\text{A}}$), 2.93 (1H, d, J 12.8, $\text{C}(16)\text{H}_{\text{B}}$), 3.12 (2H, t, J 4.8, $\text{C}(1)\text{H}_2$), 3.21 (1H, m, $\text{C}(12)\text{H}_2$), 3.37 (2H, t, J 5.7, $\text{C}(6)\text{H}_2$), 3.56 (2H, t, J 5.7, $\text{C}(5)\text{H}_2$), 3.64-3.68 (4H, m, $\text{C}(3)\text{H}_2$, $\text{C}(4)\text{H}_2$), 3.70 (2H, t, J 4.8, $\text{C}(2)\text{H}_2$), 4.32 (1H, dd, J 7.9, 4.5, $\text{C}(13)\text{H}$), 4.51 (1H, dd, J 7.9, 4.7, $\text{C}(15)\text{H}$); δ_{C} (150 MHz, CD_3OD) 26.9 ($\text{C}(9)\text{H}_2$), 29.5 ($\text{C}(11)\text{H}_2$), 29.7 ($\text{C}(10)\text{H}_2$), 36.7 ($\text{C}(8)\text{H}_2$), 40.2 (CH_2), 40.7 (CH_2), 41.7 (CH_2), 57.0 ($\text{C}(12)\text{H}$), 61.7 ($\text{C}(15)\text{H}$), 63.4 ($\text{C}(13)\text{H}$), 70.7 (CH_2), 71.3 (CH_2), 71.3 (CH_2), 71.4 (CH_2), 117.3 (q, J 289, CF_3), 161.3 (q, J 38, CF_3COO^-), 166.2 ($\text{C}(14)$), 176.3 ($\text{C}(7)$); ν_{max} (oil) 3293, 3075, 2929, 1777, 1673; m/z (CI^+) 375 (100%, $[\text{M}]^+$); HRMS (CI^+) $\text{C}_{16}\text{H}_{32}\text{N}_4\text{O}_4\text{S}^+$ ($[\text{M}+\text{H}]^+$) requires 375.20605, measured 375.20509.

6-(2-((4-(6-Aminopyridazin-3-yl)phenoxy)methyl)-5-benzoylphenyl)-N-(2-(2-(2-(biotinylamino)ethoxy)ethoxy)ethyl)hex-5-ynamide, 104.

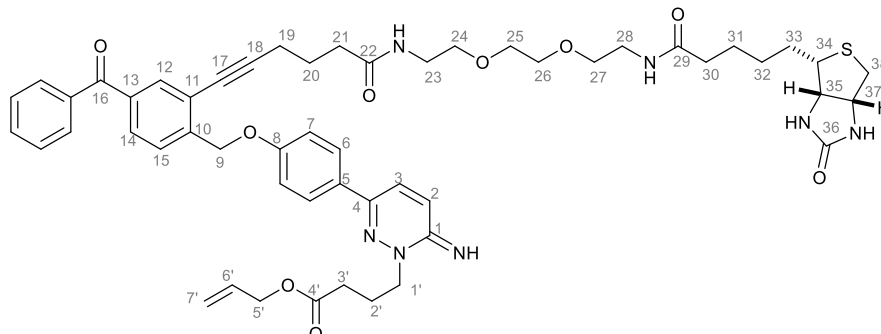


Method A: A suspension of **87** (10.4 mg, 0.021 mmol), HBTU (10.5 mg, 0.28 mmol) and DIPEA (10.8 μL , 0.063 mmol) in DMF (2 mL) was stirred for 20 mins at rt before being added via cannula to a solution of **101** (10.4 mg, 0.021 mmol) in DMF (1 mL). The reaction mixture was stirred for 2 h before the solvent was removed *in vacuo*. Purification via flash column chromatography (CH_2Cl_2 : CH_3OH , 20:1), followed by the recrystallisation out of impurity, followed by trituration (CHCl_3) gave **104** (9.86 mg, 55%) as a colourless oil.

Method B: DCC (58 mg, 0.28 mmol) was added to a solution of **87** (126 mg, 0.26 mmol) in DMF (3 mL) and the resulting mixture was stirred at 0 °C for 30 mins, then allowed to warm to rt over 20 min. Et₃N (36 μL, 0.26 mmol) and **101** (125 mg, 0.26 mmol) were then added and the reaction mixture was stirred at rt for 16 h. The reaction mixture was diluted with EtOAc (3 mL) and washed with saturated aqueous LiCl (5 mL), dried and concentrated *in vacuo*. Purification via flash column chromatography (CHCl₃:CH₃OH, 9:1) gave **104** (113 mg, 52%) as a yellow oil.

δ_{H} (600 MHz, CD₃OD) 1.37-1.42 (2H, m, C(33)H₂), 1.51-1.73 (4H, m, C(31)H₂, C(32)H₂), 1.89 (2H, quint, *J* 7.2 C(20)H₂), 2.17 (2H, t, *J* 7.3, C(30)H₂), 2.36 (2H, t, *J* 7.4, C(21)H₂), 2.53 (2H, t, *J* 7.6, C(19)H₂), 2.68 (1H, d, *J* 12.8, C(38)H_A), 2.89 (1H, d, *J* 12.8, C(38)H_B), 3.13-3.17 (1H, m, C(34)H), 3.32-3.35 (4H, m, C(23)H₂, C(28)H₂), 3.50 (4H, t, *J* 5.4, C(24)H₂, C(27)H₂), 3.57 (4H, app s, C(25)H₂, C(26)H₂), 4.26 (1H, dd, *J* 8.0, 4.4, C(35)H), 4.46 (1H, dd, *J* 8.0, 4.5, C(37)H), 5.38 (2H, s, C(9)H₂), 7.01 (1H, d, *J* 9.4, C(2)H), 7.14 (2H, d, *J* 8.6, 2×C(7)H), 7.56 (2H, t, *J* 7.9, 2×*m*-PhH), 7.67 (1H, t, *J* 7.4, C(14)H), 7.70-7.75 (2H, m, *p*-PhH, C(15)H), 7.76-7.80 (3H, m, 2×*o*-PhH, C(3)H), 7.87 (2H, d, *J* 8.6, 2×C(6)H), 7.91 (1H, s, C(12)H); δ_{C} (150 MHz, CD₃OD) 19.2 (CH₂), 25.9 (CH₂), 26.8 (CH₂), 29.5 (CH₂), 29.8 (CH₂), 36.0 (CH₂), 36.7 (CH₂), 40.3 (CH₂), 40.3 (CH₂), 41.0 (CH₂), 57.0 (CH), 61.6 (CH), 63.3 (CH), 66.9 (CH₂), 69.2 (CH₂), 70.6 (CH₂), 70.6 (CH₂), 71.3 (CH₂), 78.7 (C), 79.5 (C), 79.5 (CH), 97.3 (C), 116.2 (CH), 117.5 (CH) 124.2 (C), 128.0 (CH), 128.6 (CH), 129.7 (CH), 130.4 (CH), 131.0 (C), 131.0 (CH), 131.2 (C), 134.1 (CH), 134.4 (CH), 138.4 (C), 138.5 (C), 144.1 (C), 160.9 (C), 163.6 (C), 175.4 (C), 176.1 (C), 197.4 (C); ν_{max} (oil) 3301, 2926, 2856, 2349, 1693, 1650; m/z (ES⁺) 848 (100%, [M+H]⁺).

Allyl 4-(3-(4-((4-benzoyl-2-(5,16-dioxo-1-((3a*S*,4*S*,6a*R*)-2-oxohexahydro-1*H*-thieno[3,4-*d*]imidazol-4-yl)-9,12-dioxa-6,15-diazahenicos-20-yn-21-yl)benzyl)oxy)phenyl)-6-iminopyridazin-1(6*H*)-yl)butanoate hydrobromide, 105.

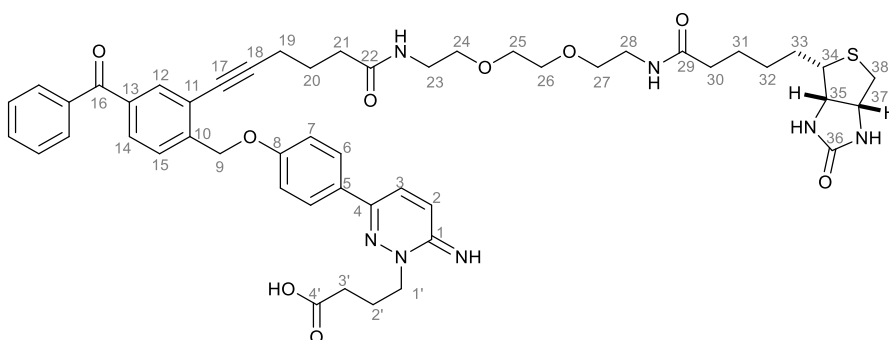


A reaction mixture of allyl 4-bromobutyrate (7.0 mg, 0.03 mmol), **67** (19 mg, 0.02 mmol) in DMF (0.1 mL) was heated to 120 °C for 16 h. The product precipitated upon addition of cold EtOAc (2 mL), and filtered to give **105** (18.2 mg, 77%) as a brown oil.

δ_{H} (600 MHz, CD_3OD) 1.37-1.44 (2H, m, C(32) H_2), 1.50-1.74 (4H, m, C(31) H_2 , C(33) H_2), 1.89 (2H, quint, J 7.3, C(20) H_2), 2.18 (2H, t, J 7.3, C(30) H_2), 2.27 (2H, t, J 6.8, C(2') H_2), 2.37 (2H, t, J 7.3, C(21) H_2), 2.53 (2H, t, J 7.0, C(19) H_2), 2.63 (2H, t, J 6.8, C(3') H_2), 2.68 (1H, d, J 13.0, C(38) H_A), 2.90 (1H, dd, J 12.6, 4.9, C(38) H_B), 3.14-3.20 (1H, m, C(34) H), 3.32-3.36 (4H, m, C(23) H_2 , C(28) H_2), 3.52 (4H, app q, J 5.8, C(24) H_2 , C(27) H_2), 3.58 (4H, app s, C(25) H_2 , C(26) H_2), 4.28 (1H, dd, J 7.7, 7.5, C(35) H), 4.44-4.50 (5H, m, C(5') H_2 , C(1') H_2 , C(37) H), 5.16 (1H, dd, J 10.5, 1.3, C(7') H_A), 5.24 (1H, dd, J 17.3, 1.3, C(7') H_B), 5.41 (2H, s, C(9) H_2), 5.80-5.88 (1H, m, C(6') H), 7.20 (2H, d, J 9.0, $2\times$ C(7) H), 7.56 (2H, t, J 7.8, $2\times$ *m*-Ph H), 7.62 (1H, d, J 9.6, C(3) H), 7.67 (1H, t, J 7.4 C(15) H), 7.70 (1H, d, J 8.1, *p*-Ph H), 7.72 (1H, td, J 7.9, 1.7, C(14) H), 7.78 (2H, d, J 8.1, $2\times$ *o*-Ph H), 7.82 (1H, s, C(12) H), 7.99 (2H, d, J 8.8, $2\times$ C(6) H), 8.32 (1H, d, J 9.6, C(2) H); δ_{C} (150 MHz, CD_3OD) 19.8 (CH $_2$), 22.5 (CH $_2$), 25.9 (CH $_2$), 26.9 (CH $_2$), 29.5 (CH $_2$), 29.8 (CH $_2$), 31.3 (CH $_2$), 36.0 (CH $_2$), 36.7 (CH $_2$),

40.3 (CH₂), 40.3 (CH₂), 41.1 (CH₂), 43.8 (CH₂), 55.9 (CH), 56.9 (CH₂), 57.0 (CH), 61.6 (CH), 63.3 (CH), 66.5 (CH₂), 69.3 (CH₂), 70.6 (CH₂), 70.6 (CH₂), 71.3 (CH₂), 81.6 (C), 97.3 (C), 116.7 (CH), 118.7 (CH₂), 122.5 (C), 126.7 (C), 127.1 (CH), 127.2 (CH), 129.5 (CH), 129.7 (CH), 130.4 (CH), 131.0 (CH), 133.5 (CH), 133.6 (CH), 134.1 (CH), 134.5 (C), 138.1 (C), 144.0 (C), 152.9 (C), 153.9 (C), 158.8 (C), 160.5 (C), 162.5 (C), 174.0 (C), 175.4 (C), 175.9 (C), 197.3 (C); ν_{\max} (oil) 3323, 2939, 1726; m/z (ES⁺) 974 (100%, [M+H]⁺).

4-(3-(4-((4-benzoyl-2-(5,16-dioxo-1-((3a*S*,4*S*,6a*R*)-2-oxohexahydro-1*H*-thieno[3,4-*d*]imidazol-4-yl)-9,12-dioxa-6,15-diazahenicos-20-yn-21-yl)benzyl)oxy)phenyl)-6-iminopyridazin-1(6*H*)-yl)butanoic acid, **106.**

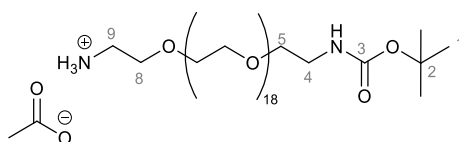


A solution of NaOH (1.0 mg, 0.025 mmol) and **105** (8.6 mg, 0.009 mmol) in THF (1 mL) and H₂O (1 mL) was stirred at 50 °C for 3 h. After cooling to 10 °C the reaction mixture was washed with EtOAc (2 mL) and the aqueous layer separated, then acidified to pH 1 by addition of 0.1 M aqueous HCl and stirred at 0 °C for 1 h. The solvent was removed *in vacuo* and the residue triturated with H₂O (1 mL) to leave **106** (11.9 mg, 65%) as a brown solid.

δ_{H} (600 MHz, CD₃OD) 1.37-1.43 (2H, m, C(32)H₂), 1.52-1.73 (4H, m, C(31)H₂, C(33)H₂), 1.88 (2H, quint, *J* 7.2, C(20)H₂), 2.15-2.24 (4H, m, C(2')H₂, C(30)H₂), 2.36 (2H, t, *J* 7.4, C(21)H₂), 2.50-2.54 (4H, m, C(3')H₂, C(19)H₂), 2.68 (1H, d, *J* 12.7,

C(38) H_A), 2.90 (1H, dd, J 12.7, 4.9, C(38) H_B), 3.14-3.18 (1H, m, C(34) H), 3.32-3.36 (4H, m, C(23) H_2 , C(28) H_2), 3.51 (4H, app q, J 5.7, C(24) H_2 , C(27) H_2), 3.58 (4H, app s, C(25) H_2 , C(26) H_2), 4.25-4.28 (1H, m, C(35) H), 4.42-4.48 (3H, m, C(1') H_2 , C(37) H), 5.41 (2H, s, C(9) H_2), 7.20 (2H, d, J 9.0, 2×C(7) H), 7.56 (2H, t, J 7.8, 2× m -Ph H), 7.62 (1H, d, J 9.6, C(3) H), 7.65-7.69 (1H, m, C(15) H), 7.70 (1H, d, J 8.1, p -Ph H), 7.74 (1H, dd, J 8.1, 1.7, C(14) H), 7.77-7.80 (2H, m, 2× o -Ph H), 7.83 (1H, d, J 1.7, C(12) H), 7.99 (2H, d, J 9.0, 2×C(6) H), 8.30 (1H, d, J 9.6, C(2) H); δ_C (150 MHz, CD₃OD) 19.8 (CH₂), 23.0 (CH₂), 25.9 (CH₂), 26.9 (CH₂), 29.5 (CH₂), 29.8 (CH₂), 31.6 (CH₂), 36.0 (CH₂), 36.7 (CH₂), 40.2 (CH₂), 40.3 (CH₂), 41.0 (CH₂), 57.0 (CH), 61.6 (CH), 61.6 (CH), 63.3 (CH), 69.3 (CH₂), 69.6 (CH₂), 70.6 (CH₂), 70.6 (CH₂), 71.3 (CH₂), 78.6 (C), 98.0 (C), 116.6 (CH), 117.2 (CH), 124.5 (C), 126.6 (C), 127.1 (CH), 128.7 (CH), 129.5 (CH), 129.7 (CH), 130.4 (CH), 131.0 (C), 132.6 (C), 134.1 (CH), 134.5 (CH), 138.4 (C), 144.0 (C), 151.8 (C), 153.0 (C), 162.5 (C), 173.7 (C), 175.4 (C), 176.1 (C), 177.1 (C), 197.4 (C); ν_{\max} (solid) 3263, 2832, 2380, 1650; mp (EtOH) 178-180 °C; m/z (ES⁺) 934, (30%, [M+H]⁺), 468 (100%); HRMS (ESI⁺) C₅₀H₅₉N₇O₉S ([M+H]⁺) requires 934.4173; measured 934.4884.

NH-OEG₈₈₀-NHBoc acetic acid salt, 108.¹¹³

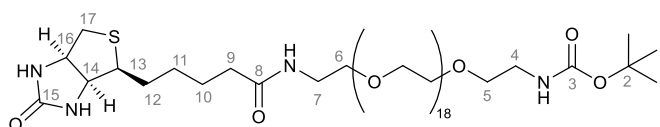


A suspension of crushed O,O'-bis(2-aminoethyl)octadecaethylene glycol (144 mg, 0.161 mmol) in CH₃OH (10 mL) was treated dropwise with a solution of Boc₂O (35.1 mg, 0.161 mmol) in CH₃OH (10 mL) over 1 h. The resulting mixture was stirred at rt for 19 h, before acetic acid (10 mL) and toluene (70 mL) were added and the reaction solvent was removed *in vacuo*. Purification via flash column chromatography

(CHCl₃:CH₃OH:CH₃CO₂H, 80:20:3) gave mono- protected OEG diamine **108** (142 mg, 83%) as a white solid.

δ_{H} (600 MHz, CDCl₃) 1.39 (9H, s, 3×C(1)H₃), 3.24-3.28 (2H, m, C(4)H₂), 3.46-3.50 (2H, m, C(5)H₂), 3.54-3.71 (~74H, m, 37×CH₂), 3.80-3.85 (2H, m, C(9)H₂); δ_{C} (150 MHz, CDCl₃) 28.5 (C(1)H₃), 40.4 (CH₂), 69.9 (CH₂), 70.0 (CH₂), 70.0 (CH₂), 70.2 (CH₂), 70.2 (CH₂), 70.2 (CH₂), 70.3 (CH₂), 70.3 (CH₂), 70.4 (CH₂), 70.4 (CH₂), 70.5 (CH₂), 70.6 (CH₂), 70.6 (CH₂), 70.6 (CH₂), 79.2 (C(2)), 156.1 (C(3)); m/z (ES⁺) 1020 (60%, [M+CH₃COO⁻]), 997, (100%, [M+H]⁺); HRMS (ES⁺) C₄₅H₉₂N₂O₂₁⁺ ([M+H]⁺) requires 997.6271; measured 997.6266.

D-Biotin-NH-OEG₈₈₀-NHBoc, **110**.¹¹³

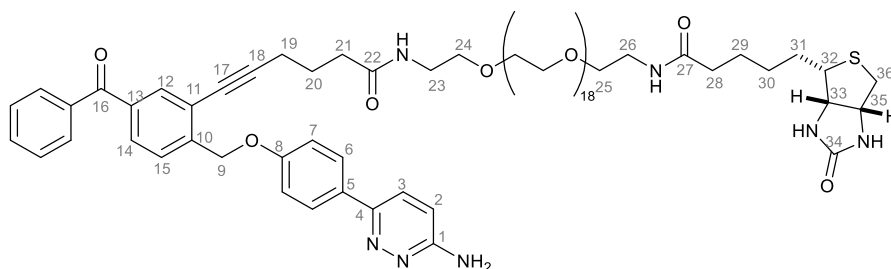


A solution of BocNH-PEG-NH₂.CH₃CO₂H **108** (40.4 mg, 0.038 mmol) in dry DMF (1 mL) was treated with D-Biotin-NHS (18.4 mg, 0.054 mmol) and triethylamine (9.1 μ L, 0.07 mmol) and stirred at rt for 24 h. The reaction was quenched upon addition of H₂O (0.5 mL), and stirred for a further 2 h. The reaction solvent was removed *in vacuo*, and the residue was redissolved in 0.2 M aqueous Na₂CO₃ (5 mL), and filtered. The filtrate was saturated with NaOH, extracted with CHCl₃ (2×50 mL) and the combined organic layers were dried and concentrated *in vacuo* to give **110** (35.2 mg, 76%) as a white solid.

δ_{H} (600 MHz, CDCl₃) 1.44 (9H, s, 3×C(1)H₃), 1.60-1.82 (6H, m, C(10)H₂, C(11)H₂, C(12)H₂), 2.18-2.26 (2H, m, C(9)H₂), 2.74 (1H, d, J 12.8, C(17)H_A), 2.92 (1H, dd, J 12.8, 4.5, C(17)H_B), 3.12-3.19 (1H, C(13)H), 3.27-3.34 (2H, m, C(7)H₂), 3.40-3.46 (2H, m, C(4)H₂), 3.50-3.58 (4H, m, C(6)H₂, C(5)H₂), 3.58-3.73 (72H, s, 36×CH₂),

4.29-4.35 (1H, m, C(14)*H*), 4.48-4.54 (1H, m, C(16)*H*), 5.08 (2H, s, C(3)*NH*), 5.89 (1H, s, *NH*), 6.70 (1H, s, *NH*); δ_{C} (150 MHz, CDCl₃) 25.6 (CH₂), 28.1 (CH₂), 28.6 (C), 35.8 (CH₂), 39.3 (CH₂), 40.6 (CH₂), 55.5 (CH), 60.3 (CH), 61.9 (CH), 70.0 (CH₂), 70.2 (CH₂), 70.4 (CH₂), 70.5 (CH₂), 70.6 (CH₂), 70.6 (CH₂), 70.6 (CH₂), 70.7 (CH₂), 79.3 (C), 166.3 (C), 167.8 (C), 173.4 (C); m/z (ES⁺) 1245, (50%, [M+H]⁺), 562 (100%); HRMS (ESI⁺) C₅₅H₁₀₆N₄O₂₃S⁺ ([M+Na]⁺) requires 124.57090, measured 124.56866.

6-(2-((4-(6-Aminopyridazin-3-yl)phenoxy)methyl)-5-benzoylphenyl)-N-(61-oxo-65-((3a*S*,4*S*,6a*R*)-2-oxohexahydro-1*H*-thieno[3,4-*d*]imidazol-4-yl)-3,6,9,12,15,18,21,24,27,30,33,36,39,42,45,48,51,54,57-nonadeca-60-azapentacontyl)hex-5-ynamide, **111.**

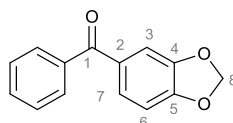


A mixture of acid **87** (29.4 mg, 0.060 mmol) and HOAt (8.2 mg, 0.060 mmol) in DMF (0.5 mL) was stirred at 0 °C for 10 minutes before DCC (13.6 mg, 0.066 mmol) was added and the resulting mixture was stirred at 0 °C for 30 min, and then at rt for 30 min. Biotin-NH-PEG₈₈₀-NHBoc **110** (74.2 mg, 0.060 mmol) and triethylamine (16.8 μ L, 0.120 mmol) were added and the reaction was stirred at rt for 20 h, before being concentrated *in vacuo*. Purification via flash column chromatography (CHCl₃:CH₃OH, 100:20) gave **111** (53.0 mg, 55%) as a yellow oil.

δ_{H} (600 MHz, CDCl₃:CD₃OD, 1:2) 1.36-1.45 (2H, m, C(30)*H*₂), 1.54-1.74 (4H, m, C(29)*H*₂, C(31)*H*₂), 1.89 (2H, quin, *J* 7.2, C(20)*H*₂), 2.16-2.23 (2H, m, C(28)*H*₂), 2.32

(2H, t, J 7.7, C(21) H_2), 2.50 (2H, t, J 7.2, C(19) H_2), 2.70 (1H, d, J 13.2, C(36) H_A), 2.89 (1H, dd, J 12.7, 5.0, C(36) H_B), 3.11-3.17 (1H, m, C(32) H), 3.32-3.37 (2H, m, C(23) H_2), 3.48-3.53 (2H, m, C(26) H_2), 3.59-3.64 (76H, m, 38 \times CH $_2$), 4.27-4.30 (1H, m, C(33) H), 4.46-4.50 (1H, m, C(35) H), 5.36 (2H, s, C(9) H_2), 7.11-7.14 (3H, m, C(2) H , 2 \times C(7) H), 7.46-7.52 (1H, m, *p*-Ph H), 7.58 (1H, d, J 9.6, C(14) H), 7.61-7.65 (2H, m, 2 \times *m*-Ph H), 7.69-7.72 (1H, m, C(3) H), 7.74-7.79 (2H, m, 2 \times *o*-Ph H), 7.83 (1H, d, J 1.7, C(12) H), 7.86-7.89 (2H, m, 2 \times C(6) H), 8.19-8.22 (1H, m, C(15) H); {Signals in ^{13}C NMR were too weak to characterise}; ν_{max} (solid) 3266, 2829, 2376, 1650; m/z (ES $^+$) 1618 (90%, [M+Na] $^+$), 1596 (70%, [M+H] $^+$), 1242 (100%); HRMS (ES $^+$), C $_{80}$ H $_{122}$ N $_7$ O $_{24}$ S $^+$ ([M+H] $^+$) requires 1596.8262, found 1596.7903.

Benzo[d][1,3]dioxol-5-yl(phenyl)methanone, **134**.¹¹⁴

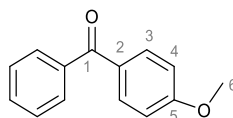


Solid FeCl $_3$ (1.00 g, 6.17 mmol) was slowly added to a solution of benzoyl chloride (703 μL , 6.06 mmol) and 1,3-benzodioxole (631 μL , 5.50 mmol) in CH $_2$ Cl $_2$ (250 mL) at 0 $^\circ\text{C}$, and the reaction mixture was stirred at rt for 3 h. The mixture was poured into ice, acidified with concentrated HCl, and extracted with CH $_2$ Cl $_2$ (2 \times 150 mL). The combined organics were washed with H $_2$ O (150 mL), dried and concentrated *in vacuo*. Purification via flash column chromatography (40-60 $^\circ\text{C}$ petrol:Et $_2$ O, 10:1) gave **134** (174 mg, 14%) as a grey solid.

δ_{H} (600 MHz, CDCl $_3$) 6.07 (2H, s, C(8) H_2), 6.86 (1H, dd, J 8.0, 0.5, C(6) H), 7.36-7.39 (2H, m, C(7) H , C(3) H), 7.47 (2H, t, J 7.3, 2 \times *m*-Ph H), 7.57 (1H, t, J 7.4, *p*-Ph H), 7.73-7.76 (2H, m, 2 \times *o*-Ph H); δ_{C} (150 MHz, CDCl $_3$) 102.0, (C(8) H_2), 107.8 (C(6) H), 110.0

(CH), 127.0 (CH), 128.3 (*m*-PhH), 129.8 (*o*-PhH), 132.0 (C(2)), 132.1 (*p*-PhH), 138.2 (*i*-Ph), 148.1 (C), 151.6 (C), 195.3 (C(1)); *m/z* (ES⁺) 227 (100%, [M+H]⁺).

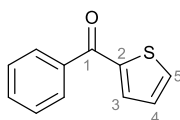
(4-Methoxyphenyl)(phenyl)methanone, 112.¹¹⁵



A solution of 4-methoxy benzoylchloride (1.00 g, 5.86 mmol) in benzene (5 mL) was treated with AlCl₃ (860 mg, 6.45 mmol), and the resulting mixture was stirred at reflux for 16 h. The reaction was then poured onto ice and extracted with CH₂Cl₂ (2×100 mL). The combined organic layers were washed with H₂O (100 mL), 5% aqueous NaOH (100 mL), dried and concentrated *in vacuo*. Purification via flash column chromatography (40-60 °C petrol:Et₂O, 10:1 to 0:1) gave **134** (168 mg, 13%) as a cream solid.

δ_{H} (600 MHz, CDCl₃) 3.86 (3H, s, C(6)H₃), 6.95 (2H, d, *J* 9.0, 2×C(4)H), 7.46 (2H, t, *J* 7.5, 2×*m*-PhH), 7.55 (1H, t, *J* 7.5, *p*-PhH), 7.75 (2H, d, *J* 8.3, 2×*o*-PhH), 7.82 (2H, d, *J* 9.0, 2×C(3)H); δ_{C} (150 MHz, CDCl₃) 51.6 (CH₃), 109.6, (CH), 124.3 (CH), 125.8 (CH), 126.2 (C), 128.0 (CH), 128.7 (CH), 134.3 (C), 159.3 (C), 191.7 (C(1)); *m/z* (CI) 213 (100%, [M+H]⁺).

Phenyl(thiophen-2-yl)methanone, 133.¹¹⁶

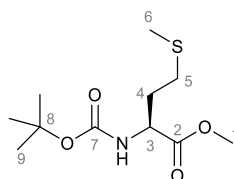


A solution of diisopropyl 1-benzoylhydrazine-1,2-dicarboxylate¹¹⁷ (308 mg, 1.00 mmol) in dry THF (20 mL) was cooled to -78 °C and thiophen-2-ylmagnesium bromide (1.0 M in THF, 2.5 mL, 2.5 mmol) was added. The reaction mixture was

stirred at $-78\text{ }^{\circ}\text{C}$ for 30 min, then at $0\text{ }^{\circ}\text{C}$ for a further 30 min before being quenched by addition of saturated aqueous NH_4Cl (5 mL). The aqueous layer was extracted with Et_2O ($3\times 50\text{ mL}$), and the combined organic layers were dried and concentrated *in vacuo*. Purification via flash column chromatography ($40\text{-}60\text{ }^{\circ}\text{C}$ petrol: Et_2O , 100:1) gave **133** (54 mg, 29%) as a white solid.

δ_{H} (600 MHz, CDCl_3) 6.16 (1H, dd, J 4.9, 3.8, C(4)*H*), 7.50 (2H, t, J 7.5 (2 \times *m*-Ph*H*), 7.59 (1H, t, J 7.5, *p*-Ph*H*), 7.65 (1H, dd, J , 3.8, 1.1, C(3)*H*), 7.72 (1H, dd, J 4.9, 1.1, C(5)*H*), 7.85-7.88 (2H, m, 2 \times *o*-Ph*H*); δ_{C} (150 MHz, CDCl_3) 128.1 (C(2)*H*), 128.5 (CH), 129.3 (CH), 132.4 (CH), 134.4 (CH), 135.0 (CH), 138.2 (C), 143.7 (C), 188.4 (C(1)); m/z (CI) 189 (100%, $[\text{M}+\text{H}]^+$).

Methyl (*tert*-butoxycarbonyl)-L-methioninate {Boc-L-Met-OMe}, **125**.¹¹⁸

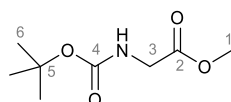


A mixture of thionyl chloride (0.80 mL, 13.2 mmol) in CH_3OH (7 mL), was stirred at $0\text{ }^{\circ}\text{C}$ for 10 min before L-methionine (4.00g, 26.8 mmol) was added and the reaction was stirred at rt for a 18 h. The reaction mixture was then concentrated *in vacuo*, redissolved in CH_2Cl_2 (250 mL), and cooled to $0\text{ }^{\circ}\text{C}$. Triethylamine (15.1 mL, 107 mmol) was then added slowly, followed by Boc_2O (10.5 g, 48.2 mmol), and the reaction was stirred at rt for 15 h before being concentrated *in vacuo*. Purification via flash column chromatography ($40\text{-}60\text{ }^{\circ}\text{C}$ petrol: Et_2O , 5:1) yielded Boc-L-Met-OMe **125** (7.00 g, 99%) as a colourless oil.

δ_{H} (600 MHz, CDCl_3) 1.43 (9H, s, 3 \times C(9)*H*₃), 1.88-1.96 (1H, m, C(4)*H*_A), 2.09 (3H, s, C(6)*H*₃), 2.09-2.16 (1H, m, C(4)*H*_B), 2.53 (2H, t, J 7.9, C(5)*H*₂), 3.75 (3H, s,

C(1) H_3), 4.39-4.44 (1H, m, C(3) H), 5.12 (1H, d, J 7.2, NH); δ_c (150 MHz, $CDCl_3$) 15.6 (C(6) H_3), 28.4 (C(9) H_3), 30.1 (C(5) H_2), 32.3 (C(4) H_2), 52.6 (C(1) H_3), 52.8 (C(3) H). 80.2 (C(8)), 155.4 (C(7)) 175.0 (C(2)); m/z (CI) 104 (100%), 264 (5%, $[M+H]^+$).

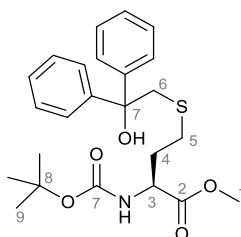
Methyl (*tert*-butoxycarbonyl)glycinate {Boc-Gly-OMe}, 126.¹¹⁹



A stirring suspension of glycine methyl ester hydrochloride (3.00 g, 23.9 mmol) and NaCl (4.74 g, 81.2 mmol) in $CHCl_3$ was treated with a solution of $NaHCO_3$ (2.01 g, 23.9 mmol) in H_2O (20 mL), followed by a solution of Boc_2O (5.22 g, 23.9 mmol) in $CHCl_3$ (30 mL). The resulting biphasic mixture was stirred vigorously at reflux for 2 h, then allowed to cool to rt, before the layers were separated. The aqueous layer was extracted with $CHCl_3$ (2×50 mL) and the combined organics were dried and concentrated *in vacuo* to yield Boc-Gly-OMe **126** (4.37 g, 97%) as a colourless oil.

δ_H (600 MHz, $CDCl_3$) 1.41 (9H, d, 3×C(3) H_3), 3.71 (3H, s, C(1) H_3), 3.88 (2H, d, J 5.7, C(3) H_2), 5.11 (1H, br s, NH); δ_c (150 MHz, $CDCl_3$) 28.4 (C(6) H_3), 42.3 (C(3) H_2), 52.3 (C(1) H_3), 80.1 (C(5)), 115.8 (C), 171.0 (C); m/z (ES^+) 190 (100%, $[M+H]^+$).

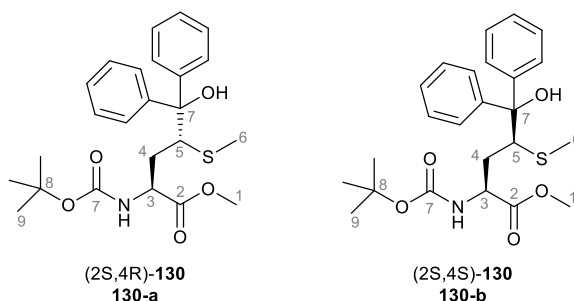
Methyl *N*-(*tert*-butoxycarbonyl)-*S*-(2-hydroxy-2,2-diphenylethyl)-*L*-homocysteinate, 129.



A reaction mixture of benzophenone (273 mg, 1.5 mmol) and Boc-L-Met-OMe **125** (502 mg, 1.91 mmol) in acetonitrile (15 mL) in a pyrex photoreactor immersion well, were degassed for 30 min, then irradiated with a 125 W, medium pressure mercury lamp for 40 min. The reaction solvent was concentrated *in vacuo*. Purification of the crude mixture via flash column chromatography (40-60 °C petrol:Et₂O, 7:3) gave benzophenone **13** (173 mg, 64%), Boc-L-Met-OMe **125** (336 mg, 67% wrt **125** starting material), ϵ -photoadduct **129** (88 mg, 13%) as a yellow oil.

δ_{H} (600 MHz, CDCl₃) 1.43 (9H, s, 3×C(9)H₃), 1.81-1.88 (1H, m, C(4)H_A), 2.02-2.08 (1H, m, C(4)H_B), 2.46 (2H, t, *J* 7.5, C(5)H₂), 3.43 (2H, s, C(6)H₂), 3.70 (3H, s, C(1)H₃), 4.36-4.42 (1H, m, C(3)H), 5.04 (1H, d, *J* 7.9, NH), 7.24 (2H, t, *J* 7.9, 2×*p*-PhH), 7.31 (4H, t, *J* 7.9, 4×*m*-PhH), 7.43 (4H, d, *J* 7.9, 4×*o*-PhH); δ_{C} (150 MHz, CDCl₃) 28.4 (CH₃), 30.0 (CH₂), 33.1 (CH₂), 46.4 (CH₂), 52.5 (CH₃), 52.6 (CH), 80.3 (C), 126.2 (CH), 127.4 (CH), 128.4 (CH), 145.6 (C), 145.7 (C), 155.4 (C), 172.9 (C); ν_{max} (solid) 2954, 2832, 2380, 1710, 1601; *m/z* (ES⁺) 468 (100%, [M+Na]⁺); HRMS (ESI⁺) C₂₄H₃₁NO₅SNa⁺ ([M+Na]⁺) requires 468.1815, measured 468.1800.

(*S,S*), (*S,R*) Benzophenone-Methionine γ -photoadduct diastereoisomers, (2*S*,2*R*)-130 and (2*S*,4*R*)-130.

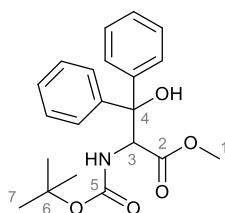


A reaction mixture of benzophenone (233 mg, 1.28 mmol) and Boc-L-Met-OMe **125** (427 mg, 1.62 mmol) in acetonitrile (30 mL) in) in a pyrex photoreactor immersion well, was degassed for 30 min, then irradiated with a 125 W, medium pressure mercury

lamp for 3 h. The reaction solvent was concentrated *in vacuo*. Purification of the crude mixture via flash column chromatography (40-60 °C petrol:Et₂O, 7:3) isolated Boc-L-Met-OMe **125** (102 mg, 24%) and γ -photoadduct (15 mg, 3%) as a 1 : 0.52 mixture of diastereoisomers **130a** and **130b**.

δ_{H} (600 MHz, CDCl₃) 1.45 (3 \times **130a**-C(9)H₃), 1.53 (3 \times **130b**-C(9)H₃), 1.59 (**130a**-C(6)H₃), 1.70 (**130b**-C(6)H₃), 1.73-1.82 (**130b**-C(4)H₂), 1.82-1.80 (**130a**-C(4)H_A), 2.12-2.18 (**130a**-C(4)H_B), 3.44 (**130b**-OH), 3.49 (**130a**-OH), 3.68 (**130b**-C(1)H₃), 3.75 (**130a**-C(1)H₃), 3.75-3.80 (**130a**-C(5)H, **130b**-C(5)H), 4.51-4.59 (**130b**-C(3)H), 5.03-5.08 (**130b**-NH), 5.20-5.26 (**130a**-NH), 7.16-7.22 (ArH), 7.26-7.33 (ArH), 7.47-7.55 (ArH); δ_{C} (150 MHz, CDCl₃) 17.3 (CH), 173 (CH), 28.5 (CH₃), 35.2 (CH₂), 36.1 (CH₂), 52.2 (CH₃), 52.4 (CH₃), 52.5 (CH₃), 55.1 (CH), 56.2 (CH), 80.1 (C), 80.2 (C), 80.4 (C), 80.5 (C), 125.7 (CH) 125.8 (CH), 125.8 (CH), 126.0 (CH), 127.1 (CH), 128.2 (CH), 128.3 (CH), 128.5 (CH), 128.6 (CH), 144.3 (C), 146.1 (C), 146.3 (C), 155.2 (C), 156.0 (C), 173.1 (C), 173.4 (C). *m/z* (FTMS) 468 (100%, [M+Na]⁺).

Methyl 2-((*tert*-butoxycarbonyl)amino)-3-hydroxy-3,3-diphenylpropanoate, **131**.



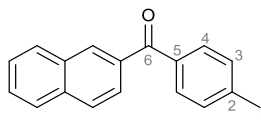
A reaction mixture of benzophenone (547 mg, 3.00 mmol) and Boc-Gly-OMe **126** (568 mg, 3.00 mmol) in acetonitrile (30 mL) in) in a pyrex photoreactor immersion well, were degassed for 30 min, then irradiated with a 125 W, medium pressure mercury lamp for 40 100 min. The reaction solvent was concentrated *in vacuo*. Purification of the crude mixture via flash column chromatography (40-60 °C petrol:Et₂O, 7:3) isolated

benzophenone (294 mg, 54%), Boc-Gly-OMe (184 mg, 32%) and photoadduct **131** (150 mg, 13%) as a yellow oil.

NB Diastereotopic protons on phenyl ring adjacent to a stereogenic centre in carbon NMR.

δ_{H} (600 MHz, CDCl_3) 1.30 (9H, s, $3\times\text{C}(7)\text{H}_3$), 3.50, (3H, s, $\text{C}(1)\text{H}_3$), 4.44 (1H, s, OH), 5.35 (1H, d, J 9.1, $\text{C}(3)\text{H}$), 5.50 (1H, s, J 9.1, NH), 7.17-7.23 (2H, m, $2\times p$ -PhH), 7.27-7.32 (4H, m, $4\times m$ -PhH), 7.46-7.52 (4H, m, $4\times o$ -PhH); δ_{C} (150 MHz, CDCl_3) 28.2 ($\text{C}(7)\text{H}_3$), 52.3 ($\text{C}(1)\text{H}_3$), 58.3 ($\text{C}(3)\text{H}$), 79.4 ($\text{C}(4)\text{H}$), 80.4 ($\text{C}(6)$), 125.3 (o -PhH), 125.7 (o -PhH), 127.4 (p -PhH), 127.7 (p -PhH), 128.4 (m -PhH), 128.6 ($2\times m$ -PhH), 142.2 (C), 144.0 (C), 173.6 (C); m/z (ES) 394 (100%, $[\text{M}+\text{Na}]^+$), 371 (15%, $[\text{M}+\text{H}]^+$).

Naphthalen-2-yl(*p*-tolyl)methanone, **116**.¹²⁰

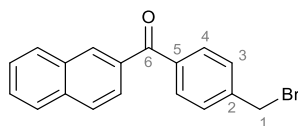


Thionyl chloride (1.0 mL, 13.8 mmol) was added dropwise to 4-methyl benzoic acid (500 mg, 3.67 mmol) and stirred at rt for 2 min, then at reflux for 2 h. The reaction mixture was cooled to rt and concentrated *in vacuo*. The residue redissolved in dry dichloroethane (100 mL) and naphthalene (941 mg, 7.34 mmol) then AlCl_3 (538mg, 4.04 mmol) were added. The resulting mixture was heated at 80 °C for 14 h, and then the reaction solvent was removed *in vacuo*. Purification via flash column chromatography (40-60 °C petrol:Et₂O, 50:1) twice yielded **116** (204 mg, 23%) as a yellow solid.

δ_{H} (600 MHz, CDCl_3) 2.43 (3H, s, $\text{C}(1)\text{H}_3$), 7.27 (2H, dd, J 8.5, 0.6, $2\times\text{C}(4)\text{H}$), 7.47-7.55 (3H, m, $3\times\text{C}(\text{Ar})\text{H}$), 7.57 (1H, dd, J 7.0, 1.3 $\text{C}(\text{Ar})\text{H}$), 7.78 (2H, br d, J 8.3,

2×C(3)H), 7.92 (1H, br d J 8.1, C(Ar)H), 8.00 (1H, dd, J 8.1, C(Ar)H), 8.05 (1H, br d, J 8.3, C(Ar)H); δ_c (150 MHz, CDCl₃) 21.9 (CH₃), 124.5 (CH), 125.8 (CH), 126.5 (CH), 127.3 (CH), 127.5 (CH), 128.5 (CH), 129.3 (CH), 130.7 (CH), 131.0 (C), 131.1 (CH), 133.8 (C), 135.8 (C), 136.8 (C), 144.4 (C), 197.9 (C(6)); ν_{\max} (oil) 3009, 2980, 2932, 2837, 1676, 1659, 1610; m/z (CI) 247 (100%, [M+H]⁺); HRMS (CI) C₁₈H₁₅O⁺ ([M+H]⁺) requires 247.11174, measured 247.11132.

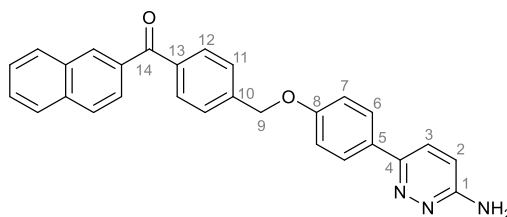
(4-(Bromomethyl)phenyl)(naphthalen-2-yl)methanone, 117.¹²⁰



A solution of naphthalen-2-yl(p-tolyl)methanone **116** (121 mg, 0.49 mmol) in benzene (3 mL) was treated with *N*-bromosuccinimide (87 mg, 0.49 mmol) then AIBN (12 mg, 0.07 mmol) and heated to 80 °C for 16 h. The reaction solvent was then removed *in vacuo*. Purification via flash column chromatography (40-60 °C petrol:Et₂O, 100:1) gave **117** (96 mg, 60%) as a yellow crystalline solid.

δ_H (600 MHz, CDCl₃) 2.52 (2H, s, C(1)H₂), 7.46-7.59 (6H, m, 6×C(Ar)H), 7.85 (2H, dt, J 8.6, 1.9, 2×C(Ar)H), 7.94 (1H, br d, J 8.1, C(Ar)H), 8.02 (1H, d, J 8.1, C(Ar)H), 8.09 (1H, d, J 8.5, C(Ar)H); δ_c (150 MHz, CDCl₃) 32.3 (CH₂), 124.5 (CH), 125.7 (CH), 126.7 (CH), 127.5 (CH), 128.0 (CH), 128.6 (CH), 129.2 (CH), 131.0 (C), 131.0 (CH), 131.6 (CH), 133.8 (C), 136.1 (C), 138.2 (C), 143.0 (C), 197.4 (C(6)); ν_{\max} (solid) 2942, 2831, 1652; m/z (CI) 326 (38%, [⁸¹M]⁺), 324 (39%, [⁷⁹M]⁺), 247 (100%, [M-Br]⁺); HRMS (CI) C₁₈H₁₄BrO⁺ requires 325.02225; measured 325.02190.

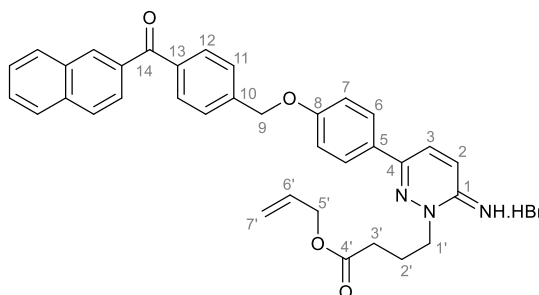
(4-((4-(6-Imino-1,6-dihydropyridazin-3-yl)phenoxy)methyl)phenyl)(naphthalen-2-yl) methanone, 118.



A solution of aryl pyridazine **31** (18.3 mg, 0.098 mmol) in DMF (0.1 mL) 2.21.1 was added to NaH (4.0 mg, 0.11 mmol) in DMF (0.3 mL) at 0 °C and stirred for 20 min. Naphthalene **117** (35 mg, 0.11 mmol) was added in one portion and the reaction mixture stirred at rt for 16 h, before the reaction solvent was removed *in vacuo*. Purification via flash column chromatography (EtOAc) gave **118** (33 mg, 77%) as a white solid.

δ_{H} (600 MHz, CDCl_3) 4.97 (2H, s, NH_2), 5.20 (2H, s, $\text{C}(9)\text{H}_2$), 6.87 (1H, d, J 9.0, $\text{C}(3)\text{H}$), 7.07 (2H, d, J 8.7, $2\times\text{C}(6)\text{H}$), 7.49-7.56 (5H, m, $5\times\text{C}(\text{Ar})\text{H}$), 7.57-7.62 (2H, m, $2\times\text{C}(\text{Ar})\text{H}$), 7.87-7.95 (4H, m, $5\times\text{C}(\text{Ar})\text{H}$), 8.01 (1H, d, J 7.9, $\text{C}(\text{Ar})\text{H}$), 8.09 (1H, d, J 8.3, $\text{C}(\text{Ar})\text{H}$); δ_{C} (150 MHz, CDCl_3) 69.5 (CH_2), 115.3 (CH), 115.4 (CH), 124.5 (CH), 125.8 (CH), 126.0 (CH), 126.6 (CH), 127.2 (CH), 127.5 (CH), 127.7 (CH), 127.9 (CH), 128.6 (CH), 130.0 (C), 130.9 (CH), 131.0 (C), 131.5 (CH), 133.8 (C), 136.3 (C), 138.0 (C), 142.5 (C), 152.2 (C), 158.0 (C), 159.3 (C), 197.7 (C); ν_{max} (solid) 2830, 2350, 1650; mp (EtOH) 101-105 °C; m/z (ES^+) 432, (100%, $[\text{M}+\text{H}]^+$); HRMS (ES^+) $\text{C}_{28}\text{H}_{22}\text{N}_3\text{O}_2^+$ ($[\text{M}+\text{H}]^+$) requires 432.1712, measured 432.1712.

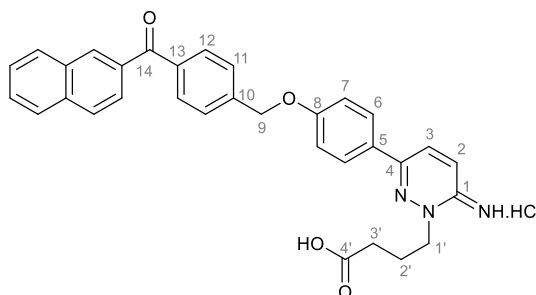
Allyl 4-(3-(4-((4-(2-naphthoyl)benzyl)oxy)phenyl)-6-iminopyridazin-1(6H)-yl)butanoate, 119.



A reaction mixture of allyl-4-bromobutrate (7.2 mg, 0.035 mmol) and pyridazine **118** (10 mg, 0.023 mmol) in DMF (0.1 mL) was heated to 80 °C for 72 h. The reaction solvent was removed *in vacuo* and the residue was triturated with EtOAc (2×5 mL) to give **119** (10 mg, 98%) as a grey solid.

δ_{H} (600 MHz, $\text{CDCl}_3:\text{CD}_3\text{OD}$, 1:1) 2.24 (2H, quin, J 7.0, $\text{C}(2')\text{H}_2$), 2.59 (2H, t, J 6.8, $\text{C}(3')\text{H}_2$), 4.41 (2H, t, J 7.3, $\text{C}(1')\text{H}_2$), 4.51 (2H, dt, J 5.8, 1.3, $\text{C}(5')\text{H}_2$), 5.18 (1H, dq, J 10.4, 1.2, $\text{C}(7')\text{H}_A$), 5.22-5.26 (3H, m, $\text{C}(9)\text{H}_2$, $\text{C}(7')\text{H}_B$), 5.78-5.85 (1H, m, $\text{C}(6')\text{H}$), 7.11 (2H, d, J 9.0, $2\times\text{C}(\text{Ar})\text{H}$), 7.47-7.57 (7H, m, $7\times\text{C}(\text{Ar})\text{H}$), 7.65 (1H, d, J 9.6, $\text{C}(\text{Ar})\text{H}$), 7.84-7.88 (3H, m, $3\times\text{C}(\text{Ar})\text{H}$), 7.94 (1H, d, J 8.1, $\text{C}(\text{Ar})\text{H}$), 8.01 (1H, d, J 8.5 $\text{C}(\text{Ar})\text{H}$), 8.04 (1H, d, J 8.0 $\text{C}(\text{Ar})\text{H}$), 8.15 (1H, d, J 9.6, $\text{C}(\text{Ar})\text{H}$); δ_{C} (150 MHz, $\text{CDCl}_3:\text{CD}_3\text{OD}$, 1:1) 22.8 ($\text{C}(2')\text{H}_2$), 31.5 ($\text{C}(3')\text{H}_2$), 57.0 ($\text{C}(1')\text{H}_2$), 67.1 ($\text{C}(5')\text{H}_2$), 70.7 ($\text{C}(9)\text{H}_2$), 117.0 (CH), 119.9 ($\text{C}(7')\text{H}_2$), 125.9 (CH), 126.7 (CH), 127.0 (CH), 127.9 (CH), 128.5 (CH), 128.7 (CH), 129.2 (CH), 129.6 (CH), 132.2 (CH), 132.7 (CH), 132.8 (C), 132.9 (CH), 133.0 (CH), 135.2 (C), 137.3 (C), 139.2 (C), 143.7 (C), 152.1 (C), 153.7 (C), 161.8 (C), 162.4 (C), 174.2 ($\text{C}(4')$), 199.8 ($\text{C}(14)$); ν_{max} (solid) 3410, 2990, 1648, 1571; mp 242-244 °C; m/z (ES^+) 558, (100%, $[\text{M}+\text{H}]^+$); HRMS (ES^+) $\text{C}_{35}\text{H}_{31}\text{N}_3\text{O}_4$ requires 558.2393; measured 560.0221 $[\text{M}+2\text{H}]^+$.

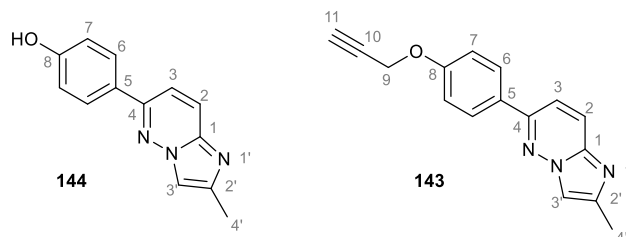
4-(3-(4-((4-(2-Naphthoyl)benzyl)oxy)phenyl)-6-iminopyridazin-1(6H)-yl)butanoic acid, 115.



To a solution of **119** (9.9 mg, 0.017 mmol) in THF (1 mL) and H₂O (1 mL) was added NaOH (5 mg) and the resulting mixture was stirred at 50 °C for 3 h. The reaction solution was then cooled to 10 °C and washed with EtOAc (5 mL). The aqueous layer was acidified to pH 1.0 by addition of 1 M aqueous HCl and then stirred for 1 h, before the solvent was removed *in vacuo*. Trituration with H₂O (3 mL) yielded **115** (9 mg, 99%) as a white solid.

δ_{H} (600 MHz, CDCl₃:CD₃OD, 1:1) 2.08-2.15 (2H, m, C(2')H₂), 2.33-2.38 (2H, m, C(3')H₂), 4.39-4.44 (2H, m, C(1')H₂), 5.28 (2H, s, C(9)H₂), 6.91 (1H, d, *J* 8.7, C(3)H), 7.14 (2H, d, *J* 8.9, 2×C(7)H), 7.47-7.65 (5H, m, 5×C(Ar)H), 7.81 (1H, d, *J* 8.7, C(2)H), 7.86 (2H, d, *J* 8.3, 2×C(Ar)H), 7.93 (2H, d, *J* 8.7, 2×C(6)H), 7.97 (1H, d, *J* 8.1, C(Ar)H), 7.99 (1H, d, *J* 8.9, C(Ar)H), 8.07 (1H, d, *J* 8.3, C(Ar)H), 8.22 (1H, d, *J* 9.4, C(Ar)H); δ_{C} (150 MHz, CDCl₃:CD₃OD, 1:1) 24.3 (CH₂), 38.4 (CH₂), 57.9 (CH₂), 70.5 (CH₂), 116.7 (CH), 117.3 (CH), 125.6 (CH), 126.5 (CH), 126.7 (CH), 127.8 (CH), 128.5 (CH), 129.0 (CH), 129.5 (CH), 129.8 (CH), 131.9 (CH), 132.1 (C), 132.5 (CH), 132.7 (CH), 135.2 (C), 137.4 (C), 139.1 (C), 144.2 (C), 153.4 (C), 153.6 (C), 153.8 (C), 179.9 (C(4')), 199.8 (C(14)); ν_{max} (solid) 3410, 2990, 1648, 1571; mp 234-237 °C; *m/z* (ES⁺) 518 (100%, [M+H]⁺); HRMS (ES⁺) C₃₂H₂₆N₃O₄⁺ (M⁺) requires 516.1923, measured 516.1971.

**4-(2-Methylimidazo[1,2-b]pyridazin-6-yl)phenol 144, and
2-Methyl-6-(4-(prop-2-yn-1-yloxy)phenyl)-2,3-dihydroimidazo[1,2-b]pyridazine,
143.**



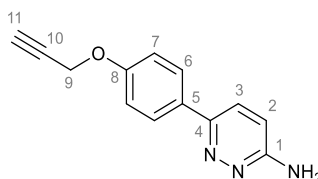
A solution of NaH (65% in mineral oil, 99 mg, 2.67 mmol) in DMF (5 mL) was added dropwise to a solution of **31** (500 mg, 2.67 mmol) in DMF (1 mL) at 0 °C. The resulting mixture was stirred at 0 °C for 30 min. Propargyl bromide (85% in toluene, 357 μ L, 3.21 mmol) was then added and the reaction was stirred at 0 °C for 90 min, before being quenched with H₂O (1 mL) and concentrated *in vacuo*. Purification via flash column chromatography (40-60 °C petrol: EtOAc, 1:1) yielded **31** (40 mg, 1%), **142** (94 mg, 16%), **144** (25 mg, 7%) and **143** (40 mg, 1%) with respect to requisite starting materials.

Data for 144: δ_{H} (600 MHz, CD₃OD) 2.45 (3H, s, C(4')H₃), 6.91 (2H, d, *J* 8.8, 2×C(7)H), 7.54 (1H, d, *J* 9.5, C(2)H), 7.79 (1H, s, C(3')H), 7.83 (3H, m, C(3)H, 2×C(6)H); δ_{C} (150 MHz, CD₃OD) 14.8 (C(4')H₃), 115.6 (C(3')H), 117.0 (C(7)H), 117.8 (C(2)H), 124.9 (C(3)H), 128.0 (C(5)), 129.7 (C(6)H), 139.1 (C(1)), 144.2 (C(2')), 153.2 (C(4)), 160.6 (C(8)); *m/z* (EI) 226 (100%, [M+H]⁺), 210 (95%); HRMS (ES⁺) C₁₃H₁₂N₃O⁺ ([M+H]⁺) requires 226.0980, measured 226.0985.

Data for 143: δ_{H} (600 MHz, CD₃OD) 2.45 (3H, s, C(4')H₃), 3.00 (1H, t, *J* 2.4, C(11)H) 4.80 (2H, d, *J* 2.4, C(9)H₂), 7.10 (2H, d, *J* 8.9, 2×C(7)H), 7.63 (1H, d, *J* 9.6, C(2)H), 7.85-7.87 (3H, m, C(3')H, C(3)H), 7.95 (2H, d, *J* 8.9, 2×C(6)H); δ_{C} (150 MHz, CD₃OD) 14.3 (C(4')H₃), 56.7 (C(9)H₂), 77.1 (C(11)H), 115.7 (C(3')H), 116.3

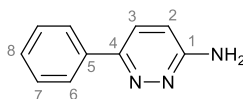
($2\times C(7)H$), 117.6 ($C(2)H$), 124.8 ($C(3)H$), 129.3 ($2\times C(6)H$), 79.5 ($C(10)$), 129.7 ($C(5)$), 139.1 ($C(1)$), 144.4 ($C(2')$), 152.6 ($C(4)$), 160.7 ($C(8)$); m/z (EI) 264 (100%, $[M+H]^+$), 279 (20%, $[M+Na]^+$); HRMS (ES^+) $C_{16}H_{14}N_3O^+$ ($[M+H]^+$) requires 264.1137, measured 264.1140.

6-(4-(Prop-2-yn-1-yloxy)phenyl)pyridazin-3-amine, **142**.³⁰



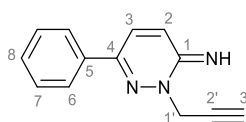
A solution of NaH (65% in mineral oil, 39.5 mg, 1.07 mmol) in DMF (5 mL) was added dropwise to a solution of **31** (200 mg, 1.07 mmol) in DMF (5 mL) over 1 h at 0 °C, and the resulting mixture was stirred at 0 °C for 90 min. Propargyl bromide (85% in toluene, 143 μ L, 1.28 mmol) was then added and the reaction was allowed to warm to rt over 4 h, before being quenched with H₂O (1 mL) and concentrated *in vacuo*. Purification via flash column chromatography (40-60 °C petrol: EtOAc, 2:3) yielded **142** (92.9 mg, 34%) as a white solid.

δ_H (600 MHz, CD₃OD) 2.94 (1H, t, J 2.4, $C(11)H$), 4.78 (2H, d, J 2.4, $C(9)H_2$), 7.00 (1H, d, J 9.3, $C(2)H$), 7.08 (2H, d, J 8.9, $2\times C(7)H$), 7.73 (1H, d, J 9.3, $C(3)H$), 7.82 (2H, d, J 8.9, $2\times C(6)H$); δ_C (150 MHz, CD₃OD) 56.7 ($C(9)H_2$), 77.0 ($C(11)H$), 79.6 ($C(10)$), 116.3 ($2\times C(7)H$), 117.6 ($C(2)H$), 128.1 ($C(3)H$), 128.5 ($C(6)H$), 131.3 (C), 152.7 (C), 159.9 (C), 161.3 (C); ν_{max} (solid) 3436, 3260, 3148, 3046, 2930, 2109, 1630, 1603; mp (EtOH) 167-168 °C; {Lit³⁰ 117-119 °C}; m/z (ES^+) 226 (10%, $[M+H]^+$), 218 (100%); HRMS (ES^+) $C_{13}H_{12}N_3O$ ($[M+H]^+$) requires 226.0980, measured 226.0989.

6-phenylpyridazin-3-amine, 148.¹²¹

A suspension of phenylboronic acid (1.00 g, 8.20 mmol), 3-amino-6-chloropyridazine **33** (886 mg, 6.83 mmol) and Pd(PPh₃)₂Cl₂ (240 mg, 0.34 mmol) in 1,4-dioxane (50 mL) was degassed and stirred at rt for 10 min. Degassed 2 M aqueous Na₂CO₃ (6.9 mL) was added and the reaction mixture was heated rapidly to reflux for 16 h. The resulting mixture was then concentrated *in vacuo*. Purification via flash column chromatography (40-60° petrol : EtOAc, 1:1 to 0:1) gave **148** (625 mg, 53%) as a white solid.

δ_{H} (600 MHz, CDCl₃) 6.97 (1H, d, *J* 9.4, C(2)*H*), 7.39 (1H, t, *J* 7.5, C(8)*H*), 7.44 (2H, t, *J* 7.5, 2×C(7)*H*), 7.67 (1H, d, *J* 9.4, C(3)*H*), 7.82 (2H, d, *J* 7.5, 2×C(6)*H*); δ_{C} (150 MHz, CDCl₃) 116.2 (C(2)*H*), 126.1 (C(6)*H*), 127.2 (C(3)*H*), 128.8 (C(7)*H*), 128.8 (C(8)*H*), 136.6 (C(5)), 152.0 (C(4)), 159.5 (C(1)); *m/z* (ES⁺) 172 (100%, [M+H]⁺).

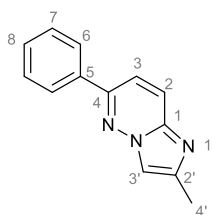
6-phenyl-2-(prop-2-yn-1-yl)pyridazin-3(2H)-imine, 147.

A reaction mixture of **148** (26 mg, 0.15 mmol) and propargyl bromide (89% in toluene, 20 μ L, 0.18 mmol) in DMF (0.1 mL) was heated at 50 °C for 3 h. After this time EtOAc (5 mL) was added and the reaction cooled to 0 °C. The resulting precipitate was filtered and washed with cold EtOAc (2 mL) to give **147** (35 mg, 80%) as a white solid.

δ_{H} (600 MHz, CD₃OD) 3.25 (1H, t, *J* 2.6, C(3')*H*), 5.29 (2H, d, *J* 2.6, C(1')*H*₂), 7.53-7.59 (3H, m, C(8)*H*, 2×C(7)*H*), 7.67 (1H, d, *J* 9.4, C(3)*H*), 7.99-8.03 (2H, m,

$2\times C(6)H$), 8.37 (1H, d, J 9.7, $C(2)H$); δ_C (150 MHz, CD_3OD) 48.2 ($C(1')H_2$), 74.4 ($C(2')$), 78.9 ($C(3')H$), 127.0 ($C(3)H$), 127.8 ($C(6)H$), 130.4 ($C(7)H$), 132.4 ($C(8)H$), 133.5 ($C(2)H$), 134.0 ($C(5)$), 152.0 ($C(4)$), 154.0 ($C(1)$); m/z (ES^+) 210 (100%, $[M+H]^+$); HRMS (ES^+) $C_{13}H_{12}N_3$ ($[M+H]^+$) requires 210.1031, measured 210.1022.

2-methyl-6-phenylimidazo[1,2-b]pyridazine, **149**.



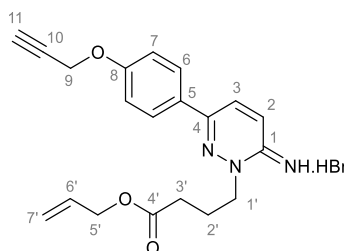
Method A: To a solution of 6-phenyl-2-(prop-2-yn-1-yl)pyridazin-3(2H)-imine, **147** (17 mg, 0.06 mmol) in DMF (0.1 mL) was added sodium hydride (4.3 mg, 0.12 mmol) at 0 °C. The reaction mixture was stirred at 0 °C for 30 min, then rt for 30 min before the reaction solvent was removed *in vacuo*. Purification via flash column chromatography (EtOAc) gave **149** (10 mg, 69%) as a white solid.

*Method B:*⁹³ A reaction mixture of 1-amino-6-phenylpyridazine **148** (100 mg, 0.58 mmol), chloroacetone (53 μ L, 0.64 mmol) in ethanol (50 mL) was heated at reflux for 3 h. The reaction mixture was cooled to rt and was treated with 1M aqueous $NaHCO_3$ (0.3 mL), before being heated at reflux for a further 14 h. The reaction solvents were removed *in vacuo*, and the resulting residue was redissolved in $CHCl_3$ (50 mL), washed with H_2O (50 mL), dried and concentrated *in vacuo* to give **149** (82 mg, 68%) as a cream solid.

δ_H (600 MHz, $CDCl_3$) 2.54, (3H, s, $C(4')H_3$), 7.44 (1H, d, J 9.4 $C(3)H$), 7.48-7.54 (3H m, $C(8)H$, $2\times C(7)H$), 7.80 (1H, s, $C(3')H$), 7.91 (1H, d, J 9.4, $C(2)H$), 7.93-7.96 (2H, m, $2\times C(6)H$); δ_C (150 MHz, $CDCl_3$) 15.0 ($C(4')H_3$), 114.5 ($C(3')H$), 115.8 ($C(3)H$), 124.6 ($C(2)H$), 127.1 ($C(6)H$), 129.2 ($C(7)H$), 136.0 ($C(5)$), 138.1 ($C(1)$), 144.4

(C(2')), 151.4 (C(4)); m/z (ES⁺) 209 (100%, [M]⁺), 214 (50%); HRMS (ES⁺) C₁₃H₁₂N₃ ([M+H]⁺) requires 210.1031, measured 210.1036.

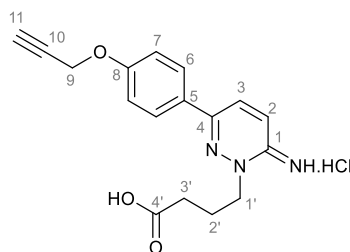
Allyl 4-(6-imino-3-(4-(prop-2-yn-1-yloxy)phenyl)pyridazin-1(6H)-yl)butanoate hydrobromide, **150.**³⁰



A reaction mixture of **142** (130 mg, 0.58 mmol) and allyl bromobutyrate (120 mg, 0.58 mmol) in DMF (0.1 mL) was heated at 80 °C for 6 h. The product precipitated upon addition of cold EtOAc (7 mL) and was filtered to yield **150** (168 mg, 67%) as a white solid.

δ_H (600 MHz, CD₃OD) 2.24 (2H, quint, J 6.8, C(2')H₂), 2.61 (2H, t, J 6.8, C(3')H₂), 3.00 (1H, t, J 2.4, C(11)H), 4.41-4.47 (4H, m, C(1')H₂, C(5')H₂), 4.81 (2H, d, J 2.4, C(9)H₂), 5.14 (1H, dd, J 10.5, 1.2, C(7')H_A), 5.22 (1H, dd, J 17.2, 1.2, C(7')H_B), 5.77-5.83 (1H, m, C(6')H), 7.13 (2H, d, J 8.9, 2×C(7)H), 7.60 (1H, d, J 9.5, C(3)H), 7.95 (2H, d, J 8.9, 2×C(6)H), 8.29 (1H, d, J 9.5, C(2)H); δ_C (150 MHz, CD₃OD) 22.5 (C(2')H₂), 31.3 (C(3')H₂), 56.8 (CH₂), 56.9 (CH₂), 66.5 (CH₂), 77.3 (C(11)H), 79.3 (C(10)), 116.7 (C(7)H), 118.7 (C(7')H₂), 126.7 (CH), 127.1 (C), 129.3 (CH), 132.6 (CH), 133.4 (CH), 151.8 (C), 153.9 (C), 161.5 (C), 174.0 (C(4')) {1 C signal unobserved}; ν_{\max} (solid) 3318, 3259, 3218, 3029, 2120; mp (EtOH) 159-161 °C {Lit³⁰107-109 °C}; m/z (ES⁺) 352 (100%, [M+H]⁺).

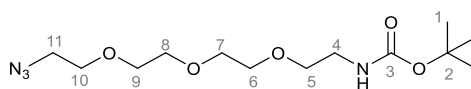
4-(6-Imino-3-(4-(prop-2-yn-1-yloxy)phenyl)pyridazin-1(6H)-yl)butanoic acid hydrochloride, **141.**³⁰



To a solution of **150** (20 mg, 0.046 mmol) in THF (1 mL) and H₂O (1 mL) was added NaOH (5 mg, 0.208 mmol) and the resulting mixture was stirred at 50 °C for 3 h. The reaction solution was then cooled to 10 °C and washed with EtOAc (5 mL). The aqueous layer was acidified to pH 1.0 by addition of 1 M aqueous HCl and then stirred for 1 h, before the solvent was removed *in vacuo*. Trituration with H₂O (3 mL) yielded **141** (18 mg, 99%) as a white solid.

δ_{H} (600 MHz, CD₃OD) 2.22 (2H, quint, J 7.1, C(2')H₂), 2.55 (2H, t, J 6.7, C(3')H₂), 2.87 (1H, t, J 2.2, C(11)H), 4.43 (2H, t, J 7.1, C(1')H₂), 4.75-4.80 (2H, m, C(9)H₂), 7.13 (2H, d, J 8.9, 2×C(7)H), 7.62 (1H, d, J 9.6, C(3)H), 7.93 (2H, d, J 8.9, 2×C(6)H), 8.24 (1H, d, J 9.6, C(2)H); δ_{C} (150 MHz, CD₃OD) 22.8 (C(2')H₂), 31.1 (C(3')H₂), 57.0 (CH₂), 57.0 (CH₂), 77.3 (C(11)), 79.4 (C(10)) 116.8 (C(7)H), 126.7 (C(3)H), 129.4 (CH), 132.7 (CH), 136.3, (C), 150.3 (C), 152.2 (C), 161.3 (C), 177.3 (C); ν_{max} (oil) 3338, 3259, 3069, 1722; mp (EtOH) 261-264 °C {Lit 180-183 °C}; m/z (ES⁺) 312 (100%, [M+H]⁺).

***tert* Butyl (2-(2-(2-(2-azidoethoxy)ethoxy)ethoxy)ethyl)carbamate, **151**.**¹²²

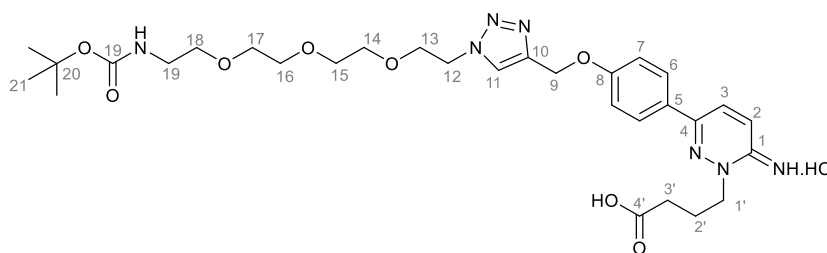


To a solution of 3,6,9-trioxaundecan-1-amine (90.9 μ L, 0.458 mmol) in ethanol (2 mL) at 0 °C was added Boc₂O (100 mg, 0.458 mmol), and the reaction mixture was

allowed to warm to rt over 12 h. The reaction solvent was removed *in vacuo*, and the residue was redissolved in CH₂Cl₂ (20 mL) before being washed with H₂O (20 mL), brine (20 mL) and dried and concentrated *in vacuo*. Purification via flash column chromatography (40-60 °C petrol:EtOAc, 1:1) gave **151** (111 mg, 76%) as a white solid.

δ_{H} (600 MHz, CDCl₃) 1.39 (9H, s, 3×C(1)H₃), 3.26 (2H, q, *J* 5.1, C(4)H₂), 3.34 (2H, t, *J* 5.1, C(11)H₂), 3.49 (2H, t, *J* 5.1, C(5)H₂), 3.55-3.58 (2H, m, CH₂), 3.59-3.61 (2H, m, CH₂), 3.61-3.65 (6H, m, 3×CH₂), 5.05 (1H, br s, NH); δ_{C} (150 MHz, CDCl₃) 28.5 (C(1)H₃), 40.4 (C(4)H₂), 50.7 (C(11)H₂), 70.1 (CH₂), 70.3 (CH₂), 70.7 (CH₂), 70.7 (CH₂), 70.8 (CH₂), 70.8 (CH₂), 79.2 (C(2)), 156.1 (C(3)); *m/z* (ES⁺) 341 (100%, [M+Na]⁺), 319 ([M+H]⁺, 15%), 219 (74%, [M-C₅H₈O₂]⁺).

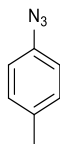
4-(3-(4-((1-(2,2-Dimethyl-4-oxo-3,8,11,14-tetraoxa-5-azahexadecan-16-yl)-1H-1,2,3-triazol-4-yl)methoxy)phenyl)-6-iminopyridazin-1(6H)-yl)butanoic acid hydrochloride, **152.**



A mixture of CuSO₄·5H₂O (1.1 mg, 0.0044 mmol) and sodium ascorbate (2.6 mg, 0.0131 mmol) were premixed in degassed H₂O (0.5 mL), then added to a suspension of **141** (10.1 mg, 0.029 mmol) and **151** (9.2 mg, 0.029 mmol) in degassed H₂O (1 mL). The reaction mixture was stirred at rt for 6 h, before the solvent was removed *in vacuo*. Purification via flash column chromatography (CHCl₃:CH₃OH, 7:3) yielded **152** (5.1 mg, 29%) as a white solid.

δ_{H} (600 MHz, CD_3OD) 1.40 (9H, s, ($3\times\text{C}(21)\text{H}_3$), 2.10-2.16 (2H, m, $\text{C}(2')\text{H}_2$), 2.47 (2H, t, J 6.3, $\text{C}(3')\text{H}_2$), 3.19 (2H, t, J 5.5, $\text{C}(19)\text{H}_2$), 3.46 (2H, t, J 5.5, $\text{C}(18)\text{H}_2$), 3.56 (6H, s, $3\times\text{CH}_2$), 3.57-3.63 (2H, m, CH_2), 3.91 (2H, t, J 4.9, CH_2), 4.42 (2H, t, J 6.3, $\text{C}(1')\text{H}_2$), 4.46 (2H, t, J 5.0, CH_2), 5.26 (2H, s, $\text{C}(9)\text{H}_2$), 7.19 (2H, d, J 8.9, $2\times\text{C}(7)\text{H}$), 7.62 (1H, d, J 9.4, $\text{C}(3)\text{H}$), 7.97 (2H, d, J 8.9, $2\times\text{C}(6)\text{H}$), 8.18 (1H, s, $\text{C}(11)\text{H}$), 8.24 (1H, d, J 9.4, $\text{C}(2)\text{H}$); δ_{C} (150 MHz, CD_3OD) 24.0 ($\text{C}(2')\text{H}_2$), 28.8 ($\text{C}(21)\text{H}_3$), 33.6 ($\text{C}(3')\text{H}_2$), 41.2 ($\text{C}(19)\text{H}_2$), 51.5 (CH_2), 57.7 ($\text{C}(1')\text{H}_2$), 62.5 (CH_2), 70.3 (CH_2), 71.0 (CH_2), 71.2 (CH_2), 71.3 (CH_2), 71.4 (CH_2), 80.3 ($\text{C}(20)$) 166.6 ($\text{C}(7)\text{H}$), 126.6 ($\text{C}(3)\text{H}$), 129.3 (CH), 129.4 (CH), 132.4 ($\text{C}(2)\text{H}$), 144.4 (C), 151.7 (C), 153.8 (C), 158.5 (C), 162.0 (C), 180.9 (C) {1 C signal unobserved}; m/z (ES^+) 630 (100%, $[\text{M}+\text{H}]^+$); HRMS (ES^+) $\text{C}_{30}\text{H}_{44}\text{N}_7\text{O}_8^+$ ($[\text{M}+\text{H}]^+$) requires 630.3251, measured 630.3261.

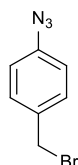
1-Azido-4-methylbenzene, **34**.¹²³



A solution of p-toluidine (1.00 g, 9.33 mmol) in 2M aqueous HCl (15 mL) was cooled to $-5\text{ }^{\circ}\text{C}$ and a solution of NaNO_2 (773 mg, 11.2 mmol) in H_2O (2.60 mL) was added. The reaction mixture was stirred at $-5\text{ }^{\circ}\text{C}$ for 5 min before urea (67.2 mg, 1.12 mmol) was added. This reaction mixture was then added to a solution of NaN_3 (1.21 g, 18.7 mmol), NaOAc (2.30 g, 28.0 mmol) in H_2O (15 mL) over 5 min whilst maintaining the temperature at $0\text{ }^{\circ}\text{C}$. The resulting solution was stirred for a further 2 h at $0\text{ }^{\circ}\text{C}$. Et_2O (50 mL) and H_2O (50 mL) were added and the organic layer was separated, washed with H_2O (50 mL), dried, and concentrated *in vacuo* to give **34** as a yellow oil (1.151 g, 93%).

δ_{H} (600 MHz, CDCl_3); 2.33 (3H, s, CH_3), 6.93 (2H, d, J 8.4, $2\times\text{C}(3)\text{H}$), 7.16 (2H, d, J 8.4, $2\times\text{C}(2)\text{H}$); δ_{C} (150 MHz, CDCl_3); 21.0 (CH_3), 118.9 (CH), 130.5 (CH), 134.7 (C), 137.2 (C); m/z (ES^+) 133 (100%, M^+).

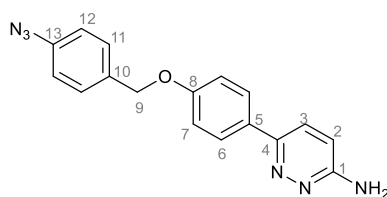
1-azido-4-(bromomethyl)benzene, 35.¹²³



To a solution of **34** (966 mg, 7.25 mmol) in PhH (100 mL) was added *N*-bromosuccinimide (1.42 g, 7.98 mmol) followed by AIBN (179 mg, 1.09 mmol) and the reaction was heated to 80 °C for 4 h. The reaction mixture was concentrated *in vacuo*. Purification via flash column chromatography (petrol 40-60 °C) yielded **35** as a yellow oil (1.175 g, 76%).

δ_{H} (600 MHz, CDCl_3); 4.48 (2H, s, CH_2), 7.00 (2H, d, J 8.6, $2\times\text{C}(3)\text{H}$), 7.38 (2H, d, J 8.6, $2\times\text{C}(2)\text{H}$); δ_{C} (150 MHz, CDCl_3); 33.1 (CH_2), 119.5 (CH), 130.7 (CH), 134.6 (C), 140.3 (C); m/z (EI) 210 (100%, $^{79}\text{M}^+$), 212 (100%, $^{81}\text{M}^+$).

6-(4-((4-Azidobenzyl)oxy)phenyl)pyridazin-3-amine, 36.³⁰

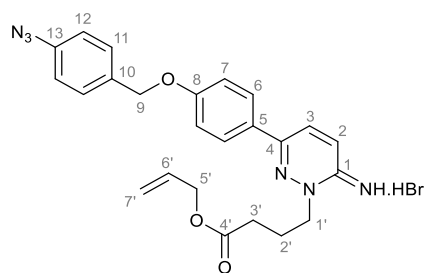


A solution of aryl pyridazine **31** (100 mg, 0.53 mmol) in DMF (0.2 mL) was added to NaH (65% in mineral oil, 20 mg, 0.53 mmol) in DMF (0.3 mL) at 0 °C and stirred for 30 min. Benzylbromide **35** (125 mg, 0.59 mmol) was added in one portion and the reaction mixture stirred at rt for 16 h, before the reaction solvent was removed *in*

vacuo. Purification via flash column chromatography (CH₂Cl₂:CH₃OH, 100:2) gave **36** (78.6 mg, 51%) as a yellow solid.

δ_{H} (600 MHz, DMSO-d₆) 5.14 (2H, s, C(9)H₂), 6.38 (2H, s, NH₂), 6.82 (1H, d, *J* 9.2, C(2)H), 7.09 (2H, d, *J* 8.9, 2×C(7)H), 7.16 (2H, d, *J* 8.6, 2×C(11)H), 7.52 (2H, d, *J* 8.6, 2×C(12)H), 7.75 (1H, d, *J* 9.2, C(3)H), 7.89 (2H, d, *J* 8.9, 2×C(6)H); δ_{C} (150 MHz, DMSO) 68.7 (CH₂), 114.3 (CH), 115.1 (CH), 119.2 (CH), 124.9 (CH), 126.6 (CH), 129.6 (CH), 133.9 (C), 139.0 (C), 148.6 (C), 149.6 (C), 154.6 (C), 159.5 (C); *m/z* (ES⁺) 319 (100%, [M+H]⁺).

Allyl 4-(3-(4-((4-azidobenzyl)oxy)phenyl)-6-iminopyridazin-1(6H)-yl)butanoate, 37.³⁰

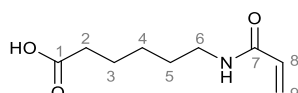


A reaction mixture of allyl 4-bromobutyrate (50 mg, 0.24 mmol), **36** (76 mg, 0.24 mmol) in DMF (0.1 mL) was heated to 50 °C for 16 h. The product precipitated upon addition of cold EtOAc (2 mL), and filtered to give a mixture of starting material and **37**, which was recrystallised twice with EtOAc (2 mL) to yield **37** (5.1 mg, 4%) as a brown oil.

δ_{H} (600 MHz, CD₃OD) 2.25 (2H, quint, *J* 6.8, C(2')H₂), 2.60 (2H, t, *J* 6.8, C(3')H₂), 4.42 (2H, t, *J* 6.8, C(1')H₂), 4.49 (2H, dt, *J* 5.8, 1.3, C(5')H₂), 5.13 (2H, s, C(9)H₂), 5.17 (1H, dd, *J* 10.5, 1.3, C(7')H_A), 5.23 (1H, dd, *J* 17.1, 1.3, C(7')H_B), 5.78-5.85 (1H, m, C(6')H), 7.06 (2H, d, *J* 8.5, 2×C(11)H), 7.10 (2H, d, *J* 9.0, 2×C(7)H), 7.45 (2H, d, *J* 8.5, 2×C(12)H), 7.61 (1H, d, *J* 9.5, C(3)H), 7.88 (2H, d, *J* 9.0, 2×C(6)H), 8.20 (1H,

d, J 9.5, C(2) H); δ_C (150 MHz, CD₃OD) 22.7 (CH₂), 31.5 (CH₂), 57.0 (CH₂), 66.9 (CH₂), 70.8 (CH₂), 116.9 (CH), 119.6 (CH₂), 120.4 (CH), 126.4 (C), 126.8 (CH), 129.5 (CH), 130.5 (CH), 132.8 (CH), 133.0 (C), 134.6 (C), 141.4 (C), 152.1 (C), 153.7 (C), 162.6 (C), 174.1 (C); m/z (EI) 524 (7%, M⁺).

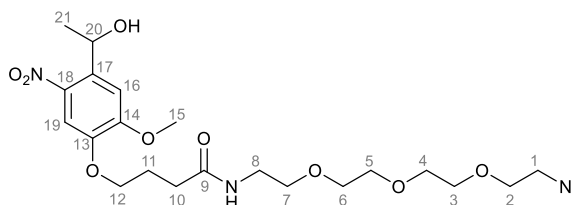
6-Acrylamidohexanoic acid, **156**.¹²⁴



Acryloyl chloride (96%, 705 μ L, 8.38 mmol) was added dropwise over 15 min to an ice-cold solution of 6-aminohexanoic acid (1.00 g, 7.62 mmol) and Ca(OH)₂ (1.02 g, 13.7 mmol) in H₂O (15 mL). The reaction was stirred at 0 °C for a further 10 min before being filtered. The filtrate was adjusted to pH 2-6 by addition of concentrated HCl and the resulting crystals were filtered to yield **156** (512 mg, 36%) as a white crystalline solid, which was used with no further purification.

δ_H (600 MHz, DMSO-d₆) 1.23-1.29 (2H, m, C(4) H_2), 1.41 (2H, quin, J 7.5, C(5) H_2), 1.49 (2H, quin, J 7.5, C(3) H_2), 2.19 (2H, t, J 7.5, C(2) H_2), 3.10 (2H, dd, J 7.5, 18.2, C(6) H_2), 5.56 (1H, dd, J 10.2, 2.3, C(9) H_A), 6.05 (1H, dd, J 16.9, 2.3, C(9) H_B), 6.19 (1H, dd, J 16.9, 10.22, C(8) H), 8.05-8.10 (1H, m, NH), 12.02 (1H, br s, CO₂H); δ_C (150 MHz, DMSO-d₆) 24.3 (C(3) H_2), 26.0 (C(4) H_2), 28.8 (C(5) H_2), 33.6 (C(2) H_2), 38.4 (C(6) H_2), 124.9 (C(9) H_2), 131.9 (C(8) H), 164.5 (C(7)), 174.5 (C(1)); m/z (ES⁺) 208 (52%, [M+Na]⁺), 186 (100%, [M+H]⁺).

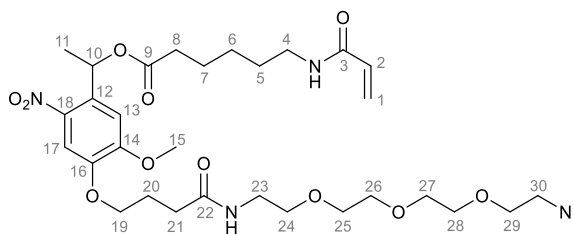
***N*-[2-(2-Azidoethoxy)ethyl]-4-(4-(1-hydroxyethyl)-2-methoxy-5-nitrophenoxy)butanamide, **158**.**



A reaction mixture of 4-[4-(1-hydroxyethyl)-2-methoxy-5-nitrophenoxy]butyric acid **155** (200 mg, 0.67 mmol), 3,6,9-trioxaundecan-1-amine (265 μ L, 1.34 mmol), HBTU (510 mg, 1.34 mmol) and HOAt (45.5 mg, 0.33 mmol) in DMF (2 mL) was stirred for 2 min at rt, before triethylamine (187 μ L, 1.34 mmol) was added, and the resulting mixture was stirred at rt for 20 h. The reaction mixture was dissolved in EtOAc (15 mL) and washed with saturated aqueous LiCl (2 \times 15 mL). The organic layer was then dried and concentrated *in vacuo*. Purification via flash column chromatography (CH₂Cl₂:CH₃OH, 50:1) yielded **158** (286 mg, 86%) as a yellow oil.

δ_{H} (600 MHz, CDCl₃) 1.55 (3H, d, *J* 6.4, C(21)H₃), 2.19 (2H, quin, *J* 6.8, C(11)H₂), 2.41 (2H, t, *J* 7.5, C(10)H₂), 3.38 (2H, t, *J* 5.3, C(1)H₂), 3.41-3.69 (14H, m, 7 \times CH₂), 3.98 (3H, s, C(15)H₃), 4.10 (2H, t, *J* 6.4, C(12)H₂), 5.56 (1H, dd, *J* 12.8, 6.4, C(20)H), 6.21 (1H, m, NH), 7.31 (1H, s, CH), 7.56 (1H, s, CH); δ_{C} (150 MHz, CDCl₃) 24.4 (C(21)H₃), 25.0 (C(11)H₂), 32.7 (C(10)H₂), 39.3, (CH₂), 50.8 (C(1)H₂), 56.5 (C(15)H₃), 65.8 (C(20)H), 68.6 (CH₂), 70.3 (CH₂), 70.6 (CH₂), 70.7 (CH₂), 70.8 (CH₂), 108.8 (CH), 109.2 (CH), 137.2 (C(17)), 139.7 (C(18)), 147.0 (C(13)), 154.2 (C(14)), 172.2 (C(9)); ν_{max} (oil) 3323, 3098, 2927, 2870, 2100, 1649; *m/z* (ES⁺) 522 (42%, [M+Na]⁺), 500 (40%, [M+H]⁺); HRMS (ES⁺) C₂₁H₃₄N₅O₉⁺ ([M+H]⁺) requires 500.2357, measured 500.2364.

1-(4-((1-Azido-13-oxo-3,6,9-trioxa-12-aza-hexadecan-16-yl)oxy)-5-methoxy-2-nitrophenyl)ethyl 6-acrylamidohexanoate, **154.**

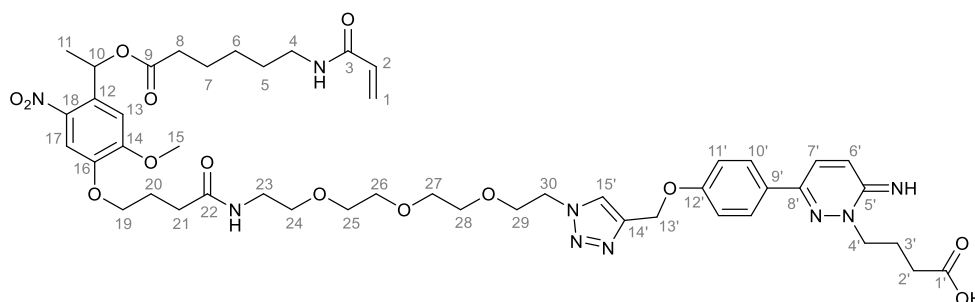


To a suspension of **158** (105 mg, 0.209 mmol) and **156** (58 mg, 0.31 mmol) in DMF (1 mL) at 0 °C was added EDC (60 mg, 0.31 mmol) and DMAP (5.11 mg, 0.042 mmol). The reaction mixture was stirred at rt for 18 h, before being wet loaded and undergoing purification via flash column chromatography (40-60 °C petrol to CH₂Cl₂:CH₃OH, 50:1) to yield **154** (104 mg, 75%) as a yellow solid.

δ_{H} (600 MHz, CDCl₃) 1.28-1.38 (2H, m, C(6)H₂), 1.53 (2H, quin, *J* 7.5, C(5)H₂), 1.61 (3H, d, *J* 6.4, C(11)H₃), 1.61-1.66 (2H, m, C(7)H₂), 2.19 (2H, quin, *J* 6.7, C(20)H₂), 2.28-2.38 (2H, m, C(8)H₂), 2.40 (2H, t, *J* 7.2, C(21)H₂), 3.30 (2H, quin, *J* 6.0, C(4)H₂), 3.36 (2H, t, *J* 4.9, C(30)H₂), 3.42-3.48 (2H, m, C(23)H₂), 3.55 (2H, t, *J* 4.9, C(24)H₂), 3.59-3.69 (10H, m, CH₂), 3.95 (3H, s, C(15)H₃), 4.10 (2H, t, *J* 6.4, C(19)H₂), 5.62, (1H, d, *J* 10.2, C(1)H_A), 5.83 (1H, br s, C(19)NH), 6.08 (1H, dd, *J* 16.9, 10.2, C(2)H), 6.23-6.29 (2H, m, C(23)NH, C(1)H_B), 6.45 (1H, q, *J* 6.4, C(10)H), 6.98 (1H, s, C(13)H), 7.56 (1H, s, C(14)H); δ_{C} (150 MHz, CDCl₃) 22.1 (C(11)H₃), 24.4 (CH₂), 24.9 (CH₂), 26.4 (C(6)H₂), 29.2 (C(5)H₂), 32.7 (C(21)H₂), 34.3 (C(8)H₂), 39.3(C(4)H₂), 39.3 (C(23)H₂), 50.8 (C(30)H₂), 56.5 (C(15)H₃), 68.3 (C(10)H), 68.6 (C(19)H₂), 70.0 (CH₂), 70.2 (CH₂), 70.3 (CH₂), 70.6 (CH₂), 70.7 (CH₂), 70.8 (CH₂), 108.3 (C(13)H), 109.1 (C(17)H), 126.4 (C(1)H₂), 131.0 (C(2)H), 133.2 (C(12)), 140.0 (C(18)), 147.4 (C(16)), 154.0 (C(14)), 165.7 (C(3)), 172.1 (C), 172.5 (C); ν_{max} (solid) 3306, 3071, 2933, 2864, 2101, 1724, 1650; mp (CH₃OH) 110-119 °C; *m/z* (ES⁺) 689

(7%, $[M+Na]^+$), 667 (100%, $[M+H]^+$); HRMS (ES^+) $C_{30}H_{47}N_6O_{11}^+$ ($[M+H]^+$) requires 667.3303, measured 667.3337.

4-(3-(4-((1-(2-(2-(4-(4-(1-((6-Acrylamidohexanoyl)oxy)ethyl)-2-methoxy-5-nitrophenoxy)butanamido)ethoxy)ethyl)-1H-1,2,3-triazol-4-yl)methoxy)phenyl)-6-iminopyridazin-1(6H)-yl)butanoic acid, **153.**

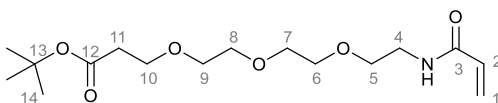


To a mixture of **141** (8.1 mg, 0.023 mmol) and **154** (15.0 mg, 0.023 mmol) in H_2O (0.1 mL) and DMF (0.1 mL) was added a solution of $CuSO_4 \cdot 5H_2O$ (1.3 mg, 0.005 mmol) and THPTA (10 mg, 0.023 mmol) in degassed H_2O (0.1 mL), followed by sodium ascorbate (3.0 mg, 0.015 mmol) in H_2O (0.1 mL). The resulting solution was stirred at 50 °C for 4 h, followed by rt for 16 h. The reaction solvent was removed *in vacuo*. Purification via flash column chromatography ($CH_2Cl_2:CH_3OH$, 10:1 to 7:3) gave **153** (4.0 mg, 18%) as a white solid.

δ_H (600 MHz, CD_3OD) 1.27-1.36 (4H, m, $2 \times CH_2$), 1.52 (2H, quin, J 7.9, CH_2), 1.59 (3H, d, J 6.8 C(11) H_3), 1.59-1.65 (2H, m, CH_2), 2.07 (2H, quin, J 6.8, CH_2), 2.35-2.40 (4H, m, $2 \times CH_2$), 3.21 (2H, t, J 7.2, CH_2), 3.31-3.35 (2H, m, PEG- CH_2), 3.48 (2H, t, J 5.3 PEG- CH_2), 3.53 (4H, s, PEG- CH_2), 3.54-3.61 (8H, m, PEG- CH_2), 3.89 (2H, t, J 4.9, CH_2), 3.91 (3H, s, C(15) H_3), 3.99-4.05 (2H, m, CH_2), 4.38-4.45 (2H, m, CH_2), 4.56 (2H, br s), 4.60 (2H, t, J 4.9, CH_2), 5.23 (2H, s, C(13') H_2), 5.63 (1H, dd, J 9.0, 3.0, C(1) H_A), 6.18-6.21 (2H, m, C(1) H_B , C(2) H), 6.32 (1H, q, J 6.8, C(10) H), 7.09 (1H, s, CH), 7.15 (2H, d, J 8.7, $2 \times CH$), 7.51 (1H, s, CH), 7.58 (1H, d, J 9.8, CH), 7.93

(2H, d, J 9.0, 2×CH), 8.17 (1H, s, C(15')H), 8.24 (1H, d J 9.4, CH); δ_C (150 MHz, CD₃OD) 22.0 (CH₃), 26.6 (CH₂), 26.4 (CH₂), 27.4 (CH₂), 30.0 (CH₂), 33.4 (CH₂), 35.0 (CH₂), 40.1 (CH₂), 40.4 (CH₂), 49.6 (CH₂), 51.5 (CH₂), 56.9 (CH₃), 57.5 (CH₂), 59.4 (CH₂), 62.5 (CH₂), 69.3 (CH), 69.6 (CH₂), 70.3 (CH₂), 70.5 (CH₂), 71.2 (CH₂), 71.4 (CH₂), 71.4 (CH₂), 71.5 (CH₂), 92.8 (C), 109.5 (CH), 109.9 (CH), 116.5 (CH), 126.5 (CH), 126.5 (CH), 129.3 (C), 132.1 (CH), 132.3 (CH), 134.0 (C), 141.4 (C), 148.8 (C), 151.6 (C), 155.4 (C), 162.1 (C), 168.1 (C), 174.2 (C), 175.3 (C); ν_{\max} (solid) 3305, 3071, 2933, 2863, 2104, 1724, 1649, 1578; mp 110-119 °C; m/z (ES⁺) 978 (100%, [M+H]⁺); HRMS (ES⁺) C₄₇H₆₄N₉O₁₄⁺ ([M+H]⁺) requires 978.4573, measured 978.4598.

***tert* Butyl 3-oxo-7,10,13-trioxa-4-aza-hexadec-1-en-16-oate, 159.**

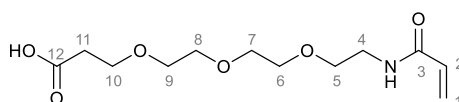


A solution of *tert* butyl 12-amino-4,7,10-trioxadodecanoate (205 mg, 0.739 mmol) and triethylamine (103 μ L, 0.739 mmol) in CH₂Cl₂ (2 mL) was stirred at 0 °C for 15 minutes, before a solution of acryloyl chloride (96%, 62 μ L, 0.74 mmol) was added dropwise. The reaction mixture was stirred at 0 °C for 1 h, then at rt for a further 2 h before being partitioned with aqueous NaHCO₃ (10 mL) and CH₂Cl₂ (10 mL). The aqueous layer was extracted with CH₂Cl₂ (3 × 10 mL) and the combined organic layers were washed with H₂O (10 mL), dried and concentrated *in vacuo*. Purification via flash column chromatography (40-60 °C petrol: EtOAc, 1:5) gave **159** (203 mg, 83%) as a colourless oil.

δ_H (600 MHz, DMSO-d₆) 1.39 (9H, s, 3×C(14)H₂), 2.41 (2H, t, J 6.2, C(11)H₂), 3.28 (2H, q, J 5.8, C(4)H₂), 3.44 (2H, t, J 5.7, C(5)H₂), 3.46-3.53 (8H, m, 4×CH₂), 3.58

(2H, t, J 6.3, C(10)H₂), 5.56 (1H, dd, J 10.3, 2.3, C(1)H_A), 6.07 (1H, dd, J 17.1, 2.2, C(1)H_B), 6.24 (1H, dd, J 17.1, 10.3, C(2)H), 8.14 (1H, s, NH); δ_C (600 MHz, DMSO-d₆) 27.8 (C(14)H₃), 35.9, 38.6 (C(11)H₂, C(4)H₂), 66.3 (C(10)H₂), 69.1, 69.6, 69.7, 69.7 (CH₂), 79.8 (C(13)), 125.0 (C(1)H₂), 131.8 (C(2)H), 164.7 (C(3)), 170.4 (C(12)); m/z (ES⁺) 332 (100%, [M+H]⁺), 354 (20%, [M+Na]⁺).

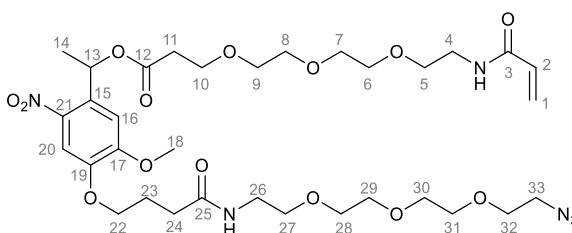
3-oxo-7,10,13-trioxa-4-azahexadec-1-en-16-oic acid, **160**.



A reaction mixture of trifluoroacetic acid (5 mL, 43.8 mmol), and ester **159** (203 mg, 0.613 mmol) in CH₂Cl₂ (10 mL) was stirred at rt for 1 h, before additional CH₂Cl₂ (50 mL) was added and all solvents were removed *in vacuo* to give **160** (168 mg, 99%) as a colourless oil.

δ_H (600 MHz, CDCl₃) 2.63 (2H, t, J 6.0, C(11)H₂), 3.54-3.58 (2H, m, C(4)H₂), 3.62-3.68 (10H, m, 5×CH₂), 3.79 (2H, t, J 6.0 C(10)H₂), 5.65 (1H, dd, J 10.2, 1.5, C(1)H_A), 6.19 (1H, dd, J 16.9, 10.2, C(2)H), 6.31 (1H, dd, J 16.9, 1.5, C(1)H_B), 6.67 (1H, s, NH); δ_C (150 MHz, CDCl₃) 35.0 (C(11)H₂), 39.6 (C(4)H₂), 66.5 (C(10)H₂), 70.1 (CH₂), 70.3 (CH₂), 70.4 (CH₂), 70.7 (CH₂), 126.9 (C(1)H₂), 130.9 (C(2)H), 166.3 (C(3)), 174.1 (C(12)); m/z (ES⁺) 276 (100%, [M+H]⁺).

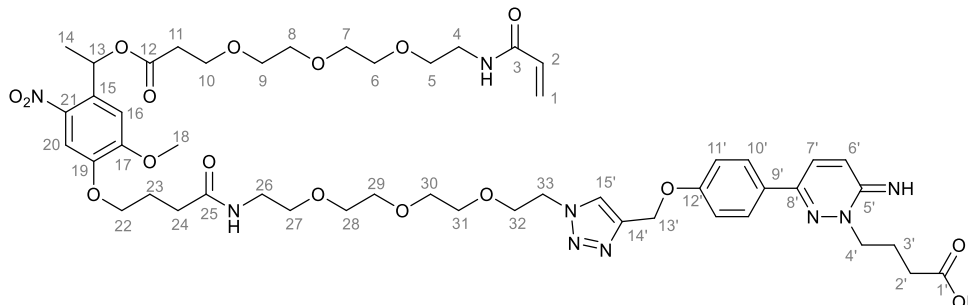
1-(4-((1-azido-13-oxo-3,6,9-trioxa-12-azahexadecan-16-yl)oxy)-5-methoxy-2-nitrophenyl)ethyl 3-oxo-7,10,13-trioxa-4-azahexadec-1-en-16-oate, **161**.



1-Ethyl-3-(3-dimethylaminopropyl)carbodiimide (93.7 mg, 0.489 mmol) and DMAP (8.0 mg, 0.07 mmol) were added to a solution of alcohol **158** (163 mg, 0.326 mmol) and acid **160** (90 mg, 0.326 mmol) in DMF (2 mL) at 0 °C. The resulting mixture was stirred at rt for 18 h before being loaded onto a column. Purification via flash column chromatography (CH₂Cl₂:CH₃OH, 100:2 to 100:15) yielded **161** (81.9 mg, 33%) as a yellow oil.

δ_{H} (600 MHz, CD₃OD) 1.62 (3H, d, *J* 6.4, C(14)H₃), 2.11 (2H, quin, *J* 6.8, C(23)H₂), 2.41 (2H, t, *J* 7.5, C(24)H₂), 2.63 (2H, t, *J* 6.0, C(4)H₂), 3.34-3.38 (4H, m, 2×CH₂), 3.42 (2H, t, *J* 5.6, C(33)H₂), 3.51-3.67 (22H, m, 11×CH₂), 3.70-3.79 (2H, m, C(5)H₂), 3.96 (3H, s, C(18)H₃), 4.08 (2H, t, *J* 6.8, C(22)H₂), 5.64 (1H, dd, *J* 9.8, 2.6, C(1)H_A), 6.17-6.28 (2H, m, C(1)H_B, C(2)H), 6.36 (1H, q, *J* 6.4, C(13)H), 7.14 (1H, s, CH), 7.59 (1H, s, CH); δ_{C} (150 MHz, CD₃OD) 22.1 (C(14)H₃), 26.4 (CH₂), 33.4 (CH₂), 36.1 (CH₂), 51.7 (C(33)H₂), 60.0 (C(18)H₃), 67.6 (CH₂), 69.7 (C(13)H), 70.4 (CH₂), 71.1 (CH₂), 71.3 (CH₂), 71.6 (CH₂), 109.7 (CH), 109.9 (CH), 126.7 (C(1)H₂), 132.0 (C(2)H), 134.1 (C(15)), 141.3 (C(21)), 148.8 (C(19)), 155.5 (C(17)), 168.1 (C(3)), 172.4 (C), 175.4 (C); ν_{max} (oil) 3310, 3056, 2871, 2103, 1736. 1661.0; *m/z* (ES⁺) 779 (100%, [M+Na]⁺); HRMS (ES⁺) C₃₃H₅₃N₆O₁₄⁺ ([M+H]⁺) requires 757.3620, measured 757.3649.

4-(3-(4-((1-(16-(4-(4,17-Dioxo-3,7,10,13-tetraoxa-16-azanonadec-18-en-2-yl)-2-methoxy-5-nitrophenoxy)-13-oxo-3,6,9-trioxa-12-azahexadecyl)-1H-1,2,3-triazol-4-yl)methoxy)phenyl)-6-iminopyridazin-1(6H-yl)butanoic acid, **163.**

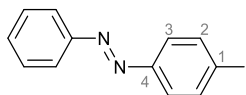


To a mixture of alkyne **141** (38 mg, 0.107 mmol) and azide **161** (81 mg, 0.107 mmol) in H₂O (0.1 mL) and DMF (0.1 mL) was added a solution of CuSO₄·5H₂O (26.7 mg, 0.107 mmol) and THPTA (47 mg, 0.107 mmol) in degassed H₂O (0.1 mL), followed by sodium ascorbate (64 mg, 0.107 mmol) in H₂O (0.1 mL). The resulting solution was stirred at 50 °C for 4 h, followed by rt for 16 h. The reaction solvent was removed *in vacuo*. Purification via flash column chromatography (CH₂Cl₂:CH₃OH, 100:5 to 50:50) gave **163** (28 mg, 24%) as a yellow oil.

δ_{H} (600 MHz, CD₃OD) 1.60 (3H, d, *J* 6.5, C(14)H₃), 2.04-2.14 (4H, m, C(23)H₂, C(2')H₂), 2.38 (2H, t, *J* 7.5, C(24)H₂), 2.63 (2H, t, *J* 5.8, C(4)H₂), 3.34 (2H, t, *J* 5.6, CH₂), 3.41 (2H, t, *J* 5.5, CH₂), 3.49 (2H, t, *J* 5.5, CH₂), 3.50-3.67 (22H, m, 11×CH₂), 3.69-3.80 (2H, m, C(5)H₂), 3.89 (2H, t, *J* 5.1, C(3')H₂), 3.93 (3H, s, C(18)H₃), 4.02 (2H, t, *J* 7.8, C(22)H₂), 4.60 (2H, t, *J* 5.2, C(4')H₂), 5.24 (2H, s, C(13')H₂), 5.63 (1H, dd, *J* 9.7, 2.2, C(1)H_A), 6.19 (1H, dd, *J* 17.1, 2.2, C(1)H_B), 6.25 (1H, dd, *J* 17.1, 9.7, C(2)H), 6.34 (1H, q, *J* 6.4, C(13)H), 7.11 (1H, s, CH), 7.15 (2H, d, *J* 8.9, 2×C(11')H), 7.51 (1H, s, CH), 7.62 (1H, d, *J* 9.4, C(7')H), 7.93 (2H, d, *J* 8.9, 2×C(10')H), 8.18 (1H, s, C(15')H), 8.25 (1H, d, *J* 9.4, C(6')H); δ_{C} (150 MHz, CD₃OD) 22.1 (C(14)H₃), 26.4 (C(23)H₂), 33.4 (C(24)H₂), 36.0, (CH₂), 40.4 (CH₂), 40.4 (CH₂), 51.5 (CH₂), 57.0 (C(18)H₃), 62.5 (CH₂), 67.6 (CH₂), 69.6 (CH₂), 69.7 (C(13)H), 70.3 (CH₂), 70.5

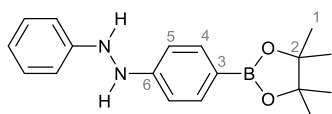
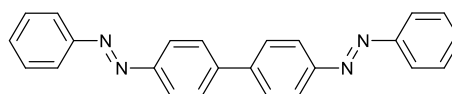
(CH₂), 70.6 (CH₂), 71.2 (CH₂), 71.3 (CH₃), 71.4 (CH₂), 71.4 (CH₂), 71.5 (CH₂), 109.7 (CH), 109.9 (CH), 116.5 (C(11')H), 126.6 (C(7')H), 127.1 (C(1)H₂), 129.4 (C(10')H), 131.9 (C(2)H), 132.4 (C(6')H), 134.1 (C(15)), 141.2 (C(21)), 148.7 (C(19)), 153.8 (C) 155.5 (C(17)), 162.1 (C), 168.2 (C(3)), 172.4 (C), 175.4 (C) {3 C signals unobserved}; ν_{\max} (oil) 3292, 2946, 2875, 2476, 2103, 1736, 1650, 1606; m/z (ES⁺) 1068 (100%, [M+H]⁺); HRMS (ES⁺) C₅₀H₇₀N₉O₁₇⁺ ([M+H]⁺) requires 1068.4890, measured 1068.4892.

1-(4-Iodophenyl)-2-phenyldiazene, **166**.¹²⁵



To a stirring solution of nitrosobenzene (200 mg, 1.87 mmol) in glacial acetic acid (12 mL) was added 4-iodoaniline (341 mg, 1.56 mmol) in one portion. The reaction mixture was stirred at 40 °C for 12 h before being poured into H₂O (40 mL). This aqueous solution was extracted with CH₂Cl₂ (3×40 mL), and the combined organic layers were washed with brine (50 mL), and dried and concentrated *in vacuo*. Purification via flash column chromatography (40-60°C petrol:Et₂O, 200:1) gave **166** (418 mg, 87%) as an orange solid.

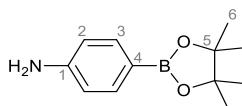
δ_{H} (600 MHz, CDCl₃) 7.48-7.55 (3H, m, 2×*m*-PhH, *p*-PhH), 7.67 (2H, d, *J* 8.3, 2×C(2)H), 7.93 (2H, d, *J* 8.7, 2×C(3)H), 7.93 (2H, d, *J* 7.2, 2×*o*-PhH); δ_{C} (150 MHz, CDCl₃); 97.8 (C(1)), 123.1 (*o*-PhH), 124.6 (C(2)H), 129.3 (*m*-PhH), 131.5 (*p*-PhH), 138.5 (C(3)H), 152.0 (C), 152.6 (C); m/z (ES⁺) 309 (100%, [M+H]⁺), 287 (75%), 268 (70%).

1-Phenyl-2-(4-(4,4,5,5-tetramethyl-1,3,2-dioxaborolan-2-yl)phenyl)hydrazine**168, 4,4'-bis(phenyldiazenyl)-1,1'-biphenyl 169.****168****169**

A solution of **166** ((91 mg, 0.295 mmol) in toluene (5 mL) was added to a suspension of 4,4,5,5-tetramethyl-1,3,2-dioxaborolane (127 μ L, 0.45 mmol), Pd(PPh₃)₂Cl₂ (4.1 mg, 0.006 mmol) in dry triethylamine (123 μ L, 0.885 mmol) and toluene (5 mL). The reaction mixture was heated to 80 °C for 2 h before EtOAc (20 mL) and brine (20 mL) were added. The organic layer was separated, dried and concentrated *in vacuo*. Purification via flash column chromatography (40-60 °C petrol: CH₂Cl₂, 3:2 to 0:1) yielded dimer **169** (8.5 mg, 4%). Further elution gave hydrazine **168** (53.0 mg, 58%), followed by azobenzene **167** (15.4 mg, 17%).

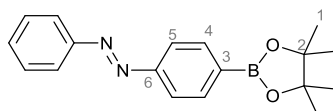
Data for **169**: δ_{H} (600 MHz, CDCl₃) 7.47-7.55 (6H, m, 6 \times CH), 7.64-7.68 (4H, m, 4 \times CH), 7.79-7.83 (4H, m, 4 \times CH), 7.90-7.94 (4H, m, 4 \times CH); δ_{C} (150 MHz, CDCl₃) 123.1 (CH), 124.5 (CH), 129.3 (CH), 131.5 (CH), 132.5 (CH), {3 C signals unobserved}; ν_{max} (solid) 3452, 3046 (C-H), 1680; mp 295-297 °C; m/z 362 (100%, [M⁺]).

Data for **168**: δ_{H} (600 MHz, CDCl₃) 1.32 (12H, s, 4 \times C(1)H₃), 5.67 (1H, s, NH), 5.76 (1H, s, NH), 6.82-6.87 (5H, m, 2 \times *o*-PhH, *p*-PhH, 2 \times C(5)H), 7.22 (2H, t, *J* 7.5, 2 \times *m*-PhH), 7.68 (2H, d, *J* 8.7, 2 \times C(4)H); δ_{C} (150 MHz, CDCl₃) 25.0 (C(1)H₃), 83.5 (C(2)), 111.4, 112.5 (C(5)H, *o*-PhH), 120.2 (*p*-PhH), 129.5 (*m*-PhH), 136.5 (C(4)H), 148.6 (C(3)), (C(6)), 151.6 (*i*-PhH); ν_{max} (solid) 3042, 2978, 2929 (N-H, C-H), 1602, 1568, 1501; mp 96-97 °C; m/z (ES⁺) 311 (100%, [M+H]⁺).

4-(4,4,5,5-Tetramethyl-1,3,2-dioxaborolan-2-yl)aniline, 170.¹²⁶

A flame dried flask containing CsCO₃ (595 mg, 1.83 mmol), bis(pinacolato)diboron (928 mg, 3.65 mmol), 4-iodoaniline (200 mg, 0.913 mmol) in CH₃OH (10 mL) was stirred at reflux for 60 h, before being passed over a short plug of neutralised Al₂O₃ (eluent Et₂O). The resulting filtrate was concentrated *in vacuo*. Purification via flash column chromatography (CH₂Cl₂) gave **170** (95.8 mg, 48%) as a brown solid.

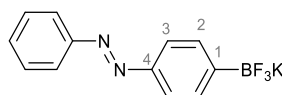
δ_{H} (600 MHz, CDCl₃) 1.32 (12H, s, 4×C(6)H₃) 6.67 (2H, d, *J* 8.3, 2×C(2)H), 7.63 (2H, d, *J* 8.3, 2×C(3)H); δ_{C} (150 MHz, CDCl₃) 25.0 (C(6)H₃), 83.4 (C(5)), 114.2 (C(2)H), 136.5 (C(3)H), 149.4 (C(4)), 149.4 (C(1)); *m/z* (ES⁺) 220 (100%, [M+H]⁺); HRMS (ES⁺) C₁₂H₁₉BNO₂⁺ ([M+H]⁺) requires 220.1511, measured 220.1362.

1-phenyl-2-(4-(4,4,5,5-tetramethyl-1,3,2-dioxaborolan-2-yl)phenyl)diazene, 167.⁹⁹

To a stirring solution of nitrosobenzene (70.2 mg, 0.656 mmol) in glacial acetic acid (5 mL) was added 4-(4,4,5,5-tetramethyl-1,3,2-dioxaborolan-2-yl)aniline **170** (95.8 mg, 0.437 mmol). The reaction mixture was heated at 90 °C for 3.5 h before being poured into H₂O (10 mL). This aqueous solution was extracted with CH₂Cl₂ (5×20 mL), and the combined organic layers were washed sequentially with saturated aqueous NaHCO₃ (20 mL), H₂O (20 mL) and brine (20 mL), and dried and concentrated *in vacuo*. Purification via flash column chromatography (CH₂Cl₂ : CH₃OH, 100:0.5) yielded **167** (21.6 mg, 27%) as a brown solid.

δ_{H} (600 MHz, CDCl_3); 1.38 (12H, s, $4\times\text{C}(1)\text{H}_3$), 7.47-7.51 (1H, m, *p*-PhH), 7.53 (2H, t, J 7.5, $2\times\text{m}$ -PhH), 7.91 (2H, d, J 8.7, $2\times\text{C}(5)\text{H}$), 7.92-7.98 (4H, m, $2\times\text{o}$ -PhH, $2\times\text{C}(4)\text{H}$); δ_{C} (150 MHz, CDCl_3) 25.0 ($\text{C}(1)\text{H}_3$), 84.2 ($\text{C}(2)$), 122.1 ($\text{C}(5)\text{H}$), 123.1 (*o*-PhH), 129.2 (*m*-PhH), 131.3 (*p*-PhH), 135.8 ($\text{C}(4)\text{H}$), 152.8 (C), 153.4 (C), 154.4 (C); ν_{max} (solid) 2980, 2923, 2852, 1602, 1503; mp (CH_2Cl_2) 95-97 °C; m/z (ES^+) 309 (100%, $[\text{M}+\text{H}]^+$); HRMS (ES^+) $\text{C}_{18}\text{H}_{22}\text{N}_2\text{O}_2\text{B}^+$ ($[\text{M}+\text{H}]^+$) requires 309.1774, measured 309.1777.

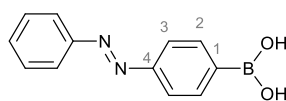
(*E*)-1-Phenyl-2-(4-(trifluoro-*l*4-boranyl)phenyl)diazene, potassium salt, **171.⁹⁹**



To a stirring suspension of nitrosobenzene (244 mg, 2.28 mmol) in glacial acetic acid (20 mL) was added **170** (500 mg, 2.28 mmol) and the reaction mixture was stirred at 90 °C for 3.5 h. The reaction solvent was removed *in vacuo* until 10 mL remained. The resulting mixture was diluted with H_2O (50 mL) and extracted with CH_2Cl_2 (3×50 mL). The combined organic layers were washed sequentially with H_2O (50 mL), saturated aqueous NaHCO_3 (50 mL), then H_2O (50 mL) and dried and concentrated *in vacuo*. To this crude mixture was added CH_3CN (3 mL), H_2O (0.3 mL), and KHF_2 (401.3 mg, 5.14 mmol), and the resulting solution was stirred at rt for 2.5 h. After this the reaction mixture was quenched with saturated aqueous NaHCO_3 (1 mL) and the solvent removed *in vacuo*. The residue was cooled to 0 °C and 40-60 °C petrol (25 mL) was added. The resulting suspension was then filtered through a short column of Celite®, and the precipitate at the top of the column was washed with petrol (25 mL) and the filtrate discarded. The precipitate was then dissolved in acetone (100 mL) and filtered through the column. This acetone filtrate was then concentrated *in vacuo* to give **171** (348 mg, 53%) as a white solid.

δ_{H} (600 MHz, acetone- d_6) 7.50 (1H, t, J 7.5, p -PhH), 7.57 (2H, t, J 7.5, $2\times m$ -PhH), 7.70 (2H, d, J 8.3, $2\times C(2)H$), 7.74 (2H, d, J 8.3, $2\times C(3)H$), 7.90 (2H, m, $2\times o$ -PhH); δ_{C} (150 MHz, acetone- d_6) 120.9 ($C(3)H$), 122.3 (o -PhH), 129.1 (m -PhH), 130.3 (p -PhH), 132.3 ($C(2)H$), 150.9 (C), 152.9 (C) {1 C signal unobserved}; ν_{max} (solid) 3643, 3040; mp 284-285 °C; m/z (ES^-) 246 (100%, [M]), 248 (50%, [M-K $^+$]).

(4-(Phenyldiazenyl)phenyl)boronic acid, 165.⁹⁹



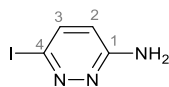
Method A: A mixture of trifluoroborate salt **171** (50 mg, 0.174 mmol) and $\text{FeCl}_3 \cdot 6\text{H}_2\text{O}$ (52 mg, 0.191 mmol) in THF (5 mL) and H_2O (5 mL) was stirred at rt for 2 h. The reaction mixture was filtered through basic alumina (THF) and concentrated *in vacuo* to give **165** as a white solid (26 mg, 66%).

Method B: A solution of 1-phenyl-2-[(4-pinacolylborane)phenyl]diazene **167** (15.6 mg, 0.05 mmol) and KHF_2 (11.8 mg, 0.15 mmol) in H_2O (0.1 mL) and CH_3CN (1 mL) was stirred at rt for 3 h. Saturated aqueous NaHCO_3 (1 mL) was added and the reaction was stirred at rt for 1 h before being partitioned between H_2O (5 mL) and Et_2O (10 mL). The aqueous layer was extracted Et_2O (8 \times 25 mL), and the combined organic layers were dried and concentrated *in vacuo* to give **165** (8.4 mg, 58%) as a yellow solid.

δ_{H} (600 MHz, acetone- d_6) 7.57-7.60 (1H, m, p -PhH), 7.60-7.64 (2H, m, $2\times m$ -PhH), 7.92 (2H, d, J 8.3, $2\times C(3)H$), 7.97 (2H, d, J 7.2, $2\times o$ -PhH), 8.09 (2H, d, J 8.3, $2\times C(2)H$); δ_{C} (150 MHz, acetone- d_6) 121.6 ($C(3)H$), 122.7 (o -PhH), 129.3 (m -PhH), 131.4 (p -PhH), 135.1 ($C(2)H$), 152.7 (C), 153.7 (C) {1 C signal unobserved}; ν_{max} (solid) 3390, 3045, 2919, 2850, 1600, 1502; mp degraded >100 °C; m/z (ES^+) 241

(95%, [$^{11}\text{M}+\text{Na}$] $^+$), 227 (100%, [$^{10}\text{M}+\text{H}$] $^+$); HRMS (ES $^+$) $\text{C}_{12}\text{H}_{12}\text{N}_2\text{O}_2\text{B}^+$ ([$^{10}\text{M}+\text{H}$] $^+$) requires 226.1028, measured 226.1024.

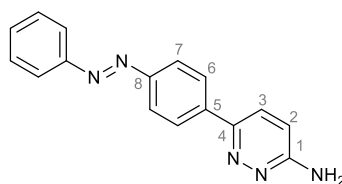
3-Amino-6-iodopyridazine, **172**.¹²¹



A reaction mixture of HI (57% aq, 4.00 mL, 7.72 mmol) and 3-amino-6-chloropyridazine (500 mg, 3.86 mmol) was refluxed for 48 h. Once cooled to rt, EtOAc (1 mL) was added and the mixture sonicated for 3 min. The precipitate was filtered and washed with EtOAc (10 mL), before being redissolved in CH_3OH (10 mL). To this mixture was added NaOH (163 mg, 4.08 mmol), and the solution was stirred at reflux for 5 min. The solvent was concentrated *in vacuo* and the residue redissolved in H_2O (5 mL). This was filtered after 15 min to give **172** (338 mg, 40%) as a cream solid. Further recrystallisation of the aqueous filtrate yielded **172** with 3-amino-6-chloropyridazine **33** impurity.

δ_{H} (600 MHz, DMSO-d_6) 6.55 (1H, d, J 9.2, C(2)H), 6.55 (2H, s, NH_2), 7.55 (1H, d, J 9.2, C(3)H); δ_{C} (150 MHz, DMSO-d_6) 111.5 (C(4)), 116.4 (C(2)H), 137.1 (C(3)H), 160.1 (C(1)); m/z (ES $^+$) 222 (100%, [$\text{M}+\text{H}$] $^+$); HRMS (ES $^+$) $\text{C}_4\text{H}_4\text{N}_3\text{I}$ requires 221.9528; measured 221.9530.

6-(4-(Phenyldiazenyl)phenyl)pyridazin-3-amine, **164**.

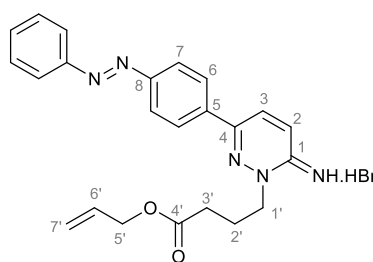


To a microwave vial containing CH_3CN (2.0 mL) and H_2O (1.3 mL) was charged with **171** (75 mg, 0.26 mmol), 3-amino-6-chloropyridazine **33** (30.6 mg, 0.237 mmol),

Pd(PPh₃)₂Cl₂ (8.3 mg, 0.012 mmol) and K₂CO₃ (98.3 mg, 0.711 mmol) and the reaction was degassed, then irradiated for 15 min at 120 °C. The crude reaction mixture was concentrated *in vacuo*. Purification via flash column chromatography (40-60 °C petrol : EtOAc, 2:1 to 1:3) gave **164** (53.8 mg, 41%) as an orange solid.

Product exists as ratio *trans*-**164** : *cis*-**164** of 0.28:1.00 under ambient light, NMR taken of a dark-adapted sample which shows peaks of thermodynamic *trans*-**164** isomer only. δ_{H} (600 MHz, CD₃OD) 7.48 (1H, d, *J* 9.8, C(2)*H*), 7.53-7.60 (3H, m, *p*-Ph*H*, 2×*m*-Ph*H*), 7.96 (2H, d, *J* 6.8, 2×*o*-Ph*H*), 8.07 (2H, d, *J* 8.3, 2×C(7)*H*), 8.18 (2H, d, *J* 8.3, 2×C(6)*H*), 8.33 (1H, d, *J* 9.8, C(3)*H*); δ_{C} (150 MHz, CD₃OD) 121.6 (CH), 124.0 (CH), 124.5 (CH), 128.1 (C), 128.5 (CH), 130.0 (C), 130.4 (CH), 132.8 (CH), 154.0 (C), 154.8 (C), 173.1 (C) {1 CH signal unobserved}; ν_{max} (oil) 3351, 3305, 3224, 3210, 3165, 1453, mp (CH₃OH) 222-224 °C; *m/z* (ES⁺) 276 (100%, [M+H]⁺); HRMS (ES⁺) C₁₆H₁₄N₅⁺ ([M+H]⁺) requires 276.1242, measured 276.1245.

Allyl 4-(6-imino-3-(4-(phenyldiazenyl)phenyl)pyridazin-1(6H)-yl)butanoate, **174**.

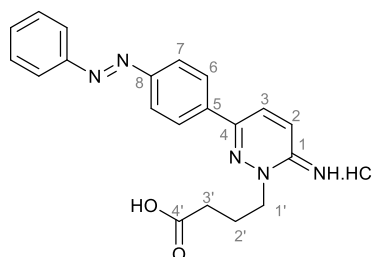


A reaction mixture of **164** (14 mg, 0.051 mmol) and allyl 4-bromobutyrate (10.5 μ L, 0.051 mmol) in DMF (0.1 mL) was heated at 80 °C for 16 h. After this time EtOAc (5 mL) was added and the reaction cooled to 0 °C. The resulting precipitate was filtered and washed with cold EtOAc (2 mL) to give **174** (14.9 mg, 73%) as a yellow solid.

Product exists as ratio *trans*-**174** : *cis*-**174** of 0.30:1.00 under ambient light, NMR taken of dark-adapted sample which shows peaks of thermodynamic *trans*-**174** isomer

only. δ_{H} (600 MHz, CD_3OD) 2.30 (2H, quin, J 6.8, $\text{C}(2')\text{H}_2$), 2.66 (2H, t, J 6.8, $\text{C}(3')\text{H}_2$), 4.48-4.52 (4H, m, $\text{C}(1')\text{H}_2$, $\text{C}(5')\text{H}_2$), 5.16 (1H, dd, J 10.4, 1.5, $\text{C}(7')\text{H}_\text{A}$), 5.25 (1H, dd, J 17.3, 1.5, $\text{C}(7')\text{H}_\text{B}$), 5.81-5.88 (1H, m, $\text{C}(6')\text{H}$), 7.54-7.60 (3H, m, p -PhH, $2\times m$ -PhH), 7.68 (1H, d, J 9.4, $\text{C}(3)\text{H}$), 7.95-7.98 (2H, m, $2\times o$ -PhH), 8.08 (2H, d, J 8.3, $2\times \text{C}(7)\text{H}$), 8.20 (2H, d, J 8.3, $2\times \text{C}(6)\text{H}$), 8.43 (1H, d, J 9.4, $\text{C}(2)\text{H}$); δ_{C} (125 MHz, CD_3OD) 22.5 (CH_2), 31.3 (CH_2), 57.1 (CH_2), 66.5 (CH_2), 118.6 (CH_2), 124.1 (CH), 124.5 (CH), 127.0 (CH), 128.8 (CH), 130.4 (CH), 132.8 (CH), 133.0 (CH), 133.4 (CH), 136.3 (C), 151.3 (C), 154.0 (C), 154.4 (C), 155.2 (C), 174.1 ($\text{C}(4')$); ν_{max} (solid) 3319, 3040, 1735; mp (CH_3OH) 169-170 °C; m/z (ES^+) 402 (100%, $[\text{M}+\text{H}]^+$); HRMS (ES^+) $\text{C}_{23}\text{H}_{24}\text{N}_5\text{O}_2$ ($[\text{M}+\text{H}]^+$) requires 402.1930, measured 402.1892.

4-(6-Imino-3-(4-(phenyldiazenyl)phenyl)pyridazin-1(6H)-yl)butanoic acid {azogabazine}, **163.**



A solution of NaOH (20 mg), **174** (14.9 mg, 0.037 mmol) in THF (1 mL) and H_2O (1 mL) was stirred at 50 °C for 3 h. The mixture was then cooled to 10 °C and washed with EtOAc (3 mL). The aqueous layer was acidified to pH 1 with 1 M aqueous HCl and stirred at rt for 1 h. The solvent was then concentrated *in vacuo*, and the residue triturated with H_2O (2 mL) to yield **163** (12.3 mg, 80%) as a yellow solid.

Product exists as ratio *trans*-**163** : *cis*-**163** of 0.33 : 1.00 under ambient light, NMR taken of dark-adapted sample which shows peaks of thermodynamic *trans*-**163** isomer only. δ_{H} (600 MHz, CD_3OD) 2.26 (2H, quin, J 6.9, $\text{C}(2')\text{H}_2$), 2.59 (2H, t, J 6.9, $\text{C}(3')\text{H}_2$), 4.50 (2H, t, J 7.1, $\text{C}(1')\text{H}_2$), 7.50-7.60 (3H, m, p -PhH, $2\times m$ -PhH), 7.70 (1H,

d, J 9.4, C(3) H), 7.96 (2H, d, J 7.5, 2 \times *o*-Ph H), 8.07 (2H, d, J 7.9, 2 \times C(7) H), 8.21 (2H, d, J 8.3, 2 \times C(6) H), 8.42 (1H, d, J 9.4, C(2) H); δ_C (150 MHz, CD₃OD) 22.6 (CH₂), 31.0 (CH₂), 57.1 (CH₂), 124.1 (CH), 124.5 (CH), 126.9 (CH), 128.9 (CH), 130.4 (CH), 132.8 (CH), 133.0 (CH), 136.4 (C), 154.0 (C), 154.4 (C), 155.2 (C), 176.4 (C), 190.5 (C); ν_{\max} (solid) 3039 (N-H, O-H, C-H), 1718; mp 242-246 °C; m/z (ES⁺) 362 (100%, [M+H]⁺); HRMS (ES⁺) C₂₀H₁₉N₅O₂⁺ ([M]⁺) requires 362.1617; measured 362.1618.

References

- ¹ Lüscher, B.; Keller, C. A. *Pharmacol. Ther.*, **2004**, *102*(3), 195-221.
- ² Nutt, D. J.; Malizia, A. L. *Br. J. Psychiatry*, **2001**, *179*(5), 390-396.
- ³ Jacob, T. C.; Moss, S. J.; Jurd, R. *Nat. Rev. Neurosci.*, **2008**, *9*, 331-343.
- ⁴ Bannai, H.; Levi, S.; Schweizer, C.; Inoue, T.; Launey, T.; Racine, V.; Sibarita, J-B.; Mikoshiba, K.; Triller, A. *Neuron* **62**, **2009**, 670-682.
- ⁵ Hausrat, T. J.; Muhia, M.; Gerrow, K.; Thomas, P.; Hirdes, W.; Tsukita, S.; Heisler, F. F.; Herich, L.; Dubroqua, S.; Breiden, P.; Feldon, J.; Schwarz, J. R.; Yee, B. K.; Smart, T. G.; Triller, A.; Kneussel, M. *Nat. Commun.*, **2015**, *6*, 6872.
- ⁶ Smart, T. G.; Moss, S. J. *Nat. Rev. Neurosci.* **2001**, *2*, 240-250.
- ⁷ Renner, M.; Schweizer, C.; Bannal, H.; Triller, A.; Levi, S. *PLOS ONE*, **2012**, 43032.
- ⁸ Froestl, W. *Future Med. Chem.* **2011**, *3*, 163-175.
- ⁹ Ballard, T. M.; Knoflach, F.; Prinssen, E.; Borroni, E.; Vivian, J. A.; Basile, J.; Gasser, R.; Moreau, J. L.; Wettstein, J. G.; Buettelmann, B.; Knust, H.; Thomas, A. W.; Trube, G.; Hernandez, M. C. *Psychopharmacology (Berl.)*, **2009**, *202*, 207-223.
- ¹⁰ Gouzer, G.; Specht, C. G.; Allain, L.; Shinoo, T.; Triller, A. *Mol. Cell. Neurosci.*, **2014**, *63*, 101-113.
- ¹¹ Singh, A.; Thornton, E. R.; Westheimer, F. H. *J. Biol. Chem.* **1962**, *237*, 3006-3008.
- ¹² Lapinsky, D. J. *Bio. Med. Chem.*, **2012**, *20*, 6237-6247.
- ¹³ Weber, R. J. A.; Beck-Sickinger, A. G. *J. Peptide. Res.* **1997**, *49*, 375-383.
- ¹⁴ Dornán, G.; Pretwich, G. D. *Biochemistry*, **1994**, *33*, 5661-5673.
- ¹⁵ Schuster, D. I.; Probst, W. C.; Ehrlich, G. K.; Singh, G. *Photochemistry and Photobiology*, **1989**, *49*, 785-804.
- ¹⁶ Johnston, G. A. R. *Current Pharmaceutical Design*, **2005**, *11*, 1867-1885.
- ¹⁷ Olsen, R. W.; Li, G.-D. *J. Can. Anesth.*, **2011**, *58*, 206-215.
- ¹⁸ Zhong, H.; Rusch, D.; Forman, S. A. *Anesthesiology*; **2008**, *108*, 103-112.
- ¹⁹ Li, G.-D.; Chiara, D. C.; Cohen, J. B.; Olsen, R. W. *J. Biol. Chem.*, **2009**, *284*, 11771-11775.
- ²⁰ Van Rijn C. M.; Willems-van Bree, E.; Dirksen R.; Rodrigues, M. J. F. *Epilepsy Res.* **1992**, *12*, 163-170.
- ²¹ Goelder, M. P.; Hawkinson, J. E.; Casida, J. E. *Tetrahedron Letters*, **1989**, *30*, 823-826.
- ²² Shimotahira, H.; Fusazaki, S.; Ikeda, I.; Ozoe, Y. *Bioorg. Med. Chem. Lett.*, **2011**, *21*, 1598-1600.
- ²³ Sirisoma, N. S.; Ratra, G. S.; Tomizawa, M.; Casida, J. E. *Bioorg. Med. Chem. Lett.*, **2001**, *11*, 2979-2981.
- ²⁴ Sammelson, R. E.; Casida, J. E. *J. Org. Chem.*, **2003**, *68*, 8075-8079.
- ²⁵ Hall, M. A.; Xi, J.; Lor, C.; Dai, S.; Pearce, R.; Dailey, W. P.; Eckenhoff, R. G. *J. Med. Chem.*, **2010**, *53*, 5667-5675.
- ²⁶ Cavalla, D.; Neff, N. H. *J. Neurochem.* **1985**, *44*, 916-921.
- ²⁷ Nielson, M.; Witt, M.-R.; Ebert, B.; Krosggaard-Larsen, P. *Eur. J. Pharma.*, **1995**, *289*, 109-12.
- ²⁸ Iqbal, F. *PhD Thesis*, UCL, **2011**.
- ²⁹ Wermuth, C.-G.; Bourguignon, J. J.; Schlewer, A.; Gies, J. P.; Schoenfelder, A.; Melikian, A.; Bouchet, M.-J.; Chantreux, D.; Molimard, J.-C.; Heaulme, M.; Cambon, J.-P.; Bizierez, K. *J. Med. Chem.*, **1987**, *30*, 239-249.
- ³⁰ Iqbal, F.; Ellwood, R.; Mortensen, M.; Smart, T. G.; Baker, J. R. *Bioorg. Med. Chem. Lett.*, **2011**, *21*, 4252-4254.
- ³¹ Perán, M.; Hooper, H.; Boulaiz, H.; Marchal, J. A.; Aranega, A.; Salas, R. *Cell Motil. Cytoskeleton*, **2006**, *63*, 747-757.
- ³² Li, X.; Cao, J.-H.; Li, Y.; Rondard, P.; Zhang, Y.; Yi, P.; Liu, J.-F.; Nan, F.-J. *J. Med. Chem.*, **2008**, *51*, 3057-3060.
- ³³ Pathak, S.; Cao, E.; Davidson, M. C.; Jin, S.; Silva, G. A. *J. Neurosci.* **2006**, *26*, 1893-1895.
- ³⁴ Bouzigues, C.; Levi, S.; Triller, A.; Dahan, M.; *Methods in Molecular Biology; Vol 374: Quantum Dots: Applications in Biology; Chapter 7*; Humana Press Inc, Totowa, NJ.
- ³⁵ Corona, C.; Bryant, B. K.; Arterburn, J. B. *Org. Lett.*, **2006**, *8*, 1883-1886.
- ³⁶ Gussin, H. A.; Tomlinson, I. D.; Muni, N. J.; Little, D. M.; Qian, H.; Rosenthal, S. J.; Pepperberg, D. R. *Bioconjugate Chem.*, **2010**, *4*, 1455-1464.
- ³⁷ Yu, G.; Liang, J.; He, Z.; Sun, M. *Chemistry & Biology*, **2006**, *13*, 723-731.
- ³⁸ Bouzigues, C.; Morel, M.; Triller, A.; Dahan, M. *Proc. Natl. Acad. Sci. U.S.A.*, **2007**, *104*, 11251-11256.

- ³⁹ Muir, J.; Arancibia-Carcamo, L.; MacAskill, A. F.; Smith, K. R.; Griffin, L. D.; Kittler, J. T. *Proc. Natl. Acad. Sci. U.S.A.*, **2010**, *107*, 16679-16684.
- ⁴⁰ De Koninck, P.; Labrecque, S.; Heyes, C. D.; Wiseman, P. W. *HFSP Journal*, **2013**, *5*.
- ⁴¹ Groc, L.; Lafourcade, M.; Heine, M.; Renner, M.; Racine, V.; Sibarita, J.-B.; Lounis, M.; Cognet, L. *J. Neurosci.*, **2007**, *27*, 12433-12437.
- ⁴² Dahan, M.; Levi, S.; Luccardini, C.; Rostaing, P.; Riveau, B.; Triller, A. *Science*, **2003**, *302*, 442-445.
- ⁴³ Bali, M.; Akabas, M. H. *J. Biol. Chem.*, **2012**, *287*, 27762-27770.
- ⁴⁴ Combs-Bachmann, R. E.; Johnson, J. N.; Vytla, D.; Hussey, A. M.; Kilfoil, M. L.; Chambers, J. J. *J. Neurochem.*, **2015**, *133*, 320-329.
- ⁴⁵ Vytla, D.; Combs-Bachmann, R. E.; Hafez, A. M.; Chambers, J. J. *Org. Biomol. Chem.*, **2011**, *9*, 7151-7161.
- ⁴⁶ Hermanson, G. T., *Bioconjugate Techniques*, 2nd Ed, Academic Press, **2010**.
- ⁴⁷ Tan, K. R.; Gonthier, A.; Baur, R.; Ernst, M.; Goeldner, M.; Sigel, E. *J. Biol. Chem.*, **2007**, *282*, 26316-26325.
- ⁴⁸ Tan, K. R.; Baur, R.; Charon, S.; Goeldner, M.; Sigel, E. *J. Neurochem.*, **2009**, *111*, 1264-1273.
- ⁴⁹ Bochet, C. G. *J. Chem. Soc., Perkin Trans. 1*, **2002**, 125-142.
- ⁵⁰ Kramer, R.; Chambers, J. J.; Trauner, D. *Nat. Chem. Bio.*, **2005**, 360-365.
- ⁵¹ Kramer, R. H.; Mouro, A.; Adesnik, H. *Nat. Neurosci.*, **2013**, *16*, 816-823.
- ⁵² Hartley, G. S. *Nature*, **1937**, *140*, 281-281.
- ⁵³ Mahimwalla, Z.; Yager, K. G.; Mamiya, J.; Shishido, A.; Priimagi, A.; Barrett, C. J. *Polym. Bull.* **2012**, *69*, 967-1006.
- ⁵⁴ Beharry, A. A.; Wong, L.; Tropepe, W.; Woolley, G. A. *Angew. Int. Ed.*, **2011**, *50*, 1325-1327.
- ⁵⁵ Samata, S.; Beharry, A. A.; Sadovski, O.; McCormick, T. M.; Babalhavaeji, A.; Tropepe, W.; Woolley, G. A. *J. Am. Chem. Soc.*, **2013**, *135*, 9777-9784.
- ⁵⁶ Beharry, A.; Woolley, G. A. *Chem. Soc. Rev.*, **2011**, *40*, 4422-4437.
- ⁵⁷ Szymański, W.; Beijerle, J. M.; Kistemaker, H. A. V.; Velema, W. A.; Feringa, B. L. *Chem. Rev.*, **2013**, *113*, 6114-6178.
- ⁵⁸ Koçer, A.; Walko, M.; Meijberg, W.; Feringa, B. L. *Science*, **2005**, *309*, 755-758.
- ⁵⁹ Klajn, R. *Chem. Soc. Rev.*, **2014**, *43*, 148-184.
- ⁶⁰ Bartels, E.; Wasserman, N. H.; Erlanger, B. F. *Proc. Natl. Acad. Sci. U.S.A.*, **1971**, *68*, 1820-1823.
- ⁶¹ Fortin, D. L.; Banghart, M. R.; Dunn, T. W.; Borges, K.; Wagenaar, D. A.; Gaudry, Q.; Karakossian, M. H.; Otis, T. S.; Kristan, W. B.; Trauner, D.; Kramer, R. H. *Nat. Methods*, **2008**, *5*, 331-338.
- ⁶² Damijonaitis, A.; Broichhagen, J.; Urushima, T.; Hüll, K.; Nagpal, J.; Laprell, L.; Schönberger, M.; Woodmansee, D. H.; Rafiq, A.; Sumser, M. P.; Kummer, W.; Gottschalk, A.; Trauner, D. *ACS Chem. Neurosci.*, **2015**, *6*, 701-707.
- ⁶³ Stein, M.; Middendorp, S. J.; Carta, V.; Pejo, E.; Raines, D. E.; Forman, S. A.; Sigel, E.; Trauner, D. *Angew. Chem. Int. Ed.*, **2012**, *51*, 10500-10504.
- ⁶⁴ Yue, L.; Pawlowski, M.; Dellal, S. S.; Xie, A.; Feng, F.; Otis, T. S.; Bruzik, K. S.; Qian, H.; Pepperberg, D. R. *Nat. Commun.*, **2012**, *3*, 1095.
- ⁶⁵ Lin, W.-C.; Davenport, C. M.; Mouro, A.; Vytla, D.; Smith, C. M.; Medeiros, K. A.; Chambers, J. J.; Kramer, R. H. *ACS Chem. Biol.*, **2014**, *9*, 1414-1419.
- ⁶⁶ Raser, P. *PhD Thesis*, Universitat Regensburg, 2014.
- ⁶⁷ Guery, S.; Parrot, I.; Rival, Y.; Wermuth, C. G. *Tet. Lett.*, **2001**, *42*(11), 2115-2117.
- ⁶⁸ Guery, S.; Parrot, I.; Rival, Y.; Wermuth, C. G. *Synthesis*, **2001**, *5*, 699-701.
- ⁶⁹ Clapham, K. M.; Batsanov, A. S.; Greenwood, R. D. R.; Bryce, M. R.; Smith, A. E.; Tarbit, B. J. *Org. Chem.*, **2008**, *73*, 2176-2181.
- ⁷⁰ Mortensen, M.; Iqbal, F.; Pandurangan, A. P.; Hannan, S.; Huckvale, R.; Topf, M.; Baker, J. R.; Smart, T. G. *Nat. Commun.*, **2014**, 4454.
- ⁷¹ Sonogashira, K.; Tohda, Y.; Hagihara, N. *Tet. Lett.*, **1975**, *16*, 4467-4470.
- ⁷² Chinchilla, R.; Najera, C. *Chem Soc. Rev.* **2011**, *40*, 5084-5121.
- ⁷³ Hundertmark, T.; Littke, A. F.; Buchwald, S. L.; Fu, G. C. *Org. Lett.*, **2000**, *2*, 1729-1731.
- ⁷⁴ Brea, R. J.; Lopez-Deber, M. P.; Castedo, L.; Granja, J. R. *J. Org. Chem.*, **2006**, *71*, 7870-7873.
- ⁷⁵ Zhu, X.-Y.; Wang, Y.; Bair, F.; Gao, G.-W.; Men J. *Arkivoc*, **2011**, 99.
- ⁷⁶ Boger, D.L.; Zhou, J. *J. Org. Chem.*, **1993**, *58*, 3018-3024.
- ⁷⁷ Chinchilla, R.; Najera, C. *Chem. Rev.*, **2007**, *107*, 874-922.
- ⁷⁸ Tashiro, M.; Yamoto, T. *J. Org. Chem.*, **1979**, *44*, 3037-3041.
- ⁷⁹ Wan, Y.; Alterman, M.; Larhed, M.; Hallberg, A. *J. Org. Chem.*, **2002**, *67*, 6232-6235.

- ⁸⁰ Guy, J.; Caron, K.; Dufresne, S.; Michnick, S. W.; Keillor, J. W. *J. Am. Chem. Soc.*, **2007**, *129*, 11969-11977.
- ⁸¹ Trester-Zedlitz, M.; Kamada, K.; Burley, S. K.; Fenyo, D.; Chait, B. T.; Muir, T. W. *J. Am. Chem. Soc.*, **2003**, *125*, 2416-2425.
- ⁸² Invitrogen Molecular Probe (R) specification data sheet, **2007**.
- ⁸³ Kaech, S.; Banker, G. *Nat. Protoc.* **1**, **2007**, 2406-2415.
- ⁸⁴ Bailey, C. E.; Ong, S. D. *Journal of Pharmacological Methods*, **1978**, *1*, 171-175.
- ⁸⁵ Demeter, A.; Horváth, K.; Böör, K.; Molnár, L.; Soós, R.; Lendvay, G. *J. Phys. Chem. A.*, **2013**, *117*, 10196-10210.
- ⁸⁶ Wittelsberger, A.; Thomas, B. E.; Mierke, D. F.; Rosenblatt, M. *FEBS Letters*, **2006**, *7*, 1872-1876.
- ⁸⁷ Churio, M. S.; Grela, J. *Chem. Educ.*, **1997**, *74*, 436.
- ⁸⁸ Oatis, J. E.; Knapp, D. R. *Tet. Lett.*, **1998**, *39*, 1665-1668.
- ⁸⁹ Alessandro, M.; Marco, C.; Fernando, F.; Huck, L. A.; Mangion, D.; Leigh, W. J.; Toniolo, C. *Proceedings of the 30th European Peptide Symposium*, **2008**.
- ⁹⁰ Wright, K.; Moretto, A.; Marco, C.; Wakselman, J. P.; Formaggio, F.; Toniolo, C. *Org. Biomol. Chem.*, **2010**, *8*, 3281-3286.
- ⁹¹ Huisgen, R. *Proc. Chem. Soc.*, **1961**, 357-396.
- ⁹² Husinec, S.; Markovic, R.; Petkovic, M.; Nasufovic, V.; Savic, V. *Org. Lett.*, **2011**, *13*, 2286-2289.
- ⁹³ Mourad, A. E.; Wise, D. S.; Townsend, L. B. *J. Heterocycl. Chem.*, **1993**, *30*, 1365-1372.
- ⁹⁴ Alam, M. S.; Huang, J.; Ozoe, F.; Matsumura, F.; Ozoe, Y. *Bioorg. Med. Chem.*, **2007**, *15*, 5090-5104.
- ⁹⁵ Bräse, S.; Gil, C.; Knepper, K.; Zimmerman, V. *Angew. Chem. Int. Ed.*, **2005**, *44*, 5188-5240.
- ⁹⁶ Chan, T. R.; Hilgraf, R.; Sharpless, K. B.; Fokin, V. V. *Org. Lett.*, **2004**, *6*, 2853-2855.
- ⁹⁷ Feliciano, M.; Vytla, D.; Medeiros, K. A.; Chambers, J. J. *Bioorg. Med. Chem.*, **2010**, *18*, 7731-7738.
- ⁹⁸ Schoenberger, M.; Damijonaitis, A.; Zhang, Z.; Nagel, D.; Trauner, D. *ACS Chem. Neurosci.*; **2014**, *5*, 514-518.
- ⁹⁹ Harvey, J. H.; Butler, B. K.; Trauner, D. *Tet. Lett.*, **2007**, *48*, 1661-1664.
- ¹⁰⁰ Merino, E.; Ribagorda, M. *Beilstein J. Org. Chem.* **2012**, *8*, 1071-1090.
- ¹⁰¹ Banghart, M. R.; Trauner, D. *Chemical Neurobiology: Methods and Protocols*, Methods in Molecular Biology, **2013**, 995.
- ¹⁰² Experimental results from Dr M. Mortensen in the Smart group.
- ¹⁰³ Lord, S.; Conley, N. R.; Lee, H. L.; Nishimura, S. Y.; Pomerantz, A. K.; Willets, K. A.; Lu, Z.; Wang, H.; Liu, N.; Samuel, R.; Weber, R.; Semyonov, A.; He, M.; Tweig, R. J.; Moerner, W. E. *Chem. Phys. Chem.*, **2009**, *10*, 55-65.
- ¹⁰⁴ Lord, S.; Conley, N. R.; Lee, H. H.; Liu, N.; Samuel, R. *Proc. SPIE*, **2009**, 7190.
- ¹⁰⁵ Yamaguchi, T.; Asanuma, M.; Nakanishi, S.; Saito, Y.; Okazaki, M.; Dodo, K.; Sodeoka, M. *Chem. Sci.*, **2014**, *5*, 1021-1029.
- ¹⁰⁶ Miller, P. S.; Aricescu, A. R. *Nature*, **2014**, *512*, 270-275.
- ¹⁰⁷ Gellerman, G.; Elgavi, A.; Salitra, Y.; Kramer, M. *J. Pept. Res.*, **2001**, *57*, 277-291.
- ¹⁰⁸ Ding, D.; Zhao, Y.; Meng, Q.; Xie, D.; Nare, B.; Chen, D.; Bacchi, C. J.; Yarlett, N.; Zhang, Y.-K.; Hernandez, V.; Xia, Y.; Freund, Y.; Abdulla, M.; Ang, K.-H.; Ratnam, J.; McKerrow, J. H.; Jacobs, R. T.; Zhou, H.; Plattner, J. J. *ACS Med. Chem. Lett.*, **2010**, *1*, 165-169.
- ¹⁰⁹ Coker, G. *G Br. Pat.* GB923727, **1963**.
- ¹¹⁰ Cram, D. J.; Allinger, N. L. *J. Am. Chem. Soc.*, **1956**, *78*, 2518-2524.
- ¹¹¹ Song, H. Y.; Ngai, M. H.; Song, Z. Y.; MacAry, P.; Hobley, J.; Lear, M. J. *Org. Biomol. Chem.*, **2009**, *7*, 3400-3406.
- ¹¹² Lee, M.; Jung, D.-W.; Williams, D.; Shin, I. *Org. Lett.*, **2005**, *7*, 5477-5480.
- ¹¹³ Kaiser, K.; Marek, M.; Haselgrübler, T.; Schindler, H.; Gruber, H. J. *Bioconjugate Chem.*, **1997**, *8*, 545-551.
- ¹¹⁴ Kunbaraci, V.; Aydogan, B.; Talinli, N.; Yagci, Y. *J. Polymer Sci.*; **2012**, *50*, 2612-2618.
- ¹¹⁵ Oikawa, A.; Kindaichi, G.; Shimotori, Y.; Okimoto, M.; Hoshi, M. *Tetrahedron*, **2015**, *71*, 1705-1711.
- ¹¹⁶ Akhbar, A. R.; Chudasama, V.; Fitzmaurice, R. J.; Powell, L.; Caddick, S. *Chem. Commun.*, **2014**, *11*, 743-746.
- ¹¹⁷ Diisopropyl 1-benzoylhydrazine-1,2-dicarboxylate was kindly donated by Dr Ahmed Akhbar.
- ¹¹⁸ Chalker, J. M.; Gunnno, S.; Boutoureira, O.; Gerstberger, S. C.; Fernández-González, M.; Bernardes, G. J. L.; Hailu, H.; Schofield, C. J.; Davies, B. G. *Chem. Sci.*, **2011**, *2*, 1666-1676.
- ¹¹⁹ Biagini, S. C. G.; Gibson, S.; Keen, S. P. *J. Chem. Soc. Perkin Trans. 1*, **1998**, 2485-2500.

- ¹²⁰ Belluti, F.; Piazza, L.; Bisi, A.; Gobbi, S.; Bartolini, M.; Cavalli, A.; Valenti, P.; Rampa, A. *Eur. J. Med. Chem.*, **2009**, *44*, 1341-1348.
- ¹²¹ Maes, B. U. W.; Lemière, G. L. F.; Dommissie, R.; Augustyns, K.; Haemers, A. *Tetrahedron*, **2000**, *56*, 1777-1781.
- ¹²² Neklesa, T. K.; Tae, H. S.; Schneekloth, A. R.; Stulberg, M. J.; Corson, T. W.; Sundberg, T. B.; Raina, K.; Holley, S. A.; Crews, C. M. *Nat. Chem. Bio.* **2011**, *7*, 538-543.
- ¹²³ Zachary, P. D.; Sharpless, B. K. *Angew. Chem. Int. Ed.*, **2002**, *41*, 2110-2113.
- ¹²⁴ Greving, N.; Keul, H.; Millaruelo, M.; Weberskirch, R.; Moeller, M. *Polym. Int.*, **2014**, *63*, 114-126.
- ¹²⁵ Volgraf, M.; Gorostiza, P.; Szobota, S.; Helix, M. R.; Isacoff, E. Y.; Trauner, D. *J. Am. Chem. Soc.* **2007**, *129*, 260-261.
- ¹²⁶ Kumar, M.; Kumar, N.; Bhalla, V.; Singh, H.; Sharma, P. R.; Kaur, T. *Org. Lett.*, **2011**, *13*, 1422-1425.